Universitat de Lleida

Adaptive syndromes of Mediterranean pines in response to drought and fire: common gardens meet high-throughput phenotyping techniques

Erica Lombardi

http://hdl.handle.net/10803/689451

Universitat de Lleida

TESI DOCTORAL

Adaptive syndromes of Mediterranean pines in response to drought and fire: common gardens meet high-throughput phenotyping techniques

Erica Lombardi

Memòria presentada per optar al grau de Doctor per la Universitat de Lleida
Programa de Doctorat en (Gestió Forestal i del Medi Natural)

Director/a
(Jordi Voltas Velasco)
(Víctor Resco de Dios)

Tutor/a
(Jordi Voltas Velasco)

To all those who don't have the possibility to pursue their dreams

INDEX

List of publications

The first three chapters of this thesis are based on the following publications:

- Lombardi, E., Ferrio, J. P., Rodríguez-Robles, U., Resco de Dios, V., & Voltas, J. (2021). Ground-Penetrating Radar as phenotyping tool for characterizing intraspecific variability in root traits of a widespread conifer. Plant and Soil, 468, 319-336.
- Lombardi, E., Shestakova, T. A., Santini, F., Resco de Dios, V., & Voltas, J. (2022). Harnessing tree-ring phenotypes to disentangle gene by environment interactions and their climate dependencies in a circum-Mediterranean pine. Annals of Botany, 130, 509-523.
- Lombardi, E., Rodríguez-Puerta, F., Santini, F., Chambel, M. R., Climent, J., Resco de Dios, V., & Voltas, J. (2022). UAV-LiDAR and RGB imagery reveal large intraspecific variation in tree-level morphometric traits across different pine species evaluated in common gardens. Remote Sensing, 14, 5904.

Manuscript submitted to a peer reviewed journal

- Remotely sensed and ground measurements reveal intraspecific differences in early season needle unfolding and senescence but lack of variability in litter flammability of *Pinus halepensis*.

Thesis overview

This thesis includes first a general introduction part, a section in which general and specific objectives are explained, and a general material and methods section. Then the thesis consists of four chapters, the first three are based upon published papers, while the last chapter is a manuscript in preparation. All chapters include the following sections: introduction, material and methods, results, discussion (and conclusions when present). Finally, a general discussion and conclusions sections are provided. Chapter sections start with a characterization of intraspecific variation in belowground growth (root morphology) of *Pinus halepensis* (Chapter 1), while Chapter 2, 3 and 4 are focused on intraspecific differentiation in aboveground growth of *Pinus halepensis* (all Chapters) and *Pinus nigra* (Chapter 3). The chapters tackle from main trunk characteristics (Chapter 2), to main trunk and crown structure and architecture (Chapter 3) ending in crown vegetation indices and flammability (Chapter 4). In more details:

Chapter 1. In the first chapter I used Ground-Penetrating Radar (GPR) as non-invasive high-throughput phenotyping technique to characterize intraspecific variation in coarse root morphology (depth, diameter and frequency) among 56 populations of *P. halepensis*.

Chapter 2. Here I analyzed interannual growth pattern and its genetic basis of 23 populations of Aleppo pine by testing genotype by environment interactions (G × E) in a common garden experiment. In this regard I linked radial growth records (ring width and early to latewood ratios) as phenotypic traits with genomic data, in particular genetic markers (SNPs) and environmental data.

Chapter 3. I evaluated the potential of two unmanned aerial vehicle (UAV) based high-throughput phenotyping techniques, LiDAR and RGB imagery, to characterize tree growth and crown structure and architecture. In this regard, I studied the suitability of these devices to characterize intraspecific variability in morphometric traits related to crown architecture and volume, primary growth and biomass in two widely distributed Mediterranean pines (P. *halepensis* and *P. nigra*).

Chapter 4. In the last chapter I used UAV-based vegetation indices along with *in situ* measuraments to characterize intraspecific differentiation and differential plasticity in litter flammability and tree phenology,

potentially related to needle senescence among *P. halepensis* populations.

Abstract

Genetic differentiation and phenotypic plasticity are important mechanisms of trees to cope with environmental changes. In this thesis I focused on intraspecific differentiation of functional traits of two pine species widely distributed in the Mediterranean basin: *Pinus halepensis* Mill. and *Pinus nigra* Arnold. I combined high-throughput phenotyping techniques (HTPTs) with *in situ* measurements to characterize intraspecific differences in functional traits potentially explanatory of different adaptive syndromes to external factors, especially those related to drought and fire. In particular, (i) the Ground Penetrating Radar (GPR) was used to detect intraspecific variability of coarse root morphology in *P. halepensis*; (ii) Unmanned Aerial Vehicles (UAVs) coupled with LiDAR sensors or RGB and multispectral cameras were used to infer intraspecific differences in crown structure and architecture in *P. halepensis* and *P. nigra*, and also in needle phenology in *P. halepensis*; and (iii) dendrochronology combined with a candidate-gene approach was applied to disentangle genetic and environmental effects determining intra-annual variation in secondary growth. Data was collected from four common garden experiments or forest provenance trials located in Spain (three of *P. halepensis*, one of *P. nigra*). These trials allowed to investigate the magnitude of genetic variation, local adaptation and phenotypic plasticity in the aforementioned characteristics, and made possible to indirectly attribute the existing phenotypic variability among populations to genetic differentiation. The findings of this thesis revealed the existence of intraspecific differentiation of functional traits related to root morphology, crown structure and volume, needle phenology and secondary growth in *P. halepensis*, and to aerial growth (tree height, crown structure and volume) in *P. nigra*. The results pointed to the existence of different adaptive syndromes and the presence of trade-offs involving miscellaneous plant compartments and functions. To conclude, by using novel phenotyping tools this thesis provides new insights about the nature of intraspecific differentiation in functional traits poorly studied to date at the intraspecific level in forest adult trees. Therefore, the combination of HTPTs, *in situ* measurements and candidate-gene approaches in common garden experiments was effective to understand phenotypic and genetic differentiation among populations of two important pine species of the Mediterranean forests.

Resumen

La diferenciación genética y la plasticidad fenotípica son importantes mecanismos de respuesta de los árboles frente a las condiciones ambientales. En esta tesis he analizado la diferenciación intra-específica de rasgos funcionales de dos especies de pino ampliamente distribuidas en la cuenca Mediterránea: *Pinus halepensis* Mill. y *Pinus nigra* Arnold. A tal efecto, he combinado técnicas de fenotipado de alto rendimiento (HTPTs) con mediciones *in situ* para estimar diferencias intra-específicas en rasgos potencialmente relacionadas con diferentes síndromes adaptativos derivados de ambientales variables especialmente relacionados con la sequía y el fuego. En particular, se utilizó el georradar (GPR) para detectar variabilidad intraespecífica en la morfología de raíces en *P. halepensis*; se utilizaron vehículos aéreos no tripulados (UAVs) equipados con sensores LiDAR y cámaras RGB y multi-espectrales para estimar diferencias intra-específicas en la estructura y arquitectura de la copa en *P. halepensis* y *P. nigra*, así como la fenología de las acículas en *P. halepensis*; y se aplicó la dendrocronología junto con aproximaciones de genes candidatos para revelar efectos genéticos y ambientales determinantes de variación intra-anual en crecimiento secundario en *P. halepensis*. Los datos se obtuvieron de cuatro ensayos genéticos forestales ubicados en España (tres de *P. halepensis* y uno de *P. nigra*). Este tipo de ensayos permite investigar la magnitud de la variación genética, la adaptación local y la plasticidad fenotípica. Los hallazgos de esta tesis revelaron la existencia de diferenciación intra-específica de rasgos funcionales relacionados con la morfología de la raíz, la estructura y el volumen de la copa, la fenología de las acículas y el crecimiento secundario de *P. halepensis*, y relacionados con el crecimiento aéreo (altura del árbol, estructura y volumen de la copa) en *P. nigra*. Todo ello indica la existencia de diferentes síndromes adaptativos y la presencia de compensaciones entre las diferentes funciones y morfología de los árboles. Para concluir, mediante el uso de herramientas de fenotipado avanzadas esta tesis proporciona información novedosa en relación a la diferenciación intra-específica en rasgos funcionales poco estudiados en árboles forestales adultos. La combinación de HTPTs, mediciones *in situ* y genes candidatos en ensayos genéticos forestales resultó sumamente eficaz para evaluar la diferenciación fenotípica y genética entre las

poblaciones de dos importantes especies de pinos mediterráneos.

Resum

La diferenciació genètica i la plasticitat fenotípica són importants mecanismes de resposta dels arbres en front a les condicions ambientals. En aquesta tesi he analitzat la diferenciació intraespecífica de trets funcionals de dues espècies de pi àmpliament distribuïdes a la conca Mediterrània: *Pinus halepensis* Mill. i *Pinus nigra* Arnold. A tal efecte, he combinat tècniques de fenotipat d'alt rendiment (HTPTs) amb mesures *in situ* per estimar diferències intra-específiques en trets potencialment relacionats amb diferents síndromes adaptatives derivades d'ambients variables, i especialment relacionades amb la sequera i el foc. En particular, es va utilitzar el georradar (GPR) per detectar variabilitat intra-específica en la morfologia de les arrels gruixudes en *P. halepensis*; es van utilitzar vehicles aeris no tripulats (UAVs) equipats amb sensors LiDAR i càmeres RGB i multiespectrals per inferir diferències intra-específiques en l'estructura i arquitectura de la capçada en *P. halepensis* i *P. nigra*, així com la fenologia de les acícules en *P. halepensis*; i es va aplicar la dendrocronologia conjuntament amb mètodes de gens candidats per revelar els efectes genètics i ambientals que determinen la variació intra-anual en el creixement secundari en *P. halepensis*. Les dades es van recollir a quatre assajos genètics forestals ubicats a Espanya (tres de *P. halepensis* i un de *P. nigra*). Aquest tipus d'assaigs permeten investigar la magnitud de la variació genètica, l'adaptació local i la plasticitat fenotípica. Les resultats d'aquesta tesi van revelar una important diferenciació intra-específica de trets funcionals relacionats amb la morfologia de l'arrel, l'estructura i el volum de la copa, la fenologia de les acícules i el creixement secundari de *P. halepensis*, i relacionats amb el creixement aeri (alçada de l'arbre, estructura i volum de la copa) en *P. nigra*. Això indica l'existència de diferents síndromes adaptatius i la presència de compensacions entre les diferents funcions i morfologia dels arbres. Per concloure, mitjançant l'aplicació d'eines de fenotipat avançades aquesta tesi proporciona nous coneixements sobre la diferenciació intraespecífica en trets funcionals poc estudiats en arbres forestals adults. La combinació de HTPTs, mesures *in situ* i gens candidats amb assaigs genètics forestals va resultar eficaç per avaluar la diferenciació fenotípica i genètica entre les poblacions de dues importants espècies de pins pròpies dels boscos mediterranis.

Introduction

Background

Forests are complex ecosystems that provide vital services to both humans and wildlife. They play a key role in carbon sequestration, soil conservation and water cycle, and they provide many other ecosystem services (Felipe-Lucia et al. 2018; Pan et al. 2013). Nowadays forests cover approximately 30% of the Earth land surface (Pan et al. 2013) and *ca*. 40% of European land (Orsi et al. 2020). Europe is home to a number of different forest types, including temperate deciduous forests, boreal forests and Mediterranean forests, each of them characterized by its unique biodiversity (Ratcliffe et al. 2017; Ruiz-Benito et al. 2017). Unfortunately, many of European's forests, especially in the Mediterranean area, are under threat due to deforestation, landscape fragmentation and climate change (Peñuelas et al. 2017; Palahi et al. 2008). Global warming is recognized as a worldwide threat, especially in arid and semiarid ecosystems (Huang etl al. 2016; Prăvălie 2016). Forests are particularly vulnerable to climate change since the rate of environmental changes is higher than the adaptation capacity of many plants (Jezkova et al. 2016). As a results, forest productivity will likely be affected and we will face a shifting in forest dynamics, including changes in forest distribution, tree species migration and local extinction, for instance (Vacek et al. 2023).

Future climate might seriously impact forest ecosystem dynamics across the Mediterranean basin, since water availability is the main limiting factor in Mediterranean ecosystems and models forecast a reduction in precipitation up to 40% (IPCC 2022) This means that in many areas forest ecosystems will likely face important prolonged drought periods (Tramblay and Hertig, 2021; Lange, 2019). The intensification of droughts coupled with increasing temperature may be lethal for many tree species (Hammond et al. 2022), as it can cause direct and indirect damages to plants, like hydraulic failure, increasing pest occurrence and, also, increasing wildfire events (Ruffault et al. 2020). Wildfire is an important abiotic threat that shapes forest ecosystems and have significant impacts on both individual trees and the overall composition and structure of the forest. Across its gradient of frequency and severity it can have positive or negative effects on forest ecosystems (Roces-Díaz et al. 2022). However, nowadays human

activity and climate change are the major drivers intensifying forest fire regimes around the globe (Moreira et al. 2023; Pausas and Keeley, 2021). Thus, fire is considered a major threat in many areas (including the Mediterranean basin) and it can cause severe damage to forest ecosystems, including those adapted to fire (Fernández-Guisuraga et al. 2019; Taboada et al. 2017).

In order to prevent or slowdown global change effects, there are ongoing efforts to protect and restore forest ecosystems, including the establishment of protected areas, reforestation activities, assisted migration and forest management practices for monitoring and assessing forest health (North et al. 2019; Leech et al. 2011). However, these practices very often do not take into account the existence of intraspecific variability in adaptive traits (Montwé et al. 2015).

Adaptation and phenotypic variation

Tree phenotypes refer to the morphophysiological characteristics of tree species, such as their size, structure and growth patterns. Phenotypes play an important role in determining how trees respond to environmental changes (Amaral et al. 2020; Heilmeier et al. 2019). For example, some tree species have evolved to develop deep root systems that allow them to access deep water sources, other species produce serotinous cones that help them to regenerate after crown fire, some other have crown structures that allow them to endure heavy snowfalls, etc. A tree phenotype is the result of both genetic and environmental factors, and disentangling the two effects is challenging under natural conditions (Bussotti et al. 2015). In fact, a given genotype can express different phenotypes under distinct environmental conditions, which is called phenotypic plasticity. Phenotypic plasticity is a heritable mechanism that allow individuals to adjust their phenotypes in responses to environmental changes at both short- and long-term (Anderson et al. 2020; Nicotra et al. 2010). The other main process that plant adopt to cope to climate change is called genetic adaptation (Westerband et al. 2021; Fady et al. 2016). Genetic adaptation refers to inherited genetic changes as a consequence of natural selection in response to environmental selection pressure (Pritzkow et al. 2020; Fady et al. 2016), and it accounts for inter- and intraspecific differences in many functional traits as adaptive response to different

ecological niches (Pritzkow et al. 2020). In this regard, populations with high genetic variability are more likely to have greater adaptability potential than other less variable counterparts (Depardieu et al. 2020; Aravanopoulos, 2018). Genetic variability can be studied through genetic (i.e. molecular markers) or phenotypic approaches. In relation to the latter, common garden experiments (e.g. provenance trials) are really useful in order to investigate genetic variability through phenotypic studies. Common gardens refer to experimental designs where individuals collected from distinct geographic locations are planted under semi natural conditions and, therefore, grow sharing the same set of environmental conditions (de Villemereuil et al. 2022). Through common garden experiments it is possible to investigate the magnitude of genetic variation, local adaptation and phenotypic plasticity (Leroy et al. 2019; Sovolainen et al. 2007), since in these trials it is possible to tease the environmental effect apart from true genetic variation. Thus, the observed phenotypic variability can indirectly be attributed to genetic differentiation (Colautti et al. 2009). With regard genetic approaches, Single Nucleotide Polymorphisms (SNPs) are likely the most used molecular markers to investigate genotype-phenotype associations (Liu et al. 2019; Mandaliya et al. 2010). SNPs are variations of a single nucleotide occurring at particular genomic positions that occur between individuals; thus, they generate genetic differentiation within a species which can be related to adaptive variation (Rellstab et al. 2017; Seifert et al. 2012). The analysis of SNPs variation through approaches like candidate genes are invaluable since it provides a straight connection to gene function, without the need to investigate the whole genome (Jaramillo-Correa et al. 2015).

High-throughput phenotyping techniques

Collecting information about phenotypic traits is not an easy task. A major limitation when studying phenotypic traits of forest trees, especially in their adult stage, is the complexity and time-consuming nature of ground-based methods (Liao et al. 2022; Ganz et al. 2019). In this regard, high-throughput phenotyping techniques (HTPTs) have the potential to provide valuable data on a large number of phenotypic traits, particularly in adult trees (Camarretta et al. 2020). These techniques have been developed in the last decades

and they are in continuous expansion, especially in agricultural applications (Mazis et al. 2020). They allow to collect numerous plant traits efficiently and with high precision at both small and large spatial scales (Feng et al. 2021; Xie and Yang, 2020). Moreover, automated measurements reduce the errors and variability associated to manual labor, leading to greater consistency of the data collected. Among the vast varieties of HTPTs we can underline remotely-sensed information obtained from satellites, unmanned aerial vehicles (UAVs) and terrestrial tools. The first satellites were launched before 1960, and after that an increasing number of satellites with different purposes of Earth monitoring have been in orbit (Guo et al. 2019). Nowadays there is a continuous increment in number of satellites with high temporal and spatial resolution that generate either private or freely accessible data that can be used for plant phenotypic studies (Zhang et al. 2020). However, one the major cons of satellites is that they are sensitive to cloudy conditions (Pàdua et al. 2017), and also their resolution is in the order of meters.

On the other hand, UAVs are characterized by higher ground resolutions, in the order of centimeters, and they are not affected by atmospheric conditions since they can fly at really low altitudes (Moe et al. 2020; Pàdua et al.2017). UAVs can be equipped with different type of sensors, like multispectral, RGB, or thermal cameras, and LiDAR, for instance. The data provided by these tools can be used for a multidimensional visualization of trees and also to obtain information about above-ground growth traits such as total height, stem diameter, crown structure and biomass at the tree level (Liao et al. 2022; Camarretta et al. 2020). In addition, multispectral and RGB sensors provide valuable information on vegetation reflectance in different wavelengths from which is possible to calculate indices related to vegetation status, phenology and leaf area for instance (Botyanszka, 2021; Klosterman at al. 2018). Complementary to this, thermal cameras capture crown temperatures, providing information of tree transpiration as a proxy of water use efficiency (Botyanszka et al. 2021; Santini et al. 2019a). Still, UAV-based HTPT are not free of cons. For example, high technical skills are still required in order to use these tools and post-process the data. In addition, even if they are not sensitive to clouds, bad weather, especially wind, may affect their performance and, also, they cover smaller areas compared to satellites. Among HTPT

terrestrial tools, we can highlight above-ground tools such as field spectrometry, field hyperspectral imaging or terrestrial laser scanning which have excellent accuracy and very high resolutions, and below-ground tools like the ground-penetrating radar, which allows investigating root structure and distribution at the tree level in a non-destructive way (Alani and Lantini, 2020; Guo et al. 2013). However, in some circumstances a high technical competence is also required for terrestrial HTPT tools in order to use these devices and process the data and, although the resolution of these tools is really high, using these devices in the field can be labor-intensive, since they have to be placed or be moved manually, and site accessibility can also compromise their applicability (Pàdua et al. 2017).

Overall HTPT can provide valuable data on plant traits in forestry, and in particular UAV-derived images and terrestrial tools are promising cost-effective techniques to investigate phenotypic variability at the tree level. Anyway, in some circumstances traditional field-phenotyping techniques are still needed in conjunction to HTPT in order to provide complementary data to validate results and, in some cases, to reduce costs.

Mediterranean pines: the case of Pinus halepensis and Pinus nigra

Pinus is a genus of coniferous trees worldwide distributed, with approximately 120 species present across the Northern hemisphere (Andini et al. 2022; Keeley, 2012). Pine trees are highly adaptable and can grow in a broad variety of habitats, from desert to mountain ecosystems. This genus is an important component of Mediterranean ecosystems, since it has great economic and ecological values (Ibrahim et al. 2022). Ten pine species naturally occur across the Mediterranean basin, including *P. halepensis* Mill (Aleppo pine) and *P. nigra* Arnold (European black pine).

P. halepensis is the most widely distributed conifer species across the Mediterranean basin (Vennetier et al. 2018), and thanks to its high intraspecific variability and plasticity, it occupies vastly different ecological niches ranging from mesic (annual precipitation exceeding 800 mm) to xeric environments (below 350 mm). It is a species well adapted to drought, since it presents an efficient hydraulic

system and is also capable of regulating its stomatal activity and adjust its growth rate depending on the severity of drought (Pasho et al. 2012; Tapias et al. 2004). It is also adapted to fire, and specifically it is described as fire embracer since it has a short-life cycle with an early reproduction stage, and it produces serotinous cones that allow for a rapid post-fire regeneration (Romero et al. 2023; Pausas, 2015).

On the other hand, *P. nigra* inhabits medium to high altitude mountain ranges across the Mediterranean basin and is less adapted to drought (Enescu et al. 2016; Isajev et al. 2003). *P. nigra* is a fast-growing and a light demanding species that grows under different soil types, and it also shows cold hardiness (Kreyling et al. 2012). It is considered a fire-tolerant species because it shows fire-related features such as a thick bark that allows survival under low intensity fires (Resco de Dios et a. 2018). It can be found in association with other pine species, including Aleppo pine (Jevšenak and Saražin, 2023).

Many studies have focused on the characterization of interspecific differentiation of functional traits in the genus *Pinus*, thereby concluding that pine species have high interspecific variability as a result of contrasting evolutionary histories and adaptability (Keeley et al. 2012). However, functional traits may substantially vary within species allowing different trees belonging to the same species to thrive under very different environmental conditions (Benito-Garzón et al. 2011).

Previous studies have investigated intraspecific differences for functional traits related to primary growth (Patsiou et al. 2020; Voltas et al. 2018), secondary growth and wood density (Hevia et al 2020), water use efficiency (Voltas et al. 2008) and photosynthetic indices (Santini et al. 2019a) among *P. halepensis* populations. Also, several subspecies have been recognized for *P. nigra* (Isajev et al. 2003) which differ in traits associated to photosynthetic indices (Santini et al. 2019b), tree height (Varelides et al. 2001) and secondary growth and wood anatomy (Fkiri et al. 2018; Esteban et al 2012). Although the importance of studying intraspecific variability has recently increased (Girard et al. 2022; Hé et al. 2021), current knowledge on differentiation in functional traits at the intraspecific level remains insufficient compared to the interspecific level (Chelli et al. 2018; Sbay et al. 2018; Albert et al. 2011). Characterizing phenotypic variability is fundamental in order to understand genotype by environment interactions (i.e.

differential plasticity), and interpret the ecological significance of functional traits in relation to the potential adaptability of populations to major environmental constraints such as drought and fire.

Objectives

The main objective of this thesis is to gain knowledge on the adaptive syndromes of two Mediterranean pines (*P. halepensis* and *P. nigra*) by analyzing populations growing in three common garden experiments. This primarily includes the characterization of genetic differentiation for functional (morphological, phenological) and fitness-related (above and belowground growth) traits, and also the evaluation of differential plasticity linked to genotype by environment interactions for some of these traits.

In this regard, three general objectives are shared by the four chapters that constitute this thesis:

Objective 1. To understand the potential of Mediterranean pines (*P. halepensis*, *P. nigra*) to respond to climate change and environmental stressors by characterizing intraspecific variability in functional traits potentially related to drought and fire (chapters 1 to 4).

Objective 2. To evaluate the possible relationships between patterns of local adaptation and their environmental drivers at the geographic origin of populations (chapters 1 to 4).

Objective 3. To evaluate novel and/or high-throughput phenotyping techniques (HTPT) informative of drought- and fire-related strategies in forest genetic trials (chapters 1, 3 and 4).

In addition to these general objectives, each chapter also develops some specific objectives as follows:

Objective 4. To evaluate if ground penetrating radar is a valid tool to infer intraspecific variability for coarse root frequency, depth and diameter in a widespread Mediterranean pine species adapted to drought such as *P. halepensis* (chapter 1).

Objective 5. To characterize the associations between coarse root traits (frequency, depth and diameter) and aboveground growth in *P. halepensis* (chapter 1).

Objective 6. To explore the genetic basis, differential plasticity and climate drivers of *P. halepensis* secondary growth at the temporal level using dendrochronology in common gardens (chapter 2).

Objective 7. To evaluate if UAV-based LiDAR and UAV-based RGB imagery are valid tools to assess

intraspecific differentiation in phenotypic traits related to primary growth, crown volume and structure, and aerial biomass in *P. halepensis* and *P. nigra* (chapter 3).

Objective 8. To characterize intraspecific variation and differential plasticity in phenology mainly associated to needle senescence and flammability among *P. halepensis* populations using HTPT (chapter 4).

References

Alani, A.M., Lantini, L. (2020). Recent Advances in Tree Root Mapping and Assessment Using Non-destructive Testing Methods: A Focus on Ground Penetrating Radar, Surveys in Geophysics. Springer Netherlands. 41, 605-646. https://doi.org/10.1007/s10712-019-09548-6

Albert, C.H., Grassein, F., Schurr, F.M., Vieilledent, G., Violle, C. (2011). Perspectives in Plant Ecology, Evolution and Systematics When and how should intraspecific variability be considered in trait-based plant ecology? PPEES. 13, 217–225. https://doi.org/10.1016/j.ppees.2011.04.003

Amaral, J., Ribeyre, Z., Vigneaud, J., et al. (2020). Advances and promises of epigenetics for forest trees. Forests. 11, 976. https://doi.org/10.3390/f11090976

Anderson, J. T., & Song, B. H. (2020). Plant adaptation to climate change—Where are we? JSE. 58, 533-545. https://doi.org/10.1111/jse.12649

Andini, R., Melinda, V., Pardede, E., Yanti, L.A., Hmon, K., Moulana, R., Indrioko, S. (2022). Morphological variation of Aceh *Pinus* (*Pinus merkusii*). IOP Conf. Ser. Earth Environ. Sci. 951. https://doi.org/10.1088/1755-1315/951/1/012091

Aravanopoulos, F.A. (2018). Do silviculture and forest management affect the genetic diversity and structure of long-impacted forest tree populations? Forests. 9, 1–14. https://doi.org/10.3390/f9060355

Benito Garzón, M., Alía, R., Robson, T.M., Zavala, M.A. (2011). Intra-specific variability and plasticity influence potential tree species distributions under climate change. Glob. Ecol. Biogeogr. 20, 766–778. https://doi.org/10.1111/j.1466-8238.2010.00646.x

Botyanszka, L. (2021). A Review of Imaging and Sensing Technologies for Field Phenotyping. Acta Hortic. Regiotect. 24, 58–69. https://doi.org/10.2478/ahr-2021-0011

Bussotti F, Pollastrini M, Holland V, Brüggemann W. (2015). Functional traits and adaptive capacity of European forests to climate change. EEB. 111: 91–113. https://doi.org/10.1016/j.envexpbot.2014.11.006

Camarretta, N., Harrison, P.A., Lucieer, A., Potts, B.M., Davidson, N., Hunt, M. (2020). From drones to phenotype: Using UAV-LiDAR to detect species and provenance variation in tree productivity and structure. Remote Sens. 12, 1–16. https://doi.org/10.3390/rs12193184

Chelli, S., Marignani, M., Barni, E., et al. (2019). All Aspects of Plant Biology Plant – environment interactions through a functional traits perspective: a review of Italian studies. PLANT Biosyst. - AN Int. J. Deal. WITH ALL Asp. PLANT Biol. 0, 1–17. https://doi.org/10.1080/11263504.2018.1559250

Colautti, R.I., Maron, J.L., Barrett, S.C.H. (2009). Common garden comparisons of native and introduced plant populations: Latitudinal clines can obscure evolutionary inferences. Evol. Appl. 2, 187–199. https://doi.org/10.1111/j.1752-4571.2008.00053.x

Depardieu, C., Girardin, M.P., Nadeau, S., Lenz, P., Bousquet, J., Isabel, N. (2020). Adaptive genetic variation to drought in a widely distributed conifer suggests a potential for increasing forest resilience in a drying climate. New Phytol. 227, 427–439. https://doi.org/10.1111/nph.16551

de Villemereuil, P., Gaggiotti, O.E., Goudet, J. (2022). Common garden experiments to study local adaptation need to account for population structure. J. Ecol. 110, 1005–1009. https://doi.org/10.1111/1365-2745.13528

Enescu, C. M., de Rigo, D., Caudullo, G., Mauri, A., Houston Durrant, T. (2016). *Pinus nigra* in Europe: distribution, habitat, usage and threats. In: San-Miguel-Ayanz J, de Rigo D, Caudullo G, Houston Durrant T, Mauri A (Eds.), European Atlas of Forest Tree Species. Publ. Off. EU, Luxembourg. 015–138

Esteban, L.G., Martín, J.A., de Palacios, P., Fernández, F.G. (2012). Influence of region of provenance and climate factors on wood anatomical traits of *Pinus nigra* Arn. subsp. *salzmannii.* Eur. J. For. Res. 131, 633–645. https://doi.org/10.1007/s10342-011-0537-x

Fady, B., Cottrell, J., Ackzell, L., Alía, R., Muys, B., Prada, A., González-Martínez, S.C. (2016). Forests and global change: what can genetics contribute to the major forest management and policy challenges of the twenty-first century? Reg. Environ. Chang. 16, 927–939. https://doi.org/10.1007/s10113-015-0843-9

Felipe-Lucia, M.R., Soliveres, S., Penone, C. et al. (2018). Multiple forest attributes underpin the supply of multiple ecosystem services. Nat Commun. 9, 4839. https://doi.org/10.1038/s41467-018-07082-4

Feng, L., Chen, S., Zhang, C., Zhang, Y., He, Y. (2021). A comprehensive review on recent applications of unmanned aerial vehicle remote sensing with various sensors for high-throughput plant phenotyping. Comput. Electron. Agric. 182, 106033. https://doi.org/10.1016/j.compag.2021.106033

Fernández-Guisuraga J., M., Calvo, L., Fernández-García, V., Marcos-Porras, Elena., Taboada, A., Suárez-Seoane, S. (2019). Efficiency of remote sensing tools for post-fire management along a climatic gradient. For. Ecol. Manag. 433, 553-562. https://doi.org/10.1016/j.foreco.2018.11.045

Fkiri, S., Guibal, F., Fady, B., Khorchani, A. El, Khaldi, A., Khouja, M.L., Nasr, Z. (2018). Tree-rings to climate relationships in nineteen provenances of four black pines sub-species (*Pinus nigra* Arn.) growing

in a common garden from Northwest Tunisia. Dendrochronologia. 50, 44–51. https://doi.org/10.1016/j.dendro.2018.05.001

Ganz, S., Käber, Y., Adler, P. (2019). Measuring tree height with remote sensing-a comparison of photogrammetric and LiDAR data with different field measurements. Forests. 10, 694. https://doi.org/10.3390/f10080694

Girard, F., Vennetier, M., Ouarmim, S., Caraglio, Y., Misson, L. (2011). Polycyclism, a fundamental tree growth process, decline with recent climate change: The example of *Pinus halepensis* Mill. in Mediterranean France. Trees - Struct. Funct. 25, 311–322. https://doi.org/10.1007/s00468-010-0507-9

Guo, L., Chen, J., Cui, X., Fan, B., Lin, H. (2013). Application of ground penetrating radar for coarse root detection and quantification: A review. Plant Soil. 362, 1–23. https://doi.org/10.1007/s11104-012-1455-5

Guo, H., Fu, W., Liu, G. (2019). Development of Earth Observation Satellites. In: Scientific Satellite and Moon-Based Earth Observation for Global Change. Springer, Singapore. 31-49. https://doi.org/10.1007/978-981-13-8031-0_2

Hammond, W.M., Williams, A.P., Abatzoglou, J.T., Adams, H.D., Klein, T., López, R., Sáenz-Romero, C., Hartmann, H., Breshears, D.D., Allen, C.D. (2022). Global field observations of tree die-off reveal hotter-drought fingerprint for Earth's forests. Nat. Commun. 13. https://doi.org/10.1038/s41467-022-29289-2

He, D., Biswas, S.R., Xu, M.-S., Yang, T.-H., You, W.-H. and Yan, E.-R. (2021), The importance of intraspecific trait variability in promoting functional niche dimensionality. Ecography. 44: 380-390. https://doi.org/10.1111/ecog.05254

Heilmeier, H. (2019). Functional traits explaining plant responses to past and future climate changes. Flora. 254, 1-11. https://doi.org/10.1016/j.flora.2019.04.004

Huang, J., Ji, M., Xie, Y., 2016. Global semi-arid climate change over last 60 years. Clim. Dyn. 46, 1131–1150. https://doi.org/10.1007/s00382-015-2636-8

Ibrahim, H. M. (2022). The importance of the species of genus Pine scattered in the Mediterranean region. Tikrit J. Agrc. Sci. 22, 157-165. https://doi.org/10.25130/tjas.22.2.17

Isajev, V.., Fady, B., Semerci, H.., Andonovski, V. (2003). EUFORGEN Technical Guidelines for genetic conservation and use for European black pine (*Pinus nigra*). Int. Plant Genet. Resour. Institute, Rome, Italy

Jevšenak, J., Saražin, J. (2023). *Pinus halepensis* is more drought tolerant and more resistant to extreme events than Pinus nigra at a sub - Mediterranean flysch site. Trees. 3-8. https://doi.org/10.1007/s00468-023-02413-5

Jezkova, T., Wiens, J.J. (2016). Rates of change in climatic niches in plant and animal populations are much slower than projected climate change. Proc. R. Soc. B Biol. Sci. 283, 20162104. https://doi.org/10.1098/rspb.2016.2104

Jaramillo-Correa, J. P., Prunier, J., Vázquez-Lobo, A., Keller, S. R., Moreno-Letelier, A. (2015). Chapter Eight - Molecular Signatures of Adaptation and Selection in Forest Trees, Eds: Plomion, C., Adam-Blondon, A. F. Advances in Botanical Research, Academic Press. 74, 265-306. https://doi.org/10.1016/bs.abr.2015.04.003

Keeley, J.E. (2012). Ecology and evolution of pine life histories. Ann. For. Sci. 64, 445–453. https://doi.org/10.1007/s13595-012-0201-8

Klosterman, S., Melaas, E., Wang, J., Martinez, A., Frederick, S., O'Keefe, J., Orwig, D.A., Wang, Z., Sun, Q., Schaaf, C., Friedl, M., Richardson, A.D. (2018). Fine-scale perspectives on landscape phenology from unmanned aerial vehicle (UAV) photography. Agric. For. Meteorol. 248, 397–407. https://doi.org/10.1016/j.agrformet.2017.10.015

Kreyling, J., Wiesenberg, G.L.B., Thiel, D., Wohlfart, C., Huber, G., Walter, J., Jentsch, A., Konnert, M., Beierkuhnlein, C. (2012). Cold hardiness of *Pinus nigra* Arnold as influenced by geographic origin, warming, and extreme summer drought. Environ. Exp. Bot. 78, 99–108. https://doi.org/10.1016/j.envexpbot.2011.12.026

Lange, M.A., 2019. Climate Change in the Mediterranean: Environmental Impacts and Extreme Events. IEMed: Mediterranean Yearbook. 10, 455. https://doi.org/10.3390/atmos10080455

Leech, S. M., Almuedo, P. L., & O'Neill, G. (2011). Assisted migration: adapting forest management to a changing climate. JEM. 12, 18-34. https://doi.org/10.22230/jem.2011v12n3a91

Leroy, T., Louvet, J.M., Lalanne, C., Le Provost, G., Labadie, K., Aury, J.M., Delzon, S., Plomion, C., Kremer, A. (2020). Adaptive introgression as a driver of local adaptation to climate in European white oaks. New Phytol. 226, 1171–1182. https://doi.org/10.1111/nph.16095

Liao, L., Cao, L., Xie, Y., Luo, J., Wang, G. (2022). Phenotypic Traits Extraction and Genetic Characteristics Assessment of Eucalyptus Trials Based on UAV-Borne LiDAR and RGB Images. Remot. Sens. 14,

765. https://doi.org/10.3390/rs14030765

Liu, Y., Wang, D., He, F., Wang, J., Joshi, T., Xu, D. (2019). Phenotype Prediction and Genome-Wide Association Study Using Deep Convolutional Neural Network of Soybean. Front. Genet. 10, 1–10. https://doi.org/10.3389/fgene.2019.01091

Lombardi, E., Ferrio, J.P., Rodríguez-Robles, U., Resco de Dios, V., Voltas, J. (2021). Ground-Penetrating Radar as phenotyping tool for characterizing intraspecific variability in root traits of a widespread conifer. Plant Soil 468, 319–336. https://doi.org/10.1007/s11104-021-05135-0

Mandaliya, V.B., Pandya, R. V, Thaker, V.S. (2010). Single nucleotide polymorphism (snp): a trend in genetics and genome analyses of plants. Gen. Appl. plant Physiol. 36, 159–166

Mazis, A., Choudhury, S. Das, Morgan, P. B., Stoerger, V., Hiller, J., Ge, Y., Awada, T. (2020). Application of high-throughput plant phenotyping for assessing biophysical traits and drought response in two oak species under controlled environment. For. Ecol. Manage. 465, 118101. https://doi.org/10.1016/j.foreco.2020.118101

Montwé, D., Isaac-Renton, M., Hamann, A., & Spiecker, H. (2015). Drought tolerance and growth in populations of a wide-ranging tree species indicate climate change risks for the boreal north. Glob. Chang. Biol. 22, 806-815. https://doi.org/10.1111/gcb.13123

Moreira, F., Leal, M., Bergonse, R., Canadas, M. J., Novais, A., Oliveira, S., Ribeiro P. F., Zêzre, J. L., Santos, J. L. (2023). Recent Trends in Fire Regimes and Associated Territorial Features in a Fire-Prone Mediterranean Region. Fire. 6, 60. https://doi.org/10.3390/fire6020060

Nicotra AB, Atkin OK, Bonser SP, et al. (2010). Plant phenotypic plasticity in a changing climate. Trends Plant Sci. 15, 684–692. https://doi.org/10.1016/j.tplants.2010.09.008

North, M. P., Stevens, J. T., Greene D. F., et al. (2019). Review: Reforestation for resilience in dry western U.S. forests. For. Ecol. Manag. 432, 209-224. https://doi.org/10.1016/j.foreco.2018.09.007

Orsi, F., Ciolli, M., Primmer, E., Varumo, L., Geneletti, D. (2020). Mapping hotspots and bundles of forest ecosystem services across the European Union. Land use policy. 99, 104840. https://doi.org/10.1016/j.landusepol.2020.104840

Pádua, L., Vanko, J., Hruška, J., Adão, T., Sousa, J.J., Peres, E., Morais, R. (2017). UAS, sensors, and data processing in agroforestry: a review towards practical applications. Int. J. Remote Sens. 38, 2349–2391. https://doi.org/10.1080/01431161.2017.1297548

Palahi, M., Mavsar, R., Gracia, C., Birot, Y. (2008). Mediterranean forests under focus. Int. For. Rev. 10, 676–688. https://doi.org/10.1505/ifor.10.4.676

Pan, Y., Birdsey, R.A., Phillips, O.L., Jackson, R.B. (2013). The structure, distribution, and biomass of the world's forests. Annu. Rev. Ecol. Evol. Syst. 44, 593–622. https://doi.org/10.1146/annurev-ecolsys-110512-135914

Pasho, E., Camarero, J.J., Vicente-Serrano, S.M. (2012). Climatic impacts and drought control of radial growth and seasonal wood formation in *Pinus halepensis*. Trees - Struct. Funct. 26, 1875–1886. https://doi.org/10.1007/s00468-012-0756-x

Patsiou, T.S., Shestakova, T.A., Klein, T., di Matteo, G., Sbay, H., Chambel, M.R., Zas, R., Voltas, J. (2020). Intraspecific responses to climate reveal nonintuitive warming impacts on a widespread thermophilic conifer. New Phytol. 228, 525-540. https://doi.org/10.1111/nph.16656

Pausas, J.G. (2015). Evolutionary fire ecology: Lessons learned from pines. Trends Plant Sci. 20, 318–324. https://doi.org/10.1016/j.tplants.2015.03.001

Pausas, J. G., & Keeley, J. E. (2021). Wildfires and global change. Front. Ecol. Environ. 19, 387-395. https://doi.org/10.1002/fee.2359

Peñuelas, J., Sardans, J., Filella, I., et al. (2017). Impacts of Global Change on Mediterranean Forests and Their Services. Forests. 8, 463. https://doi.org/10.3390/f8120463

Pörtner, H. O., Roberts, D. C., Adams, H., et al. (2022). Climate change 2022: Impacts, adaptation and vulnerability. 3056. Geneva, Switzerland: IPCC 2022

Prăvălie R. (2016). Drylands extent and environmental issues. A global approach. Earth Sci. Rev. 161, 259-278. https://doi.org/10.1016/j.earscirev.2016.08.003

Pritzkow, C., Williamson, V., Szota, C., Trouvé, R., Arndt, S.K. (2020). Phenotypic plasticity and genetic adaptation of functional traits influences intra-specific variation in hydraulic efficiency and safety. Tree Physiol. 40, 215–229. https://doi.org/10.1093/treephys/tpz121

Ratcliffe, S., Wirth, C., Jucker, T., et al. (2017). Biodiversity and ecosystem functioning relations in

European forests depend on environmental context. Ecol. Lett. 20, 1414–1426. https://doi.org/10.1111/ele.12849

Rellstab, C., Fischer, M.C., Zoller, S., Graf, R., Tedder, A., Shimizu, K.K., Widmer, A., Holderegger, R., Gugerli, F. (2017). Local adaptation (mostly) remains local: Reassessing environmental associations of climate-related candidate SNPs in Arabidopsis halleri. Heredity (Edinb). 118, 193–201. https://doi.org/10.1038/hdy.2016.82

Resco de Dios, V., Arteaga, C., Hedo, J., Gil-Pelegrín, E., Voltas, J. (2018). A trade-off between embolism resistance and bark thickness in conifers: are drought and fire adaptations antagonistic? Plant Ecol. Divers. 11, 253–258. https://doi.org/10.1080/17550874.2018.1504238

Roces-Díaz, J. V., Santín, C., Martínez-Vilalta, J., & Doerr, S. H. (2022). A global synthesis of fire effects on ecosystem services of forests and woodlands. Front. Ecol. Environ. 20, 170-178. https://doi.org/10.1002/fee.2349

Romero, B., Scotti, I., Fady, B., Ganteaume, A. (2023). Fire frequency, as well as stress response and developmental gene control serotiny level variation in a widespread pioneer Mediterranean conifer, *Pinus halepensis.* Ecol. Evol. 13, e9919. https://doi.org/10.1002/ece3.9919

Ruffault, J., Curt, T., Moron, V. et al. (2020). Increased likelihood of heat-induced large wildfires in the Mediterranean Basin. Sci Rep. 10, 13790. https://doi.org/10.1038/s41598-020-70069-z

Ruiz-Benito, P., Ratcliffe, S., Jump, A.S., Gómez-Aparicio, L., Madrigal-González, J., Wirth, C., Kändler, G., Lehtonen, A., Dahlgren, J., Kattge, J. and Zavala, M.A. (2017). Functional diversity underlies

demographic responses to environmental variation in European forests. Global Ecol. Biogeogr. 26: 128-141. https://doi.org/10.1111/geb.12515

Santini, F., Kefauver, S.C., Resco de Dios, V., Araus, J.L., Voltas, J. (2019a). Using unmanned aerial vehicle-based multispectral, RGB and thermal imagery for phenotyping of forest genetic trials: A case study in *Pinus halepensis*. Ann. Appl. Biol. 174, 262–276. https://doi.org/10.1111/aab.12484

Santini, F., Serrano, L., Kefauver, S.C., Abdullah-Al, M., Aguilera, M., Sin, E., Voltas, J. (2019b). Morpho-physiological variability of *Pinus nigra* populations reveals climate-driven local adaptation but weak water use differentiation. Environ. Exp. Bot. 166, 103828. https://doi.org/10.1016/j.envexpbot.2019.103828

Savolainen, O., Pyhäjärvi, T., Knürr, T. (2007). Gene flow and local adaptation in trees. Annu. Rev. Ecol. Evol. Syst. 38, 595–619. https://doi.org/10.1146/annurev.ecolsys.38.091206.095646

Sbay, H., Zas, R. (2018). Geographic variation in growth, survival, and susceptibility to the processionary moth (*Thaumetopoea pityocampa* Dennis & Schiff.) of *Pinus halepensis* Mill. and *P. brutia* Ten.: results from common gardens in Morocco. Ann. For. Sci. 75. https://doi.org/10.1007/s13595-018-0746-2

Seifert, S., Vornam, B., Finkeldey, R., 2012. DNA sequence variation and development of SNP markers in beech (Fagus sylvatica L.). Eur. J. For. Res. 131, 1761-1770. https://doi.org/10.1007/s10342-012-0630-9

Taboada, A., Tárrega, R., Marcos, E., Valbuena, L., Suárez-Seoane, S., Calvo L. (2017). Fire recurrence and emergency post-fire management influence seedling recruitment and growth by altering plant interactions in fire-prone ecosystems. For. Ecol. Manag. 402, 63-75. https://doi.org/10.1016/j.foreco.2017.07.029.

Tapias, R., Climent, J., Pardos, J.A., Gil, L. (2004). Life histories of Mediterranean pines. Plant Ecol. 171, 53–68. https://doi.org/10.1023/B:VEGE.0000029383.72609.f0

Tramblay, Y., Hertig, E. (2018). Modelling extreme dry spells in the Mediterranean region in connection with atmospheric circulation. Atmos. Res. 202, 40–48. https://doi.org/10.1016/j.atmosres.2017.11.015

Vacek, S., Cukor, J. (2023). European forests under global climate change: Review of tree growth processes, crises and management strategies. J. Environ. Manage. 15, 332. https://doi.org/10.1016/j.jenvman.2023.117353

Varelides, C., Brofas, G., Varelides, Y. (2011). Provenance variation in *Pinus nigra* at three sites in Northern Greece. Ann. For. Sci. 58, 893-900. https://doi.org/10.1051/FOREST:20011003

Vennetier, M., Ripert, C., Rathgeber, C. (2018). Autecology and growth of Aleppo pine (*Pinus halepensis* Mill.): A comprehensive study in France. For. Ecol. Manage. 413, 32–47. https://doi.org/10.1016/j.foreco.2018.01.028

Voltas, J., Chambel, M.R., Prada, M.A., Ferrio, J.P. (2008). Climate-related variability in carbon and oxygen stable isotopes among populations of Aleppo pine grown in common-garden tests. Trees - Struct. Funct. 22, 759–769. https://doi.org/10.1007/s00468-008-0236-5

Westerband, A.C., Funk, J.L., Barton, K.E. (2021). Intraspecific trait variation in plants: A renewed focus on its role in ecological processes. Ann. Bot. 127, 397–410. https://doi.org/10.1093/aob/mcab011

Xie, C., Yang, C. (2020). A review on plant high-throughput phenotyping traits using UAV-based sensors.

Comput. Electron. Agric. 178, 105731. https://doi.org/10.1016/j.compag.2020.105731

Zhang, C., Marzougui, A., Sankaran, S. (2020). High-resolution satellite imagery applications in crop phenotyping: An overview. Comput. Electron. Agric. 175, 105584. https://doi.org/10.1016/j.compag.2020.105584

Material and Methods

Common garden experiments

The data analyzed in this thesis was collected from four provenance trials (common garden experiments) located in Spain (Fig. 1). These trials were established by the Spanish government in the 1990s with the objective to investigate patterns of local adaptation and potential for evolutionary responses of Spanish populations and their Mediterranean counterparts of different pine species. Three provenance trials (Altura, Valdeolmos and Zuera) consisted of 56 populations of *P. halepensis* originating from the Iberian Peninsula, Balearic Islands, France, Greece, Italy and Tunisia, which are representative of the current distribution range of the species. The trial in Altura is located in Castellón province (39°49′29″N, 00°34′22″W, 640 m a.s.l.) and presents a mean annual temperature of 13.8°C and a mean annual precipitation of 468 mm. The trial in Valdeolmos is situated in Madrid province (40°38′37″N, 03°26′26″W, 738 m a.s.l.), with a mean annual temperature of 13.2 °C and a mean annual precipitation of 407 mm. The third trial of *P. halepensis* is located in Zuera, Zaragoza province (41°52′24″N, 00°38′57″W, 425 m a.s.l.), and is characterized by a mean annual temperature of 14.5°C and a mean annual precipitation of 420 mm. The last common garden experiment used in this thesis is composed of 18 populations of *P. nigra* belonging to the subspecies *laricio*, *nigra*, *salzmannii*, *pallasiana* and *calabrica*, and it is situated in La Mata de Valsaín, Segovia province (40°54′42″N, 04°00′50″W, 1137 m a.s.l.). This trial presents a mean annual temperature of 10.4°C and a mean annual precipitation of 516 mm. All the provenance trials were established following standard practices. Seeds of 20 to 30 trees of the same population, spaced at least 100 m apart, were collected at origin of each population. Then, they were nursed in containers and one-year-old seedlings were transplanted following a randomized block design with four replicates (Valdeolmos) or 12 replicates (Valsaín), or a Latinised row-column design with four replicates (Altura and Zuera). The provenance trials were not subjected to common management protocols, since management actions depend, in this case, mostly on the growth rate and tree density of each trial. For example, in Zuera trial, where trees grow more slowly due to the particular climate conditions, no management action was taken so far; on the contrary the

Altura trial was thinned in 2019, and Valsaín trial in 2017, where *ca.* half of the trees present in the trial were cut. For the third trial of Aleppo pine (Valdeolmos) a future thinning action is planned, but for now the trial has not been subjected to any management protocol.

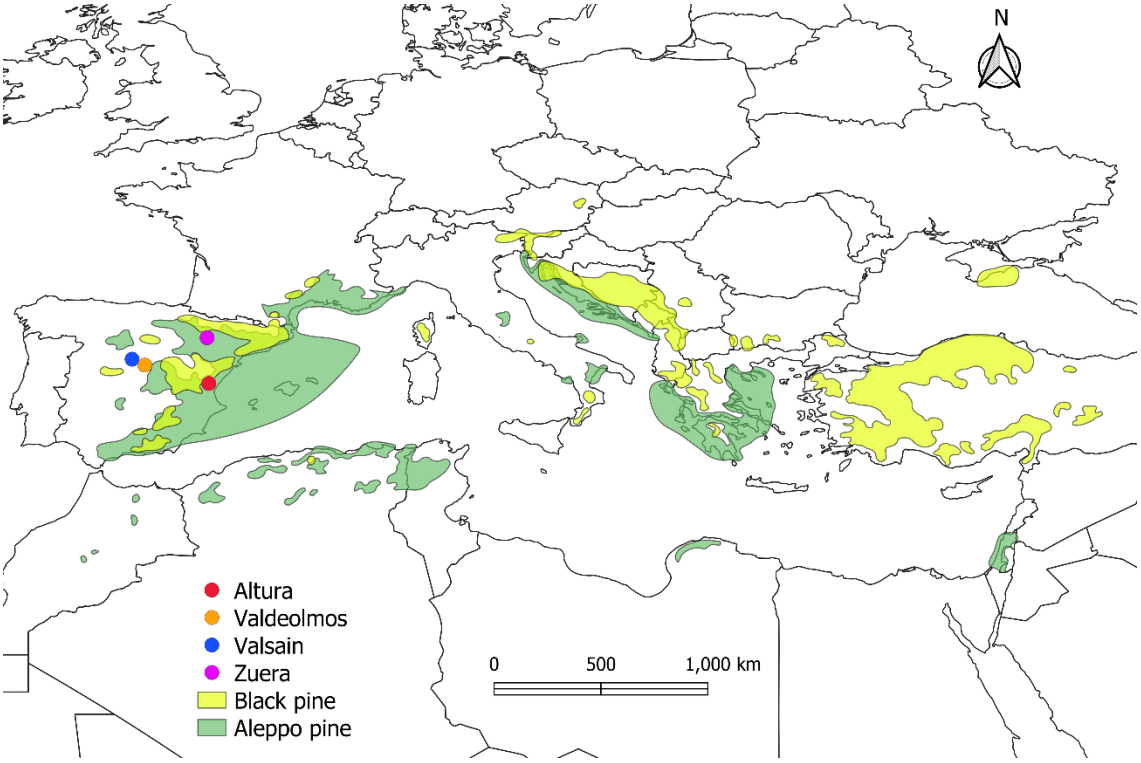

Fig 1. Location of the four common gardens experiments analysed in this thesis: Altura (Castellón province, Spain), Valdeolmos (Madrid province, Spain), Valsain (Segovia province, Spain) and Zuera (Zaragoza province, Spain). The dark green area represents the natural distribution of *P. halepensis* and the light green area indicates the natural distribution of *P. nigra* according to EUFORGEN (http://www.euforgen.org/species).

High-throughput phenotyping tools

Ground penetrating radar

A Ground-Penetrating Radar (GPR) MALÅ RAMAC X3M GPR (MALÅ Geoscience AB, Sweden) equipped with an 800 MHz shielded antenna was used in the first chapter as a high-throughput phenotyping technique in order to characterize coarse root morphology (frequency, depth and diameter) in a non-destructive way. GPR records were obtained in a single day in mid-June 2015 and they were taken

continuously along three linear profiles (P1, P2, P3) following the trial's column direction and passing through the two central trees of each experimental unit. Coarse roots were identified through hyperbolic signatures on radargrams. First, GPR radargrams were examined using RadExplorer v1.42 software (MALÅ Geoscience AB, Sweden) through visual inspection of the hyperbolae, and then several pre-processing filter functions were applied in order to reduce noise and improve the identification of hyperbolae.

Aerial remote sensing

In chapters 3 and 4, unmanned aerial vehicles (UAVs) were employed to obtain LiDAR (chapter 3), RGB (chapter 3 and 4) and multispectral (chapter 4) records. In particular, in chapter 3 an octocopter UAV equipped with a LiDAR (sensor Velodyne VLP-16 Puck Lite) and a DJI (Phantom 4 pro v2) equipped with a RGB camera having a sensor size of 5472 × 3648 pixels and a focal distance of 8.86 mm were used for the *P. nigra* trial. In the case of *P. halepensis* trial, aerial laser scanning (ALS) data were acquired with an octocopter UAV equipped with a LiDAR (sensor Velodyne VLP-32C), whereas a RGB camera with sensor size 6000 × 4000 pixels and focal distance 12 mm was mounted on a DJI (m300) to collect RGB images. In chapter 4, RGB and multispectral images were acquired through a UAV DJI Mavic (2 Pro, China) RGB camera of 20 MP, and through a UAV Mikrokopter (6S12 XL, Germany) equipped with an RGB camera (Lumiz GX7, Panasonic, Japan) with 16 MP resolution and with a multispectral camera (Tetracram micro-MCA, USA). For both chapters (3 and 4), I applied the following workflow to pre-process the LiDAR and RGB point clouds using LAStools and US Forest Service FUSION/LDV 3.42 software. First, I filtered points of noise in the point clouds, then the ground points were computed and the point cloud was normalized, and the points were classified as ground and non-ground (vegetation). Then I built a digital terrain model (DTM) and a canopy height model (CHM) with a resolution of 10 cm using the GridSurfaceCreate and CanopyModel procedures, respectively, of FUSION/LDV. In the case of chapter 4, multispectral and RGB images were previously aligned using Agisoft PhotoScan Professional software (Agisoft LLC, St. Petersburg, Russia) to produce dense points clouds and orthomosaic images. ForestTools

R package (Plowright 2018) was used to identify individual treetops and to segmented tree crowns.

Field-based phenotyping methods

A vast number of phenotyping traits were measured for every trial. The most common ones that were measured in almost every trial are total tree height (H) and diameter at the breast height (DBH), which were obtained through a Vertex hypsometer and a diameter tape, respectively. Another standard phenotyping approach that is worth highlighting in this section, since it is the principal method used in chapter 2, is based on dendrochronological principles. Tree-ring width was measured for a subset of 130 individuals of *P. halepensis* through a semi-automatic process in WinDendro 2014a (Regent instrument Inc., Quebec, Canada). Each tree-ring series was cross-dated and the cross-dating was quality-checked with COFECHA (Holmes 1983). In addition, earlywood width (EW) and latewood width (LW) were estimated using WinDendro coupled with a computer-integrated Leica binocular microscope (5X zoom), and the EW to LW ratio (EL) was then calculated for each tree ring. Ring-width and EL indices (RWI and ELI) were obtained for each tree-ring series and afterwards a master chronology was built for both indices using R studio.

Chapter 1

Ground-Penetrating Radar as phenotyping tool for characterizing intraspecific variability in root traits of a widespread conifer

Erica Lombardi1,2, Juan Pedro Ferrio3,4, Ulises Rodríguez-Robles5, Víctor Resco de Dios1,2,6, Jordi Voltas1,2*

1Joint Research Unit CTFC–AGROTECNIO–CERCA, Av. Alcalde Rovira Roure 191, E-25198 Lleida, Spain;

2 Department of Crop and Forest Sciences, University of Lleida, Av. Alcalde Rovira Roure 191, E-25198 Lleida, Spain;

3Aragon Agency for Research and Development (ARAID), E-50018 Zaragoza, Spain;

4Unidad de Recursos Forestales, Centro de Investigación y Tecnología Agroalimentaria de Aragón (CITA), Avda. Montañana 930, E-50059 Zaragoza, Spain;

5Departamento de Ecología y Recursos Naturales, Centro Universitario de la Costa Sur, Universidad de Guadalajara, Autlán de Navarro, Mexico;

6School of Life Science and Engineering, Southwest University of Science and Technology, 59 Qinglong Ave., Mianyang 621010, China

Abstract

Drought is the main abiotic stress affecting Mediterranean forests. Root systems are responsible for water uptake, but intraspecific variability in tree root morphology is poorly understood mainly owing to sampling difficulties. The aim of this study was to gain knowledge on the adaptive relevance of rooting traits for a widespread pine using a non-invasive, high-throughput phenotyping technique. In this regard, Ground-Penetrating Radar (GPR) was used to characterize variability in coarse root features (depth, diameter and frequency) among populations of the Mediterranean conifer *Pinus halepensis* evaluated in a common garden. GPR records were examined in relation to aboveground growth and climate variables at origin of populations. Variability was detected for root traits among 56 range-wide populations categorized into 16 ecotypes. Root diameter decreased eastward within the Mediterranean basin. In turn, root frequency, but not depth and diameter, decreased following a northward gradient. Root traits also varied with climatic variables at origin such as the ratio of summer to annual precipitation, summer temperature or solar radiation. Particularly, root frequency increased with aridity, whereas root depth and diameter were maximum for ecotypes occupying the thermal midpoint of the species distribution range. Our findings showed that GPR is a high-throughput phenotyping tool that allows detection of intraspecific variation in root traits of *P. halepensis* and its dependencies on eco-geographic characteristics at origin, thereby informing on the adaptive relevance of root systems for the species. It is also potentially suited for inferring population divergence in resource allocation above- and belowground in forest genetic trials.

Keywords: Aleppo pine; Climatic adaptation; Ground-Penetrating Radar; Root depth; Root diameter; Root frequency

Introduction

Climate models forecast an increase in temperature along with an intensification of extreme weather events that will likely lead to more prolonged and intense drought periods around the globe (IPCC 2007, 2014). This future climate may have serious impacts on ecosystem dynamics in the Mediterranean basin (Resco de Dios et el. 2007; Sardans and Peñuelas 2013). Seasonal drought is one of the main factors affecting Mediterranean forests, and forest tree species use different strategies to respond to changes in water availability. Among those, access to deep water pools is fundamental to survive dry periods (Dawson et al. 2020; Ripullone et al. 2020; Rossatto et al. 2012), because water uptake is dependent on root architecture (Hernández et al. 2010). A number of functional traits related to hydraulic conductivity such as root vessel diameter are determined by root xylem anatomy, which in turn is influenced by root diameter and rooting depth (Kirfel et al. 2017; Wang et al. 2015). Thus, root structure and morphology play a key role on the ability of plants to explore and access the deeper subsurface when shallower soil layers dry out (Andivia et al. 2019; Padilla and Pugnaire 2007). Species-specific and intraspecific differences in rooting patterns are still poorly characterized, however. This is mainly due to the inherent complexity of underground sampling (Alani and Lantini 2020) and the fact that traditional approaches for root monitoring, such as the Auger and the Monolith methods, are destructive and non-repeatable (Krainyukov and Lyaksa 2016).

The Ground-Penetrating Radar (GPR) is a non-destructive geophysical prospecting device that utilizes electromagnetic wave pulses for subsurface detection based on the different dielectric properties of materials, as well as on the physical properties of the medium (Lorenzo et al. 2010). GPR transmits electromagnetic signals into a surface and records the reflection of the signal transmitted by a receiving shielded antenna. The amplitude of the reflected pulses and its receiving time can be used in order to estimate the position and the size of the material that generates a discontinuous signal (Butnor et al. 2001). GPR is widely used for many purposes, such as the detection of bedrock structure (Loudes et al. 2011; Valerio et al. 2012) or the quantification of soil water content (Klotzsche et al. 2018). Also, it has been used as non-invasive tool for the detection of root features and belowground biomass estimation (Barton et al. 2004; Butnor et al. 2001, 2003; Guo et al. 2013; Lorenzo et al. 2010). Roots have a different dielectric

permittivity compared to soil and, as a result, GPR allows defining the number (or frequency of occurrence; frequency herein), position (depth) and size (diameter) of coarse roots through the timing and features of back-reflected signals induced by hyperbolic reflections on radargrams (Hirano et al. 2012, 2009; Wu et al. 2014). The reflected waves are detectable as hyperbolas, where the hyperbolic signatures' peak (or the maximum amplitude of the hyperbola) corresponds to the center of every object detected, which is recorded on a portable control unit (Hirano et al. 2012). However, the successful identification of roots with GPR depends on different factors, with soil moisture, root water content and soil properties influencing wave frequency and thus root detection (Barton et al. 2004; Hirano et al. 2009).

Pinus halepensis Mill. (Aleppo pine) is the most widely distributed conifer species across the Mediterranean basin (Vennetier et al. 2018), occupying vastly different ecological niches ranging from mesic (annual precipitation exceeding 800 mm) to xeric environments (below 350 mm). The widespread distribution of Aleppo pine suggests the existence of intraspecific adaptive divergence (Grivet et al. 2009; Ruiz Daniels et al. 2018). Indeed, there is strong evidence for genetic variability among populations originating from distinct environments to tolerate water stress, which involves traits such as water-use efficiency (Voltas et al. 2008), wood anatomy (Esteban et al. 2010), biomass allocation (Chambel et al. 2007), or use of water sources (Voltas et al. 2015). Deeper and more developed root systems might also be related to the ability of Aleppo pine to cope with water deficit (Andivia et al. 2019; Voltas et al. 2015). As a result, root morphology may be a key characteristic to understand water use strategies and, consequently, drought resistance mechanisms in this species. Although a large investment in roots is often related to enhanced survival under drought (Grossnickle et al. 2005; Matias et al. 2014), and Aleppo pine has a greater ability for colonizing the soil subsurface and produce a more efficient root system in dry environments than mountain pines (Andivia et al. 2019), the existence of intraspecific divergence in root traits for this Mediterranean pine has barely been investigated thus far (Voltas et al. 2015).

In this work, we applied GPR root detection to a common garden of adult Aleppo pine trees where populations representative of the circum-Mediterranean distribution of the species were tested. Our purpose was to evaluate if GPR is a valid tool to infer intraspecific variability for coarse root frequency, depth and

diameter in a widespread tree species. We hypothesized that populations originating from xeric environments would present deeper, thicker and more numerous coarse roots than their mesic counterparts as a result of different adaptive mechanisms underlying the use of soil water pools. In addition, we also hypothesized that variability in root traits among populations of the species is related, to some extent, to intraspecific divergence in aboveground growth, which may point to the existence of allocation trade-offs to aerial growth or belowground dry matter. Therefore, we aimed to: (1) test the use of GPR as a high-throughput root phenotyping technique to assess population differentiation in coarse root architecture for Aleppo pine; (2) relate intraspecific differences in coarse root traits (frequency, depth and diameter) among Aleppo pine populations to their climate at origin, which can be informative of different adaptive strategies in the species; and (3) describe the associations between such root traits and aboveground growth and define potential allocation trade-offs at the intraspecific level.

Material and Methods

Plant material and experimental site

Seeds from 56 populations of *P. halepensis* originating from mainland Spain, Balearic Islands, France, Greece, Italy and Tunisia were used in this study. These populations are representative of most of the current distribution range of the species (Fig. 1). The seeds were collected in 1995 from 20 to 30 adult individuals per population, spaced at least 100 m apart, and were sown in a forest nursery in Spain using standard container practices (Landis et al. 1990) the following year. In 1997, 896 one-year old seedlings (16 seedlings per population) were transplanted at the study site (provenance trial), which is located in Altura, Castellón province, Spain (39°49′29″N, 00°34′22″W, 640 m a.s.l.). The experimental design was a Latinised row-column design with four replicated blocks (John and Williams, 1998). The spacing between each consecutive tree at row or column distances was 2.5 m. Each row was *ca*. 70 m long and was composed of seven linear plots or experimental units consisting of four trees of the same provenance per plot (Fig. S1). The total area of the provenance trial was about 0.8 ha. For this study, we used three of the four available blocks, as some individuals from the fourth block were affected by fire in 2012. The Latinised row-column

design allowed to efficiently control for inherent intra-site variability as systematic changes in both column and row directions were incorporated into the fitted mathematical models.

The soil at the study site is a calcic cambisol (Soil Map of Generalitat Valenciana 1996) with loam texture (44.2% sand, 24.3% clay and 31.5% silt) and a maximum depth of *ca*. 40 cm followed by a petrocalcic horizon with vertical fractures (visual inspection). The general features of the soil are outlined in Table S1. The site has climatic characteristics similar to the average climate of the species across the Mediterranean basin (Santini et al. 2019a). The mean annual temperature is 13.8 °C and the mean annual precipitation is 468 mm, with 18% falling in summer.

Climate variables

For each population, climate data at origin for the period 1970-2000 were obtained from the WorldClim database (Fick and Hijmans, 2017) at 1 km^2 spatial resolution. The following climate variables were retrieved, based on previous studies on the climatic drivers of ecotypic variation in Mediterranean pines (Climent et al. 2008; Tapias et al. 2004): mean annual temperature (MAT), mean summer temperature (MST), temperature annual range (TAR; T_{max}-T_{min}), mean annual precipitation (MAP) and summer to annual precipitation ratio (PsP). Moreover, solar radiation accounting for cloud cover (SR) was retrieved from WorldClim and monthly means of day-time vapour pressure deficit for the warmest (summer) quarter (VPD_s) were calculated for each population by subtracting the water vapour pressure (VP) from the monthly average of saturation water vapour (VP_{sat}) obtained at daily level. VP was estimated as in Ferrio and Voltas (2005):

$$\ln(VP) = 6.34 + 0.047T_m + 0.96(P_m/1000) - 0.22(Z/1000) \quad (1)$$

where T_m is mean monthly temperature, P_m is monthly precipitation and Z is altitude (in m).

In turn, VP_{sat} was estimated from day-time temperature (T_{day}) as (Jones 1992):

$$VP_{sat} = 613.75 \exp\left(17.50 \frac{T_{day}}{240.97 + T_{day}}\right) \quad (2)$$

The populations were further categorised into 16 ecotypes (Fig. 1, Table S2) following previously published

approaches based on climate attributes (Climent et al. 2008).

Aboveground growth

Tree height (H) and diameter at breast height (DBH), measured in 2013 (at age 17 years), were used as aboveground growth traits. Additionally, tree crown area was estimated from aerial RGB imagery taken in summer 2016 (at age 20 years) through a canopy height model using the R package ForestTools (Plowright 2018), as reported in Santini et al. (2020). We assumed constancy of phenotypic ranking in tree growth from age 15 onwards, as previously reported for *P. halepensis* (Sbay and Zas, 2018).

GPR data collection

GPR records were obtained in a single day in mid-June 2015, when trees were 19 years old, and the number (frequency), depth and diameter of coarse roots were estimated using a MALÅ RAMAC X3M GPR (MALÅ Geoscience AB, Sweden) equipped with an 800 MHz shielded antenna coupled to an inspection cartwheel. The 800 MHz antenna was used because it has been shown to provide the best possible resolution in calcic soils (Rodríguez-Robles et al. 2017), which are distinctive of the study site. In particular, roots reaching a depth of up to *ca*. 0.9 m could be identified within the petrocalcic fractures underneath the lower soil layer of 40 cm, and roots with a diameter of *ca*. 2 cm or higher were also detectable (Fig. 2) after *in situ* calibration (see subsection "GPR data processing"), as also shown in previous studies (Butnor et al. 2001; Barton and Montagu 2004; Rodríguez-Robles et al. 2017).

GPR measurements were taken continuously along three linear profiles (P1, P2, P3) following the trial's column direction and passing through the two central trees of each experimental unit (Fig. 3a, b). For every experimental unit, P1 and P3 were settled at *ca.* 0.30 m distance from the main trunk of the two central trees, while P2 was positioned halfway from both trees, that is, at *ca*. 1.25 m (Fig. 3c). In order to assign each detected root to a particular experimental unit, the position of trees along each linear profile was manually recorded in the RAMAC XV Monitor implemented in the GPR, along with GPR measurements. With this information, relevant data could be retrieved at sub-plot level in the profile (see

"GPR data processing" subsection).

GPR data processing

Coarse roots were identified through hyperbolic signatures on radargrams. First, GPR radargrams were examined using RadExplorer v1.42 software (MALÅ Geoscience AB, Sweden) through visual inspection of the hyperbolae ("manual dataset"), which allowed to determine trends in the distribution of roots along the linear profiles.

Based on this preliminary information, a second dataset was created in RadExplorer using a built-in detection procedure along predefined sub-plots ("automatic dataset"), which was subjected to several pre-processing filter functions, in order to reduce noise and improve the identification of hyperbolae. Particularly, we applied background removal filters in order to remove parallel bands, often derived from ground surface reflection. Then we eliminated the initial current signal component (DC) from the GPR control unit (RAMAC XV Monitor and ProEx system – adjust signal position) to guarantee that depth estimates started from 0. Afterwards, a *high/low bandpass* filter was applied in order to remove unwanted noise. *Stolt F-K migration* was also used in order to improve GPR image and to correct for root position (Rodríguez-Robles et al. 2017; Barton and Montagu 2004). This procedure did not allow for a case-by-case assessment of hyperbolae; however, it was able to detect a larger number of roots than the visual inspection of radargrams while being free of its subjectivity, allowing for a more robust analysis.

The automatic dataset was generated for three different sub-plot sizes. In all cases, their cross-sections extended from P1 through P3 and, therefore, were centred at each experimental unit's mid-point, but had different lengths of 50, 100 and 250 cm (hereafter S_{50}, S_{100} and S_{250} sub-plots, respectively; Fig. 3c). Note that the largest sub-plot length (S_{250}) was equivalent to the mean inter-plot distance (Fig. 3c). This strategy allowed to identify a particular sub-plot area maximising population differences in root traits, as described in section 2.5.

Although pre-processing filters were applied to the original GPR information, a calibration was needed since the depth and size of an object cannot be inferred directly by the GPR. Thus, we measured

depth and diameter *in situ* of 12 coarse roots. Coarse roots were excavated through soil digging underneath GPR scan line profiles (P1, P2, P3), in different experimental units across the trial. Root depth and diameter were then GPR-estimated through the so-called 'time interval between zero crossing' (Rodríguez-Robles et al. 2017; Guo et al. 2013a; Tanikawa et al. 2013). Time interval between zero crossing is the time elapsed between signal emission and registration by the shielded antenna, which is manually adjusted to time zero before processing the data to set the instant in which the radar signal leaves the antenna. A linear regression between root diameter measured *in situ* and time interval between zero crossing was applied, and the resulting equation used for calibration of root diameter (Rodríguez-Robles et al. 2017).

Statistical analyses

The definition of a proper sub-plot size is important for optimal GPR-based root detection in experimental trials. While using a too large sub-plot size could potentially capture coarse roots of trees from neighbouring experimental units, a too small sub-plot could underestimate the actual number of coarse roots for each unit. To handle this issue, the variability in root number (frequency) was evaluated as a function of the linear distance from the trunk along the aforementioned profiles using evenly spaced bins of 10 cm. Overall, a high number of roots was found at small and medium distances, followed by a progressive decrease in root number and a sudden increase after some value, hence denoting overlapping with roots from neighbouring trees (see Results, subsection 3.1). In addition, the 'optimal' sub-plot length (S_{50}, S_{100} or S_{250}) was explored through linear mixed-effects analysis of variance (ANOVA) fitted to the automatic dataset independently for each sub-plot size. The ANOVA included block, column and population as fixed effects, while row within block and column by block interaction were defined as random effects in order to account for systematic variability at the trial site. We retained as optimal sub-plot the one that maximised the F value for population differences in the ANOVAs for coarse root traits (diameter, depth, and frequency), which approximately matched the optimal distance previously identified in the manual dataset (Table 1, Table S3). The mixed-effects ANOVAs were further extended to partition the variability among populations into fixed ecotype and between-population within-ecotype effects, hence testing for ecotypic structure in root traits.

As indirect validation of our phenotyping approach, we compared the information obtained through GPR measurements with estimates of the relative contribution of two consecutive soil layers (0-15 cm, upper soil; 15-40 cm, lower soil) to the total amount of water taken up by the different populations, as inferred through the analysis of the isotopic composition ($\delta^{18}O$ and $\delta^{2}H$) of soil and xylem water in 2010 (data retrieved from Voltas et al. [2015]). Additionally, simple correlations were calculated between GPR-based root traits and xylem water $\delta^{18}O$ at plot level.

Population (or ecotype) least squares means of root depth, diameter and frequency were subjected to linear and quadratic regressions as a function of long-term climate conditions of each population (or ecotype) at origin. The three populations of ecotype 16MC (reforestations of Northern Spain) were not used in the regression analysis because they have uncertain geographic origins. Linear and quadratic regressions of root traits were also performed on Euclidean geographic distances and climatic distances (Gower's distances) of each population (or ecotype) from the trial site. Gower's distances indicate dissimilarities among entities, in this case climate dissimilarities between populations (ecotypes) at origin and the trial site, and were calculated following Rutter and Fenster (2007):

$$GD = \frac{1}{p} \sum_{i=1}^{p} \frac{|A_i - B_i|}{r_i} \quad (3)$$

Where p is the number of climate variables, A_i and B_i are the values of each climate variable (MAT, TAR, MAP, PsP) at site A (trial) and B (population or ecotype origin), and r_i is the range of each climate variable in the dataset.

Finally, linear and quadratic regressions were calculated for root traits as a function of aboveground growth variables (H, DBH and crown area), both at population and ecotype level. The associations of aboveground growth variables with those climate variables at origin found to be related to population or ecotypic variability in root traits were also evaluated. For model selection, the best fitting model for each explanatory variable (linear, quadratic) was chosen considering its overall significance (F-value) and goodness of fit (adjusted R^2).

Results

Root detection using GPR

Manual measurements of root diameter showed a positive correlation (r = 0.95; $p < 0.001$) with GPR records (Fig. 4a). Measured and GPR-estimated root depth also showed a positive association (r = 0.98; $p < 0.001$) (Fig. 4b). Following the visual inspection of radargrams, we detected the largest number of roots at distances between 10 cm and 50 cm from each tree trunk along the trial's column direction, with a progressive decrease at larger distances (Fig. 4c). However, the number of detected roots increased again starting at 1 m apart from each tree. This observation suggested that GPR was detecting roots corresponding to trees from adjacent experimental units for distances higher than 90 cm from each targeted tree trunk (Fig. 4c). This was confirmed by analyses of variance carried out on the automatic dataset for three different sub-plot sizes (S_{50}, S_{100}, S_{250}). Particularly, the results showed that the sub-plot size that maximised population differentiation in root traits was S_{100} (Tables 1 and S3). Further analyses were therefore performed for S_{100}. At sub-plot level (S_{100}), GPR estimates of coarse root traits varied between 3.0 cm and 5.0 cm (diameter), between 14.7 cm and 44.3 cm (depth), and between 3 and 19 roots (frequency).

Phenotypic variation in root traits

We detected significant variation in coarse root diameter among populations ($p = 0.030$), but the effect was only marginally significant among ecotypes ($p = 0.091$; Table 1). Mean diameter values of ecotypes varied between 3.5 cm (15TU, Tunisia; Table S2) and 4.0 cm (3ALC, Spanish Southern Plateau). Differences among populations in coarse root depth (Table 1) were marginally significant ($p = 0.086$), while significant differences were detected among ecotypes ($p = 0.011$). Mean depth values of ecotypes varied between 21 cm (15TU) and 30 cm (16MC, reforestations of Northern Spain). These results suggested a stronger ecotypic structure for rooting depth than for root diameter. We did not observe significant differences in root frequency among populations ($p = 0.460$), whereas marginally significant differences were detected among ecotypes ($p = 0.096$). Mean frequency values of ecotypes varied between 8.9 (2MO, Spanish Ebro depression) and 13.1 (7BM, Spanish Betic system). Estimates of coarse root depth and diameter were significantly and positively correlated both at population (r = 0.42, $p = 0.001$) (Fig. S2a) and ecotype level

(r = 0.63, p = 0.009), but root frequency did not correlate significantly with root depth or diameter (Fig. S2b, c).

The variability of root traits was in good agreement with xylem water isotopes records obtained in 2010 for the same trial, with the exception of root frequency. At population level, we observed significant negative correlations between coarse root diameter or depth and $\delta^{18}O$ of xylem water in early autumn (r = 0.62, $p < 0.001$, and r = 0.50, $p < 0.001$, respectively; Fig. S3), but not in peak summer (mid-July) ($p > 0.10$, Fig. S3). At ecotype level, a negative association between root diameter and the relative contribution of the upper soil layer to xylem water in early autumn was also observed (Fig. 5a); this relationship was non-significant for root depth (Fig. 5b) and root frequency (Fig. 5c). There was also a negative association between the relative contribution of bottom soil layer in early autumn and root diameter at ecotype level (Fig. 5d). However, this association was non-significant for root depth (Fig. 5e) and root frequency (Fig. 5f).

Phenotypic associations with aboveground growth

At ecotype level, root diameter and root depth showed marginally significant quadratic relationships (p = 0.064 and p = 0.102, respectively) with tree height (Fig. 6, Table S4), while root frequency was unrelated to vertical growth. These results suggested that shallower and smaller roots were indistinctly found in ecotypes having lower or higher than average height growth. Other aboveground growth variables (DBH, crown area) were unrelated to root depth, diameter or frequency (Table S4).

Associations with geographic variables and climate at origin

Coarse root traits were related to some geographic and climatic variables at origin of populations, either linearly or quadratically (Table 2a). Root traits decreased linearly (albeit weakly) with geographic distance to the trial and also with longitude (Table 2a). These results suggested geographically structured differences between populations located near the trial site (i.e. the westernmost distribution of Aleppo pine) and those from the eastern Mediterranean basin. A significant quadratic dependence of root depth on Gower's distance

(Table 2a) was also observed, indicating that populations with climate at origin either most similar or most dissimilar to the trial site presented shallower roots.

Root diameter showed a quadratic dependence on solar radiation (p = 0.014), with thicker roots occurring in populations having intermediate solar radiation at origin. In turn, root depth showed a quadratic dependence on PsP (p = 0.035) and, marginally, on MST (p = 0.067), with shallower roots observed under low and high values of both climate variables (Table 2a). Root frequency was linearly dependent on solar radiation ($p < 0.001$) and marginally on PsP ($p = 0.060$), with more roots observed under high solar radiation and low PsP at origin. In addition, we also detected significant or marginally significant positive linear dependencies of root frequency on VPD_s (p = 0.003) and TAR (p =0.073). Although these relations hinted on the dependence of roots traits on climate conditions of populations at origin, the proportion of explained variance was relatively low ($R^2 < 0.25$).

Similar dependencies of coarse root traits on geographic and climatic factors occurred at ecotype level, with relationships being either linear or quadratic (Table 2b). In particular, we observed a negative linear dependency of root diameter on longitude and a positive linear association of root frequency on latitude. There were also marginally significant quadratic relationships between root depth and latitude and between both root depth or diameter and altitude (Fig. S4, Table 2b). The quadratic relationships were such that northern and southern ecotypes tended to present shallower roots, while deeper and thicker roots were distinctive of ecotypes from either low or high altitudes. Based on Gower's distances, ecotypes having high or low climate similarities with the trial climate showed shallower and finer roots, but they were not distinctive with regard root frequency (Fig. S4).

Root frequency showed a negative linear dependence on PsP (Table 2b), while quadratic dependencies of coarse root traits on MST were detected for root depth and diameter, but not for root frequency (Fig. 7a,b,c). Both root depth and diameter showed also a quadratic relationship with solar radiation, while root frequency showed a positive relationship with this variable (Fig. 7d,e,f). These results suggested that shallower and finer roots were present in ecotypes having either relatively low and high MST or solar radiation values at origin. Also, root depth showed a marginally significant (negative) linear

dependence on VPD_s (Fig. 7e,f), denoting that ecotypes subjected to higher summer transpirative demand tended to show shallower roots. As for root depth, tree height showed a negative dependence on VPD_s (p = 0.029). On the contrary, tree height was negatively related to SR (p = 0.035) and unrelated to MST (results not shown).

Discussion

GPR applicability to root phenotyping of forest trees

This study showcases the use of GPR devices as high-throughput phenotyping tools to assess intraspecific differentiation in coarse roots potentially related to water use and drought tolerance strategies of forest trees. It broadens the customary use of GPR for tree root detection in ecological studies carried out since the turn of this century (Guo et al. 2013; Hruska et al. 1999). By using an 800 MHz antenna we were able to detect 1,835 roots with diameters equal to or above 2.2 cm at a maximum depth of 88 cm for about 330 trees monitored in a common garden of *ca*. 0.8 ha.

In situ calibration provided direct evidence of the adequacy of GPR measurements for root detection. An additional (indirect) indication of the potential of GPR for root detection was the observation that the variability detected in coarse root traits for Aleppo pine agreed (at least partly) with the information derived from xylem water isotopes on the use of water sources by the same trees (Voltas et al., 2015). However, we should note that only associations involving $\delta^{18}O$ of xylem water in early autumn were significant, whereas no relevant relationships with GPR records were detected in peak summer. This suggests that the existing electromagnetic gradient between roots and soil at the time of GPR measurements (i.e. mid-June) could have identified more roots than those effectively taking up water during the acute summer drought typical of end-July. For an isohydric species such as Aleppo pine, a fraction of coarse roots might have remained in a quiescent condition during soil dry-down in summer as avoidance strategy against hydraulic failure. This condition might be the result of a reversible development of water transport barriers such as suberin or cutin, stimulated by nutrient scarcity and drought stress (Vandeleur et al. 2008; Schreiber 2010; Barberon et al. 2016). Roots might be also subjected to seasonal embolism, since partial cavitation

in roots is less deleterious than xylem failure because roots can recover after drought by refilling the embolized conduit (Domec et al. 2004). Changes in root turnover and turgor are some of the prevailing consequences of high soil temperature and water deficit stress in plants (Brunner et al. 2015, Gill and Jackson 2000), and both have been widely described for the case of fine roots (Gill and Jackson 2000; Kitajima et al. 2010; Montagnoli et al. 2019). However, there is no evidence of inactivation of coarse roots in forest tree species thus far. This possibility would deserve detailed investigation through e.g. temporal assessment of GPR signals following changes in soil water status during the growing season.

Evidence for intraspecific variability in root traits of Aleppo pine

It is known that root system architecture varies among Iberian pines, with mountain species (e.g. *Pinus sylvestris*) usually having shallower roots than typical Mediterranean species (e.g. *Pinus pinaster*, *P. halepensis*) (Andivia et al. 2019). This variability correlates with the species' ecological niches and the intensity of drought stress present in their environments (Andivia et al. 2019). However, there is still a lack of information on the variability of functional root traits at the intraspecific level, which determines the efficiency of water acquisition by trees (Kirfel et al. 2017). A main goal of this work was to fill this knowledge gap for a Mediterranean pine species and, particularly, to characterize intraspecific patterns of coarse root traits potentially related to different strategies of water uptake and use in Aleppo pine.

We found population differentiation for root traits in *P. halepensis*, which was geographically structured following an ecotypic pattern. Such patterns have been previously reported in *P. halepensis* for traits related to the tree's water budget such as water-use efficiency (Voltas et al. 2008), transpiration (Santini et al. 2019b) and the use of water sources (Voltas et al. 2015). Also, we observed greater variability in coarse root traits among populations originating from the Iberian Peninsula than among their eastern Mediterranean counterparts in spite of the loss of genetic diversity that Aleppo pine suffered after the post-glacial recolonization from the eastern Mediterranean (Grivet et al. 2009). This result, however, requires confirmation because comparatively less populations were available from the eastern Mediterranean compared to the western Mediterranean basin, being also distributed within a narrower latitudinal gradient.

Relationships between root traits and aboveground growth

We found quadratic associations of coarse root depth with tree height and diameter at the intraspecific level. Although these relationships were only marginally significant, they suggest predictable allometric patterns linking below and aboveground growth, which are partially consistent with the general allometric scaling theory (West et al. 1999). In particular, proportionality of carbon investment to above and belowground growth is suggested for ecotypes reaching up to *ca*. 6 m height at age 19 years in the study site (root to shoot biomass is known to stabilize once pines reach the reproductive stage; Peichl and Arain [2007], Cao et al. [2012]). Above this height threshold, a negative association between aerial growth and investment in roots could be observed at the ecotype level. This suggests a preferential mass allocation to aerial carbon stocks for mesic ecotypes having high growth potential (Climent et al. 2008; Voltas et al. 2018), as exemplified by ecotypes 12GR and 14IT originating from the center-eastern Mediterranean basin. These ecotypes experience mild climate conditions at origin (either having MAP> 500 mm or MSP> 60 mm) and are known to exhibit a larger tree height plasticity compared with xeric ecotypes across water availability gradients (Patsiou et al. 2020). This superior plasticity might be associated with a progressively large carbon allocation to roots under harsher (i.e. drier or nutrient-poor) conditions. In any case, our results suggest that these mesic ecotypes allocate relatively more resources to aerial growth than to root development under the relatively favorable conditions encountered in the trial, as compared with xeric ecotypes. This result partially agrees with previous studies stating that forest trees allocate carbon preferentially to the root system as a response to poor nutrient availability (Hermans et al. 2006; Vicca et al. 2012), which precedes synthesis of secondary metabolites (Prescott et al. 2020).

Variability in root traits of Aleppo pine follows geographical and climatic gradients

The assessment of geographic dependencies of roots traits suggests that root diameter decreases across an eastward longitudinal cline in Aleppo pine populations. This cline agrees with previous results being indirectly informative of allocation patterns to roots in *P. halepensis*, which reported decreases in

reproductive investment (Climent et al. 2008) and water-use efficiency (Voltas et al. 2008) in eastern populations. On the other hand, the larger proportion of shallow roots in populations originating from either extreme of the species' latitudinal range disagrees with our initial hypothesis. However, root frequency decreased as latitude increased, suggesting that southern populations, which generally are exposed to a drier climate, have more abundance of coarse roots than northern populations, regardless of their root depth. This discrepancy could be related to the higher costs of construction and maintenance of deep roots (Schenk 2008a) in ecotypes with low growth potential and high reproductive allotment, leading to carbon allocation shifts towards shallower and more abundant roots in dry and resource-poor habitats. This could be an advantageous strategy in habitats where the uppermost soil layers may present higher nutrients and moisture as a result of discrete precipitation pulses (Schenk 2008a, b).

Previous studies have shown that rooting depth increases with water shortage in pine species (Andivia et al. 2019), an interspecific pattern that only partially agrees with our results at the intraspecific level. In fact, only root frequency increased with aridity at origin of populations of Aleppo pine. On the other hand, intraspecific relationships between root depth or diameter and temperature were hump-shaped, and peaked towards the thermal midpoint of the species distribution range (Albert et al. 2010). This finding may be related to the existence of different adaptive strategies imprinted in a number of life-history traits and their potential trade-offs – in addition to rooting traits – to cope with the conditions encountered by the species along its distribution range, as modulated by stresses (drought, cold temperatures, pests) and disturbances (fire). For example, the associations between aerial growth or rooting traits and incoming radiation might indicate allocation trade-offs related to higher selective pressures for increased competition for light in the case of Greek and Italian mesic ecotypes. This result also suggests that the existence of trade-offs between reproduction, defense and vegetative growth in Aleppo pine (Climent et al. 2008; Santini et al. 2019a; Voltas et al. 2008) may imply a decrease of C allocation to coarse roots in fire-prone, dry and warm habitats. The negative dependency of rooting depth on VPD_s has to be carefully interpreted, however, since this relation was mostly driven by the Tunisian ecotype (15TU), which has shallow roots despite being exposed to high summer evapotranspiration. This could be explained as the result of conflicting functional

strategies typical of stressed and disturbed environments (Santini et al. 2019a), implying a relatively low allocation to growth (both aerial and belowground) compared with reproduction (Climent et al. 2008; Santos-del-Blanco et al. 2013). Such possibility is supported by the negative intraspecific association found between tree height and VPD_s.

Methodological limitations

Despite its high detection capability and non-destructive assessment of root features, GPR is not devoid of technical limitations for tree phenotyping studies. These are related to the existing variability in root orientation, since overlapping roots and roots underneath the tree trunk are underestimated by the device (Butnor et al. 2016; Li et al. 2016). However, GPR have been recognized as a proxy tool sufficiently precise to estimate coarse root frequency (Butnor et al. 2003; Hirano et al. 2009, Hirano et al. 2012; Guo et al. 2013a). Also, the existing electromagnetic gradient between roots and soil makes a previous calibration strictly necessary to reduce the background noise produced by the particular physicochemical characteristics of the soil. In particular, it should be noted that GPR detection capacity is seriously impaired in both nearly saturated (Hirano et al. 2009; Rodríguez-Robles et al 2017) and very dry soils (Hirano et al. 2009). In this last case, GPR detection is limited if roots have low water content (e.g. under 20% volumetric water content in *Cryptomeria japonica*; Hirano et al. 2009). In this regard, our field campaign targeted a period of full vegetative activity of trees while avoiding such extremes in soil water status (e.g. abundant precipitation in April-early May and acute drought in July-August).

Conclusions

This study provides new avenues for the examination of intraspecific variability in root traits of forest tree species using GPR as high-throughput phenotyping method. We observed population differentiation in *P. halepensis* following east-west (root diameter) and north-south (root frequency) geographical patterns. Conversely, the interspecific pattern described for the genus *Pinus*, by which species originating from xeric conditions exhibit large allocation to roots, was not strictly found at the intraspecific level for Aleppo pine.

This observation may be attributable to the existence of different adaptive strategies under varying environmental conditions for the species, which likely lead to trade-offs involving the use of resources. In this regard, our work contributes to unravel the evolutionary complexity of a widespread conifer of high ecological significance in the Mediterranean basin.

Authors' contribution

Erica Lombardi: Formal analysis, Writing - Original Draft, Visualization. **Juan Pedro Ferrio:** Conceptualization, Formal analysis, Writing - Review & Editing. **Ulises Rodríguez-Robles:** Methodology, Data curation, Formal analysis, Writing - Review & Editing. **Víctor Resco de Dios:** Formal analysis, Writing - Review & Editing. **Jordi Voltas:** Conceptualization, Formal analysis, Writing - Review & Editing, Funding acquisition.

References

Alani, A.M., Lantini, L. (2020). Recent Advances in Tree Root Mapping and Assessment Using Non-destructive Testing Methods: A Focus on Ground Penetrating Radar, Surveys in Geophysics. Springer Netherlands. https://doi.org/10.1007/s10712-019-09548-6

Albert, C.H., Thuiller, W., Yoccoz, N., G., Soudant, A., Boucher, F., Saccone, P., Lavorel, S. (2010). Intraspecific functional variability: Extent, structure and sources of variation. J. Ecol. 98, 604–613. https://doi.org/10.1111/j.1365-2745.2010.01651.x

Andivia, E., Zuccarini, P., Grau, B., de Herralde, F., Villar-Salvador, P., Savé, R. (2019). Rooting big and deep rapidly: the ecological roots of pine species distribution in southern Europe. Trees Struct. Funct. 33, 293–303. https://doi.org/10.1007/s00468-018-1777-x

Barberon, M., Vermeer, J.E.M., De Bellis, D., Wang, P., Naseer, S., Andersen, T.G., Humbel, B.M., Nawrath, C., Takano, J., Salt, D.E., Geldner, N. (2016). Adaptation of root function by nutrient-induced plasticity of endodermal differentiation. Cell. 164, 447–459. https://doi.org/10.1016/j.cell.2015.12.021

Barton, C.V.M., Montagu, K.D. (2004). Detection of tree roots and determination of root diameters by ground penetrating radar under optimal conditions. Tree. Physiol. 24, 1323–1331. https://doi.org/10.1093/treephys/24.12.1323

Brunner, I., Herzog, C., Dawes, M.A., Arend, M., Sperisen, C. (2015). How tree roots respond to drought. Front. Plant Sci. 6, 1–16. https://doi.org/10.3389/fpls.2015.00547

Butnor, J.R., Doolittle, J.A., Johnsen, K.H., Samuelson, L., Stokes, T., Kress, L. (2003). Utility of ground-penetrating radar as a root biomass survey tool in forest systems. Soil Sci. Soc. Am. J. 67, 1607–1615.

https://doi.org/10.2136/sssaj2003.1607

Butnor, J.R., Samuelson, L.J., Stokes, T.A., Johnsen, K.H., Anderson, P.H., González-Benecke, C.A. (2016). Surface-based GPR underestimates below-stump root biomass. Plant Soil. 402, 47–62. https://doi.org/10.1007/s11104-015-2768-y

Cao, J., Wang, X., Tian, Y., Wen, Z., Zha, T. (2012). Pattern of carbon allocation across three different stages of stand development of a Chinese pine (*Pinus tabulaeformis*) forest. Ecol. Res. 27, 883–892. https://doi.org/10.1007/s11284-012-0965-1

Chambel, M.R., Climent, J., Alía, R. (2007). Divergence among species and populations of Mediterranean pines in biomass allocation of seedlings grown under two watering regimes. Ann. For. Sci. 64, 7–97. https://doi.org/10.1051/forest:2006092

Climent, J., Prada, M.A., Calama, R., Chambel, M.R., De Ron, D.S., Alía, R. (2008). To grow or to seed: Ecotypic variation in reproductive allocation and cone production by young female Aleppo pine (*Pinus halepensis*, *Pinaceae*). Am. J. Bot. 95, 833–842. https://doi.org/10.3732/ajb.2007354

Dawson, T.E., Hahm, W.J., Crutchfield-Peters, K. (2020). Digging deeper: what the critical zone perspective adds to the study of plant ecophysiology. New Phytol. 226, 666–671. https://doi.org/10.1111/nph.16410

Esteban, L.G., Martín, J.A., de Palacios, P., Fernández, F.G., López, R. (2010). Adaptive anatomy of *Pinus halepensis* trees from different mediterranean environments in Spain. Trees Struct. Funct. 24, 19–30. https://doi.org/10.1007/s00468-009-0375-3

Ferrio, J.P., Voltas, J. (2005). Carbon and oxygen isotope ratios in wood constituents of *Pinus halepensis* as indicators of precipitation, temperature and vapour pressure deficit. Tellus B. Chem. Phys. Meteorol. 57, 164–173. https://doi.org/10.1111/j.1600-0889.2005.00137.x

Fick, S.E., Hijmans, R.J. (2017). WorldClim 2: new 1-km spatial resolution climate surfaces for global land areas. Int. J. Climatol. 37, 4302-4315. https://doi.org/10.1002/joc.5086

Gill, R.A., Jackson, R.B. (2000). Global patterns of root turnover for terrestrial ecosystems. New. Phytol. 147, 13–31. https://doi.org/10.1046/j.1469-8137.2000.00681.x

Grivet, D., Climent, J., Zabal-Aguirre, M., Neale, D.B., Vendramin, G.G., González-Martínez, S.C. (2013). Adaptive evolution of Mediterranean pines. Mol. Phylogenet. Evol. 68, 555–566. https://doi.org/10.1016/j.ympev.2013.03.032

Grivet, D., Sebastiani, F., González-Martínez, S.C., & Vendramin, G.G. (2009). Patterns of polymorphism resulting from long-range colonization in the Mediterranean conifer Aleppo pine. New Phytol. 184, 1016–1028. https://doi.org/10.1111/j.1469-8137.2009.03015.x

Grossnickle, S.C. (2005). Importance of root growth in overcoming planting stress. New For. 30, 273–294. https://doi.org/10.1007/s11056-004-8303-2

Guo, L., Chen, J., Cui, X., Fan, B., Lin, H. (2013a). Application of ground penetrating radar for coarse root detection and quantification: a review. Plant Soil. 362, 1–23. https://doi.org/10.1007/s11104-012-1455-5

Guo, L., Lin, H., Fan, B., Cui, X., Chen, J. (2013b). Impact of root water content on root biomass estimation using ground penetrating radar: Evidence from forward simulations and field controlled experiments. Plant

Soil. 371, 503–520. https://doi.org/10.1007/s11104-013-1710-4

Hermans, C., Hammond, J.P., White, P.J., Verbruggen, N. (2006). How do plants respond to nutrient shortage by biomass allocation? Trends Plant Sci. 11, 610–617. https://doi.org/10.1016/j.tplants.2006.10.007

Hernández, E.I., Vilagrosa, A., Pausas, J.G., Bellot, J. (2010). Morphological traits and water use strategies in seedlings of Mediterranean coexisting species. Plant Ecol. 207, 233–244. https://doi.org/10.1007/s11258-009-9668-2

Hirano, Y., Dannoura, M., Aono, K., Igarashi, T., Ishii, M., Yamase, K., Makita, N., Kanazawa, Y. (2009). Limiting factors in the detection of tree roots using ground-penetrating radar. Plant Soil. 319, 15–24. https://doi.org/10.1007/s11104-008-9845-4

Hirano, Y., Yamamoto, R., Dannoura, M., Aono, K., Igarashi, T., Ishii, M., Yamase, K., Makita, N., Kanazawa, Y. (2012). Detection frequency of *Pinus thunbergii* roots by ground-penetrating radar is related to root biomass. Plant Soil. 360, 363–373. https://doi.org/10.1007/s11104-012-1252-1

Hruska, J., Cermák, J., Sustek, S. (1999). Mapping tree root systems with ground-penetrating radar. Tree Physiol. 19, 125–130. https://doi.org/10.1093/treephys/19.2.125

John, J., Williams, E. (1998). t-Latinized Designs. Statist. NZJ. 40, 111-118. https://doi.org/10.1111/1467-842X.00012

Jones, H.G., Corlett, J.E. (1992). Current topics in drought physiology. J. Agric. Sci. 119, 291–296. https://doi.org/10.1017/S0021859600012144

Kirfel, K., Leuschner, C., Hertel, D., Schuldt, B. (2017). Influence of root diameter and soil depth on the xylem anatomy of fine-to medium-sized roots of mature beech trees in the top- and subsoil. Front. Plant. Sci. 8, 1–13. https://doi.org/10.3389/fpls.2017.01194

Kitajima, K., Anderson, K.E., Allen, M.F. (2010). Effect of soil temperature and soil water content on fine root turnover rate in a California mixed conifer ecosystem. J. Geophys. Res. Biogeosciences. 115, 1–12. https://doi.org/10.1029/2009JG001210

Klotzsche, A., Jonard, F., Looms, M.C., van der Kruk, J., Huisman, J.A. (2018). Measuring Soil Water Content with Ground Penetrating Radar: A Decade of Progress. Vadose Zo. J. 17, 180052. https://doi.org/10.2136/vzj2018.03.0052

Krainyukoy, A., Lyaksa, I. (2016). Detection of tree roots in an urban area with the use of ground penetrating radar. Transp. Telecommun. 17, 362–370. https://doi.org/10.1515/ttj-2016-0032

Landis, T.D., Tinus, R.W., McDonald, S.E., Barnett, J.P. (1990). Containers and growing media, Vol. 2. The Container Tree Nursery Manual. Agric. Handbk. 674. Washington, D.C: U.S. Department of Agriculture, Forest Service, 88

Li, W., Cui, X., Guo, L., Chen, J., Chen, X., Cao, X. (2016). Tree root automatic recognition in Ground penetrating radar profiles based on randomized Hough transform. Remote Sens. 8. https://doi.org/10.3390/rs8050430

Lorenzo, H., Pérez-Gracia, V., Novo, A., Armesto, J. (2010). Forestry applications of ground-penetrating radar. For. Syst. 19, 5. https://doi.org/10.5424/fs/2010191-01163

Luodes, H., Sutinen, H. (2011). Evaluation and modelling of natural stone rock quality using ground penetrating radar (GPR). Spec. Pap. Geol. Surv. Finl. 2011, 83–90

Matías, L., González-Díaz, P., Jump, A.S. (2014). Larger investment in roots in southern range-edge populations of Scots pine is associated with increased growth and seedling resistance to extreme drought in response to simulated climate change. Environ. Exp. Bot. 105, 32–38. https://doi.org/10.1016/j.envexpbot.2014.04.003

Montagnoli, A., Dumroese, R.K., Terzaghi, M., Onelli, E., Scippa, G.S., Chiatante, D. (2019). Seasonality of fine root dynamics and activity of root and shoot vascular cambium in a *Quercus ilex* L. forest (Italy). For. Ecol. Manage. 431, 26–34. https://doi.org/10.1016/j.foreco.2018.06.044

Padilla, F.M., Pugnaire, F.I. (2007). Rooting depth and soil moisture control Mediterranean woody seedling survival during drought. Funct. Ecol. 21, 489–495. https://doi.org/10.1111/j.1365-2435.2007.01267.x

Patsiou, T.S., Shestakova, T.A., Klein, T., di Matteo, G., Sbay, H., Chambel, M.R., Zas, R., Voltas, J. (2020). Intraspecific responses to climate reveal nonintuitive warming impacts on a widespread thermophilic conifer. New Phytol. 228, 525-540. https://doi.org/10.1111/nph.16656

Peichl, M., Arain, M.A. (2007). Allometry and partitioning of above- and belowground tree biomass in an age-sequence of white pine forests. For. Ecol. Manag. 253, 68–80. https://doi.org/10.1016/j.foreco.2007.07.003

Plowright, A. (2018). ForestTools: analyzing remotely sensed forest data. Version 0.2.0. Available via https://CRAN.R-project.org/package=ForestTools

Prescott, C.E., Grayston, S.J., Helmisaari, H.S., Kaštovská, E., Körner, C., Lambers, H., Meier, I.C., Millard, P., Ostonen, I. (2020). Surplus carbon drives allocation and plant–soil interactions. Trends Ecol. Evol. 35, 1110–1118. https://doi.org/10.1016/j.tree.2020.08.007

Resco De Dios, V., Fischer, C., Colinas, C. (2007). Climate change effects on mediterranean forests and preventive measures. New For. 33, 29–40. https://doi.org/10.1007/s11056-006-9011-x

Ripullone, F., Camarero, J.J., Colangelo, M., Voltas, J. (2020). Variation in the access to deep soil water pools explains tree-to-tree differences in drought-triggered dieback of Mediterranean oaks. Tree Physiol. 40, 591–604. https://doi.org/10.1093/treephys/tpaa026

Rodríguez-Robles, U., Arredondo, T., Huber-Sannwald, E., Ramos-Leal, J.A., Yépez, E.A. (2017). Technical note: Application of geophysical tools for tree root studies in forest ecosystems in complex soils. Biogeosciences. 14, 5343–5357. https://doi.org/10.5194/bg-14-5343-2017

Rossatto, D.R., de Carvalho Ramos Silva, L., Villalobos-Vega, R., Sternberg, L. da S.L., Franco, A.C. (2012). Depth of water uptake in woody plants relates to groundwater level and vegetation structure along a topographic gradient in a neotropical savanna. Environ. Exp. Bot. 77, 259–266. https://doi.org/10.1016/j.envexpbot.2011.11.025

Ruiz Daniels, R., Taylor, R.S., Serra-Varela, M.J., Vendramin, G.G., González-Martínez, S.C., Grivet, D. (2018). Inferring selection in instances of long-range colonization: The Aleppo pine (*Pinus halepensis*) in the Mediterranean Basin. Mol. Ecol. 27, 3331–3345. https://doi.org/10.1111/mec.14786

Rutter, M.T., Fenster, C.B. (2007). Testing for adaptation to climate in *Arabidopsis thaliana*: A calibrated common garden approach. Ann. Bot. 99, 529–536. https://doi.org/10.1093/aob/mcl282

Santini, F., Climent, J.M., Voltas, J. (2019a). Phenotypic integration and life history strategies among populations of *Pinus halepensis*: an insight through structural equation modelling. Ann. Bot. 124, 1161–1171. https://doi.org/10.1093/aob/mcz088

Santini, F., Kefauver, S.C., Resco de Dios, V., Araus, J.L., Voltas, J. (2019b). Using unmanned aerial vehicle-based multispectral, RGB and thermal imagery for phenotyping of forest genetic trials: A case study in *Pinus halepensis*. Ann. Appl. Biol. 174, 262–276. https://doi.org/10.1111/aab.12484

Santini, F., Kefauver, S.C., Araus, J.L., Resco de Dios, V., Martín García, S., Grivet, D., Voltas, J. (2020). Bridging the genotype–phenotype gap for a Mediterranean pine by semi-automatic crown identification and multispectral imagery. New Phytol. 229, 245-258 https://doi.org/10.1111/nph.16862

Santos-del-Blanco, L., Bonser, S.P., Valladares, F., Chambel, M.R., Climent, J. (2013). Plasticity in reproduction and growth among 52 range-wide populations of a Mediterranean conifer: Adaptive responses to environmental stress. J. Evol. Biol. 26, 1912–1924. https://doi.org/10.1111/jeb.12187

Sardans, J., Peñuelas, J. (2013). Plant-soil interactions in Mediterranean forest and shrublands: Impacts of climatic change. Plant Soil. 365, 1–33. https://doi.org/10.1007/s11104-013-1591-6

Sbay, H., Zas, R. (2018). Geographic variation in growth, survival, and susceptibility to the processionary moth (*Thaumetopoea pityocampa* Dennis & Schiff.) of *Pinus halepensis* Mill. and *P. brutia* Ten.: results from common gardens in Morocco. Ann. For. Sci. 75. https://doi.org/10.1007/s13595-018-0746-2

Schenk, H.J. (2008a). The shallowest possible water extraction profile: A null model for global root distributions. Vadose Zo. J. 7, 1119–1124. https://doi.org/10.2136/vzj2007.0119

Schenk, H.J. (2008b). Soil depth, plant rooting strategies and species' niches. New Phytol. 178, 223-

225. https://doi.org/10.1111/j.1469-8137.2008.02427.x

Schreiber, L. (2010). Transport barriers made of cutin, suberin and associated waxes. Trends Plant Sci. 15, 546–553. https://doi.org/10.1016/j.tplants.2010.06.004

Tanikawa, T., Hirano, Y., Dannoura, M., Yamase, K., Aono, K., Ishii, M., Igarashi, T., Ikeno, H., Kanazawa, Y. (2013). Root orientation can affect detection accuracy of ground-penetrating radar. Plant Soil. 373, 317–327. https://doi.org/10.1007/s11104-013-1798-6

Tapias, R., Climent, J., Pardos, J.A., Gil, L. (2004). Life histories of Mediterranean pines. Plant Ecol. 171, 53–68. https://doi.org/10.1023/B:VEGE.0000029383.72609.f0

Valerio, G., Galli, A., Barone, P.M., Lauro, S.E., Mattei, E., Pettinelli, E. (2012). GPR detectability of rocks in a Martian-like shallow subsoil: A numerical approach. Planet Space Sci. 62, 31–40. https://doi.org/https://doi.org/10.1016/j.pss.2011.12.003

Vandeleur, R.K., Mayo, G., Shelden, M.C., Gilliham, M., Kaiser, B.N., Tyerman, S.D. (2009). The role of plasma membrane intrinsic protein aquaporins in water transport through roots: Diurnal and drought stress responses reveal different strategies between isohydric and anisohydric cultivars of grapevine. Plant Physiol. 149, 445–460. https://doi.org/10.1104/pp.108.128645

Vennetier. M., Ripert, C., Rathgeber, C. (2018). Autecology and growth of Aleppo pine (*Pinus halepensis* Mill.): A comprehensive study in France. For Ecol. Manage. 413, 32–47. https://doi.org/10.1016/j.foreco.2018.01.028

Vicca, S., Luyssaert, S., Peñuelas, J., Campioli, M., Chapin, F.S., Ciais, P., Heinemeyer, A., Högberg, P.,

Kutsch, W.L., Law, B.E., Malhi, Y., Papale, D., Piao, S.L., Reichstein, M., Schulze, E.D., Janssens, I.A. (2012). Fertile forests produce biomass more efficiently. Ecol. Lett. 15, 520–526. https://doi.org/10.1111/j.1461-0248.2012.01775.x

Voltas, J., Chambel, M.R., Prada, M.A., Ferrio, J.P. (2008). Climate-related variability in carbon and oxygen stable isotopes among populations of Aleppo pine grown in common-garden tests. Trees Struct. Funct. 22, 759–769. https://doi.org/10.1007/s00468-008-0236-5

Voltas, J., Lucabaugh, D., Chambel, M.R., Ferrio, J.P. (2015). Intraspecific variation in the use of water sources by the circum-Mediterranean conifer *Pinus halepensis*. New Phytol. 208, 1031–1041. https://doi.org/10.1111/nph.13569

Voltas. J., Shestakova, T.A., Patsiou, T., di Matteo, G., Klein, T. (2018). Ecotypic variation and stability in growth performance of the thermophilic conifer *Pinus halepensis* across the Mediterranean basin. For. Ecol. Manage. 424, 205–215. https://doi.org/10.1016/j.foreco.2018.04.058

Wang, Y., Dong, X., Wang, H., Wang, Z., Gu, J. (2015). Root tip morphology, anatomy, chemistry and potential hydraulic conductivity vary with soil depth in three temperate hardwood species. Tree Physiol. 36, 99–108. https://doi.org/10.1093/treephys/tpv094

West, G.B., Brown, J.H., Enquist, B.J. (1999). A general model for the structure and allometry of plant vascular systems. Nature. 400, 664–667. https://doi.org/10.1038/23251

Wu. Y., Guo, L., Cui, X., Chen, J., Cao, X., Lin, H. (2014). Ground-penetrating radar-based automatic reconstruction of three-dimensional coarse root system architecture. Plant Soil. 383, 155–172. https://doi.org/10.1007/s11104-014-2139-0

Chapter 1 – Tables and Figures

Table 1 Mixed-effects model analysis of variance for root diameter (cm), root depth (cm) and root frequency (number of roots) of 56 populations of Aleppo pine categorized into 16 ecotypes grown in a common garden in Altura (Spain). Data refer to sub-plot S_{100}. Only fixed effects are reported.

Source of variation	Num. df	Root diameter			Root depth			Root frequency		
		Den. df	*F*-value	$p > F$	Den. df	*F*-value	$p > F$	Den. df	*F*-value	$p > F$
Block	2	13.4	1.49	0.226	9.8	0.26	0.773	7.6	1.92	0.146
Column	6	92.4	4.05	<0.001	12.2	1.30	0.252	11.6	2.62	0.015
Population (P)	55	84.6	1.39	0.030	73.2	1.27	0.086	89.8	1.01	0.460
Ecotype	15	97.3	1.51	0.091	87.9	2.00	0.012	97.6	1.50	0.096
P(Ecotype)	40	90.6	1.16	0.227	81.1	1.03	0.410	93.9	0.84	0.756

Table 2. Coefficients of determination (R^2) of linear and quadratic regressions of root traits (diameter, depth, frequency) at population (a) and ecotype level (b) as a function of several ecogeographical variables at origin of 53 populations grouped into 15 ecotypes of Aleppo pine tested in a common garden in Altura (Spain). Associated probabilities between 0.10 and 0.05 are represented in italics, while significant probabilities <0.05 are shown in bold characters. Ecotype 16 corresponds to reforestations of the Northern Plateau (Spain) of uncertain geographic origin and therefore it has not been included in the analysis. MAT= mean annual temperature; TAR = temperature annual range; MST = mean summer temperature; MAP = mean annual precipitation; PsP = summer to annual precipitation ratio; VPD_s = vapor pressure deficit of the warmest (summer) quarter.

(a)		Populations											
		MAT	TAR	MST	MAP	PsP	VDP_s	Solar radiation	Geographical distance	Gower's distance	Latitude	Longitude	Altitude
Diameter	Linear	0.01	0.00	0.01	0.03	0.00	0.02	0.01	**0.08**	0.01	0.00	**0.08**	0.02
	Quadratic	0.02	0.00	0.02	0.03	0.02	0.02	**0.16**	*0.10*	0.06	0.08	*0.10*	0.02
Depth	Linear	0.02	0.00	0.03	0.00	0.04	0.00	0.00	**0.08**	0.05	0.01	*0.06*	0.03
	Quadratic	0.04	0.00	*0.10*	0.00	**0.13**	0.01	*0.09*	*0.11*	**0.13**	**0.12**	0.06	0.03
Frequency	Linear	0.02	*0.06*	0.01	0.05	*0.07*	**0.16**	**0.22**	*0.06*	0.00	**0.15**	**0.11**	**0.14**
	Quadratic	0.07	0.08	0.06	0.05	*0.09*	**0.16**	**0.22**	*0.10*	0.02	**0.16**	*0.11*	**0.14**

(b)		Ecotypes											
		MAT	TAR	MST	MAP	PsP	VDP_s	Solar radiation	Geographical distance	Gower's distance	Latitude	Longitude	Altitude
Diameter	Linear	0.16	0.01	0.12	0.03	0.02	0.10	0.00	*0.20*	0.04	0.01	*0.24*	0.15
	Quadratic	0.16	0.02	*0.32*	0.07	0.03	0.23	*0.37*	0.30	*0.33*	0.16	*0.34*	*0.36*
Depth	Linear	0.01	0.04	0.06	0.04	0.05	*0.21*	0.02	0.12	0.05	0.05	0.06	0.01
	Quadratic	0.17	0.05	**0.58**	0.04	0.25	0.22	*0.33*	0.24	**0.71**	*0.37*	0.06	*0.32*
Frequency	Linear	0.19	0.18	0.16	0.05	**0.28**	0.09	**0.49**	0.11	0.17	*0.23*	0.19	0.11
	Quadratic	0.04	0.12	0.06	0.06	*0.35*	0.09	**0.49**	0.23	0.26	0.29	0.19	0.30

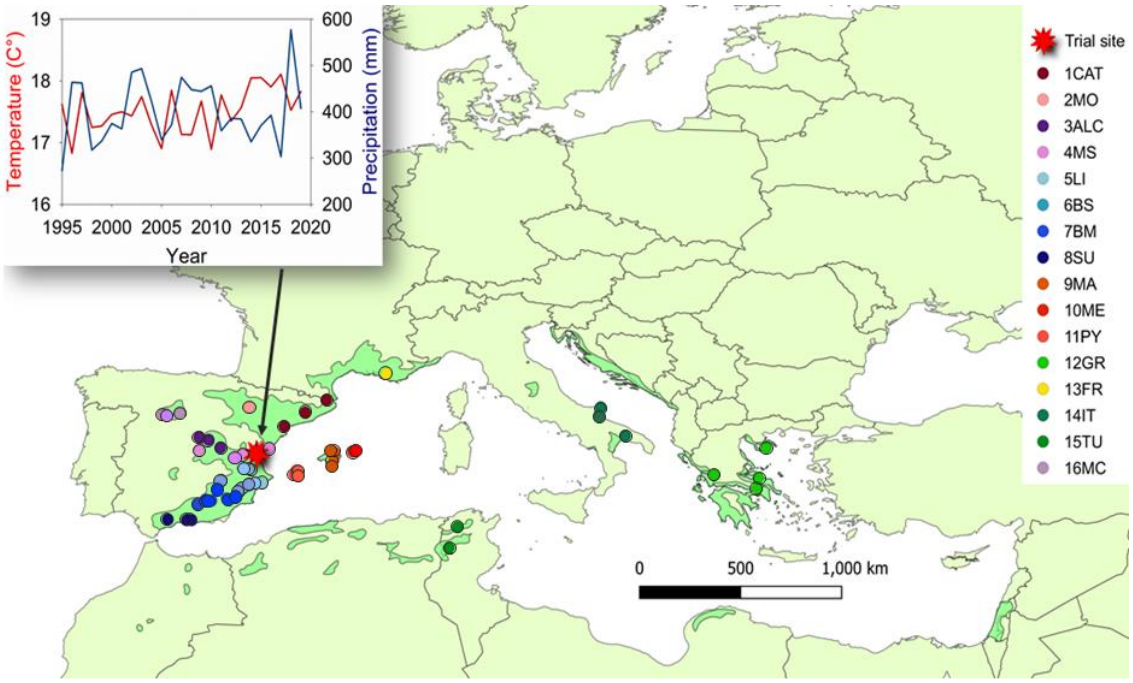

Fig. 1 Geographic origin of 56 *Pinus halepensis* populations (coloured dots) evaluated in a common garden (red star) located in Altura (Castellón province, Spain). The legend shows ecotype codes as defined in Table S2. The dark green area represents the natural distribution of *P. halepensis* according to EUFORGEN (http://www.euforgen.org/species/pinus-halepensis/). A climograph of the trial site is included (mean climate of 1995-2019 obtained from Worldclim).

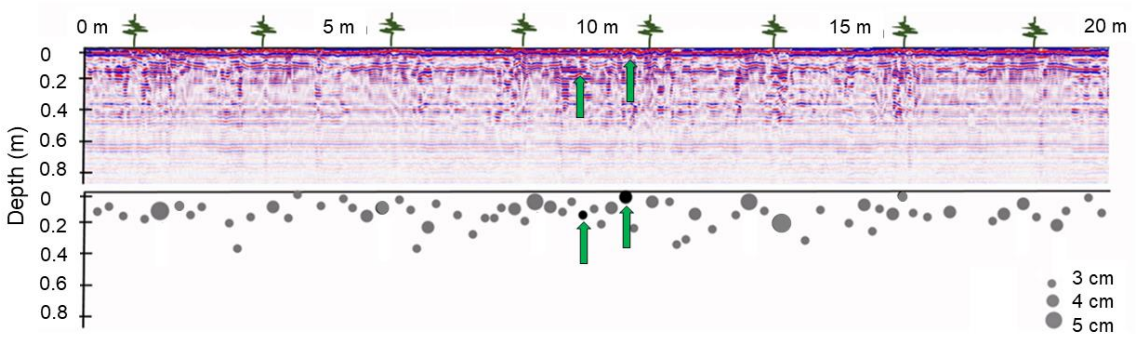

Fig. 2 Example of root detection along a linear profile section of the trial (marked in Fig. S1) using a Ground-Penetrating Radar (GPR). The GPR radargram was generated with a 800 MHz shielded antenna and band pass filters (both high-pass and low-pass filter) to eliminate low and high frequency noise (Rodríguez-Robles et al. 2017). The upper panel shows hyperbolically shaped reflections representing root reflections (dark purple hyperbolae). The lower panel illustrates the roots detected from the hyperbolae signatures (grey dots), and additional roots measured *in situ* for calibration purposes are depicted by black dots.

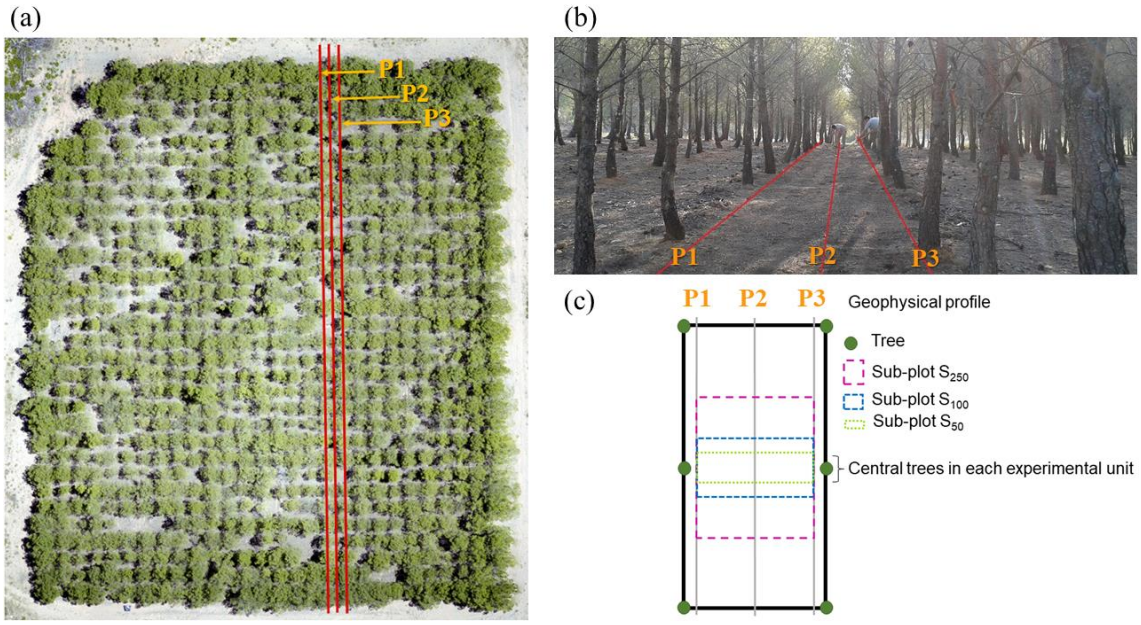

Fig. 3 a) Aerial image of the study site exemplifying the three geophysical GPR profiles (P1, P2, P3) used at plot level following the column direction of the common garden of *P. halepensis*. Measurements were done between the two central trees of every plot (experimental unit). b) Detailed view of the geophysical GPR profiles: P1 and P3 are at a row distance of 0.30 m from one or another central tree, while the position of P2 is at mid-distance (1.25 m) between central trees. c) Scheme (top view) showing the geophysical profiles and the three different sub-plot areas (S_{50}, S_{100}, S_{250}) evaluated, where sub-plots correspond to column distances of ± 0.25 m, ± 0.50 m and ± 1.25 m, respectively, from the two central trees of an experimental unit.

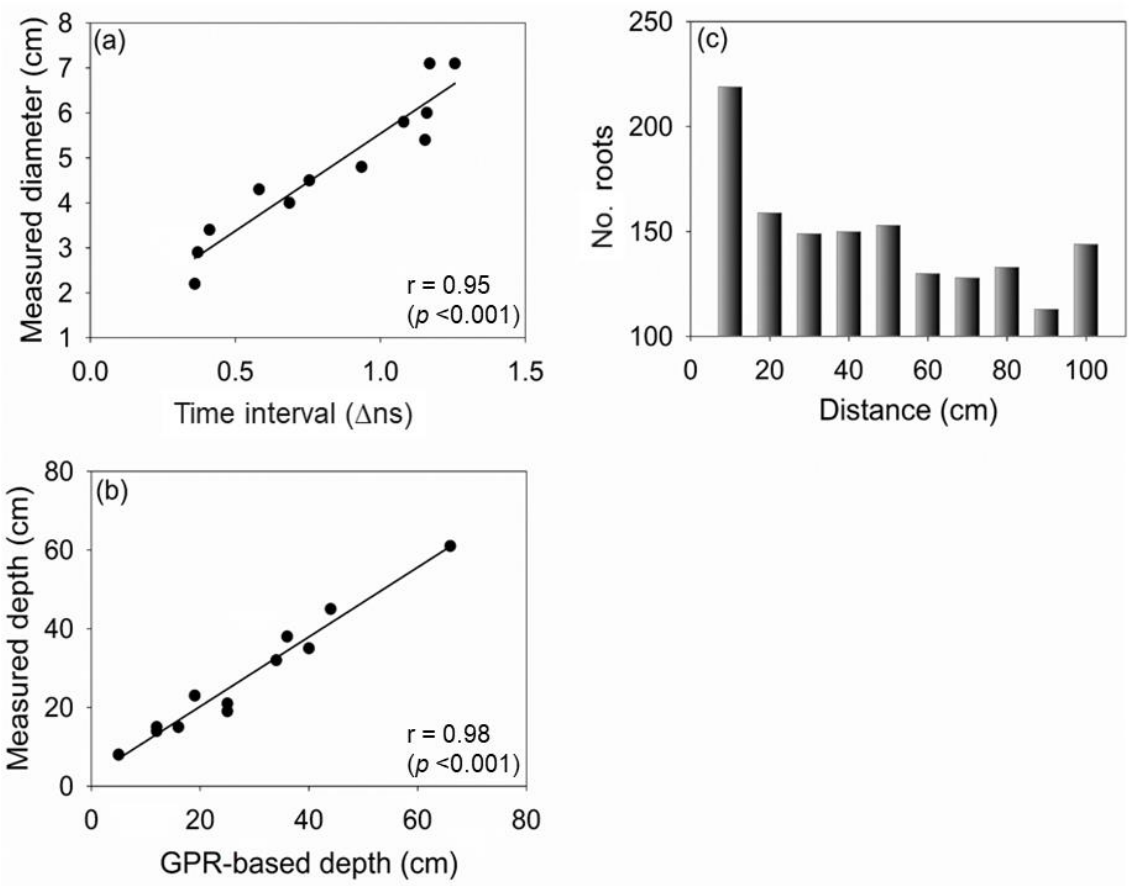

Fig. 4 Calibration of GPR mesurements. a) Relationship between root diameter obtained *in situ* through soil digging and time interval between zero crossing (measured in nanoseconds; Δns) obtained using the GPR radargram (n = 12). b) Relationship between root depth measured *in situ* and root depth inferred by GPR. c) Total number of roots manually detected from GPR radagrams as a function of distance from the tree trunk.

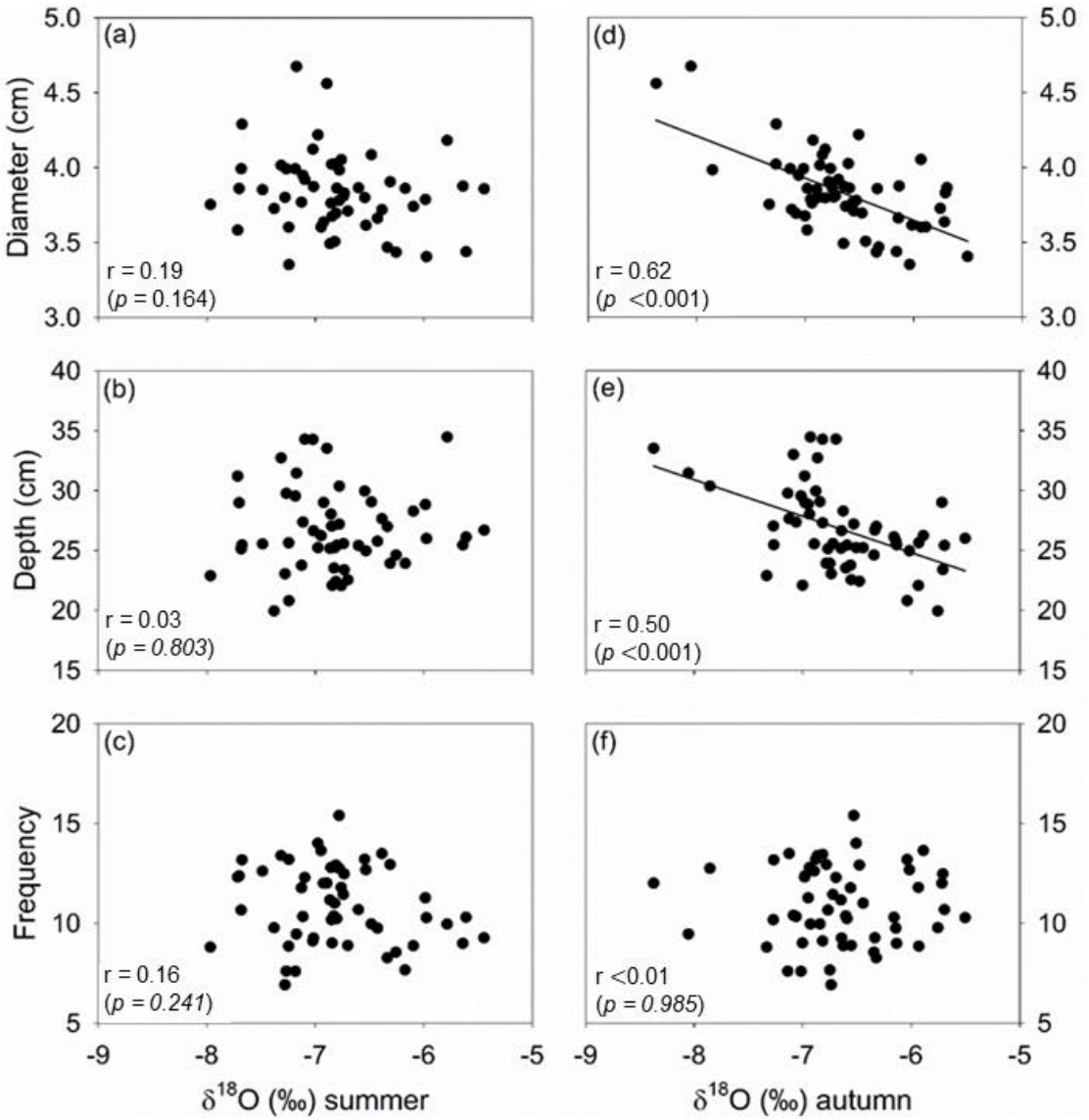

Fig. 5. Simple correlations between GPR-derived population means of root diameter (a, d), root depth (b, e) or root frequency (c, f) and xylem oxygen isotope composition ($\delta^{18}O$) obtained in mid-July (a, b, c) or late-September (d, e, f) of 56 populations of Aleppo pine tested in a common garden in Altura (Spain). Isotopic records were retrieved from Voltas et al. (2015).

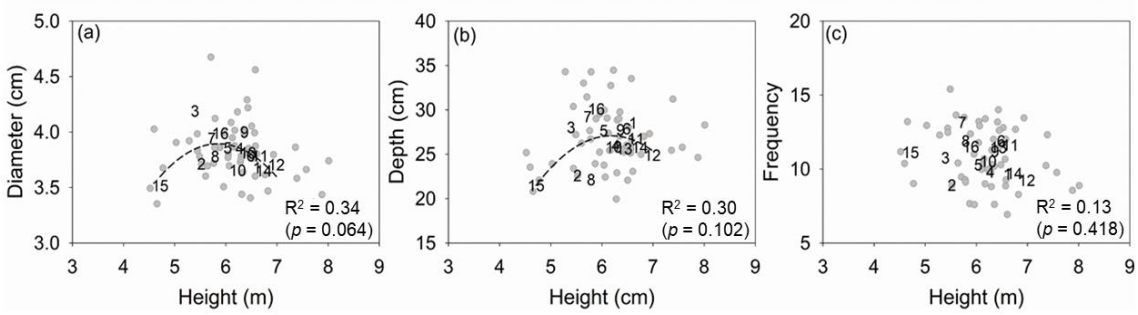

Fig. 6 Regressions of root diameter, depth and frequency as a function of tree height. Data correspond to 56 populations of Aleppo pine (grey dots) grouped into 16 ecotypes (numbers) (ecological region codes are defined in Table S2) and tested in a common garden in Altura (Spain). Each panel shows the regression (linear or quadratic) that better fits the data at ecotype level. Significant ($p \leq 0.05$) and marginally significant ($p \leq 0.10$) regressions are indicated with continuous and dashed lines, respectively. Non-significant regressions are also accompanied by the coefficient of determination (R^2) and associated probability (linear case only).

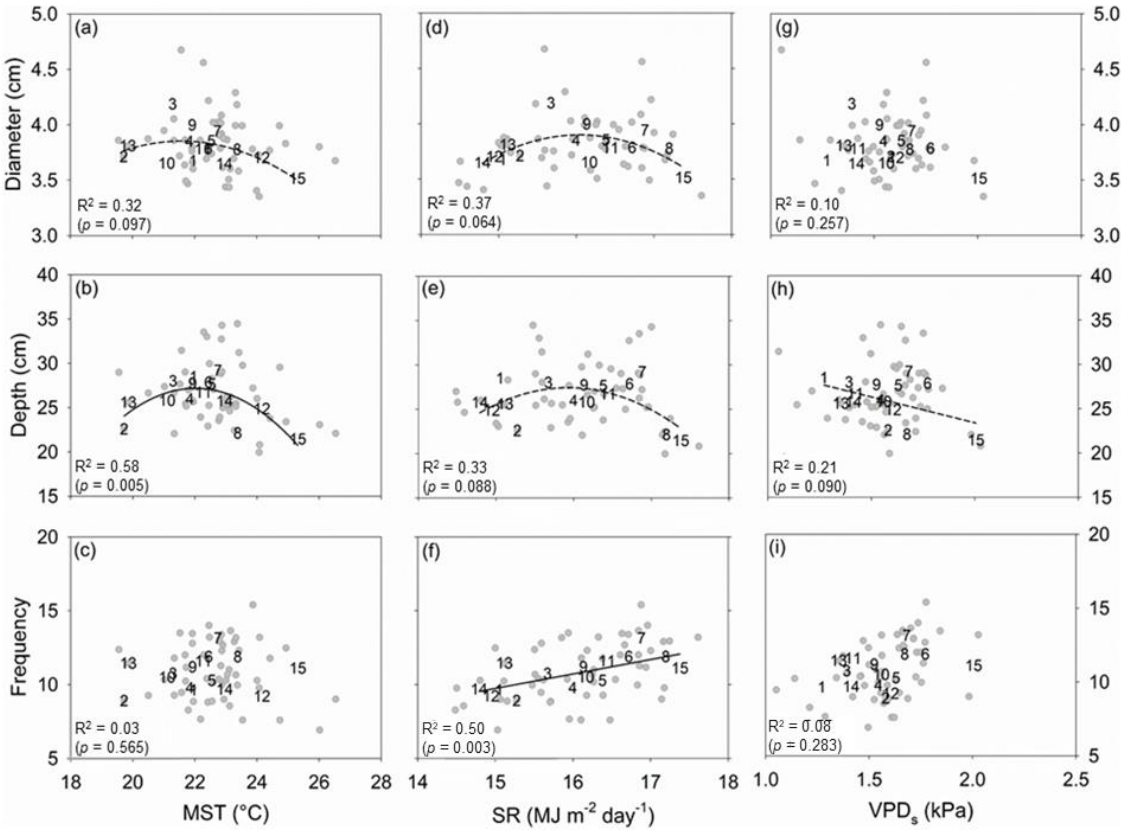

Fig. 7 Regressions of root diameter, depth and frequency as a function of climate variables at the origin of populations: (a, b, c) mean summer temperature (MST), (d, e, f) solar radiation (SR), (g, h, i) summer vapour pressure deficit (VDP_s). Top panels depict regressions for root diameter, central panels for root depth and bottom panels for root frequency. Data correspond to 53 populations of Aleppo pine (grey dots) grouped into 15 ecotypes (numbers) (ecological region codes are defined in Table S2) and tested in a common garden in Altura (Spain). Ecotype 16 (and three associated populations) corresponds to reforestations of uncertain geographic origin of the Northern Spanish Plateau and has not been included in the analysis. Each panel shows the regression (linear or quadratic) that better fits the data at ecotype level. Significant ($p \leq 0.05$) and marginally significant ($p \leq 0.10$) regressions are indicated with continuous and dashed lines, respectively. Non-significant regressions are also accompanied by the coefficient of determination (R^2) and associated probability (linear case only).

Chapter 1 – Supplementary material

Table S1. Soil parameters at the study site located in Altura (Spain).

Soil parameters	Value	Method	Result
pH	8.4	Potentiometry	Moderately basic
Electrical conductivity (dS/m)	0.2	Conductimetry	No limitant
Organic matter (% s.m.s.)	2.8	Calculation	Medium-high
Calcium carbonate equivalent (% s.m.s.)	44.0	Potentiometric titration	Extremely calcareous
N-NO_3 (mg/kg s.m.s.)	<1.0	Colorimetry	Normal
P (mg/kg s.m.s.)	<5.0	Spectrophotometry	Low
K (mg/kg s.m.s.)	234.0	Spectrometry	Normal
Ca (mg/kg s.m.s.)	7464.0	"	High
Mg (mg/kg s.m.s.)	121.0	"	Normal
Na (mg/kg s.m.s.)	<15.0	"	Normal
Fe (mg/kg s.m.s.)	104.0	"	
Cu (mg/kg s.m.s.)	3.5	"	
Mn (mg/kg s.m.s.)	82.0	"	
Zn (mg/kg s.m.s.)	1.8	"	
Sand (0.05 D < 2 mm) (%)	44.2	Gravimetry	
Tick silt (0.02 D < 0.05 mm) (%)	9.5	"	
Fine silt (0.002 D < 0.02 mm) (%)	22.0	"	
Clay (%) (D < 0.002 mm)	24.3	"	

Table S2. Characteristics of the 56 populations of Aleppo pine grouped into 16 ecotypes (or ecological regions) used in this study.

Name of provenances	Population code	Ecological region code	Region	Country	Longitude	Latitude	Altitude	MAT (°C)	MAP (mm)	PsP (%)
Cabanelles	11	1CAT	Catalonia	Spain	2°47'E	42°15'	258	14.6	720	22
Tivissa	21	1CAT	Catalonia	Spain	0°50'E	42°20'	336	14.8	587	21
Sant Salvador Guardiola	31	1CAT	Catalonia	Spain	1°45'E	41°40'	318	14.4	628	26
Zuera	61	2MO	Ebro Depression	Spain	0°55'E	41°55'	576	12.0	474	21
Valdeconcha	82	3ALC	Southern Plateau	Spain	2°52'W	40°27'	837	12.8	433	14
Alcantud	83	3ALC	Southern Plateau	Spain	2°18'W	40°34'	1057	10.8	505	19
Colmenar de Oreja	84	3ALC	Southern Plateau	Spain	3°20'W	40°05'	692	13.7	433	11
Cirat	91	4MS	Iberian Range	Spain	0°28'W	40°03'	445	14.6	440	21
Tuéar	92	4MS	Iberian Range	Spain	1°09'W	39°49'	729	13.2	424	20
Enguidanos	93	4MS	Iberian Range	Spain	1°39'W	39°38'	990	11.9	485	19
Altura	102	4MS	Iberian Range	Spain	0°37'W	39°47'	662	13.1	546	16
Benicàssim	111	4MS	Iberian Range	Spain	0°01'E	40°05'	468	13.8	472	21
Gilet	112	4MS	Iberian Range	Spain	0°21'W	39°40'	152	13.1	462	17
Tibi	101	5LI	East Spain	Spain	0°39'W	38°31'	976	14.8	428	17
Villa de Ves	103	5LI	East Spain	Spain	1°15'W	39°11'	864	14.7	454	18
Jarafuel	104	5LI	East Spain	Spain	1°01'W	39°10'	563	15.2	386	17
Bicorp	105	5LI	East Spain	Spain	0°51'W	39°06'	587	14.7	523	21
Commercial Seed	109	5LI	East Spain	Spain	1°00'W	39°09'		16.6	451	20
Villajoyosa	131	6BS	N. Betic Mts	Spain	0°18'W	38°30'	126	17.7	422	15
Ricote	141	6BS	N. Betic Mts	Spain	1°26'W	38°09'	688	14.8	398	14
Monovar	142	6BS	N. Betic Mts	Spain	0°57'W	38°23'	820	14.0	467	15
Monovar	143	6BS	N. Betic Mts	Spain	0°55'W	38°24'	601	15.1	416	15
Paterna	144	6BS	N. Betic Mts	Spain	2°17'W	38°38'	1028	12.8	470	13
Abarán	145	6BS	N. Betic Mts	Spain	1°16'W	38°17'	657	14.9	403	15
Quéntar	151	7BM	S. Betic Mts	Spain	3°25'W	37°14'	1226	12.8	578	07
Benamaurel	152	7BM	S. Betic Mts	Spain	2°44'W	37°42'	908	14.2	452	10
Vélez Blanco	153	7BM	S. Betic Mts	Spain	2°01W	37°47'	785	14.1	416	12
Santiago de la Espada	154	7BM	S. Betic Mts	Spain	2°28'W	38°14'	842	14.1	432	11
Lorca	156	7BM	S. Betic Mts	Spain	1°32'W	37°52'	831	14.1	427	13
Alhama de Murcia	157	7BM	S. Betic Mts	Spain	3°01'W	37°45'	765	15.0	449	09

Quesada	158	7BM	S. Betic Mts	Spain	1°57'W	37°45'	757	15.1	373	12
Lentergi	171	8SU	South Spain	Spain	3°41'W	36°49'	363	16.7	378	04
Carratraca	172	8SU	South Spain	Spain	4°50'W	36°51'	635	15.4	695	04
Frigiliana	173	8SU	South Spain	Spain	3°55'E	36°49'	595	15.7	456	04
Palma de Mallorca	182	9MA	Majorca	Spain	2°56'E	39°09'	32	16.7	563	14
Santanyí	183	9MA	Majorca	Spain	3°03'E	39°17'	19	16.8	568	14
Alcudia	184	9MA	Majorca	Spain	03°10'E	39°52'	185	15.7	704	15
Calvia	185	9MA	Majorca	Spain	03°08'E	39°33'	243	15.8	526	17
Marcadal	186	10ME	Menorca	Spain	4°10'E	39°58'	85	16.6	613	15
Atàlix	187	10ME	Menorca	Spain	4°03'E	39°55'	67	16.9	608	15
Cala d'Hort	191	11PY	Ibiza	Spain	1°15'E	38°53'	329	15.9	542	16
Ses Salines	192	11PY	Ibiza	Spain	1°24'E	38°50'	10	17.5	443	16
Ses Salandres	193	11PY	Ibiza	Spain	1°20'E	39°03'	65	17.1	467	17
Istaia-eyboia	211	12GR	Greece	Greece	23°31'E	38°44'	53	17.5	506	07
Amfilohia (likely seed orchard)	212	12GR	Greece	Greece	21°18'E	38°53'	429	14.2	975	07
Tatoi-attica	213	12GR	Greece	Greece	23°28'E	38°27'	253	16.3	552	07
Kassandra	214	12GR	Greece	Greece	23°54'E	40°05'	402	14.4	510	13
Gemenos	221	13FR	France	France	5°40'E	43°25'	391	12.4	707	14
Litorale Tarantino	231	14IT	Italy	Italy	17°07'E	40°37'	204	15.2	551	14
Gargano Monte Pucci	232	14IT	Italy	Italy	15°57'E	41°54'	382	14.2	524	17
Gargano Marzini	233	14IT	Italy	Italy	15°51'E	41°330	0	16.1	472	16
Thala	241	15TU	Tunisia	Tunisia	8°39'E	35°34'	948	14.9	467	13
Tabarka	242	15TU	Tunisia	Tunisia	9°04'E	36°30'	287	17.7	558	09
Valbuena de Duero	201	16MC	North Plateau (Reforestation)	Spain	04°16'W	41°39'	825			
Vega de Valdetronco	202	16MC	North Plateau (Reforestation)	Spain	05°04'W	43°35'	820			
Villavieja Tordesillas	203	16MC	North Plateau (Reforestation)	Spain	04°55'W	41°36'	820			

Table S3. Mixed-effects model analysis of variance for coarse root diameter (cm) and depth (cm) for 56 populations of Aleppo pine categorized into 16 ecotypes grown in a common garden in Altura (Spain) for sub-plot sizes (a) S_{50} and (b) S_{250}. Only fixed effects are reported.

(a)

Source of variation	Num. df	Diameter			Depth		
		Den. df	*F*-value	*p* > *F*	Den. Df	*F*-value	*p* > *F*
Block	2	8.5	1.48	0.282	8.7	1.10	0.376
Column	6	11.8	1.04	0.446	11.7	1.37	0.305
Population (P)	55	92.0	0.96	0.563	92.3	0.81	0.080
Ecotype	15	96.6	1.08	0.383	96.3	0.96	0.498
P (Ecotype)	40	94.7	0.90	0.632	94.8	0.72	0.876

(b)

Source of variation	Num. df	Diameter			Depth		
		Den. df	*F*-value	*p* > *F*	Den. Df	*F*-value	*p* > *F*
Block	2	3.5	0.46	0.665	10.8	0.87	0.448
Column	6	10.3	0.62	0.708	94.2	3.00	0.010
Population (P)	55	73.7	1.06	0.404	81.3	1.00	0.478
Ecotype	15	92.3	1.37	0.179	98.8	1.20	0.284
P (Ecotype)	40	82.3	0.97	0.593	88.5	0.96	0.549

Table S4. Coefficients of determination (R^2) of (a) linear and (b) quadratic regressions and their associated probabilities (in parenthesis) of coarse root parameters (diameter, depth and frequency) as a function of three growth variables (Height, DBH, and Crown Area) of 56 populations grouped into 16 ecotypes of Aleppo pine tested in a common garden in Altura (Spain). The regressions are calculated at both population and ecotype level.

(a)	Populations			Ecotypes		
	Height	DBH	Crown Area	Height	DBH	Crown Area
Diameter	0.01 (0.685)	0.01 (0.614)	0.00 (0.874)	0.11 (0.208)	0.06 (0.351)	0.01 (0.695)
Depth	0.01 (0.501)	0.02 (0.294)	0.01 (0.447)	0.01 (0.739)	0.02 (0.604)	0.01 (0.803)
Frequency	0.04 (0.126)	0.03 (0.193)	0.00 (0.994)	0.14 (0.387)	0.09 (0.274)	0.04 (0.481)

(b)	Populations			Ecotypes		
	Height	DBH	Crown Area	Height	DBH	Crown Area
Diameter	0.10 (0.057)	0.05 (0.279)	0.01 (0.756)	0.34 (0.064)	0.23 (0.183)	0.04 (0.748)
Depth	0.05 (0.292)	0.03 (0.398)	0.07 (0.150)	0.30 (0.102)	0.21 (0.220)	0.04 (0.782)
Frequency	0.05 (0.269)	0.04 (0.356)	0.00 (0.999)	0.13 (0.418)	0.14 (0.384)	0.04 (0.762)

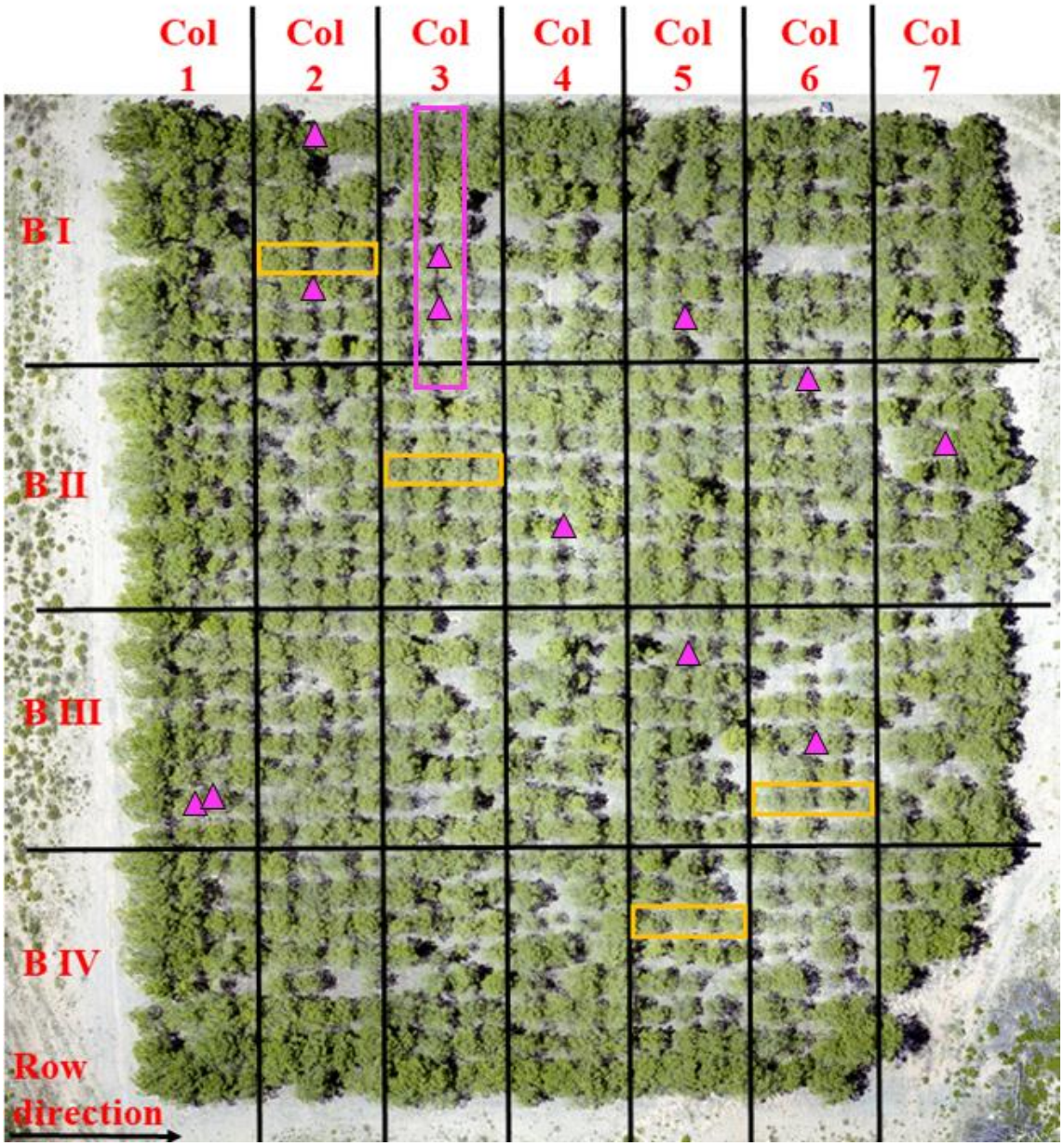

Fig. S1. Aerial view of the common garden of *Pinus halepensis* located in Altura (Castellón province, Spain). The orange rectangles exemplify four experimental units composed of four individuals each belonging to the same population and repeated across four blocks. Blocks (B), columns (Col) and rows within blocks are also indicated corresponding to a Latinised row-column design. The purple triangles indicate the position of 12 excavated roots while the purple rectangle indicates the profile section represented in Fig. 2.

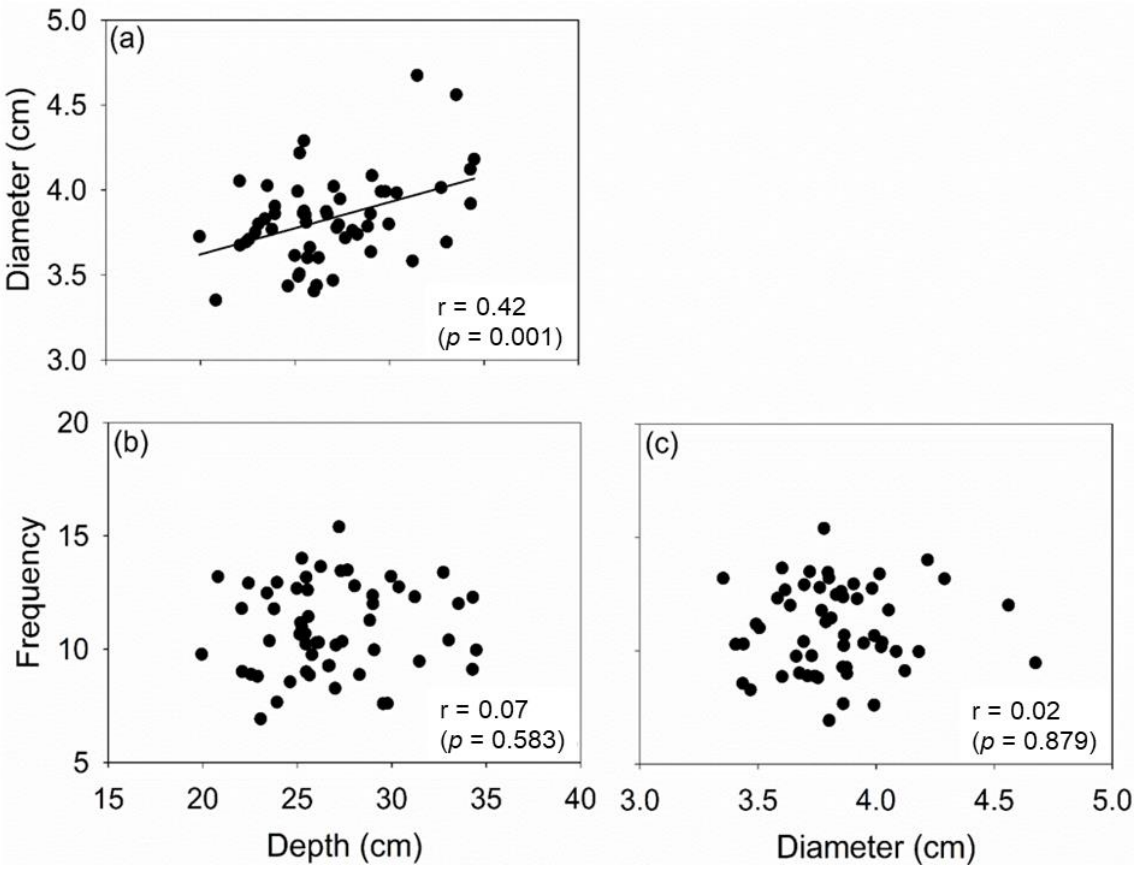

Fig. S2. Simple correlations among coarse root parameters (diameter, depth and frequency): a) root depth *vs*. root diameter, b) root depth *vs*. root frequency, c) root diameter *vs*. root frequency. Data correspond to 56 populations of Aleppo pine tested in a common garden experiment in Altura (Spain). Significant ($p \leq 0.05$) correlations for ecotypes are depicted with a continuous line.

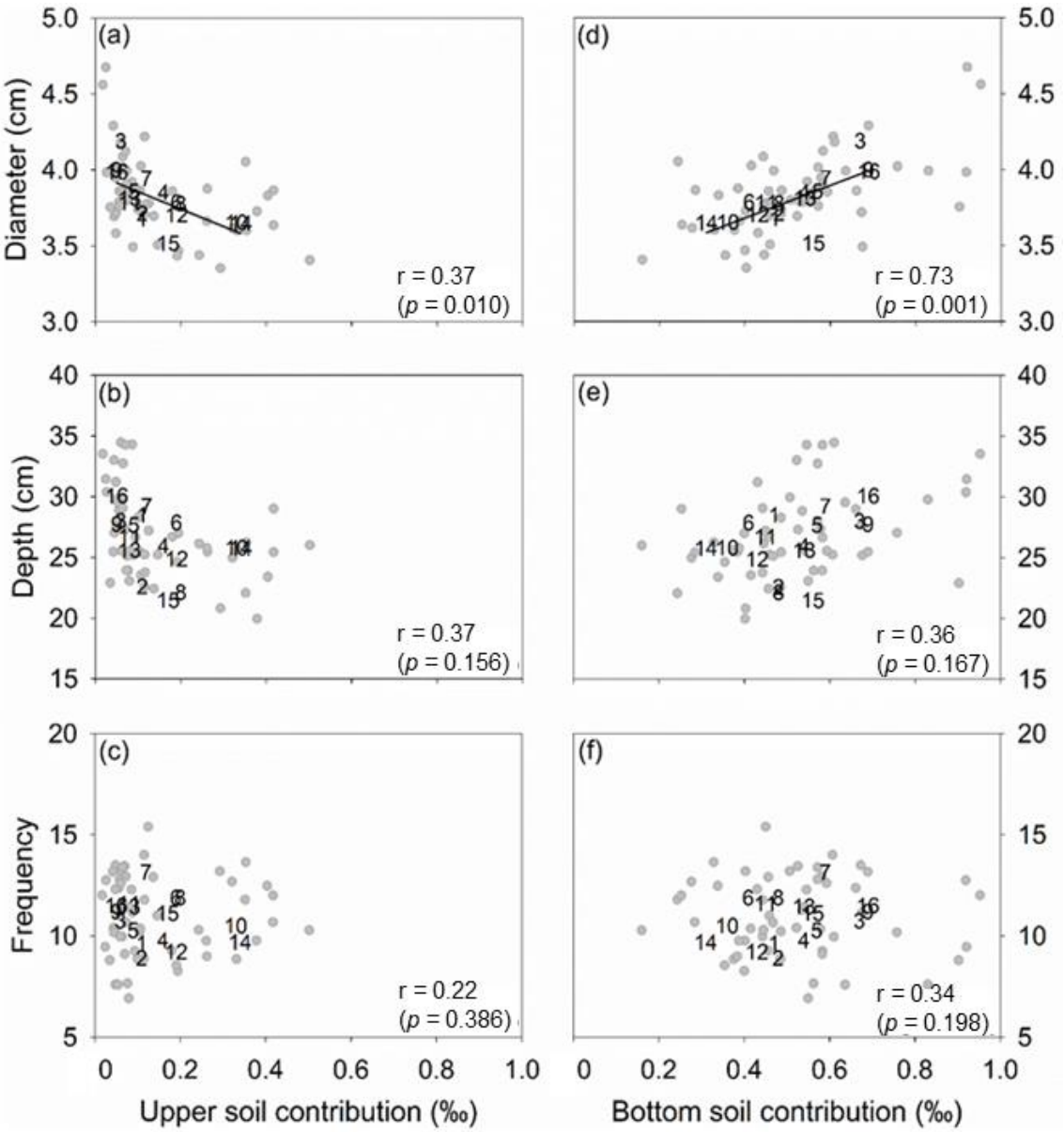

Fig. S3. Relationships between root diameter, root depth or root frequency and the relative water contribution (%) of different soil layers taken up by trees in early autumn inferred from xylem water isotopes in 2010 (Voltas et al. 2015). (a) Upper soil (0-15 cm) vs. diameter. (b) Upper soil vs. depth. (c) Upper soil vs. frequency. (d) Lower soil (15-40 cm) vs. diameter. (e) Lower soil vs. depth. (f) Lower soil vs. frequency. Populations are represented by gray dots and are grouped into 16 ecotypes (code numbers as in Table S2) evaluated in a common garden in Altura (Spain). Significant ($p \leq 0.05$) correlations for ecotypes are depicted with a continuous line.

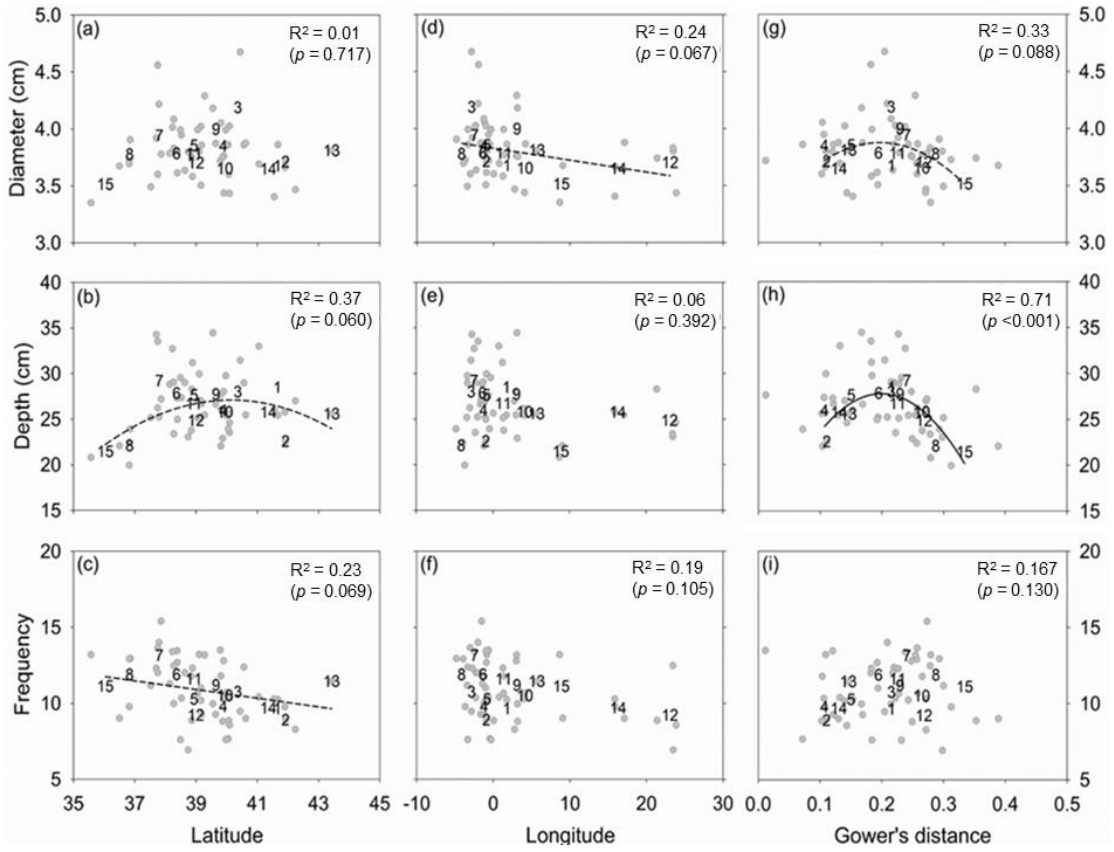

Fig. S4. Regressions of coarse root diameter, depth and frequency as a function of geographic variables at the origin of each population: (a, b, c) latitude, (d, e, f) longitude, and (g, h, i) Gower's distance. Top panels depict regressions for root diameter, central panels for root depth and bottom panels for root frequency. Data correspond to 53 populations of Aleppo pine (gray dots) grouped into 15 ecotypes (numbers) (ecological region codes are defined in Table S2) and tested in a common garden in Altura (Spain). Ecotype 16 (and three associated populations) corresponds to reforestations of uncertain geographic origin of the Northern Spanish Plateau and has not been included in the analysis. Each panel shows the regression (linear or quadratic) that better fits the data at ecotype level. Significant ($p \leq 0.05$) and marginally significant ($p \leq 0.10$) regressions are indicated with continuous and dashed lines, respectively. Non-significant regressions are also accompanied by the coefficient of determination (R^2) and associated probability (linear case only).

Chapter 2

Harnessing tree-ring phenotypes to disentangle gene by environment interactions and their climate dependencies in a circum-Mediterranean pine

Erica Lombardi[1,2,*], Tatiana A. Shestakova[3], Filippo Santini[1,2], Víctor Resco de Dios[1,2], Jordi Voltas[1,2]

[1]Joint Research Unit CTFC – AGROTECNIO – CERCA, Av. Alcalde Rovira Roure 191, Lleida E-25198, España

[2]Departament of Crop and Forest Sciences, University of Lleida, Av. Alcalde Rovira Roure 191, Lleida E-25198, España

[3]Woodwell Climate Research Center, 149 Woods Hole Road, Falmouth, MA 02540, USA

Abstract

Understanding the genetic basis of adaptation and plasticity in trees constitutes a knowledge gap. We linked dendrochronology and genomics (SNPs) for a widespread conifer (*Pinus halepensis* Mill.) to characterise intraspecific growth differences elicited by climate. The analysis comprised 20-yr tree-ring series of 130 trees structured in 23 populations evaluated in a common garden. We tested for genotype by environment interactions (G×E) of indexed ring width (RWI) and early to latewood ratios (ELI) using factorial regression, which describes G×E as differential gene sensitivity to climate. We found that the species' annual growth was positively influenced by winter temperature and spring moisture and negatively influenced by previous autumn precipitation and warm springs. Four and five climate factors explained 10% (RWI) and 16% (ELI) of population-specific interannual variability, respectively, with populations from drought-prone areas and uneven precipitation experiencing larger growth reductions during dry vegetative periods. Furthermore, four and two SNPs explained 14% (RWI) and 10% (ELI) of interannual variability among trees, respectively. Two SNPs played a putative role in adaptation to climate: one identified from transcriptome sequencing of *P. halepensis* and another involved in response regulation to environmental stressors. Our findings highlight how tree-ring phenotypes, obtained from a common garden experiment, combined with a candidate-gene approach allows quantifying genetic and environmental effects determining adaptation for a conifer with a large and complex genome.

Keywords: adaptive variation; common garden; dendroecology; factorial regression; *Pinus halepensis*; phenotypic plasticity; single nucleotide polymorphisms

Introduction

Tree growth performance is limited in dry areas like the Mediterranean region, where seasonal drought along with the intensification in the length, frequency and severity of extreme climate events are limiting ecosystem functioning (Martín-Benito *et al.*, 2010; Forner *et al.*, 2018; Helluy *et al.*, 2020). Changes in the population dynamics of tree species, which are partly linked to migration processes and genetic adaptedness, are therefore expected under future climate (Housset *et al.*, 2018; Royer-Tardif *et al.*, 2021). The pace of genetic adaptations to new conditions, however, is likely to be too slow to conveniently track global warming (Jezkova *et al.*, 2016). At the same time, responses to environmental factors may strongly differ among populations. This is because trees are usually locally adapted because of inter and intraspecific genetic differentiation; in turn, disparate selective pressures also trigger differential plasticity among individuals (Benito Garzón *et al.*, 2011; Grivet *et al.*, 2011). Thus, some populations may have higher adaptive potential than others when facing climate instability. Yet, the prediction of tree responses to future climate is constrained by knowledge gaps on the genetic basis of adaptation as well as on the prevailing climate drivers of growth and survival (Housset *et al.*, 2018).

Pinus halepensis Mill. (Aleppo pine) is a very plastic, drought-resistant conifer able to adjust its growth rate during extended drought periods (Camarero *et al.*, 2010; Pasho *et al.*, 2012). It presents large intraspecific variability in life-history traits (Climent *et al.*, 2008; Voltas *et al.*, 2018; Santini *et al.*, 2019), which is reflected in local adaptations to the different niches inhabited by this species (Patsiou *et al.*, 2020; Hevia *et al.*, 2020). Previous works have demonstrated that the intraspecific variation in traits related to growth (Voltas *et al.*, 2018; Patsiou *et al.*, 2020), wood anatomy (Hevia *et al.*, 2020) or reproduction (Climent *et al.*, 2008) is differentially affected by changing environmental conditions (i.e. differential phenotypic plasticity). To identify the genetic basis of this differentiation, recent studies have targeted single nucleotide polymorphism (SNP) markers (Pinosio *et al.*, 2014) potentially related to adaptive variation (Daniels *et al.*, 2019; Santini et al., 2020). SNPs offer a straight link to gene functions (i.e. candidate gene approach)

without the need to investigate the whole genome (Jaramillo-Correa et al., 2015).

Intraspecific variation in Aleppo pine is customarily examined through functional traits measured at a particular age (Klein et al., 2013; Santini et al., 2019). Trait expression can be therefore considered as the outcome of an individual's response to the environment at a certain time (e.g. physiological attributes), or as the integrative response over an individual's life measured in that particular moment (e.g. morphometric characters). As an alternative, investigating wood growth traits (i.e. secondary growth) in common gardens, in combination with a candidate-gene approach, constitutes an exceptional opportunity to characterise the importance of genetic and environmental effects determining tree performance dynamics on a multi-annual scale (Depardieu et al., 2021). Basic wood features such as tree-ring width are suitable to assess adaptation and plasticity during climate fluctuations (Montwé et al., 2016; Martínez-Sancho et al., 2021) since tree rings reflect climatic sensitivity across the lifespan of individuals (Housset et al., 2016). Additional information on tree growth sensitivity to climate can also be provided by alternative traits such as the relative proportion of early to latewood within a ring since the formation of these wood components is related to the prevailing climate occurring during specific seasonal windows (Torbenson et al., 2016). The early to latewood ratio is particularly informative with regard to the hydraulic and mechanical properties of the main trunk (Domec and Gartner, 2002; De Luis et al., 2011; Novak et al., 2013). A high earlywood to latewood proportion is related to a more conductive wood with wider xylem vessels, whereas a high latewood proportion implies a denser wood. The relative importance of these wood types is mainly determined by rainfall seasonality (i.e. spring to autumn precipitation) and it influences the trade-off among hydraulic conductivity, resistance to cavitation, and mechanical stability of trees (De Luis *et al*., 2011; Camarero *et al*., 2021).

In this study, we analysed the interannual growth patterns of 23 Aleppo pine populations covering most of the species' natural distribution range that were growing in a common garden experiment representative of the average climate conditions for the species. To explore the genetic basis of secondary growth determination, we attempted to link genes and phenotypes structured

in populations with potential climate drivers of growth variability. For this purpose, we tested for genotype by (multi-year) environment interactions (G×E) using ring widths and early to latewood ratios as phenotypic traits. We used a factorial regression approach as a meaningful method for the analysis and interpretation of G×E (van Eeuwijk *et al.*, 2002). Factorial regression allows the inclusion of explicit environmental and genetic information (i.e. covariates) in G×E models along with a direct evaluation (i.e. quantification) of the importance of these covariates for G×E explanation (Malosetti *et al.*, 2013; Sixto *et al.*, 2016). We tested models in which environmental covariables were represented by monthly climate factors and genetic predictors were defined by particular SNPs localized in known candidate genes, aiming at describing G×E through explicit (biophysical and genetic) underlying factors. Importantly, genetic markers allow for investigating the relevance of additive and nonadditive genetic variation in trait expression. Thus, we evaluated different genetic effects (additive, dominant, first-order epistasis) on secondary growth by defining the type of action of candidate genes relevant for the explanation of differential expression across years (Malosetti *et al.*, 2004; Vargas *et al.*, 2006; Calleja-Rodríguez *et al.*, 2021).

We expected a diverse set of interannual growth patterns among populations of Aleppo pine as a result of adaptive divergence, as previously described for many functional traits (e.g. Climent *et al.*, 2008; Martín-Sanz *et al.*, 2019; Lombardi *et al.*, 2021), including secondary growth (Hevia *et al.*, 2020). In particular, we expected populations from warmer and drier origins to be less affected by hot and dry growth periods (i.e. having wider rings and larger early to latewood ratios) compared with their wetter and colder counterparts as the result of local adaptation, in line with previous results in other conifers (Depardieu *et al.*, 2020). We also hypothesised that interannual divergence in secondary growth can be explained, at least in part, by some SNP loci previously linked to morpho-physiological variability of Aleppo pine in the same trial (Santini *et al.*, 2020), thereby modulating adaptive differentiation elicited by climate. This study is novel in the sense that it models G×E interactions of tree growth for a widespread conifer by integrating information on climate and genomics (SNPs associated with candidate genes) at an interannual scale using

tree-ring phenotypes. It benefits from dendrochronological series of secondary growth which constitute archived and readily available phenotypic information in forest trees.

Material and Methods

Genetic trials

The genetic trial (common garden) was established in 1997 and is located in the municipality of Altura (39°49′29″N, 00°34′22″W, 640 m a.s.l; Castellón Province, eastern Spain). The site is representative of the average climate condition of the species distribution range, with a mean annual temperature of 13.8°C and mean annual precipitation of 468 mm (Patsiou *et al.*, 2020; Lombardi *et al.*, 2021). It consists of 896 individual adults of Aleppo pine belonging to 56 populations that cover most of the species' natural distribution range across the Mediterranean basin. Seeds from these populations were collected in 1995 from *ca.* 25 trees spaced at least 100 m apart to minimise the kinship of individuals within populations. Seeds were sown in a forest nursery in Spain and seedlings were planted at the study site at one-year-old at a spacing of 2.5 m following row and column directions. Each experimental unit comprised four individual trees of the same population planted across the same row. The trial was set up according to a Latinised row-column design with four replicates. Out of the 412 surviving trees in November 2019, 130 trees belonging to 23 populations representative of the natural habitat of the species were used because of a thinning treatment conducted in November 2019, where about half of the trees originally presented in the trial had been systematically cut.

Meteorological data

Values of monthly maximum, minimum and mean temperatures (T_{max}, T_{min}, T_{mean}, respectively) as well as monthly precipitation (P) were retrieved from the nearest grid point to the trial location of the gridded climate dataset (Climate Research Unit, CRU TS 4.04 data set, Harris *et al.*, 2020) for 2000–2019. The CRU provides monthly climate series on a 0.5° × 0.5° grid-box basis, interpolated from meteorological stations across the globe. We used this interpolated dataset due

to the lack of continuous local climate records in the area. In addition, the Standardised Precipitation Evapotranspiration Index (SPEI) was used as a measure of drought intensity and was calculated at 1-month and 6-month scales (SPEI1 and SPEI6, respectively) using the package *SPEI* in R (Vicente-Serrano *et al.*, 2010).

For each population origin, mean historical climate records were instead obtained from the higher spatial resolution WorldClim database (Fick and Hijmans, 2017). WorldClim provides averages for 1970–2000 of 19 bioclimatic variables derived from temperature and precipitation records at 30-arcsecond resolution (*ca.*1 km^2). In particular, and based on previous studies of climatic drivers of ecotypic variation in Mediterranean pines (Tapias *et al.*, 2004; Climent *et al.*, 2008), we focused on the mean annual temperature (MAT), mean temperature of the warmest quarter (or summer temperature; MST), mean temperature of the coldest quarter (or winter temperature; MWT), maximum temperature of the warmest month ($T_{max}W$), minimum temperature of the coldest month ($T_{min}C$), mean annual precipitation (MAP), precipitation seasonality (or the coefficient of variation in monthly precipitation over the year, PS), precipitation of the driest quarter (PDQ) and the summer to annual precipitation ratio (PsP).

Tree ring records

For the subset of 130 individuals, we collected cross-sections of about 5 cm thick from the basal part of the trunk. The cross-sections were cut into planks of about 5 cm width, which comprised both ends of each slice, with the pith centred longitudinally. The planks were dried and sanded with progressively finer sandpaper until the surface was smooth enough and the rings were clearly visible.

Tree-ring width was measured with a precision of 0.01 mm through a semi-automatic process in WinDendro 2014a (Regent instrument Inc., Quebec, Canada), and manual corrections were made when necessary. Each tree-ring series was cross-dated and the cross-dating was quality-checked with COFECHA (Holmes 1983). In addition, earlywood width (EW) and latewood width (LW) were estimated using WinDendro coupled with a computer-integrated Leica

binocular microscope (5X zoom). The transition between EW and LW was visually discerned based on changes in wood colour within each ring, where EW corresponded to the light-coloured portion and LW to the darker coloured part of the ring (Griffin *et al.*, 2011; Cabral-Alemán *et al.*, 2017). The EW to LW ratio (EL) was then calculated for each tree ring. Ring-width and EL indices (RWI and ELI hereafter) were obtained for each tree-ring series using the *detrend* function of the R package *dplR* (Bunn, 2008; Bunn *et al*. 2021). To this end, we applied a cubic spline with a 50% frequency cut-off of a wavelength of half the total number of years to remove non-climatic (i.e. ontogenic) trends from each tree-ring series. This procedure generated a stationary (mean = 1) series of dimensionless indices that preserved a common variance encompassing interannual time scales. Afterwards, the master chronology of both indices (i.e. across all available trees and populations) was built through the *crn* function (R package *dplR*) using Tukey's biweight robust mean.

Genetic data

We used a subset of 20 SNPs derived from a dataset of 294 SNPs originally disclosed from comprehensive transcriptome analyses of *P. halepensis* and re-sequenced loci identified in *P. taeda* (Pinosio *et al.*, 2014). The subset of 20 SNPs (Table S2) was selected from a previous genome-wide association study (GWAS) which tested associations among morphological and multispectral-derived physiological traits and genotypes at single loci (Santini *et al.*, 2020). The GWAS analysis was carried out taking into account the neutral genetic structure of populations, thus the subset of SNPs used in our study were previously detected after correction for this structure. As a result, SNPs were found as being directly related to tree growth or indirectly related to (remotely-sensed) leaf area, photosynthetic pigments and leaf water content in Aleppo pine (Santini *et al.*, 2020) (Table S2).

For those SNPs significantly explaining RWI and ELI variability (see *Factorial regression* subsection), we re-examined their associated gene functions (previously described in Santini *et al.*, 2020) through *Blast* tools since sequence databases are continuously updated. The

original SNP sequence (Pinosio *et al.*, 2014) was implemented in the *Blastn* tool and the best match from *Blastn* was then used as the input in the *Blastx* tool. The best result given by *Blastx* was then used to identify the protein function of every SNP based on the protein knowledgebase *UniProtKB* (Boutet *et al.*, 2016).

Statistical analyses

General analyses of variance

To test for differences in tree size among populations, the following mixed model was fitted to trunk diameter records:

$$y_{iklm} = \mu + P_i + B_k + (PB)_{ik} + T(P)_{il} + C_m + e_{iklm} \quad (1)$$

where y_{iklm} is the observation of the *l*th tree of the *i*th population in the *k*th replicate and *m*th column, μ is the general mean, P_i is the fixed effect of the *i*th population, B_k is the fixed effect of replicate *k*, $(PB)_{ik}$ is the random interaction between the *i*th population and *k*th replicate, $T(P)_{il}$ is the fixed effect of the *l*th tree nested to the *i*th population, C_m is the fixed effect of column *m* and e_{iklm} is the random residual effect of the interaction between the *l*th tree nested to the *i*th population, the *m*th column and the *k*th replicate. Equation [1] was fitted to the 130 sampled trees plus those remaining trees belonging to the 23 studied populations after the thinning treatment (i.e. the total of four trees per experimental unit). In all cases, tree diameter at breast height (DBH; 1.30 m height) was measured at the time of thinning.

A second (fixed) model (herein *general model*) was fitted to each tree growth trait (RWI, ELI) testing for population differentiation in annual radial growth patterns as follows:

$$y_{ijl} = \mu + P_i + T(P)_{il} + Y_j + (PY)_{ij} + e_{ijl} \quad (2)$$

where y_{ijl} is the observation of the *l*th tree of the *i*th population in the *j*th year, μ is the general mean, P_i is the fixed effect of the *i*th population, $T(P)_{il}$ is the fixed effect of the *l*th tree nested to the *i*th population, Y_j is the fixed effect of the *j*th year, $(PY)_{ij}$ is the fixed effect of interaction between the *i*th population and the *j*th year, and e_{ijl} is the random residual effect of the interaction

between the *l*th tree nested to the *i*th population and the *j*th year. Since all tree-ring data (RWI and ELI) were detrended (i.e. they shared the same mean value among trees), the terms P_i and $T(P)_{il}$ do not capture any significant variation (as neither do the design factors block and column, which can be saved). This implies that the variability in tree-ring records can be attributed exclusively to interannual fluctuations, Y_j, the interaction between the effects of population and year, $(PY)_{ij}$, and the residual term, e_{ijl}.

Factorial regression

The general equation [2] was expanded to include explicit genetic and environmental (i.e. climatic) covariables to the levels of the tree and year effects, respectively. To this end, we fitted two alternative genotypes by environment interaction (G×E) models using factorial regression approaches (van Eeuwijk *et al.*, 2005 Voltas *et al.*, 2005), which principally focused on the partition of the population by year effects. The first model investigated the genetic basis (SNP [or gene] g_1, …., g_m) of interannual variability in RWI and ELI (herein *genetic model*; equation [3]). The second model aimed at identifying differential population sensitivities of radial growth and early- to latewood ratios to climate drivers (z_1, …, z_p) (herein *climate model*; equation [4]). The order in which covariables are included in the model is relevant for the amount of G×E accounted for by each covariable (provided the explanatory variables are not completely orthogonal). Therefore, we progressively included the different covariables in the models sorted by the amount of G×E explained by each of them until the last significant covariable entered the model, ideally leaving a non-significant population by year residual. Type I (sequential) sum of squares was used for hypothesis testing (Nelder, 1994). In this way, population by year effects were adjusted for genetic effects (equation [3]) or climate factors (equation [4]) using covariables as follows (van Eeuwijk *et al.*, 2005):

$$y_{ijl} = \mu + P_i + T(P)_{il} + Y_j + \sum_{n=1}^{N} g_{ln} Y_{jn} + (PY)_{ij} + e_{ijl} \quad (3)$$

$$y_{ijl} = \mu + P_i + T(P)_{il} + Y_j + \sum_{p=1}^{P} \beta_{ip} z_{jp} + (PY)_{ij} + e_{ijl} \quad (4)$$

where y_{ijl} is the observation of the *l*th tree of the *i*th population in the *j*th year, μ is the general

mean, P_i is the fixed effect of the *i*th population, $T(P)_{il}$ is the fixed effect of the *l*th tree nested to the *i*th population, Y_j is the fixed effect of the *j*th year, $g_{ln}Y_{jn}$ refers to the *n*th gene or covariable (SNP loci; qualitative factor with three levels or genotypes: *aa*, *ab* and *bb*) of the *l*th tree of the *i*th population interacting with the *j*th year in equation [3], β_{ip} is the *i*th population sensitivity to the *p*th climatic covariable *z* for year *j* in equation [4], $(PY)_{ij}$ is the (residual) fixed effect of interaction between the *i*th population and the *j*th year, and e_{ijl} is the random residual effect of the interaction between the *l*th tree nested to the *i*th population and the *j*th year. To facilitate interpretation of the β_i's, the climate covariables were centred to zero means. As an extension of [3], the population structure (Pstr, K=2; Santini et al. 2020) was also incorporated as genetic covariable as additional Pstr × Y term prior to SNP testing.

The *genetic model* (equation [3]) was further expanded to determine the type of gene action of relevant SNPs underlying G×E, that is, additive (A) or dominance (D) effects as well as possible first-order epistasis (van Eeuwijk *et al.*, 2002; Calleja-Rodríguez *et al.*, 2021). Additive and dominance effects were sequentially tested for each SNP individually in equation [3] by creating dummy variables as follows: each SNP loci was coded as (–1, 0, +1) (accounting for additive effects) and (0, +1, 0) or (0, –1, 0) (accounting for dominance effects) at the tree level (van Eeuwijk *et al.*, 2002). Once the type of gene action was identified as significant (either additive or dominant), relevant SNP loci were coded as (0, 1, 2) (additive) or otherwise (1, 1, 0) or (0, 1, 1) (dominant) and added to the final equation [5] below.

First-order epistatic interactions were also evaluated independently for each significant SNP by considering potential gene interactions with other SNPs that were not necessarily relevant themselves for G×E explanation. For this purpose, the SNP term was initially considered a qualitative factor. Afterwards, additive and dominance genetic effects were coded as above per SNP locus and successively tested by considering any possible effect combination between the two SNPs involved in the epistatic effect (additive × additive, additive × dominant, dominant × additive or dominant × dominant), as follows:

$$\sum_{n=1}^{N} g_{ln} Y_{jn} = \sum_{n=1}^{N} g_{(A)ln} Y_{jn} + \sum_{n=1}^{N} g_{(D)ln} Y_{jn} + \sum_{n=1}^{N} g_{(A)ln} g_{(A)ln'} Y_{jn} +$$

$$\sum_{n=1}^{N} g_{(D)ln} g_{(A)ln'} Y_{jn} + \sum_{n=1}^{N} g_{(A)ln} g_{(D)ln'} Y_{jn} + \sum_{n=1}^{N} g_{(D)ln} g_{(D)ln'} Y_{jn} \quad (5)$$

where g_{ln} refers to the nth gene (SNP, quantitative factor, coded as additive, $g_{(A)}$, or dominant, $g_{(D)}$) of the lth tree interacting with the nth gene of the same tree (also coded as additive, $g_{(A)}$, or dominant, $g_{(D)}$) and the jth year. Non-additive and epistatic genetic effects can largely influence phenotypes (Holliday *et al.*, 2012; Du *et al.*, 2015; Calleja-Rodríguez *et al.*, 2021) and it is, therefore, important to consider those effects in G×E models. Since all the genetic factors present in the models follow a hierarchical order (sequential testing), the significance of genetic effects (both single SNP and epistatic) is contingent on the significance of the additive type of gene action. For example, if the SNP effect is dominant, both the additive and the dominant effect would result in significance in the model.

Additionally, the different SNPs and climate factors previously identified in the *genetic* and *climate models* (equations [3] and [4] respectively) were tested as pair combinations of one SNP and one climate factor. If significant, the common variability explained by these factors was included – as an extension of equations [3] and [4] – into models that incorporated a cross-product involving one genetic and one climate variable underlying the population by year and the tree nested to the population by year interaction terms. In this case, population sensitivities β_i to an environmental variable z_j were replaced by a constant, c, times a genetic (SNP) variable, x_i, (β_i = c x_i), where the constant c was estimated from the data. These cross-products allowed us to estimate how particular allelic substitutions affected either the interannual tree growth or the proportion of early to latewood for every unit change in relevant climate factors.

All models were fitted using the MIXED procedure of SAS/STAT (Littell *et al.*, 1998).

Climate-growth associations at the species level and their dependencies on climate at the origin of populations

To determine the main climate drivers of interannual growth for Aleppo pine across populations (i.e. at the species level) we calculated bootstrapped Pearson correlations between the RWI or ELI

master chronology and monthly climate data during 2000–2019. These relationships were analysed from September of the previous year to October of the current year using the *treeclim* R package (Zang and Biondi 2015). Moreover, population sensitivities to relevant climate factors (β_i*'s* as defined in equation [4]) were correlated with climatic characteristics at the origin of populations.

Results

Growth differences among populations

We found significant differences (p<0.05) in DBH among populations at the trial site (Table S3). The populations showing the highest DBH values originated from Greece (Kassandra), southern Italy (Litorale Tarantino) and southern Spain (Monovar), with mean (± SE) trunk diameters of 18.4 ± 1.4, 16.9 ± 1.4 and 16.7 ± 1.3 cm, respectively. On the other hand, the populations with the lowest DBH values were from Tunisia (Tabarka) and Mallorca Island (Santanyí and Palma de Mallorca), with mean values of 11.3 ± 1.4, 11.8 ± 1.5 and 12.1 ± 1.2 cm respectively (Table S4). The relative difference between the most and least grown populations was 63%.

Climate-growth relationships

At the species level (i.e. across populations), RWI was negatively correlated with previous September and current May and June temperatures, as well as with previous November precipitation and SPEI1. On the other hand, January temperature, May precipitation, May and June precipitation as well as the SPEI1, and SPEI6 of late spring and summer (May to August), had positive effects on RWI (Fig. 2). Similar climate factors affected the proportion of latewood relative to earlywood (ELI). Particularly, high temperatures of previous September and current May and June, along with high previous November precipitation and SPEI1, decreased ELI; conversely, high current May and June precipitation and SPEI1 and high current summer SPEI6 (June to August) increased ELI (Fig. 2).

Genetic and climate factors involved in G×E

There was significant year-to-year variability in RWI and ELI that was contingent on population (i.e. significant population by year interaction, Fig. 3). This interaction explained 10% and 16% of the total sum of squares (SS) for RWI (Table 1) and ELI (Table 2), respectively. Four SNPs explained 14% altogether of interannual differentiation in RWI among trees (or G×E, subsumed in population by year and tree nested to the population by year interaction SS; Table 1). These were SNP_{201}, SNP_{151}, SNP_{133} and SNP_{9}, along with two epistatic effects encompassing SNP_{151} and SNP_{133}, as well as SNP_{151} and SNP_{9}. The inclusion of population structure in the genetic models did not substantially change the results (Tables S5 and S6). Alternatively, four climate factors unfolded 38% of the population by year interaction SS for RWI (Table 1): May maximum temperature (accounting for 12% of interaction SS), previous year November precipitation (10%), October SPEI6 (9%) and previous September SPEI1 (8%).

For ELI, SNP_{159} and SNP_{133} and their epistatic effect partly explained interannual tree variability, accounting for 9% of G×E (Table 2). In turn, populations reacted differently to five climate factors, which explained 41% of the population by year interaction term (Table 2): previous November SPEI1 (accounting for 9% of the population by year interaction), previous December precipitation (9%), June mean temperature (8%), March minimum temperature (8%) and September SPEI1 (7%) (Table 2). Both the genetic and climate models had non-significant population by year interaction residuals (except for the genetic model for ELI), thereby indicating the suitability of selected molecular markers and climate factors for the explanation of differential population performance (Tables 1, 2).

Population sensitivities to climate factors and relationships with climate at the origin

Five populations showed a significant RWI sensitivity to May maximum temperature, either positive (two populations) or negative (three populations) relative to a hypothetical average population. Another five populations exhibited a significant (positive or negative) RWI sensitivity to previous November precipitation, and three populations showed a significant RWI sensitivity

to October SPEI6 (Table S7). Regarding ELI, six populations had a significant sensitivity (positive or negative) to previous November SPEI1, while five populations showed a significant sensitivity to previous December precipitation, four populations to previous September SPEI1, three populations to June mean temperature and five populations to March minimum temperature (Table S8).

We found significant associations between population sensitivities to climate at the trial site and climate at the origin of these populations for RWI (Table 5). The temperature was the climate factor most related to these sensitivities, with populations from warmer environments (i.e. with higher MAT and MST) and experiencing more severe winter conditions, (i.e. lower MWT) being less sensitive to high May temperatures, high previous November precipitation and dry growing seasons (October SPEI6) (Table 5, Fig. 4). On the other hand, populations undergoing higher precipitation seasonality (Fig. 4) and lower summer to annual precipitation ratio at origin, as well as those belonging to the southernmost areas of the species distribution range, were more sensitive to dry growing seasons than their wetter counterparts (Table 5). For ELI we did not find relevant associations between population sensitivities to climate and climate at a population's origin (Table S9).

Genes interacting with climate for the explanation of G×E

All individual SNPs included in the genetic models showed additive effects for both RWI and ELI, while two epistatic interactions for RWI had dominant × dominant or dominant × additive gene actions and one epistatic interaction for ELI had a dominant × additive gene action. For RWI, we found significant cross-products between SNP_{201} and two climate factors (May maximum temperature and previous November precipitation). However, only the cross-product between SNP_{201} and previous November precipitation significantly explained the interaction between populations and years (albeit only accounting for 1% of interaction SS, Table 1). For ELI, SNP_{159} significantly interacted with June mean temperature; however, it explained only interannual variability of trees nested to populations, but not among populations (Table 2).

For the abovementioned SNPs, the effect of allelic substitutions as related to climate was estimated. In particular, replacing the C allele with the A allele in SNP_{201} decreased RWI by 0.029 and 0.001 (standardised) units per every 1°C increase in May maximum temperature and every 1 mm increase in previous November precipitation, respectively (Table 4). In turn, replacing the G allele with the A allele in SNP_{159} increased ELI by 0.060 (standardised) units per every 1°C increase in June mean temperature (Table 4). Known gene functions of every SNP with particular relevance in G×E models are annotated in Table 3. For most SNPs, it was possible to retrieve the related biological functions of their associated proteins.

Discussion

Aleppo pine harbours a large variability in life-history traits related to growth, defence and reproduction (Santos-del-Blanco et al 2013), which results in a complex adaptive syndrome that tailors individual performances to the array of conditions encountered by the species (Sbay and Zas, 2018; Santini *et al.*, 2019). It is therefore expected that some populations may respond better to climate instability and warming than others because of the combined effects of local adaptation and differential phenotypic plasticity on functional traits (Voltas *et al.*, 2018; Hevia *et al.*, 2020; Patsiou *et al.*, 2020). Factorial regression provided first-hand information on the genetic basis of differentiation in annual growth responses and their climate drivers for this emblematic Mediterranean conifer. The major novelty of this approach is that it quantified with precision growth variability among individuals explained by particular SNPs while characterizing the relationship between the effect of allele substitutions in dendrophenotypes and climate. In this regard, this approach can be regarded as complementary to methods that analyse high-dimensional genomic information in relation to environmental variables but where phenotypic information is absent (e.g. Redundancy analysis; Capblancq and Forester [2021], Varas-Myrik *et al*. [2022]), or that investigate long-term or specific-year tree-ring traits searching for genotype-phenotype associations but disregarding G×E (Housset et al. 2018).

Climate responses at the species level

Populations with larger trunk diameters were from coastal eastern Mediterranean areas and cool climates, while populations that showed smaller sizes originated from warm and dry areas (Voltas *et al.*, 2018). This observation anticipates that low water availability and high temperatures are the main climatic constraints for Aleppo pine growth (de Luis *et al.*, 2013). At the same time, both factors likely had a variable effect on growth depending on the geographic origin of populations (Patsiou *et al.*, 2020), as suggested by significant population by year interactions for ring width and early to latewood ratio.

At the whole species level (i.e. across populations), annual growth was mainly controlled by late spring (May-June) climate (Pasho *et al.*, 2012; Novak *et al.*, 2013). Water stress in spring, modulated by temperature, is known to negatively affect xylogenesis, thereby inducing a decline in secondary growth as a likely result of meristematic constraints (de Luis *et al.*, 2013; Puri *et al.*, 2015; Gazol *et al.*, 2017; Hevia *et al.*, 2020). In addition, RWI and ELI were influenced negatively by previous September and positively by January temperatures. The former effect is often interpreted as an indication of reserves depletion, hence decreasing secondary growth (Kagawa *et al.*, 2006; Choury *et al.*, 2017) and early to latewood proportion. The latter suggests that this thermophilic pine is constrained by cold winters, which influences its ability to resume cambial activity earlier in the growing season (Camarero *et al.*, 2010; Housset *et al.*, 2018). The negative response of RWI and ELI to previous autumn precipitation (November), earlier reported for the region (Shestakova *et al.*, 2017; Hevia *et al.*, 2020), might be related to the impairment of photosynthesis and, hence, of carbon storage due to prolonged cloudiness. This would lead to a decrease in earlywood and total ring width (Camarero *et al.*, 2010; Royo-Navascués *et al.*, 2021).

How do populations differentially respond to annual climate variability?

Our findings revealed the existence of different radial growth patterns among Aleppo pine populations. This array of growth responses could be related to particular climate factors at the trial site. Therefore, in addition to genetic variation in tree diameter among populations,

adaptation in Aleppo pine appears as partly driven by differential plasticity in secondary growth (Voltas *et al.*, 2018; Hevia *et al.*, 2020; Patsiou *et al.*, 2020). This differential plasticity, as explained by G×E interaction effects, is better related to water availability than to temperature (compare their relevance in the explanation of G×E; cf. Tables 1, 2). This observation broadens previous results on natural stands (as opposed to common garden observations), which anticipate such plastic effects in wood traits for this species (de Luis *et al.*, 2013; Novak *et al.*, 2013).

Some populations were particularly sensitive to one or several climate factors at the trial site. A comparison with their climate responses at origin (i.e. in natural stands), as reported in earlier studies, provides hints on the adaptive significance of such sensitivities. For example, Tabarka (Tunisia) is a population from a sub-humid environment of the Maghreb that was extremely dependent on water availability at the trial site. This suggests that carbohydrates synthetized under favorable conditions (autumn) may be particularly important for spring growth resumption, and is consistent with *in situ* observations indicating that drought during the previous autumn through spring is most limiting for Tunisian Aleppo pine forests (Bachtobji Bouachir *et al.*, 2017). Another population from a sub-humid coastal area (Kassandra, Greece) showed high sensitivity to elevated temperatures during late spring. This is in concord with a previous study indicating that very warm springs strongly limit Aleppo pine growth in Greece due to excessive evapotranspiration rates (Papadopoulos *et al.*, 2001). This performance can be explained by the extreme plasticity of Greek populations adjusting the timing of earlywood formation (Hevia *et al.*, 2020). Conversely, the sensitivity to hot summers in terms of decreased early to latewood ratio detected for dry Iberian populations (e.g. Benicàssim) points to a conservative water-use strategy: a strongly reduced earlywood in unfavourable years is likely indicative of an earlier growth cessation before peak summer and hence higher drought resistance (Hevia *et al.*, 2020; Royo-Navascués *et al.*, 2021).

Variation in population sensitivities to the abovementioned climate factors showed significant associations with climate at origin, suggesting distinct adaptations (George *et al.*, 2019; Depardieu *et al.*, 2020). The observation that populations from warm areas present less

growth reductions under high May temperatures likely reflects specific adaptation to hot springs (Housset *et al.*, 2018). On the other hand, populations from similarly warm areas but experiencing high precipitation seasonality and low summer rainfall were the most growth-sensitive to dry vegetative periods. This counterintuitive finding may be attributed to the combined effect of traits involved in local adaptation to drought, i.e. a particular realisation of the species' adaptive syndrome as materialised in a particular life history strategy (Santini *et al.*, 2019). Hence, these populations may present a strong summer cambial dormancy, thereby decreasing tracheid formation and thus secondary growth during dry periods, improving resistance to embolism (Camarero *et al.*, 2010; De Luis *et al.*, 2011). This agrees with intra-annual density fluctuation (IADF) records from a common garden experiment, in which populations from drier areas experienced more IADFs (Hevia *et al.*, 2020).

Interpreting the genetic basis of secondary growth and its climate dependencies

The differential growth responses among individuals were related to allele-specific expressions of a subset of candidate genes, with four and two SNPs partially explaining annual variability in ring width and the early to latewood ratio, respectively. Despite the limited explanation of G×E effects (<15%), our candidate gene approach proved to be partly effective for unveiling the genetic basis of secondary growth. However, most growth variability related to differential gene expression did not bear a clear population structure, which prevents interpreting such variability in terms of ecotypic differentiation in phenotypic plasticity. In this regard, the traits analysed are very likely under strong polygenic control, as shown for tree height in the taxonomically close *Pinus pinaster* (de Miguel *et al.* 2022). Thus it is likely that many more SNPs may have been involved in the variability of secondary growth, some with very low effect and thus statistically difficult to detect (de Miguel *et al*. 2022). Incorporating a substantially larger amount of candidate genes into G×E modelling approaches that could effectively integrate this high-dimensional genetic complexity (e.g. partial least squares estimation [Vargas *et al*. 2006] or random reaction norm models [Jarquín *et al*. 2014]) could capitalise upon the increasing wealth of genomic and

environmental information available, particularly for pine species with large and complex genomes. On the other hand, factorial regression may be particularly adequate for precise testing and quantification of the role of specific genes of annotated function in the determination of dendrophenotypes (or other longitudinal data) and, hence, for clarifying the existing relations between genomes and phenomes in forest trees.

The interplay between gene markers and climate indicated that two SNPs had putative roles in tree adaptation to climate. SNP_{201} (related to ring width) interacted with previous November precipitation and May maximum temperature. SNP_{201} has been referred to as the *P. halepensis* transcriptome (Pinosio *et al.*, 2014), but the molecular and biological function of its associated gene has not been described so far. Notably, a previous GWAS study conducted in the same common garden (Santini *et al.*, 2020) linked SNP_{201} to variation in photosynthetic rate among trees. Alternatively, SNP_{159} (related to early to latewood ratio) interacted with June mean temperature. Calcium-dependent protein kinases (CDPKs) are associated with a candidate gene corresponding to SNP_{159}. CDPKs constitute a large multigene family involved in metabolic, ion flux and gene expression alteration and related to phytohormone activity, such as the modulation of GA3 homeostasis (Schulz *et al.*, 2013). CPDKs have been shown to play a role in many physiological processes, including development and growth (Asano *et al.*, 2012; Boudsocq *et al.*, 2013). CDPKs are also recognised as positive regulators to environmental stresses (Schulz *et al.*, 2013), with the G allele of SNP_{159} seemingly providing adaptation to high temperatures during the peak growing season for Aleppo pine.

The remaining SNP loci relevant for G×E explanation could not be related to any explicit climate factor, which may indicate the need to screen for alternative temporal windows or environmental records to fully decipher the genetic basis of differential growth plasticity in the species as related to climate. In any case, the biological function of these SNPs is known (except SNP_9), and it is related to growth traits in Aleppo pine (Santini *et al.*, 2020; Table 3). In particular, the gene associated with SNP_{151} encodes for proteins of the PEX family that are involved in photomorphogenesis, which can influence leaf development (Santini *et al.*, 2020) and

photosynthesis (Kaur *et al.*, 2013). These mechanisms may affect the allocation of photosynthetic products to secondary growth throughout the year. On the other hand, the gene corresponding to SNP_{133} (involved in G×E of both RWI and ELI) is associated with polygalacturonases influencing tissue development and defence signals (Rui *et al.*, 2017; Gallego-Giraldo *et al.*, 2020). Interestingly, our study showed that the influence of SNP_{133} on ring width and early to latewood ratio was in both cases dependent on the joint expression of genes associated with SNP_{151} and SNP_{159}, with effects of double dominance and simple dominance, respectively.

Conclusions

This study contributes to improving our knowledge on the genetic basis and climate controls of growth variation of a widespread Mediterranean conifer. The different interannual responses among Aleppo pine populations could be described by climate factors mainly related to water availability, and could be successfully related to differential SNP expression of a subset of candidate genes. We therefore show how tree-ring phenotypes obtained from common garden experiments in combination with a candidate-gene approach constitute a great opportunity to disentangle the importance of genetic and environmental effects determining tree adaptation. While genomic data are now widely used as a source of insight into adaptation patterns for non-model species (Fitzpatrick and Keller, 2015; Sork *et al.*, 2013; Wadgymar *et al.*, 2017; Mahony *et al.*, 2020), this is, to the best of our knowledge, the first attempt to integrate genetic and environmental information into statistical G×E models for a forest tree species by considering longitudinal records of ring width and early to latewood ratio as phenotypic traits. In particular, a major novelty of this study is the possibility to quantify with precision the phenotypic changes attributable to SNPs associated to candidate genes and the associated effect of allelic substitutions in relation to climate variables. Future studies could consider alternative environmental variables that may also drive secondary growth of Aleppo pine (e.g. soil moisture, wind) while integrating a larger set of genetic markers associated with candidate genes. The precise molecular mechanisms underlying the adaptation patterns showed by some individuals carrying certain

allele substitutions could also be a target for future research.

Acknowledgments

We thank Ricardo Alía and Delphine Grivet (CIFOR-INIA) for providing the genomic data.

References

Asano. T., Hayashi, N., Kikuchi, S., Ohsugi, R. (2012). CDPK-mediated abiotic stress signaling. Plant Signal. Behavior. 7, 817–821. https://doi.org/10.4161/psb.20351

Bachtobji Bouachir, B., Khorchani, A., Guibal, F., El Aouni, M.H., Khaldi, A. (2017). Dendroecological study of *Pinus halepensis* and *Pinus pinea* in northeast coastal dunes in Tunisia according to distance from the shoreline and dieback intensity. Dendrochronologia. 45, 62–72. https://doi.org/10.1016/j.dendro.2017.06.008

Benito Garzón, M., Alía, R., Robson, T.M., Zavala, M.A. (2011). Intra-specific variability and plasticity influence potential tree species distributions under climate change. Glob. Ecol. Biogeogr. 20, 766–778. https://doi.org/10.1111/j.1466-8238.2010.00646.x

Boudsocq, M., Sheen, J. (2013). CDPKs in immune and stress signaling. Trends Plant Sci. 18, 30–40. https://doi.org/10.1016/j.tplants.2012.08.008

Boutet, E., Lieberherr, D., Tognolli, M., et al. (2016). UniProtKB/Swiss-Prot, the Manually Annotated Section of the UniProt KnowledgeBase: How to Use the Entry View. In: Edwards D, eds. Plant Bioinformatics: Methods in Molecular Biology. New York: Humana Press. 1374, 23-54. https://doi.org/10.1007/978-1-4939-3167-5_2

Bunn, A.G. (2008). A dendrochronology program library in R (dplR). Dendrochronologia. 26, 115–124. https://doi.org/10.1016/j.dendro.2008.01.002

Bunn, A., Korpela, M., Biondi, F., Campelo, F., Mérian, P., Qeadan, F., Zang, C. (2021). *dplR:* Dendrochronology Program Library in R. R package version 1.7.2, https://CRAN.R-project.org/package=dplR.

Cabral-Alemán, C., Pompa-García, M., Acosta-Hernández, A.C., Zúñiga-Vásquez, J.M., Camarero, J.J. (2017). Earlywood and latewood widths of *Picea chihuahuana* show contrasting sensitivity to seasonal climate. Forests. 8, 1–11. https://doi.org/10.3390/f8050173

Calleja-Rodríguez, A., Chen, Z., Suontama, M., Pan, J., Wu, H.X. (2021). Genomic Predictions With Nonadditive Effects Improved Estimates of Additive Effects and Predictions of Total Genetic Values in *Pinus sylvestris*. Front. Plant Sci. 12, 666820. https://doi.org/10.3389/fpls.2021.666820

Camarero, J.J., Olano, J.M., Parras, A. (2010). Plastic bimodal xylogenesis in conifers from continental Mediterranean climates. New Phytol. 185, 471–480. https://doi.org/10.1111/j.1469-8137.2009.03073.x

Camarero, J.J., Collado, E., Martínez-de-Aragón, J., et al. (2021). Associations between climate and earlywood and latewood width in boreal and Mediterranean Scots pine forests. Trees Struct. Funct. 35, 155–169. https://doi.org/10.1007/s00468-020-02028-0

Capblancq, T., Forester, B.R. (2021). Redundancy analysis: A Swiss Army Knife for landscape genomics. Methods Ecol. Evol. 12, 2298–2309. https://doi.org/10.1111/2041-210X.13722

Choury, Z., Shestakova, T.A., Himrane, H., et al. (2017). Quarantining the Sahara Desert: growth and water-use efficiency of Aleppo pine in the Algerian Green Barrier. Eur. J. For. Res. 136, 139–152. https://doi.org/ 10.1007/s10342-016-1014-3

Climent, J., Prada, M.A., Calama, R., Chambel, M.R., De Ron, D.S., Alía, R. (2008). To grow or to seed: Ecotypic variation in reproductive allocation and cone production by young female

Aleppo pine (*Pinus halepensis*, Pinaceae). Am. J. Bot. 95, 833–842. https://doi.org/10.3732/ajb.2007354

Daniels, R.R., Taylor, R.S., Martínez, S.C.G., et al. (2019). Looking for local adaptation: Convergent microevolution in aleppo pine (P*inus halepensis*). Genes. 10, 673. https://doi.org/10.3390/genes10090673

De Luis, M., Novak, K., Raventós, J., Gričar, J., Prislan, P., Čufar, K. (2011). Cambial activity, wood formation and sapling survival of *Pinus halepensis* exposed to different irrigation regimes. For. Ecol. Manag. 262, 1630–1638. https://doi.org/10.1016/j.foreco.2011.07.013

De Luis, M., Čufar, K., Di Filippo, A., et al. (2013). Plasticity in dendroclimatic response across the distribution range of Aleppo pine (*Pinus halepensis*). *PLoS ONE* 8: e83550. https://doi.org/10.1371/journal.pone.0083550

de Miguel, M., Rodríguez-Quilón, I., Heuertz, M., et al. (2022). Polygenic adaptation and negative selection across traits, years and environments in a long-lived plant species (*Pinus pinaster Ait.,* Pinaceae). Mol. Ecol. 31, 2089–2105. https://doi.org/10.1111/mec.16367

Depardieu, C., Girardin, M.P., Nadeau, S., Lenz, P., Bousquet, J., Isabel, N. (2020). Adaptive genetic variation to drought in a widely distributed conifer suggests a potential for increasing forest resilience in a drying climate. New Phytol. 227, 427–439. https://doi.org/10.1111/nph.16551

Depardieu, C., Gérardi, S., Nadeau, S., et al. (2021). Connecting tree-ring phenotypes, genetic associations and transcriptomics to decipher the genomic architecture of drought adaptation in a widespread conifer. Mol. Ecol. 30, 3898–3917.

https://doi.org/10.1111/mec.15846

Domec, J.C., Gartner, B.L. (2002). How do water transport and water storage differ in coniferous earlywood and latewood? J. Exp. Bot. 53, 2369–2379. https://doi.org/10.1093/jxb/erf100

Du, Q., Tian, J., Yang, X., et al. (2015). Identification of additive, dominant, and epistatic variation conferred by key genes in cellulose biosynthesis pathway in *Populus tomentosa*. DNA Res. 22, 53–67. https://doi.org/10.1093/dnares/dsu040

Fick, S.E., Hijmans, R.J. (2017). WorldClim 2: new 1-km spatial resolution climate surfaces for global land areas. Int. J. Climatol. 37, 4302–4315. https://doi.org/10.1002/joc.5086

Fitzpatrick, M.C., Keller, S.R. (2015). Ecological genomics meets community-level modelling of biodiversity: Mapping the genomic landscape of current and future environmental adaptation. Ecol. 18, 1–16. https://doi.org/10.1111/ele.12376

Forner, A., Valladares, F., Bonal, D., Granier, A., Grossiord, C., Aranda, I. (2018). Extreme droughts affecting Mediterranean tree species' growth and water-use efficiency: The importance of timing. Tree Physiol. 38, 1127–1137. https://doi.org/10.1093/treephys/tpy022

Gallego-Giraldo, L., Liu, C., Pose-Albacete, S., et al. (2020). ARABIDOPSIS DEHISCENCE ZONE POLYGALACTURONASE 1 (ADPG1) releases latent defense signals in stems with reduced lignin content. Proc. Nat. Acad. Sci. USA 117, 3281–3290. https://doi.org/10.1073/pnas.1914422117

Gazol, A., Ribas, M., Gutiérrez, E., Camarero, J.J. (2017). Aleppo pine forests from across Spain show drought-induced growth decline and partial recovery. Agric. For. Meteorol. 232, 186–194.

https://doi.org/10.1016/j.agrformet.2016.08.014

George, J.P., Grabner, M., Campelo, F, et al. (2019). Intra-specific variation in growth and wood density traits under water-limited conditions: Long-term-, short-term-, and sudden responses of four conifer tree species. Sci. Total Environ. 660, 631–643. https://doi.org/10.1016/j.scitotenv.2018.12.478

Griffin, D., Meko, D.M., Touchan, R., Leavitt, S.W., Woodhouse, C.A. (2011). Latewood chronology development for summer-moisture reconstruction in the US Southwest. Tree Ring Res. 67, 87–101. https://doi.org/10.3959/2011-4.1

Grivet, D., Sebastiani, F., Alía, R., et al. (2011). Molecular footprints of local adaptation in two mediterranean conifers. Mol. Biol. Evol. 28, 101–116. https://doi.org/10.1093/molbev/msq190

Harris, I., Osborn, T.J., Jones, P., Lister, D. (2020). Version 4 of the CRU TS monthly high-resolution gridded multivariate climate dataset. Sci. Data. 7, 1–18. https://doi.org/10.1038/s41597-020-0453-3

Helluy, M., Prévosto, B., Cailleret, M., Fernandez, C., Balandier, P. (2020). Competition and water stress indices as predictors of *Pinus halepensis* Mill. radial growth under drought. For. Ecol. Manag. 460, 117877. https://doi.org/10.1016/j.foreco.2020.117877Get rights and content

Hevia, A., Campelo, F., Chambel, R., et al. (2020). Which matters more for wood traits in *Pinus halepensis* Mill., provenance or climate? Ann. For. Sci. 77, 1-24. https://doi.org/10.1007/s13595-020-00956-y

Holliday, J.A., Wang, T., Aitken, S. (2012). Predicting adaptive phenotypes from multilocus

genotypes in sitka spruce (*Picea sitchensis*) using random forest. G3: Genes Genom. Genet. 2: 1085–1093. https://doi.org/10.1534/g3.112.002733

Holmes, R.L. (1983). Computer-assisted quality control in tree- ring dating and measurement. Tree-ring Bull. 43, 69–78.

Housset, J.M., Carcaillet, C., Girardin, M.P., Xu, H., Tremblay, F., Bergeron, Y. (2016). In situ comparison of tree-ring responses to climate and population genetics: The need to control for local climate and site variables. Front. Ecol. Evol. 4, 1–12. https://doi.org/10.3389/fevo.2016.00123

Housset, J.M., Nadeau, S., Isabel, N., et al. (2018). Tree rings provide a new class of phenotypes for genetic associations that foster insights into adaptation of conifers to climate change. New Phytol. 218, 630–645. https://doi.org/10.1111/nph.14968

Jaramillo-Correa, J.P., Rodríguez-Quilón, I., Grivet, D., et al. (2015). Molecular proxies for climate. Genetics 199, 793–807. https://doi.org/10.1534/genetics.114.173252

Jarquín, D., Crossa, J., Lacaze, X., et al. (2014). A reaction norm model for genomic selection using high-dimensional genomic and environmental data. Theor. Appl. Genet. 127, 595–607. https://doi.org/10.1007/s00122-013-2243-1

Jezkova, T., Wiens, J.J. (2016). Rates of change in climatic niches in plant and animal populations are much slower than projected climate change. Proc. Royal Soc. B. Biol. Sci. 283, 1-9. https://doi.org/10.1098/rspb.2016.2104

Kagawa, A., Sugimoto, A., Maximov, T.C. (2006). 13CO2 pulse-labelling of photoassimilates

reveals carbon allocation within and between tree rings. Plant Cell Environ. 29, 1571–1584. https://doi.org/10.1111/j.1365-3040.2006.01533.x

Kaur, N., Li, J., Hu, J. (2013). Peroxisomes and Photomorphogenesis. In: del Río L, eds. *Peroxisomes and their Key Role in Cellular Signaling and Metabolism*. Subcellular Biochemistry. Dordrecht: Springer, 69: 195-211. https://doi.org/10.1007/978-94-007-6889-5_11

Klein, T., Di Matteo, G., Rotenberg, E., Cohen, S., Yakir, D. (2013). Differential ecophysiological response of a major Mediterranean pine species across a climatic gradient. Tree Physiol. 33, 26–36. https://doi.org/10.1093/treephys/tps116

Littell, R.C., Henry, P.R., Ammerman, C.B. (1998). Statistical Analysis of Repeated Measures Data Using SAS Procedures. J. Anim. Sci. 76, 1216–1231. https://doi.org/10.2527/1998.7641216x

Lombardi, E., Ferrio, J.P., Rodríguez-Robles, U., Resco de Dios, V., Voltas, J. (2021). Ground-Penetrating Radar as phenotyping tool for characterizing intraspecific variability in root traits of a widespread conifer. Plant Soil. 468, 319-336. https://doi.org/10.1007/s11104-021-05135-0

Mahony, C.R., MacLachlan, I.R., Lind, B.M., Yoder, J.B., Wang, T., Aitken, S.N. (2020). Evaluating genomic data for management of local adaptation in a changing climate: A lodgepole pine case study. Evol. Appl. 13, 116–131. https://doi.org/10.1111/eva.12871

Malosetti, M., Ribaut, J.M., van Eeuwijk, F.A. (2013). The statistical analysis of multi-environment data: Modeling genotype-by-environment interaction and its genetic basis. Front. Physiol. 4, 1–17. https://doi.org/10.3389/fphys.2013.00044

Malosetti, M., Voltas, J., Romagosa, I., Ullrich, S.E., Eeuwijk, F.A.V. (2004). Mixed models including environmental covariables for studying QTL by environment interaction. Euphytica 137, 139–145. https://doi.org/10.1023/B:EUPH.0000040511.46388.ef

Martín-Benito, D., Del Río, M., Cañellas, I. (2010). Black pine (*Pinus nigra* Arn.) growth divergence along a latitudinal gradient in Western Mediterranean mountains. Ann. For. Sci. 67, 401. https://doi.org/10.1051/forest/2009121

Martín-Sanz, R.C., San-Martín, R., Poorter, H., Vázquez, A., Climent, J. (2019). How does water availability affect the allocation to bark in a mediterranean conifer? Front. Plant Sci. 10, 1–13. https://doi.org/10.3389/fpls.2019.00607

Martínez-Sancho, E., Rellstab, C., Guillaume, F., et al. (2021). Post-glacial re-colonization and natural selection have shaped growth responses of silver fir across Europe. Sci. Total Environ. 779, 146393. https://doi.org/10.1016/j.scitotenv.2021.146393

Montwé, D., Isaac-Renton, M., Hamann, A., Spiecker, H. (2016). Drought tolerance and growth in populations of a wide-ranging tree species indicate climate change risks for the boreal north. Glob. Chang. Biol. 22, 806–815. https://doi.org/10.1111/gcb.13123

Novak, K., de Luís, M., Raventós, J., Čufar, K. (2013). Climatic signals in tree-ring widths and wood structure of *Pinus halepensis* in contrasted environmental conditions. Trees Struct. Funct. 27, 927–936. https://doi.org/10.1007/s00468-013-0845-5

Papadopoulos, A., Serre-Bachet, F., Tessier, L. (2001). Tree ring to climate relationships of Aleppo pine (*Pinus halepensis* Mill.) in Greece. Ecol. Mediterr. 27, 89–98. https://doi.org/10.3406/ecmed.2001.1908

Pasho, E., Camarero, J.J., Vicente-Serrano, S.M. (2012). Climatic impacts and drought control of radial growth and seasonal wood formation in *Pinus halepensis*. Trees Struct. Funct. 26, 1875–1886. http://hdl.handle.net/10261/66161

Patsiou, T.S., Shestakova, T.A., Klein, T., et al. (2020). Intraspecific responses to climate reveal nonintuitive warming impacts on a widespread thermophilic conifer. New Phytol. 228, 525-540. https://doi.org/10.1111/nph.16656

Pinosio, S., González-Martínez, S.C., Bagnoli, F., et al. (2014). First insights into the transcriptome and development of new genomic tools of a widespread circum-Mediterranean tree species, *Pinus halepensis* Mill. Mol. Ecol. Resour. 14, 846–856. https://doi.org/10.1111/1755-0998.12232

Puri, E., Hoch, G., Körner, C. (2015). Defoliation reduces growth but not carbon reserves in Mediterranean *Pinus pinaster* trees. Trees Struct. Funct. 29, 1187–1196. https://doi.org/10.1007/s00468-015-1199-y

Royer-Tardif, S., Boisvert-Marsh, L., Godbout, J., Isabel, N., Aubin, I. (2021). Finding common ground: Toward comparable indicators of adaptive capacity of tree species to a changing climate. Ecol. Evol. 11, 13081–13100. https://doi.org/10.1002/ece3.8024

Royo-Navascues, M., Del Castillo, E.M., Serrano-Notivoli, R., et al. (2021). When density matters: The spatial balance between early and latewood. Forests. 12, 1–17. https://doi.org/10.3390/f12070818

Rui, Y., Xiao, C., Yi, H., et al. (2017). POLYGALACTURONASE INVOLVED IN

EXPANSION3 functions in seedling development, rosette growth, and stomatal dynamics in *Arabidopsis thaliana*. Plant Cell. 29, 2413–2432. https://doi.org/10.1105/tpc.17.00568

Santini, F., Climent, J.M., Voltas, J. (2019). Phenotypic integration and life history strategies among populations of *Pinus halepensis*: an insight through structural equation modelling. *Ann. Bot.* 124, 1161–1171. https://doi.org/10.1093/aob/mcz088

Santini, F., Kefauver, S.C., Araus, J.L., et al. (2020). Bridging the genotype–phenotype gap for a Mediterranean pine by semi-automatic crown identification and multispectral imagery. New Phytol. 229, 245-258. https://doi.org/10.1111/nph.16862

Santos-del-Blanco, L., Bonser, S.P., Valladares, F., Chambel, M.R., Climent, J. (2013). Plasticity in reproduction and growth among 52 range-wide populations of a Mediterranean conifer: Adaptive responses to environmental stress. J. Evol. Biol. 26, 1912–1924. https://doi.org/10.1111/jeb.12187

Sbay, H., Zas, R. (2018). Geographic variation in growth, survival, and susceptibility to the processionary moth (Thaumetopoea pityocampa Dennis & Schiff.) of *Pinus halepensis* Mill. and P. brutia Ten.: results from common gardens in Morocco. Ann. For. Sci. 75: 1-15. https://doi.org/10.1007/s13595-018-0746-2

Schulz, P., Herde, M., Romeis, T. (2013). Calcium-dependent protein kinases: Hubs in plant stress signalling and development. Plant Physiol. 163, 523–530. https://doi.org/10.1104/pp.113.222539

Shestakova, T.A., Camarero, J.J., Ferrio, J.P., Knorre, A.A., Gutiérrez, E., Voltas, J. (2017). Increasing drought effects on five European pines modulate Δ13C-growth coupling along a Mediterranean altitudinal gradient. Funct. Ecol. 31, 1359–1370. https://doi.org/10.1111/1365-

2435.12857

Sixto, H., Gil, P.M., Ciria, P., Camps, F., Cañellas, I., Voltas, J. (2016). Interpreting genotype-by-environment interaction for biomass production in hybrid poplars under short-rotation coppice in Mediterranean environments. GCB Bioenergy. 8, 1124–1135. https://doi.org/10.1111/gcbb.12313

Sork, V.L., Aitken, S.N., Dyer, R.J., Eckert, A.J., Legendre, P., Neale, D.B. (2013). Putting the landscape into the genomics of trees: Approaches for understanding local adaptation and population responses to changing climate. Tree Genet. Genom. 9, 901–911. https://doi.org/10.1007/s11295-013-0596-x

Tapias, R., Climent, J., Pardos, J.A., Gil, L. (2004). Life histories of Mediterranean pines. Plant Ecol. 171, 53–68. https://doi.org/10.1023/B:VEGE.0000029383.72609.f0

Torbenson, M.C.A., Stahle, D.W., Villanueva Díaz, J., Cook, E.R., Griffin, D. (2016). The Relationship between Earlywood and Latewood Ring-Growth Across North America. Tree Ring Res. 72, 53–66. https://doi.org/10.3959/1536-1098-72.02.53

Van Eeuwijk, F.A., Crossa, J., Vargas, M., Ribaut, J.M. (2002). Analysing QTL by environment interaction by factorial regression, with an application to the CIMMYT drought and low nitrogen stress programme in maize. In: M.S. Kang, eds. Quantitative Genetics, Genomics and Plant. 245-256. https://doi.org/10.1079/9780851996011.0245

Van Eeuwijk, F.A., Malosetti, M., Yin, X., Struik, P.C., Stam, P. (2005). Statistical models for genotype by environment data: from conventional ANOVA models to eco-physiological QTL models. Aust. J. Agric. Res. 56, 883–894. https://doi.org/10.1071/AR05153

Varas-Myrik, A., Sepúlveda-Espinoza, F., Fajardo, A., et al. (2022). Predicting climate change-related genetic offset for the endangered southern South American conifer *Araucaria araucana*. For. Ecol. Manag. 504, 119856. https://doi.org/10.1016/j.foreco.2021.119856

Vargas, M., Van Eeuwijk, F.A., Crossa, J., Ribaut, J.M. (2006). Mapping QTLs and QTL x environment interaction for CIMMYT maize drought stress program using factorial regression and partial least squares methods. Theor. Appl. Genet. 112, 1009-1023. https://doi.org/10.1007/s00122-005-0204-z

Vicente-Serrano, S.M., Beguería, S., López-Moreno, J.I. (2010). A multiscalar drought index sensitive to global warming: The standardized precipitation evapotranspiration index. J. Clim. 23, 1696–1718. https://doi.org/10.1175/2009JCLI2909.1

Voltas, J., López-Córcoles, H., Borrás, G. (2005). Use of biplot analysis and factorial regression for the investigation of superior genotypes in multi-environment trials. Eur. J. Agron. 22, 309–324. https://doi.org/10.1016/j.eja.2004.04.005

Voltas, J., Shestakova, T.A., Patsiou, T., di Matteo, G., Klein, T. (2018). Ecotypic variation and stability in growth performance of the thermophilic conifer Pinus halepensis across the Mediterranean basin. For. Ecol. Manag. 424, 205–215. https://doi.org/10.1016/j.foreco.2018.04.058

Wadgymar, S.M., Lowry, D.B., Gould, B.A., Byron, C.N., Mactavish, R.M., Anderson, J.T. (2017). Identifying targets and agents of selection: innovative methods to evaluate the processes that contribute to local adaptation. Methods Ecol. Evol. 8, 738–749. https://doi.org/10.1111/2041-210X.12777

Zang, C., Biondi, F. (2015). Treeclim: An R package for the numerical calibration of proxy-climate relationships. Ecography. 38, 431–436. https://doi.org/10.1111/ecog.01335

Chapter 2 – Tables and Figures

Table 1. Analysis of variance (*general model*) and factorial regression modelling of genotype by environment (G×E) interaction effects using either molecular markers (*genetic model*) or climate information (*climate model*) of indexed ring width (RWI) involving 130 individuals belonging to 23 populations of Aleppo pine grown in a common garden in Altura (Spain).

		RWI				
		general model				
Source	*df*	SS	MS	F-Value	Pr (> F)	R^2 (%)
Population (P)	22	0.14	0.007	0.12	1.000	0.1
Tree (within P)	107	0.63	0.006	0.11	1.000	0.2
Year (Y)	19	131.71	6.932	124.92	< **0.001**	48.5
P × Y	418	26.34	0.063	1.14	**0.043**	9.7
Error (Ɛ)	2033	112.82	0.055			41.5
		G×E partition (genetic model)				
$SNP_{201(A)}$ × Y	19	2.60	0.137	2.58	< **0.001**	1.9
$SNP_{151(A)}$ × Y	19	2.29	0.121	2.28	**0.001**	1.6
$SNP_{151(D)}$ × Y	19	1.34	0.071	1.34	0.150	1.0
$SNP_{133(A)}$ × Y	19	1.00	0.052	0.99	0.469	0.7
$SNP_{133(D)}$ × Y	19	1.22	0.064	1.21	0.236	0.9
$SNP_{9(A)}$ × Y	19	0.86	0.045	0.85	0.646	0.6
$SNP_{151(A)}$ × $SNP_{133(A)}$ × Y	19	1.60	0.084	1.59	**0.050**	1.1
$SNP_{151(D)}$ × $SNP_{133(A)}$ × Y	19	1.57	0.083	1.56	0.058	1.1
$SNP_{151(A)}$ × $SNP_{133(D)}$ × Y	19	1.58	0.083	1.57	0.056	1.1
$SNP_{151(D)}$ × $SNP_{133(D)}$ × Y	19	1.68	0.088	1.67	**0.035**	1.2
$SNP_{151(A)}$ × $SNP_{9(A)}$ × Y	19	1.63	0.086	1.62	**0.044**	1.2
$SNP_{151(D)}$ × $SNP_{9(A)}$ × Y	19	1.92	0.101	1.91	**0.010**	1.4
P × Y	418	24.49	0.059	1.11	0.090	
Error (Ɛ)	1786	94.63	0.053			
		G×E partition (climate model)				
P × T_{max}_May	22	3.24	0.147	2.68	< **0.001**	12.3
$SNP_{201(A)}$ × T_{max} May *between P*	1	0.14	0.141	2.56	0.110	0.5
$SNP_{201(A)}$ × T_{max} May *within P*	1	0.68	0.676	12.28	< **0.001**	0.6
P × P $Nov_{(-1)}$	22	2.52	0.115	2.08	**0.002**	9.6
$SNP_{201(A)}$ × P $Nov_{(-1)}$ *between P*	1	0.22	0.225	4.08	**0.044**	0.9
$SNP_{201(A)}$ × P $Nov_{(-1)}$ *within P*	1	0.00	0.000	-	-	0.0
P × SPEI6 Oct	22	2.29	0.104	1.89	**0.008**	8.7
P × SPEI1 $Sep_{(-1)}$	22	2.03	0.092	1.67	**0.026**	7.7

P × Y	330	16.26	0.049	0.90	0.899
Error (ε)	2031	111.78	0.055		

Significant terms are shown in bold ($p < 0.05$).

Abbreviations: T_{max} May: maximum temperature of May; P $Nov_{(-1)}$: previous November precipitation; SPEI6 Oct: SPEI at 6-months scale of October; SPEI1 $Sep_{(-1)}$: previous September SPEI at 1-month scale

Table 2. Analysis of variance (*general model*) and factorial regression modelling of genotype by environment (G×E) interaction effects using either molecular markers (*genetic model*) or climate information (*climate model*) of indexed early- to latewood ratio (ELI) involving 130 individuals belonging to 23 populations of Aleppo pine grown in a common garden in Altura (Spain).

		ELI				
		general model				
Source	*df*	SS	MS	F-Value	Pr (> F)	R^2 (%)
Population (P)	22	0.05	0.002	0.02	1.000	0.0
Tree (within P)	107	0.18	0.001	0.01	1.000	0.0
Year (Y)	19	86.56	4.556	38.83	< **0.001**	22.2
P × Y	418	63.97	0.153	1.30	< **0.001**	16.4
Error (Ɛ)	2033	238.51	0.120			61.3
		G×E partition (genetic model)				
$SNP_{159(A)}$ × Y	19	4.46	0.244	2.09	**0.004**	1.5
$SNP_{159(D)}$ × Y	19	3.01	0.160	1.40	0.117	1.0
$SNP_{133(A)}$ × Y	19	2.95	0.160	1.37	0.131	1.0
$SNP_{133(D)}$ × Y	19	2.45	0.130	1.14	0.304	0.8
$SNP_{159(A)}$ × $SNP_{133(A)}$ × Y	19	5.69	0.300	2.64	**0.001**	1.9
$SNP_{159(D)}$ × $SNP_{133(A)}$ × Y	19	1.92	0.100	0.89	0.593	0.6
$SNP_{159(A)}$ × $SNP_{133(D)}$ × Y	19	4.59	0.240	2.13	**0.003**	1.5
$SNP_{159(D)}$ × $SNP_{133(D)}$ × Y	19	1.14	0.060	0.53	0.951	0.4
P × Y	399	60.87	0.150	1.35	< **0.001**	
Error (Ɛ)	1900	215.22	0.110			
		G×E partition (climate model)				
P × SPEI1 $Nov_{(-1)}$	22	6.02	0.274	2.34	< **0.001**	9.4
P × Prec $Dec_{(-1)}$	22	6.00	0.273	2.33	< **0.001**	9.4
P × T_{mean} Jun	22	4.90	0.223	1.91	**0.007**	7.7
$SNP159_{(A)}$ × T_{mean} Jun $_{between\ P}$	1	0.00	0.000	-	-	
$SNP159_{(A)}$ × T_{mean} Jun $_{within\ P}$	1	0.93	0.931	7.96	**0.005**	0.3
P × T_{min} Mar	22	5.32	0.242	2.07	**0.003**	8.3
P × SPEI1 Sep	22	4.25	0.193	1.65	**0.029**	6.6
P × Y	309	37.46	0.121	1.04	0.331	
Error (ε)	2031	237.58	0.117			

Significant terms are shown in bold ($p < 0.05$).

Abbreviations: MAT: mean annual temperature; MST: mean summer temperature; MWT: mean winter temperature; $T_{max}W$: maximum temperature of the hottest month; $T_{min}C$: minimum temperature of the coldest month; PS: precipitation seasonality; PDQ: mean precipitation of the driest quarter; PsP: summer to annual precipitation ratio.

Table 3. Annotation of the homologous protein and its biological function of single nucleotide polymorphisms (SNPs) that were informative of either indexed ring width (RWI) or early- to latewood ratio (ELI) variation in the partition of genotype by year effects using factorial regression.

SNP code	Known annotation	Species	Biological function	Trait (GWAS) Santini et. al (2020)
SNP_{9}	Hypothetical protein 2_1014_01	*Pinus pinaster*	-	Crown area
SNP_{133}	Hypothetical protein 2_7803_01: Glycosidase, Hydrolase	*Pinus taeda*	Carbohydrate metabolic process	Water content; height
SNP_{151}	Peroxisome membrane protein 11C	*Morella rubra*	Peroxisome fission; Photomorphogenesis	Leaf area
SNP_{159}	Putative calcium-dependent protein kinase transferase	*Cupressus sempervirens*	Mediates responses to abiotic and biotic stressor.	Height
SNP_{201}	No similarity found	*Pinus halepensis*	-	Photosynthetic pigments

Table 4. Effect of allelic substitutions of selected SNPs on indexed ring width (RWI) and early- to latewood ratio (ELI) for every unit change in (standardized) relevant climate factors following the identification of significant cross-products in factorial regression G×E models of Aleppo pine grown in a common garden in Altura (Spain). Significant terms are shown in bold ($p < 0.05$).

Trait	Estimate	SE	t-value	Pr > |t|
Ring width (RWI)				
SNP_{201}(A) (C→A) × P $Nov_{(-1)}$	-0.001	0.000	-2.020	**0.044**
SNP_{201}(A) (C→A) × T_{max} May	-0.029	0.009	-3.370	**0.001**
Early- to latewood ratio (ELI)				
SNP_{159}(A) (G→A) × T_{mean} Jun	0.060	0.021	2.820	**0.005**

Abbreviations: P $Nov_{(-1)}$: previous November precipitation; T_{max} May: maximum temperature of May; T_{mean} Jun: mean temperature of June.

Table 5. Correlations coefficients between population sensitivities (βs') of indexed ring width (RWI) to four climate factors at the trial site (in row order: maximum temperature of May [T_{max} May], precipitation of previous November [P $Nov_{(-1)}$], SPEI at a 6-months scale of October [SPEI6 Oct], and SPEI at a 1-month scale of previous November [SPEI1 $Sep_{(-1)}$]) and selected climate factors at population origin. Correlation coefficients (*r*) and their associated probabilities (*p*, in parentheses) are shown; bold characters indicate probabilities <0.05.

	Latitude	MAT	MST	MWT	T_{max}HT	T_{min}CM	MAP	PS	PQdr	PsP
T_{max} May	-0.22 (0.327)	0.44 (**0.039**)	0.40 (0.057)	0.41 (**0.048**)	0.22 (0.302)	0.39 (0.066)	-0.23 (0.300)	0.08 (0.725)	-0.15 (0.497)	-0.07 (0.767)
P $Nov_{(-1)}$	-0.34 (0.114)	0.39 (0.066)	0.42 (**0.046**)	0.31 (0.149)	0.32 (0.132)	0.24 (0.271)	-0.15 (0.484)	0.40 (0.059)	-0.32 (0.140)	-0.38 (0.077)
SPEI6 Oct	0.41 (0.053)	-0.62 (**0.002**)	-0.61 (**0.002**)	-0.55 (**0.007**)	-0.37 (0.080)	-0.54 (**0.008**)	0.48 (0.829)	-0.63 (**0.001**)	0.48 (**0.020**)	0.44 (**0.037**)
SPEI1 $Sep_{(-1)}$	0.07 (0.758)	-0.21 (0.324)	-0.10 (0.658)	-0.28 (0.196)	0.05 (0.835)	-0.29 (0.179)	0.13 (0.179)	-0.02 (0.940)	<0.01 (0.982)	0.10 (0.643)

Abbreviations: MAT: mean annual temperature; MST: mean summer temperature; MWT: mean winter temperature; T_{max}W: maximum temperature of the hottest month; T_{min}C: minimum temperature of the coldest month; PS: precipitation seasonality; PDQ: mean precipitation of the driest quarter; PsP: summer to annual precipitation ratio.

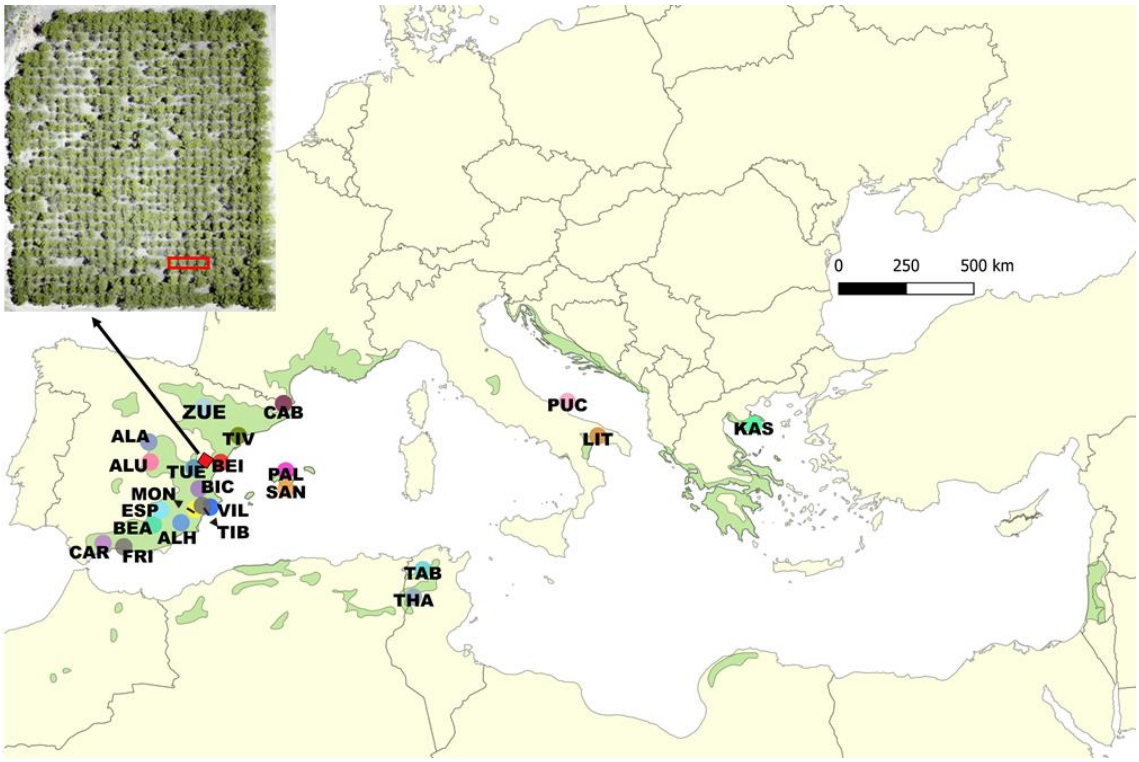

Fig. 1 Geographic origin of 23 Aleppo pine populations (coloured dots) growing in a common garden (black dot) located in Altura (Castellón province, Spain). Population acronyms (described in Table S1) are shown on top of each population origin. The dark green areas represent the natural distribution of Aleppo pine according to EUFORGEN (http://www.euforgen.org/species/pinus-halepensis/). An aerial picture of the trial is also included, where the red rectangle exemplifies an experimental unit consisting of four trees of the same population.

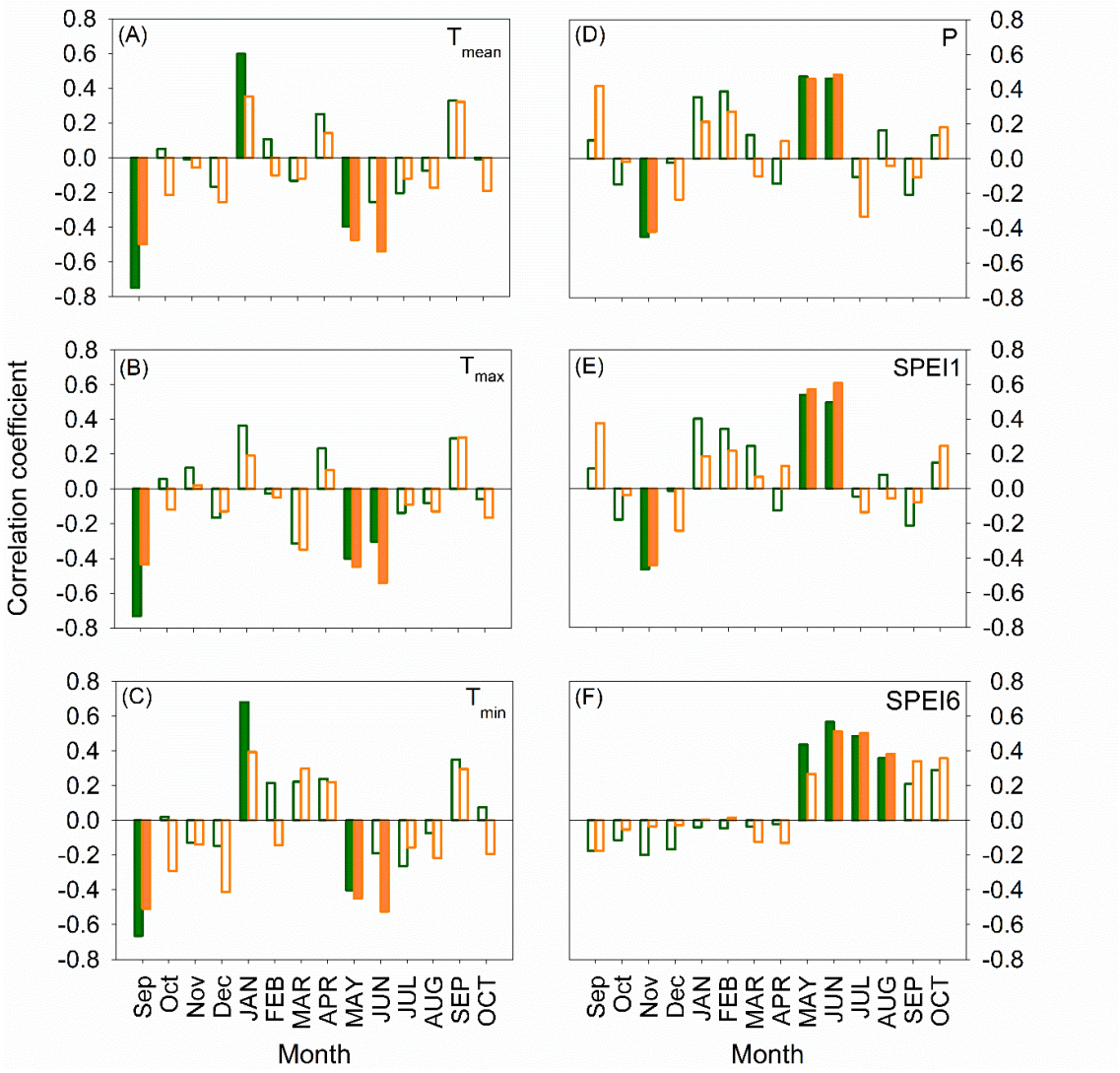

Fig. 2 Bootstrapped correlation coefficients between the master chronology (i.e. obtained across populations) of indexed mean tree ring-width series (green bars) or early to latewood ratio indices (orange bars) and six monthly climate factors calculated from previous September to current October (months of the previous year are indicated with lowercase letters) during the period of 2000–2019. Climate factors were mean temperature (T_{mean}), maximum temperature (T_{max}), minimum temperature (T_{min}), precipitation (P), and SPEI at 1- and 6-months scale (SPEI1 and SPEI6, respectively). Filled bars indicate significant bootstrapped correlations ($p < 0.05$).

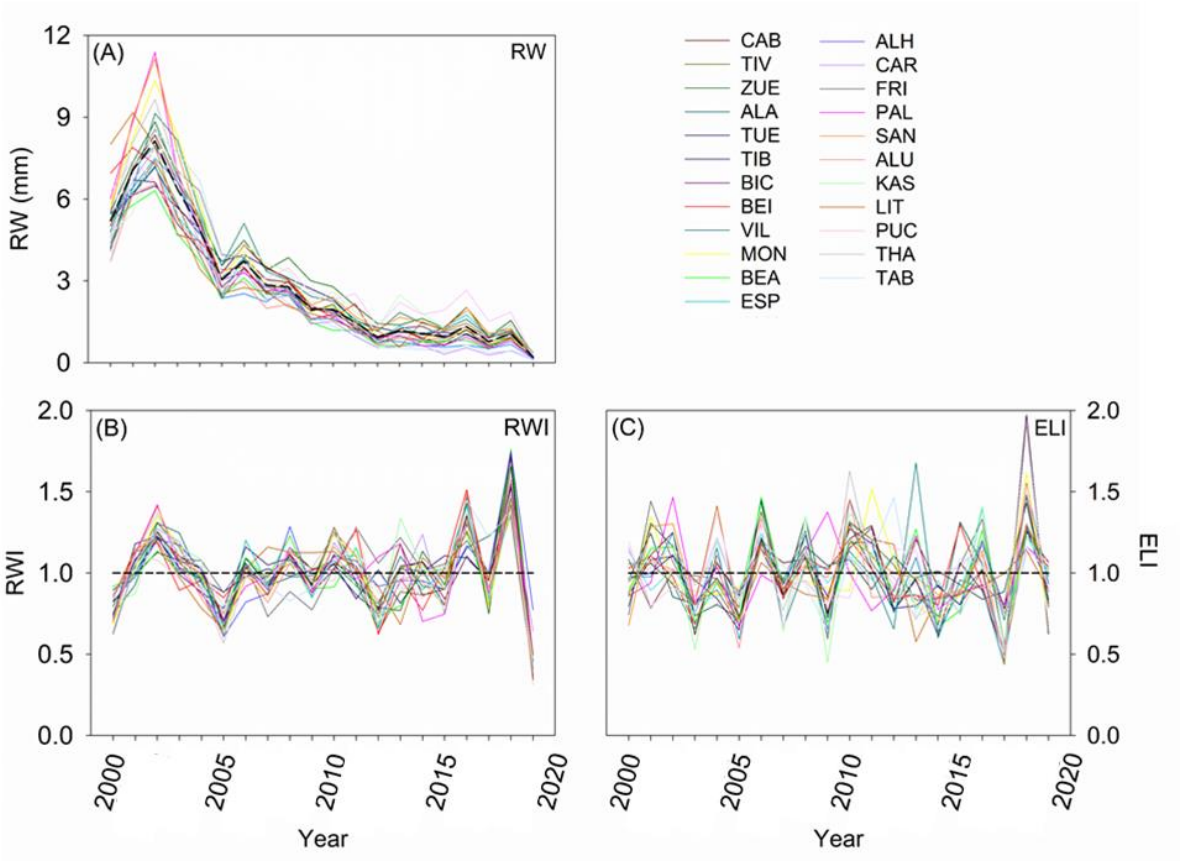

Fig. 3 Interannual population variability of raw tree-ring width (RW; mm) (A), tree ring width index (RWI) (B), and indexed early- to latewood ratio (ELI) (C) of 23 populations of Aleppo pine grown in a common garden in Altura (Spain). Each population is represented by a line of different colour; populations acronyms are listed in the legend and described in Table S1.

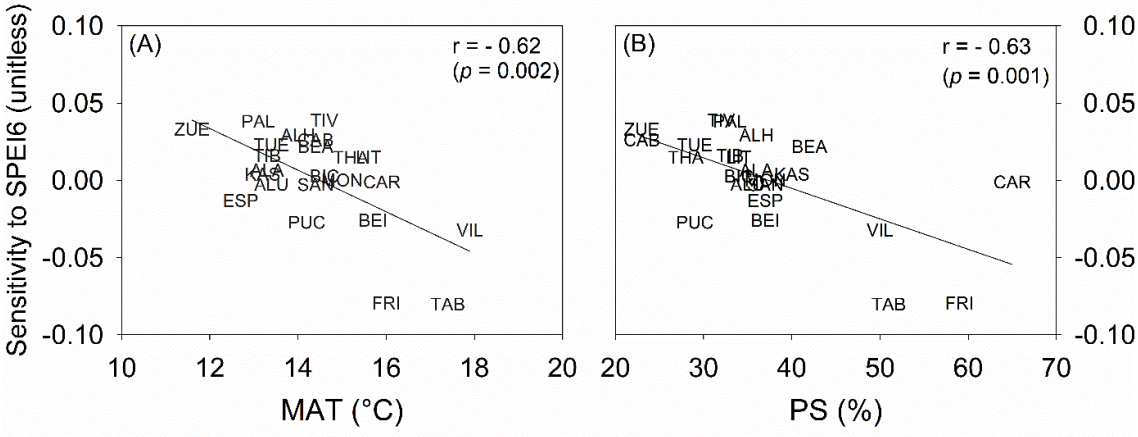

Fig. 4 Correlations between population sensitivities of ring width (RWI) to October SPEI-6 at the trial site and selected climate factors (MAT, mean annual temperature; PS, precipitation seasonality) at the origin of 23 Aleppo pine populations grown in a common garden in Altura (Spain). Population acronyms are defined in Table S1.

Chapter 2 – Supplementary material

Table S1. Characteristics of 23 populations of Aleppo pine grown in a common garden in Altura (Castellón province, eastern Spain).

Name of provenances	Population code	Country	Longitude	Latitude	Altitude	MAT (°C)	MAP (mm)
Kassandra	KAS	Greece	23°54'E	40°05'	402	14.4	510
Tabarka	TAB	Tunisia	9°04'E	36°30'	287	17.8	558
Alcantud	ALA	Spain	2°18'W	40°34'	1057	10.8	505
Alhama de Murcia	ALH	Spain	3°01'W	37°45'	765	15.1	449
Benamaurel	BEA	Spain	2°44'W	37°42'	908	14.2	452
Bicorp	BIC	Spain	0°51'W	39°06'	587	14.7	523
Santiago de la Espada	ESP	Spain	2°28'W	38°14'	842	14.1	432
Tibi	TIB	Spain	0°39'W	38°31'	976	14.8	428
Tuéjar	TUE	Spain	1°09'W	39°49'	729	13.2	424
Carratraca	CAR	Spain	4°50'W	36°51'	635	15.4	695
Frigiliana	FRI	Spain	3°55'E	36°49'	595	15.7	456
Monovar	MON	Spain	0°57'W	38°23'	820	14.0	467
Thala	THA	Tunisia	8°39'E	35°34'	948	14.9	467
Villajoyosa	VIL	Spain	0°18'W	38°30'	126	17.7	422
Cabanelles	CAB	Spain	2°47'E	42°15'	258	14.6	720
Alcudia	ALU	Spain	03°10'E	39°52'	185	15.7	704
Benicàssim	BEI	Spain	0°01'E	40°05'	468	13.8	472
Litorale Tarantino	LIT	Italy	17°07'E	40°37'	204	15.2	551
Palma de Mallorca	PAL	Spain	2°56'E	39°09'	32	16.7	563
Gargano Monte Pucci	PUC	Italy	15°57'E	41°54'	382	14.2	524
Santanyí	SAN	Spain	3°03'E	39°17'	19	16.8	568
Tivissa	TIV	Spain	0°50'E	42°20'	336	14.8	587
Zuera	ZUE	Spain	0°55'E	41°55'	576	12.0	474

Table S2. Annotation of the homologous protein and its known biological function of single nucleotide polymorphisms (SNPs) that were not informative of either indexed ring width (RWI) or early- to latewood ratio (ELI) variation in the partition of genotype by year effects using factorial regression.

SNP code	Accession	Known annotation	Species	E-value *Blastx*	Biological function	ID Sequence (Pinosio *et al.*, 2014)	Trait of GWAS Santini et. al (2020)
SNP_{2}	XP_019422240.1	Glyco_trans_20 domain-containing protein	*Lupinus angustifolius*	3,00E-28	Trehalose biosynthetic process. Catalytic activity	6890-2409	Crown area
SNP_{9}	ATP72615.1	Hypothetical protein 2_1014_01	*Pinus pinaster*	4,00E-98	-	2_1014_01-183	Crown Area
SNP_{18}	ACJ09662.1	Putative calcium-dependent protein kinase	*Cupressus sempervirens*	9,00E-45	-	CL2332Contig1_01-316	Height
SNP_{67}	ATP65193.1	Hypothetical protein : 0_7454_01	*Pinus pinaster*	4,00E-75	-	0_7454_01-210	Photosynthetic pigments
SNP_{91}	Anonymous locus genomic sequence	/	*Pinus nigra*	-	-	0_13957_02-252	Water content
SNP_{108}	AEW08319.1	Hypothetical protein : 2_6351_01	*Pinus radiata*	7,00E-92	Hsp70 protein binding. Ribosome binding	2_6351_01-114	Leaf area; Water content; Height
SNP_{133}	AFG57437.1	Hypothetical protein 2_7803_01: Glycosidase, Hydrolase	*Pinus taeda*	2,00E-93	Carbohydrate metabolic process	2_7803_01-178	Water Content; Height

SNP_{140}	AAC32124.1	Rac-like GTP binding protein	*Picea Mariana*	4,00E-132	GTPase mediated signal transduction	16593-1162	Canopy temperature
SNP_{151}	KAB1214439.1	Peroxisome membrane protein 11C	*Morella rubra*	1,00E-19	Peroxisome fission; Photomorphogenesis	0_8992_01-119	Leaf area
SNP_{159}	ACJ09662.1	Putative calcium-dependent protein kinase transferase	*Cupressus sempervirens*	6,00E-09	Mediates responses to abiotic and biotic stressor.	cpK3-134	Height
SNP_{201}	*P. halepensis* transcriptome	No similarity found	*Pinus halepensis*	-	-	9519-1324	Photosynthetic pigments
SNP_{206}	AHX59161.2	GPD-mannose phrophosphorylase	*Pinus taeda*	2,00E-88	Nucleotidyltransferase activity	10381-1617	Height
SNP_{217}	AHX59161.2	Hypothetical protein : 0_4394_01	*Pinus pinaster*	1,00E-57	-	0_4394_01-352	Height
SNP_{241}	ATP71577.1	Hypothetical protein : 0_4105_01	*Pinus pinaster*	0,01	-	0_4105_01-175	Leaf area
SNP_{250}	*P. halepensis* transcriptome	/	*Pinus halepensis*	-	-	8256-2343	Height
SNP_{258}	AJP06341.1	Auxin efflux carrier component	*Pinus tabuliformis*	0,00	Auxin-activated signalling pathway. Transmembrane transport	9882-2209	Photosynthetic pigments

SNP_{265}	*P. halepensis* transcriptome	/	*Pinus halepensis*	-	-	47393-248	Water content
SNP_{273}	AEW70215.1	Cellulose synthase	*Pinus sylvestris*	8,00E-15	Cellulose biosynthetic process	7485-4551	Leaf area; Height
SNP_{340}	ABR15469.1	GDP-mannose pyrophosphorylase	*Pinus taeda*	0,00	Biosynthetic process	10381-827	Height
SNP_{350}	AEX11977.1	Uncharacterised protein	*Pinus taeda*	2,00E-78	-	0_18322_01-50	Leaf area; Water content; Height

Table S3. Analysis of variance (fixed effects only) of DBH measurements at age 23 years old for 23 populations of Aleppo pine grown in a common garden in Altura (Spain).

Source	*df*	SS	F-Value	Pr (> F)
Block	3	44.52	1.03	0.398
Column	6	324.46	3.74	0.001
Population	22	647.03	2.04	0.005

Table S4. Least squares means for DBH of 23 Aleppo pine populations (age 23 years old) grown in a common garden in Altura (Spain).

Population	Population Code	Mean (cm)	SE
Cabanelles	CAB	15.8	1.28
Tivissa	TIV	13.8	1.22
Zuera	ZUE	12.1	1.33
Alcantud	ALA	14.4	1.30
Tuéjar	TUE	14.6	1.37
Tibi	TIB	13.5	1.28
Bicorp	BIC	14.4	1.24
Benamaurel	BEA	14.8	1.24
Villajoyosa	VIL	14.0	1.47
Monovar	MON	16.7	1.35
Benamaurel	BEA	13.0	1.39
Santiago de la Espada	ESP	15.7	1.26
Alhama de Murcia	ALH	15.2	1.37
Carratraca	CAR	12.1	1.39
Frigiliana	FRI	14.1	1.47
Palma de Mallorca	PAL	12.1	1.24
Santanyí	SAN	11.8	1.55
Alcudia	ALU	12.5	1.74
Kassandra	KAS	18.4	1.38
Litorale Tarantino	LIT	16.9	1.39
Gargano Monte Pucci	PUC	14.6	1.13
Thala	THA	12.6	1.39
Tabarka	TAB	11.3	1.40

Table S5. Factorial regression modelling of genotype by environment (G×E) interaction effects using molecular markers (genetic model) of indexed ring width (RWI), incorporating the population structure as genetic covariable, involving 130 individuals belonging to 23 populations of Aleppo pine grown in a common garden in Altura (Spain).

	RWI *(genetic model)*					
Source	*df*	SS	MS	F-Value	Pr (> F)	R^2 (%)
Population structure (Pstr)	1	0.00	0.001	0.02	0.882	0.0
Population (P)	22	0.13	0.006	0.11	1.000	0.0
Tree-within-P	107	0.60	0.006	0.11	1.000	0.2
Year (Y)	19	129.32	6.806	128.52	**<0.001**	48.1
Pstr × Y	19	0.80	0.416	0.79	0.727	0.6
$SNP_{201(A)}$ × Y	19	2.96	0.156	2.95	**< 0.001**	2.1
$SNP_{151(A)}$ × Y	19	2.15	0.113	2.14	**0.003**	1.5
$SNP_{151(D)}$ × Y	19	1.15	0.061	1.15	0.298	0.8
$SNP_{133(A)}$ × Y	19	0.97	0.051	0.97	0.495	0.7
$SNP_{133(D)}$ × Y	19	1.12	0.059	1.11	0.189	0.8
$SNP_{9(A)}$ × Y	19	0.85	0.045	0.85	0.334	0.6
$SNP_{151(A)}$ × $SNP_{133(A)}$ × Y	19	1.47	0.077	1.46	0.091	1.0
$SNP_{151(D)}$ × $SNP_{133(A)}$ × Y	19	1.52	0.080	1.51	0.072	1.1
$SNP_{151(A)}$ × $SNP_{133(D)}$ × Y	19	1.49	0.078	1.48	0.082	1.1
$SNP_{151(D)}$ × $SNP_{133(D)}$ × Y	19	1.69	0.089	1.70	**0.031**	1.2
$SNP_{151(A)}$ × $SNP_{9(A)}$ × Y	19	1.59	0.084	1.59	0.052	1.1
$SNP_{151(D)}$ × $SNP_{9(A)}$ × Y	19	1.67	0.088	1.66	**0.036**	1.2
P × Y	418	23.91	0.057	1.08	0.153	
Error (Ɛ)	1729	91.56	0.053			

Significant terms are shown in bold ($p < 0.05$).

Table S6. Factorial regression modelling of genotype by environment (G×E) interaction effects using molecular markers (genetic model) of indexed early to latewood ratio (ELI), incorporating the population structure as genetic covariable, involving 130 individuals belonging to 23 populations of Aleppo pine grown in a common garden in Altura (Spain).

	ELI *(genetic model)*					
Source	*df*	SS	MS	F-Value	Pr (> F)	R^2 (%)
Population structure (Pstr)	1	0.00	0.000	0.00	0.992	0.0
Population (P)	22	0.04	0.002	0.02	1.000	0.0
Tree-within-P	107	0.13	0.001	0.01	1.000	0.0
Year (Y)	19	89.97	4.735	44.84	**<0.001**	24.3
Pstr × Y	19	3.24	0.171	1.62	**0.044**	1.1
$SNP_{159(A)}$ × Y	19	6.94	0.365	3.46	**<0.001**	2.4
$SNP_{159(D)}$ × Y	19	2.60	0.137	1.29	0.177	0.9
$SNP_{133(A)}$ × Y	19	1.91	0.101	0.95	0.517	0.7
$SNP_{133(D)}$ × Y	19	1.43	0.075	0.71	0.810	0.5
$SNP_{159(A)}$ × $SNP_{133(A)}$ × Y	19	3.31	0.174	1.65	**0.038**	1.2
$SNP_{159(D)}$ × $SNP_{133(A)}$ × Y	19	2.59	0.136	1.29	0.177	0.9
$SNP_{159(A)}$ × $SNP_{133(D)}$ × Y	19	5.54	0.291	2.76	**<0.001**	1.9
$SNP_{159(D)}$ × $SNP_{133(D)}$ × Y	19	1.14	0.060	0.57	0.930	0.4
P × Y	399	52.08	0.130	1.24	**0.003**	
Error (Ɛ)	1843	194.62	0.106			

Significant terms are shown in bold ($p < 0.05$).

Table S7. Population sensitivities (β's) of ring width index (RWI) to relevant climate factors according to factorial regression models for Aleppo pine grown in a common garden in Altura (Spain). Significant (and marginally significant) correlations are indicated by †$p \leq 0.10$; *$p \leq 0.05$; **$p \leq 0.001$. Population acronyms are defined in Table S1. Abbreviations: T_{max} May: maximum temperature of May; P $Nov_{(-1)}$: precipitation of previous November; SPEI6 Oct: SPEI at 6-month scale of October; SPEI1 $Sep_{(-1)}$: SPEI at 1-month scale of previous September.

	RWI climate sensitivities (unitless)			
Population code	T_{max} May	P $Nov_{(-1)}$	SPEI6 Oct	SPEI1 $Sep_{(-1)}$
KAS	-0.07*	0.03	0.00	0.05*
TAB	0.05*	0.05*	-0.08**	-0.03
ALA	-0.04*	-0.03	0.01	0.04†
ALH	-0.01	0.00	0.03	-0.03
BEA	0.03	-0.04	0.02	-0.04
BIC	0.00	-0.02	0.00	-0.03†
ESP	0.00	0.01	-0.01	0.05*
TIB	-0.01	0.00	0.02	-0.01
TUE	0.06*	0.04†	0.02	-0.05*
CAR	-0.03	-0.02	0.00	0.03
FRI	0.02	0.07*	-0.08**	-0.05*
MON	-0.03	-0.01	0.00	0.04
THA	0.02	-0.01	0.01	0.02
VIL	0.04	0.06*	-0.03	-0.01
CAB	-0.05*	0.00	0.03	0.00
ALU	-0.01	-0.04	0.00	0.01
BEI	0.02	-0.03	-0.03	0.01
LIT	0.07**	-0.01	0.01	-0.02
PAL	-0.04	0.04	0.04	0.00
PUC	0.01	-0.01	-0.03	-0.02
SAN	-0.02	0.01	0.00	0.03
TIV	-0.01	-0.04*	0.04*	0.02

ZUE	0.00	-0.05*	0.03	-0.01

Table S8. Population sensitivities (β's) of indexed early to latewood ratio (ELI) to relevant climate factors according to factorial regression models for Aleppo pine grown in a common garden in Altura (Spain). Significant (and marginally significant) correlations are indicated by †$p \leq 0.10$; *$p \leq 0.05$; **$p \leq 0.001$. Population acronyms are defined in Table S1. Abbreviations: SPEI1 Nov$_{(-1)}$: SPEI at 1-month scale of previous September; P Dec$_{(-1)}$: precipitation of previous December; T_{mean} Jun: mean temperature of June; T_{min} Mar: minimum temperature of March; SPEI1 Sep$_{(-1)}$: SPEI at 1-month scale of previous September.

	ELI climate sensitivities (unitless)				
Population code	SPEI1 Nov$_{(-1)}$	P Dec$_{(-1)}$	T_{mean} Jun	T_{min} Mar	SPEI1 Sep$_{(-1)}$
KAS	-0.03	-0.01	-0.06†	0.02	-0.08*
TAB	0.07*	-0.05	0.05†	-0.06†	0.02
ALA	-0.04	0.07*	-0.02	0.06*	0.02
ALH	0.03	-0.01	0.02	-0.07*	-0.03
BEA	0.00	-0.04	0.03	-0.09*	0.01
BIC	-0.03	0.01	0.01	0.00	0.07*
ESP	0.01	0.01	-0.04	0.01	-0.08*
TIB	-0.08*	-0.02	-0.04	0.07*	0.02
TUE	-0.03	0.05	0.02	-0.03	-0.03
CAR	0.07*	0.11*	0.05	0.03	-0.01
FRI	-0.07*	0.02	-0.03	0.04	0.01
MON	0.03	-0.04	-0.05	0.04	-0.04
THA	-0.12**	0.04	-0.03	-0.02	-0.01
VIL	-0.03	-0.02	0.05	0.01	0.02
CAB	0.02	-0.02	-0.08*	0.01	-0.03
ALU	-0.01	0.04	0.02	0.00	0.01
BEI	0.02	-0.06*	-0.09*	0.08*	0.02
LIT	0.03	0.08*	0.09*	-0.05†	-0.02
PAL	0.09*	0.01	0.04	-0.02	0.05
PUC	0.04	-0.10**	0.01	-0.03	-0.02

SAN	0.01	0.00	-0.01	0.02	0.04
TIV	-0.01	0.01	0.03	-0.04	-0.03
ZUE	0.04	-0.05	0.03	0.00	0.10*

Table S9. Correlations coefficients between population sensitivities of indexed early- to latewood ratio (ELI) to five climate factors at the trial site (in order: SPEI at 1-month scale of previous November [SPEI1 $Nov_{(-1)}$], precipitation of previous December [P $Dec_{(-1)}$], mean temperature of Jun [T_{mean} Jun], minimum temperature of March [T_{min} Mar] and SPEI at 1-month scale September [SPEI1 Sep]) and different climate factors at population origin. Correlation coefficients (*r*) and their associated probabilities (*p*, in parentheses) are shown.

	Latitude	MAT	MST	MWT	T_{max}HT	T_{min}CM	MAP	PS	PQdr	PsP
SPEI1 $Nov_{(-1)}$	0.27 (0.220)	0.02 (0.935)	-0.02 (0.915)	0.05 (0.808)	-0.07 (0.752)	0.12 (0.594)	0.32 (0.141)	0.11 (0.608)	0.03 (0.897)	-0.10 (0.643)
P $Dec_{(-1)}$	-0.22 (0.307)	0.01 (0.972)	0.09 (0.668)	-0.04 (0.865)	0.22 (0.309)	-0.07 (0.738)	0.05 (0.738)	0.25 (0.254)	-0.26 (0.229)	-0.27 (0.220)
T_{mean} Jun	-0.07 (0.751)	0.23 (0.291)	0.26 (0.224)	0.18 (0.393)	0.24 (0.259)	0.17 (0.437)	-0.06 (0.772)	0.22 (0.315)	-0.29 (0.175)	-0.25 (0.241)
T_{min} Mar	0.08 (0.700)	-0.05 (0.817)	-0.19 (0.383)	0.03 (0.887)	-0.24 (0.278)	0.04 (0.843)	0.02 (0.942)	0.13 (0.566)	-0.01 (0.971)	0.21 (0.339)
SPEI1 Sep	0.06 (0.779)	-0.02 (0.936)	-0.03 (0.882)	-0.03 (0.900)	0.10 (0.643)	-0.06 (0.767)	-0.24 (0.262)	-0.05 (0.812)	-0.09 (0.675)	0.18 (0.413)

Abbreviations: MAT = mean annual temperature; MST = mean summer temperature; MWT = mean winter temperature; T_{max}W = maximum temperature of the hottest month; T_{min}C = minimum temperature of the coldest month; PS = precipitation seasonality; PDQ = mean precipitation of the driest quarter; PsP = summer to annual precipitation ratio

Chapter 3

UAV-LiDAR and RGB Imagery Reveal Large Intraspecific Variation in Tree-level Morphometric Traits Across Different Pine Species Evaluated in Common Gardens

Erica Lombardi[1,2,*], Francisco Rodríguez-Puerta[3], Filippo Santini[1,2], Maria Regina Chambel[4], José Climent[4], Víctor Resco de Dios[1,2] and Jordi Voltas[1,2]

1 Joint Research Unit CTFC – AGROTECNIO – CERCA, Av. Alcalde Rovira Roure 191, Lleida E-25198, Spain

2 Department of Crop and Forest Sciences, Av. Alcalde Rovira Roure 191, Lleida E-25198, Spain

3 EiFAB-iuFOR, Campus Deques de Soria s/n, Universidad de Valladolid, Soria E-42004, Spain

4 Centro de Investigación Forestal (CIFOR-INIA-CSIC). Ctra. de La Coruña km 7.5, Madrid E-28040, Spain

* Correspondence: erica.lombardi@udl.cat; Tel.: +34 973702226

Abstract

Remote sensing is increasingly used in forest inventories. However, its application to assess genetic variation in forest trees is still rare, particularly in conifers. Here we evaluate the potential of LiDAR and RGB imagery obtained through unmanned aerial vehicles (UAVs) as high-throughput phenotyping tools for the characterization of tree growth and crown structure in two representative Mediterranean pine species. To this end, we investigated the suitability of these tools to evaluate intraspecific differentiation in a wide array of morphometric traits for Pinus nigra (European black pine) and Pinus halepensis (Aleppo pine). Morphometric traits related to crown architecture and volume, primary growth, and biomass were retrieved at tree level in two genetic trials located in central Spain, and compared with ground-truth data. Both UAV-based methods were then tested for their accuracy to detect genotypic differentiation among black pine and Aleppo pine populations and their subspecies (black pine) or ecotypes (Aleppo pine). The possible relation between intraspecific variation of morphometric traits and life-history strategies of populations was also tested by correlating traits to climate factors at origin of populations. Finally, we investigated which traits distinguished better among black pine subspecies or Aleppo pine ecotypes. Overall, the results demonstrate the usefulness of UAV-based LiDAR and RGB records to disclose tree architectural intraspecific differences in pine species potentially related to adaptive divergence among populations. In particular, three LiDAR-derived traits related to crown volume, crown architecture and main trunk or, alternatively, the latter (RGB-derived) two traits discriminated the most among black pine subspecies. In turn, Aleppo pine ecotypes were partly distinguishable using two LiDAR-derived traits related to crown architecture and crown volume, or three RGB-derived traits related to tree biomass and main trunk. To conclude, remote sensing derived-traits related to main trunk, tree biomass, crown architecture and crown volume were associated to environmental characteristics at origin of populations of black pine and Aleppo pine, which hints to divergent environmental stress-induced local adaptation to drought, wildfire and snowfall in both species.

Keywords: Aleppo pine; black pine; crown architecture; climate adaptation; intraspecific variability; LiDAR; remote sensing; RGB

Introduction

Progress in characterizing intraspecific differentiation in morpho-physiological traits of forest trees can substantially increase our knowledge on their adaptability to environmental changes. Aboveground features such as total height, crown volume and crown structure are strongly influenced by environmental factors such as temperature, light availability, precipitation or wind (Poorter et al. 2021; Voltas et al. 2018), and also by disturbances like fire or insect outbreaks (Karna et al. 2019; Grote et al. 2016; Ordóñez et al. 2005). They are also under genetic control and therefore subject to genotype by environment interactions (Lombardi et al. 2022). Genetic changes and their associated interactions with the environment ultimately produce different phenotypes among individuals of the same species, and forest genetic trials are of paramount interest for understanding such phenotypic variation.

A major limitation when phenotyping forest trees in their adult stage in the context of evolutionary studies or breeding programs is the inherent complexity and time-consuming process of field-based measurements (Liao et al. 2022; Leite et al. 2020; Ganz et al. 2019). In this regard, high-throughput-phenotyping techniques have been developed in the last decade from different remote sensing tools (Ganz et al. 2019; Camarretta et al. 2020). In particular, light detection and ranging (LiDAR) and red, green blue (RGB) imagery are effective tools with enough resolution for routine forestry applications (Liu et al. 2020; Moe et al. 2020).

RGB cameras are often mounted on unmanned aerial vehicles (UAVs), thereby providing aerial images of the visible spectrum (400-700 nm). By overlapping RGB images it is possible to indirectly derive a point cloud holding 3D information. Airborne LiDAR scanning systems can be mounted on different platforms, including aircrafts or UAVs. LiDAR provides accurate 3D information about forest canopy cover since laser pulses can penetrate through vegetation. LiDAR is often considered as a more effective approach than RGB imagery for the acquisition of stand and individual tree traits, because it provides detailed information not only on the top of the tree crown, but also about the underlying branches and ancillary crown architecture (Ganz et al. 2018; Mielcarek et al. 2020). However, RGB cameras can be mounted in smaller UAVs and are cheaper than LiDAR, which makes it a more practical and convenient tool in some circumstances. LiDAR and RGB imagery are already replacing traditional field-based measurements in certain forest operations such as forest

inventories (Liao et al.2022; Goodbody et al. 2019), but the application of these technologies for the purpose of assessing phenotypic variation in genetic trials of forest species has been only seldom reported in the literature (Camarretta et al. 2020; Solvin et al. 2020; Santini et al. 2019a).

In this study we investigate the accuracy of these remote sensing approaches (LiDAR- and RGB-based) mounted on UAVs to estimate commonly measured phenotypic traits such as tree height and biomass, but also other more complex traits related to crown architecture and volume. Particularly, we sought to evaluate if both remote sensing tools are valid to assess intraspecific differentiation in phenotypic traits of pine species. Previous attempts to assess the usefulness of these UAV-borne approaches have been restricted to hardwoods such as Eucalyptus spp. (Camarretta et al. 2020) or conifers such as *Picea abies* (Solvin et al. 2020) or *Pseudotsuga menziesii* (du Toit et al. 2020). However, studies simultaneously evaluating both methods for their accuracy as phenotyping tools of forest genetic trials are still scarce (Ganz et al. 2019), and non-existent in pines.

In this context, we hypothesized that traits related to aboveground growth such as total height, trunk diameter (derived from allometric equations, taking into account crown area and total tree height) and tree biomass of adult pines can be estimated with similar accuracy using UAV-based remote sensing systems (LiDAR- and RGB-based) compared to traditional field-methods, but more promptly. We also hypothesized that UAV-LiDAR and (in a lower degree) UAV-RGB can provide reliable information of complex traits related to canopy architecture and canopy volume, whose estimation with traditional-field methods is time-consuming and not very efficient (Colaço et al. 2017). To test these hypotheses, we obtained remote sensing data of two Mediterranean pine species, *Pinus nigra* Arn. (European black pine) and *Pinus halepensis* Mill. (Aleppo pine), from two provenance genetic trials (or common gardens) located in central-western Spain. By using provenance trials, we aimed to describe intraspecific genetic variation in morphological traits derived from traditional field-based and high-throughput methods. In a common garden trees of the same species, but belonging to different populations with different geographic origins grow under similar environmental conditions, thus it is possible to characterize intraspecific differentiation by analyzing relevant phenotypic traits which, in turn, may be potentially informative of tree adaptability to external factors such as climate.

Here we focused on two widespread conifers of the Mediterranean basin, black pine and Aleppo pine, that present different evolutionary histories and adaptive divergence (Tapias et al. 2004).

Black pine is a non-serotinous, drought-sensitive species that exits at altitudes ranging from 350 m to 2200 m (Enescu et al. 2016; Isajev et al. 2003). Different subspecies have been recognized (Isajev et al. 2003; Santini et al. 2019b): *P. nigra salzmannii* (Dunal) is found in the Iberian Peninsula and southern France areas; *P. nigra nigra* (Höss) is present in the Apennines, Alps, Balkan Mountains and Greece; *P. nigra pallasiana* (Lamb.) covers areas in Greece and Turkey; *P. nigra dalmatica* is found in some areas of Croatia; *P. nigra laricio* (Poiret) inhabits the Corsica island; finally, *P. nigra calabrica* (Murray) is present in south Italy, although this subspecies is often considered as *P. nigra* subsp. *laricio*. Previous studies have documented intraspecific variation in miscellaneous traits such as radial growth (Fkiri et al. 2018), wood structure (Estebam et al. 2012), total height and tree survival (Varelides et al. 2001), vegetation indices, and reserves (Santini et al. 2019b). However, genotypic variability of morphological traits has been mainly described for seedling and juvenile stages (Bachofen et al. 2021; Topacoglu, 2013; Kreyling et al. 2012). Aleppo pine is a thermophilic, fire-embracer species with high ecological importance, especially in dry areas due to its drought resistance (Chambel et al. 2013). Because of its wide distribution range, Aleppo pine is a species with high intraspecific variation that has been described for many functional and life-history traits such as reproduction (Climent et al. 2008), height growth (Voltas et al. 2018) or photosynthetic indices (Solvin et al. 2015).

Altogether, we expected to find intraspecific differentiation for the analyzed traits in both species as a result of their adaptation to very different ecological niches. However, we hypothesized that this variability, especially regarding crown structure, would be higher in black pine than in Aleppo pine due to the larger phylogeographic divergence of the former. Black pine presents a high morphological variability associated to environmental factors such as snowfall, water availability and wildfire which influence crown structure and main trunk growth (Stevens et al. 2020; Aubrey et al. 2007). In this regard, we also hypothesized that climate at origin of populations of both pine species could have played an important role in shaping morphological variability of aboveground traits, in agreement with their evolutionary histories and adaptive differentiation. In particular, we expected that black pine populations from snowy origin had less dense canopy, while Aleppo

pine populations coming from xeric environments showed high aerial growth (e.g. tree height, tree biomass and crown volume).

Material and Methods

Study site and field measurements

This study was carried out in two provenance trials (common gardens) located in central Spain (Table S1). The first trial is located in La Mata de Valsaín, Segovia (degree-minute-second coordinate system: 40°54′42″ N, 04°00′50″ W). It is composed of 18 populations of adult individuals of *P. nigra* with subspecies *laricio*, *nigra*, *salzmannii*, *pallasiana* and *calabrica* (Table S1). Seeds were collected in 1995 from 20 to 30 trees of the same populations, spaced at least 100 m apart. They were nursed following standard container practices (Landis, 1990). In 1996, 800 one-year-old seedlings were transplanted following a complete randomized block design with 12 replicates, with each experimental unit consisting of a rectangular plot of four seedlings, spaced 4.0 × 1.5 m apart. In 2016, the trial was subjected to a systematic thinning by which two out of four trees were logged in each experimental unit to avoid excess competition among trees. A total of 385 trees remained in the trial, and due to sampling issues, we included 345 trees in our analyses.

The second provenance trial is located in Valdeolmos, Madrid (degree-minute-second coordinate system: 39°49′29″ N, 00°34′22″ W). It consists of 56 range-wide populations of *P. halepensis* (Aleppo pine; Table S2). Seeds were collected following the same procedure as for *P. nigra*. In 1997, 896 one-year-old seedlings were systematically planted with a distance of 2.5 × 2.5 m following a complete randomized block design with four replicates. Each experimental unit was composed of four individuals of the same population planted in a linear plot. One block was excluded in this study due to high mortality caused by rabbits during the early plantlet age, and so the total number of trees in the trial is 698, excluding this block. Aleppo pine populations were grouped into five ecotypes according to Patsiou et al. (2020), which used a hierarchical cluster analysis to identify ecotypes based on climatic information. These climate-based ecotypes were: dry-summer/semiarid/temperate (DST), dry-summer/semiarid/cold (DSC), dry-summer/sub-humid/temperate (DHT), wet-summer/semiarid/temperate (WST), and wet-summer/sub-humid/cool (WHC) (Patsiou et al. 2020).

Diameter at breast height (*dbh*) and tree height were measured using a diameter tape and a Vertex hypsometer, respectively, in February 2022 (Valdeolmos, age 26 years) and in July 2020 (Valsaín, age 25 years), while tree biomass was estimated from published allometric equations (Table 1).

Remote sensing data collection

In Valsaín, aerial laser scanning (ALS) records were acquired through an octocopter unmanned aerial vehicle (UAV) equipped with a LiDAR (sensor Velodyne VLP-16 Puck Lite). RGB images were obtained using a DJI (Phantom 4 pro v2) equipped with a camera having a sensor size of 5472 × 3648 pixels and a focal distance of 8.86 mm. Both flights were performed the same day in July 2020 at an altitude of 40 m and speed of 5 m s-1. In Valdeolmos, ALS data were acquired with an octocopter UAV equipped with a LiDAR (sensor Velodyne VLP-32C), whereas a RGB camera with sensor size 6000 × 4000 pixels and focal distance 12 mm was mounted on a DJI (m300) to collect RGB images. Both flights were performed the same day in November 2021 at an altitude of 50 m and speed of 5 m s-1. Examples of aerial RGB images and LiDAR point clouds are given in Fig. 1 for both trials.

Imagery processing

RGB and LIDAR pre-processing, treetop detection and crown segmentation

The workflow applied to pre-process the LiDAR and RGB point clouds used LAStools (Isenburg et al. 2017) and US Forest Service FUSION/LDV 3.42 (McGaughey et al. 2015) software. The workflow is summarized in Fig. 2. First, we filtered points of noise in the point clouds using *lasnoise*. Then, the ground points were computed with *lasground* and later normalized through the identification of the height above the ground of each point using *lasheight*. Finally, the points were classified as ground and non-ground (vegetation) through *lasclassify*. Once the data had been filtered and classified, we built a digital terrain model (DTM) and a canopy height model (CHM) with a resolution of 10 cm using the *GridSurfaceCreate* and *CanopyModel* procedures, respectively, of FUSION/LDV. We created slices every 1 m, directly from the LiDAR point clouds, starting from 1 m to 11 m for Valdeolmos, and from 2 m to 13 m for Valsaín and then we made a CHM for every slice. These bins were chosen based on the height of the tallest tree and on the thinning strategy applied in Valsaín.

For Valdeolmos, we additionally created two slices (one at 0.20 m and another at 0.50 m) because the trial was not pruned, and tree crowns started roughly from the trunk base.

Individual tree detection was performed for each approach independently using the *vwf* function implemented in the ForestTools R package (Plowright, 2018). This function uses a variable window filter algorithm to detect the local maxima (Popescu & Wynne, 2004) from the canopy height model. We visually evaluated the optimal window size, after testing different values. Crowns were automatically segmented starting from each treetop using the *mcws* function implemented in ForestTools. We manually corrected the segmented crowns in QGIS in order to eliminate false trees detected by the automatic procedure and, also, to add a segmentation where the algorithm failed to segment a crown. We then proceeded with the segmentation of each CHM slice (only for LiDAR-derived CHM).

Once individual trees were recognized, we calculated maximum height and crown area for each segmented slice using first the zonal statistic and then the area function in QGIS.

LIDAR- and RGB-derived traits

We obtained individual tree point clouds of each trial by segmenting the LiDAR-derived normalized point clouds over the respective crown segmented shape file. For Valsaín, we first estimated the crown base height (*CBH*) and, afterwards, we obtained several descriptive statistics to characterize the crown architecture of trees, as summarized in Table 1. To estimate *CBH* we first filtered the point cloud up to 1.3 m, since the trial is pruned and no branches are present below this height value. Then, we generated histograms with 0.1 m bins to visualize the vertical distribution of each individual point cloud, and applied a cubic smooth spline for which the first and the second derivatives were calculated. Since the inflection points of a smooth spline curve correspond to the zero crossing of their second derivative, we calculated all height values at which the second derivative equaled zero. Then, we matched this height value with the closest height at which the number of points within the individual point cloud was minimum (Arkin et al. 2021; Luo et al. 2018). In this manner, we were able to identify the *CBH* without mistakenly selecting understory vegetation (Luo et al. 2018). We then computed crown volume using the alphashape3d R package (Lafarge et al. 2017) with an alpha value of 0.25. Alphashape3d allows to reconstruct a set of points in a three-dimensional space and produces accurate

estimates of crown volume from LiDAR point cloud data (Ahongshangbam et al. 2019; Yan et al. 2019; Korhonen et al. 2013).

We then estimated a rather large set of morphometric characteristics and grouped them into traits related to i) main trunk, ii) tree biomass, iii) crown architecture or iv) crown volume (see Table 1 for full details). For Valdeolmos, we did not calculate LiDAR-derived traits relative to *CBH* since this trial had not been pruned and trees could have living or dead branches at ground level. Thus, we just filtered each individual point cloud at 0.20 m to avoid noise originating from small understory. Afterwards, we calculated the same canopy

architecture traits as for Valsaín except for *CBH*, crown length (*CL*) and crown skewness (*CL skew*) (Table 1). We also estimated RGB-derived traits, which included total tree height, trunk diameter, tree biomass, crown area and the ratio between total tree height and crown area (see Table 1).

Validation of UAV-derived height and trunk diameter and accuracy of treetops detection

In order to estimate the accuracy of treetop detection, following the local maxima algorithm [38] applied to both LiDAR and RGB canopy height models, we calculated recall (Rc), precision (Pr) and F-score (F) values. R and P represent the completeness and correctness of the detected tree with respect to a reference dataset, respectively, and F is an overall indicator that varies from 0 to 1, with higher values indicating a more accurate segmentation (Neuville et al. 2021).

$$Rc = TP / TP + FN, \quad (1)$$

$$Pr = TP / TP + FP, \quad (2)$$

$$F = 2 \times (P \times R / P + R), \quad (3)$$

where TP denotes the number of true positives (trees that are correctly individualized), FP represents the number of false positive (trees that are identified but do not exist), and FN refers to the number of false negative (trees that have not been identified).

Tree height (*h*) and *dbh* measured *in situ* were used to validate *h* and *dbh* estimates obtained from LiDAR and RGB canopy height models, which were estimated through allometric equations using LiDAR-

and RGB-derived tree height and crown area (see Table 1). We used the root mean square error (RMSE), the mean absolute error (MAE) and the coefficient of determination (R^2) statistics for comparison between approaches.

Statistical analyses

In order to test for population differentiation, traits measured *in situ* and UAV-derived traits were independently subjected to analysis of variance (ANOVA), with population and replicates as fixed terms for both trials. We also tested for subspecies (black pine) or ecotypic (Aleppo pine) differentiation by partitioning the population term into subspecies (or ecotype) and population nested to subspecies (or ecotype) effects, which were also considered as fixed terms. In the latter analysis, two populations of *P. nigra* and four populations of *P. halepensis* were discarded due to their uncertain geographic origin (Tables S1 and S2).

In order to reduce the dimensionality of our dataset and evaluate which traits better explained the allometric patterns of subspecies (or ecotypes), we performed a stepwise discriminant analysis for traits that showed significant subspecies (or ecotypic) structure. The significance level corresponding to the F-value to be included or excluded in the model was set at $P = 0.15$ (Dillon et al. 1984). We ran linear discriminant analysis when the null hypothesis of multivariate normality tested through Mardia's test (Mardia, 1970) was not rejected; otherwise, a quadratic discriminant analysis was performed. Moreover, populations' means of traits having a significant population effect were correlated to climate at populations' origin. Partial correlations were also applied to the same population means for the purpose of controlling for subspecies (or ecotypic) structure in the dataset. The statistical analyses were performed in SAS/STAT (Little et al. 1998).

Results

Accuracy of tree detection

The identification of treetops was most accurate using LiDAR-derived CHM in both provenance trials, showing a recall (R) value of 0.92 and 0.93 for Valsaín and Valdeolmos respectively. This implied that over 90% of trees were correctly detected at trial level. The overestimation of treetops was quite low (P = 99% for Valsaín; P = 97% for Valdeolmos), and the overall indicator of accuracy F was also high (above 95%),

indicating accurate treetop identification (Table S3). Treetop identification was less accurate using RGB-derived CHM, although F was above 91% (Table S3).

Validation with in situ measurements

LiDAR-derived *h* and *dbh* estimates were slightly better than RGB-derived estimates for both species, especially for black pine. For this species, LiDAR- and RGB-derived *h* showed a RMSE of 0.36 m and 0.40 m, a MAE of 0.24 m and 0.29 m (Table S4), and a R^2 of 0.92 and 0.90 (Fig. S1a, b), respectively. The regression between LiDAR- and RGB-derived *h* showed a R^2 of 0.98 (Fig. S1c). LiDAR- and RGB-derived *dbh* had a RMSE of 1.61 cm and 1.74 cm, a MAE of 1.25 cm and 1.37 cm (Table S4), and a R^2 of 0.67 and 0.65 (Fig. S2a, b), respectively. The R^2 of the regression between LiDAR- and the RGB-derived *dbh* was 0.95 (Fig. S2c).

For Aleppo pine, LiDAR- and RGB-derived *h* showed a RMSE of 0.43 m and 0.45 m, a MAE of 0.31 m and 0.34 m (Table S4), and a R^2 of 0.83 and 0.76 (Fig. S3a, b), respectively. The R^2 of the regression between LiDAR- and RGB-derived *h* was 0.86 (Fig. S3c). LiDAR- and RGB-derived *dbh* had RMSE of 1.67 cm and 1.76 cm, a MAE of 1.26 cm (in both cases) (Table S4), and a R^2 of 0.73 and 0.69, respectively (Fig. S4a, b). The regression between LiDAR- and RGB- derived *dbh* showed a R^2 of 0.83 (Fig. S4c).

Intraspecific variability of in situ traits and of LiDAR- and RGB-derived traits

Black pine

We detected intraspecific variability for both *in situ* traits and RGB-derived traits and, also, for most LiDAR-derived traits (Table 2). Significant differences among subspecies were also found for every trait showing significant variability among populations, except for two LiDAR-derived traits which exhibited intraspecific variation only at the population level (Table 2).

Three LiDAR-derived traits (coefficient of variation of crown length points (CV_{CL}), crown volume ($Cvol_{025}$) and *h*) discriminated the most among subspecies. Discriminant analysis indicated that subspecies *calabrica* was associated with high crown volume, opposite to subspecies *nigra* (Fig. 3a). Low *h*, high $Cvol_{025}$ and high CV_{CL} characterized the subspecies *laricio*, while subspecies *salzmannii* showed the opposite pattern

(Fig. 3a). The average squared canonical correlation suggested that ca. 60% of the between-subspecies to within-subspecies variability was explained by the first two discriminant axes, which described 99% of the between-subspecies variation (Fig. 3a). The RGB-derived traits that best explained differences among subspecies were *h* and the ratio between height and crown area (*h:CA*), with an average squared canonical correlation of 46% (Table 3). The canonical correlation was a bit higher in the case of *in situ* traits (68%), with *h*, *dbh* and biomass of medium branches as traits that disclosed better the differences between subspecies (Table 3).

Aleppo pine

Tree biomass (stem biomass (*Ws*), medium branches biomass (*Wb2-7*), thin branches and needles biomass (*Wb2+n*) and root biomass (*Wr*)) and main trunk growth traits (*h* and *dbh*) showed significant population effects in the case of *in situ* traits, and also for both remote sensing-derived approaches (Table 4). Additionally, LiDAR-derived traits showed intraspecific variability also for main trunk traits (specifically, *half h*), crown architecture traits (height of the widest crown section (*HWCS*), height skewness (*h skew*), CV_{CL}, and quartile coefficient dispersion of crown length points (*QCD*)), and crown volume traits (density of points at 99th, 75th and 50th quartiles (*Q99d*, *Q75d*, *Q50d*, respectively) and ratio of crown volume to crown area ($Cvol_{025}$*:CA*)). All traits mentioned above showed a significant ecotypic structure, except for three LiDAR-derived traits (Table 4).

Discriminant analysis summarized the ecotypic structure for the species by means of two LiDAR-derived traits: CV_{CL} and *Q75d* (Table 3; Fig. 3b). The analysis indicated that ecotype DHT had a denser canopy, as opposed to ecotypes DST and DSC, while ecotype WST showed a high CV_{CL} values (Fig. 3b). However, the average squared canonical correlation was low, thereby indicating a relatively low discrimination, with the first two discriminant axes explaining only 15% of the between- to within-ecotype variability (Table 3). Three RGB-derived traits (*h*, *dbh* and *Wb2-7*) discriminated the most among ecotypes, however only 13% of the between- to within-ecotype variability was explained by the first two discriminant axes (Table 3). Regarding *in situ* traits, only the biomass of medium branches was identified in the stepwise discriminant analysis (Table 3).

Relationships between in situ or UAV traits and climate at populations' origin

Black pine

The LiDAR-derived traits showing a larger number of significant correlations with climate at the origin of populations were those related to main trunk (*h*), crown architecture (ratio between tree height and widest crown section (*h:HWCS*), *h skew*, CV_{CL}, and *QCD*), and crown volume (*Q99d*, *Q75d*, and *Q55d*) (Fig. 4a). The latter traits related to crown density also showed negative correlations with altitude. Traits related to crown architecture showed a positive correlation with longitude, mean annual precipitation (MAP), precipitation of the wettest quarter and winter precipitation (PwtQ and Pw, respectively), and a negative correlation with temperature annual range (TAR) (Fig. 4a). TAR was the climate variable having the highest number of significant relationships with the entire set of traits analyzed. This variable showed negative associations with traits descriptive of tree height, regardless of the approach used for its estimation, and canopy architecture (Fig. 4a).

After accounting for subspecies structure, TAR was no longer the most influential climate variable, suggesting that all previously significant correlations were driven by large differences among subspecies (Fig. 4b). This pattern was also common to any other significant correlation described above, except for three traits related to crown volume and two traits related to crown architecture, which were negatively related to altitude (Fig. 4b).

Aleppo pine

In situ measures of trunk diameter and estimates of tree biomass were positively correlated with longitude, MAP and PwtQ, and negatively correlated with altitude and TAR (Fig. 5). Regarding RGB-derived traits, only those related to tree biomass showed significant correlations with climate. In particular, *Wb2-7* and *Wb+n* showed the same correlation pattern as for *in situ* measures, while the remaining RGB-derived biomass traits showed significant relationships with TAR (negative) and with MAP and PwtQ (positive) (Fig. 5). The same pattern was found for LiDAR-derived *Wb2+n*, while *Wb2-7* was also negatively correlated to altitude and positively correlated to longitude. Additionally, *Ws* was positively correlated with PwtQ and MAP, and *Wr* had a positive correlation with MAP only. Crown volume traits such as *Q99d*, *Q75d* and *Q50d* showed positive

correlations with longitude, and *Q75d* had also a negative correlation with altitude. Similarly, a negative correlation with altitude was observed for *HWCS*, which also had a negative correlation with TAR. Finally, CV_{CL} was positively correlated with the temperature of the coldest quarter (TCQ) (Fig. 5).

Partial correlations accounting for differences among ecotypes did not show any significant relationship between the analyzed traits and the climate at origin of populations, suggesting a lack of finer-scale ecogeographic patterns beyond the ecotypic structure of the species (results not shown).

Discussion

This study applied high-throughput, UAV-based phenotyping techniques for the assessment of genetic differentiation in morphological traits of two widespread Mediterranean pines (black pine and Aleppo pine). In particular, the effectiveness of LiDAR and RGB imagery was investigated to characterize tree phenotypes and their variability at population and meta-population (subspecies, ecotypes) level. Thus, we demonstrate the potential of these indirect approaches to disclose tree architectural differences potentially related to intraspecific adaptive divergence in pine species.

Tree segmentation accuracy and field validation

Our study showed that individual tree detection and segmentation obtained from UAV-LiDAR had a slightly higher overall accuracy than that obtained through UAV-RGB for both pine species. However, it also indicated that trees correctly identified and segmented using UAV-RGB were over 90%, which is still an excellent outcome compared to other studies involving alternative forest tree species such as *Pinus sylvestris L.*, *Picea abies* (L.) *H. Karts.* and *Quercus rubra L.*, among others (Vauhkonen et al. 2012), and in line with other studies performed in common gardens (Liao et al. 2022; Santini et al. 2019a).

The validation of LiDAR- and RGB-derived tree height and *dbh* against *in situ* measurements indicated that UAV-LiDAR estimated tree height and *dbh* better than UAV-RGB in both species, and especially for black pine, which showed a lower estimated error and a higher R^2. The fact that treetops and tree height were estimated with more accuracy and less error in black pine compared to Aleppo pine might be attributable to the thinning and pruning treatments applied in Valsaín, which produced a sparser canopy cover.

As a result, more ground points could be easily classified within the point clouds, generating a more accurate DTM (Mielcarek et al. 2020; Reutebuch et al. 2005) and, subsequently, a more accurate CHM from which tree height could be estimated with better accuracy. In addition, we speculate that morphological differences between these species, especially related to canopy architecture (denser in Aleppo pine) and total tree height (higher in black pine), could have also influenced accuracy, as described in previous studies for mixed temperate forests (Balenović et al. 2015). We would like to emphasize that, even though RGB imagery is less expensive than aerial LiDAR, both methods showed high accuracy in the identification of individual trees and, also, in the estimation of morphological traits commonly used in forest studies such as *dbh* and total tree height.

Intraspecific differentiation in black pine and associations with climate at origin

This study emphasizes the great intraspecific variability of growth traits and crown structure in European black pine. In particular, our results showed that populations belonging to *P. nigra* ssp. *nigra* presented the lowest aerial growth, regardless of methodology (*in situ*, LiDAR- or RGB-derived). Conversely, populations from south Italy, belonging to the subspecies *calabrica*, showed the opposite pattern. These results are in line with previous studies that described *P. nigra* ssp. *nigra* as slow growing (Santini et al. 2019b), but highly frost-tolerant species (Kreyling et al. 2012). Thus, traits related to crown structure could also be related to the large cold hardiness of this subspecies, especially crown density. Indeed, a slender, shorter and sparser canopy may shield the tree from snow canopy damage, as previously described for other pine species (Stevens et al. 2020; fish et al. 2006).

Also, according to our findings, intraspecific variability in crown complexity and shape indicates genetic differentiation in growth habit that may be related to particular responses to environmental stresses such as drought, snowfall and fire. Particularly, populations originating from mesic environments (i.e. Corsica), which belong to the subspecies *laricio*, showed a higher crown volume and a more expanded crown. These populations have been described as less conservative, fast growing (Santini et al. 2019b) and frost sensitive (Kreyling et al. 2012) than populations from xeric areas (i.e. Iberian Peninsula), belonging to the subspecies *salzmannii*, which showed the opposite pattern. The Iberian subspecies occupies areas in the southernmost distribution range of black pine, where drought and snowfall are the main limiting factors for

growth, although there seems to exist some growth differences between southern and northern populations within this region (Navarro-Cerrillo et al. 2014; Amodei et al. 2013). Southernmost populations occupy higher altitude, so they are subject to intense summer drought but also to heavy snowfalls in winter. These populations may have undergone more intense selection where snow is a key selective factor that influence crown structure (Climent Maldonado et al. 2017). This was hinted in our results, in which partial correlation analysis suggested that altitude was the only environmental variable showing an eco-geographic pattern beyond the subspecies structure of black pine.

Fire intensity and frequency can also play an important role for this fire-tolerant species (Resco de Dios et al. 2018), and the fact that populations from xeric environment showed a smallest and more homogeneous crown and a lower height in which the widest crown is found might be the result of selective factors that prioritize reserve accumulation and traits potentially related to surface fire-resistance that can facilitate survival under moderate-intensity surface fires (Aubrey et al. 2007), at the expenses of above-ground growth.

Intraspecific differentiation in Aleppo pine and associations with climate at origin

Significant variation was detected in Aleppo pine at population and ecotype level for many *in situ* as well as LiDAR- and RGB-derived traits. As hypothesized, however, ecotypic differentiation was by far less structured and somehow blurry compared to the strong subspecies structure exhibited by *P. nigra*.

Populations belonging to ecotypes WST and DSC (native to the Balearic Islands, Italy and central-south Iberian Peninsula) showed lower primary growth and crown volume. This is in clear contrast to populations from France, northern Spain and Greece, belonging to ecotypes WHC and DHT, which presented the opposite pattern. The latter ecotypes, originating from mesic environments, are characterized by higher phenotypic plasticity and generally grow faster than their counterparts from xeric areas (Ramírez-Valiente et al. 2022; Patsiou et al. 2020). The observed pattern can be the result of an adaptive syndrome in which populations from the east Mediterranean basin and from mesic origins invest more in aboveground growth compared to other plant compartments related to reproduction (Climent et al. 2008) or roots (Lombardi et al. 2021) and also to water-use efficiency (Voltas et al. 2015), among others. This can also be interpreted as a

genetically-based shade-avoidance strategy adopted by ecotypes from more favorable environments and therefore subject to higher competition, since a more expanded crown might enhance light capture and carbon gain (Duursma et al. 2007). These features may indeed reduce the negative effect of competition (Brisson et al. 2001). On the other hand, some morphological traits related to tree biomass, *dbh* and crown architecture showed a negative relationship with altitude and continentality (annual range temperature), thereby highlighting the thermophilic characteristic of this species (Vennetier et al. 2018). In addition, as fire-embracer species (Resco de Dios et al. 2018), Aleppo pine populations (and ecotypes) from xeric environments could assign more resources to reproduction, in particular to the production of serotine cones as post-fire regeneration strategy, at the expense of other functional traits related e.g. to primary growth (Aubrey et al. 2007). Limited height and lower height in which the widest crown is found may indeed enhance tree flammability, favoring surface fire to become crown fire (Ne´eman et al. 2004).

Conclusions

This study demonstrates the adequacy of two remote sensing approaches (UAV-LiDAR and UAV-RGB) to assess genetic variability of morphometric traits in adult trees of pine species at the intraspecific level. UAV-LiDAR accuracy was slightly better for the identification of individual trees and for the estimation of *dbh* and total tree height. However, the accuracy of UAV-RGB was still very good and, depending on the objective and available resources of the study, it might be appropriate to trade some accuracy for affordability. We conclude that genetic differentiation in tree structural differences potentially driven by environmental conditions at origin of populations of pine species can be effectively disclosed using UAV-based, high-throughput phenotyping approaches. Indeed, these methods also overcome the complex and time-consuming traditional measures of adult trees under field conditions.

Supplementary Materials: The following supporting information can be downloaded at: www.mdpi.com/xxx/s1, Fig. S1: Linear regressions between *in situ*-measured *h* and LiDAR- or RGB-derived *h* of black pine; Fig. S2: title; Linear regressions between *in situ*-measured db*h* and LiDAR- or RGB-derived *dbh* of black pine; Fig. S3: Linear regressions between *in situ*-measured *h* and LiDAR- or RGB-derived *h* of

Aleppo pine; Fig. S4: title; Linear regressions between *in situ*-measured db*h* and LiDAR- or RGB-derived *dbh* of Aleppo pine; Table S1: Name, code, subspecies, geographic origin and environmental conditions of 18 populations of European black pine; Table S2: Name, code, subspecies, geographic origin and environmental conditions of 18 populations of Aleppo pine; Table S3: Treetops accuracy detection of the local maxima algorithm applied to LiDAR and RGB canopy height models; Table S4: Validation of *h* and *dbh* derived from LiDAR and RGB canopy height models against *h* and *dbh* measured *in situ*.

Author Contributions: Conceptualization, J.V.; methodology, E.L., F.R.P., F.S.; formal analysis, E.L., F.R.P., J.V.; investigation, E.L., F.R.P., M.R.C., J.C., J.V.; writing—original draft preparation, E.L.; writing—review and editing, F.R.P., F.S., M.R.C., J.C., V.R.D., J.V; supervision, V.R.D., J.V.; funding acquisition, V.R.D., J.V. All authors have read and agreed to the published version of the manuscript."

Funding: This work was partly supported by the Spanish Government, grant numbers RTI2018-094691-B-C31 and RTI2018-094691-B-C33 (MCIU/AEI/FEDER, EU). E. Lombardi was supported by a AGAUR FI-2021 pre-doctoral fellowship (with the support from the Secretariat for Universities and Research of the Ministry of Business and Knowledge of the Government of Catalonia and the European Social Fund).

Data Availability Statement: The data supporting the results of this study will be made available at the CORA open repository (https://dataverse.csuc.cat/) upon acceptance of this article. Accession number will be provided during review stage.

Acknowledgments: In this section, you can acknowledge any support given which is not covered by the author contribution or funding sections. This may include administrative and technical support, or donations in kind (e.g., materials used for experiments).

Conflicts of Interest: The authors declare no conflict of interest.

References

Aguilar, F.J., Nemmaoui, A., Aguilar, M.A., Jiménez-Lao, R. (2022). Aleppo Pine Allometric Modeling Through Integrating Uav Image-Based Point Clouds and Ground-Based Data. ISPRS Ann. Photogramm. Remote Sens. Spat. Inf. Sci. V-3–2022, 353–360. https://doi.org/10.5194/isprs-annals-v-3-2022-353-2022

Ahongshangbam, J., Khokthong, W., Ellsäßer, F., Hendrayanto, H., Hölscher, D., Röll, A. (2019). Drone-based photogrammetry-derived crown metrics for predicting tree and oil palm water use. Ecohydrology. 12, e2115. https://doi.org/10.1002/eco.2115

Amodei, T., Guibal, F., Fady, B. (2013). Relationships between climate and radial growth in black pine (*Pinus nigra arnold* ssp. *salzmannii* (dunal) franco) from the south of France. Ann. For. Sci. 70, 41–47. https://doi.org/10.1007/s13595-012-0237-9

Arkin, J., Coops, N.C., Daniels, L.D., Plowright, A. (2021). Estimation of vertical fuel layers in tree crowns using high density lidar data. Remote Sens. 13, 1–17. https://doi.org/10.3390/rs13224598

Aubrey, D.P., Coleman, M.D., Coyle, D.R. (2007). Ice damage in loblolly pine: understanding the factors that influence susceptibility. For. Sci. 53, 580–589

Bachofen, C., Perret-Gentil, A., Wohlgemuth, T., Vollenweider, P., Moser, B. (2021). Phenotypic Plasticity versus Ecotypic Differentiation under Recurrent Summer Drought in Two Drought-Tolerant Pine Species. *J.* Ecol. 109, 3861–3876. https://doi.org/10.1111/1365-2745.13762

Balenović, I., Jazbec, A., Marjanović, H., Paladinić, E., Vuletić, D. (2015). Modeling Tree Characteristics of Individual Black Pine (*Pinus Nigra Arn.*) Trees for Use in Remote Sensing-Based Inventory. Forests. 6, 492–509. https://doi.org/10.3390/f6020492

Brisson, J. (2001). Neighborhood competition and crown asymmetry in Acer saccharum. Can. J. For. Res. 31, 2151–2159. https://doi.org/10.1139/cjfr-31-12-2151

Camarretta, N., Harrison, P.A., Lucieer, A., Potts, B.M., Davidson, N., Hunt, M. (2020). From drones to phenotype: using UAV-LiDAR to detect species and provenance variation in tree productivity and structure. Remote Sens. 12, 1–16. https://doi.org/doi:10.3390/rs12193184

Chambel, M.R., Climent, J., Pichot, C., Ducci, F. (2013). Mediterranean pines (*Pinus halepensis Mill*. and *brutia Ten*.). In *Forest Tree Breeding in Europe. Managing Forest Ecosystems*, Pâques, L. Eds.; Publisher: Springer, Dordrecht. 25, 229–265

Climent, J., Prada, M.A., Calama, R., Chambel, M.R., De Ron, D.S., Alía, R. (2008). To grow or to seed: ecotypic variation in reproductive allocation and cone production by young female Aleppo pine (*Pinus halepensis*, *pinaceae*). Am. J. Bot. 95, 833–842. https://doi.org/10.3732/ajb.2007354

Climent Maldonado, J., M., Sierra de grado, R. (2017). El derecho a crecer torcido: ¿es adaptativa la rectitud del tronco? Proceedings of VII Congreso Forestal Español, Plasencia, Spain, 26-30 June 2017

Colaço, A.F., Trevisan, R.G., Molin, J.P., Rosell-Polo, J.R., Escolà, A. (2017). A Method to Obtain Orange Crop Geometry Information Using a Mobile Terrestrial Laser Scanner and 3D Modeling. Remote Sens. 9, 10–13. https://doi.org/10.3390/rs9080763

Dillon, W. R., and Goldstein, M. (1984). Multivariate analysis: methods and applications, Publisher: Wiley. 360-393

Duursma, R.A., Mäkelä, A. (2007). Summary models for light interception and light-use efficiency of non-homogeneous canopies. Tree Physiol. 27, 859–870. https://doi.org/10.1093/treephys/27.6.859

du Toit, F., Coops, N.C., Tompalski, P., Goodbody, T.R.H., El-Kassaby, Y.A., Stoehr, M., Turner, D., Lucieer, A. (2020). Characterizing variations in growth characteristics between Douglas-fir with different genetic gain levels using airborne laser scanning. Trees Struct. Funct. 34, 649–664. https://doi.org/10.1007/s00468-019-01946-y

Enescu, C.M., de Rigo, D., Caudullo, G., Mauri, A., Houston Durrant, T., (2016). *Pinus nigra* in Europe: distribution, habitat, usage and threats. In *European Atlas of Forest Tree Species*, San- Miguel-Ayanz, J., de Rigo, D., Caudullo, G., Houston Durrant, T., Mauri, A. Eds., Publisher: Off EU, Luxembourg, 2016, 126–127

Esteban, L.G., Martín, J.A., de Palacios, P., Fernández, F.G. (2012). Influence of region of provenance and climate factors on wood anatomical traits of *Pinus nigra Arn*. subsp. *salzmannii*. Eur. J. For. Res. 131, 633–645. https://doi.org/10.1007/s10342-011-0537-x

Fish, H., Lieffers, V.J., Silins, U., Hall, R.J. (2006). Crown shyness in lodgepole pine stands of varying stand height, density, and site index in the upper foothills of Alberta. Can. J. For. Res. 36, 2104–2111. https://doi.org/10.1139/X06-107

Fkiri, S., Guibal, F., Fady, B., Khorchani, A., El Khaldi, A., Khouja, M.L., Nasr, Z. (2018). Tree-rings to climate relationships in nineteen provenances of four black pines sub-species (*Pinus nigra Arn*.) growing in a common garden from northwest Tunisia. Dendrochronologia. 50, 44–51. https://doi.org/10.1016/j.dendro.2018.05.001.

Ganz, S., Käber, Y., Adler, P. (2019). Measuring tree height with remote sensing-a comparison of photogrammetric and LiDAR data with different field measurements. Forests. 10, 694. https://doi.org/10.3390/f10080694

Goodbody, T.R.H., Coops, N.C., White, J.C. (2019). Digital Aerial Photogrammetry for Updating Area-Based Forest Inventories: A Review of Opportunities, Challenges, and Future Directions. Curr. For. Reports. 55–75. https://doi.org/10.1007/s40725-019-00087-2

Grote, R., Gessler, A., Hommel, R., Poschenrieder, W., Priesack, E. (2016). Importance of tree height and social position for drought-related stress on tree growth and mortality. Trees - Struct. Funct. 30, 1467–1482. https://doi.org/10.1007/s00468-016-1446-x

Isajev, V., Fady, B., Semerci, H., Andonovski, V. (2003). EUFORGEN technical guidelines for genetic conservation and use for European Black pine *(Pinus nigra)*. Int. Plant Genet. Resour. Institute, Rome, Italy

Isenburg, M. (2017). LAStools-Efficient LiDAR Processing Software, Version 141017, academic. Available online: http://rapidlasso. com.

Karna, Y.K., Penman, T.D., Aponte, C. (2019). Remote Sensing assessing legacy effects of wildfires on the crown structure of fire-SAR and LIDAR Fusion: Experiments and Applications. Remote Sens. 11, 2433. https://doi.org/10.3390/rs11202433

Korhonen, L., Vauhkonen, J., Virolainen, A., Hovi, A., Korpela, I. (2013). Estimation of tree crown volume from airborne Lidar data using computational geometry. Int. J. Remote Sens. 34, 7236–7248, https://doi.org/10.1080/01431161.2013.817715

Kreyling, J., Wiesenberg, G.L.B., Thiel, D., Wohlfart, C., Huber, G., Walter, J., Jentsch, A., Konnert, M., Beierkuhnlein, C. (2012). Cold hardiness of *Pinus nigra Arnold* as influenced by geographic origin, warming, and extreme summer drought. Environ. Exp. Bot. 78, 99–108. https://doi.org/10.1016/j.envexpbot.2011.12.026

Lafarge, T., and Pateiro-Lopez, B. (2017). Alphashape3d: implementation of the 3D Alpha-Shape for the reconstruction of 3D sets from a point cloud. Available online: https://cran.r-project.org/package=alphashape3d.

Landis, T.D. (1990). Containers type and functions. In *The Container Tree Nursery Manual, Landis*, T.D.; Tinus, R.W.; McDonald, S.E.; Barnett, J.P., Eds., Publisher: USDA Forest Service, Washington DC. 2, 1-39.

Leite, R.V., Silva, C.A., Mohan, M., et al. (2020). Individual tree attribute estimation and uniformity assessment in fast-growing Eucalyptus Spp. forest plantations using Lidar and linear mixed-effects models. Remote Sens. 12, 1–20. https://doi.org/10.3390/rs12213599

Liao, L., Cao, L., Xie, Y., Luo, J., Wang, G. (2022). Phenotypic traits extraction and genetic characteristics assessment of eucalyptus trials based on UAV-borne LiDAR and RGB images. Remote Sens. 14, 765. https://doi.org/10.3390/rs14030765

Liu, Q., Fu, L., Chen, Q., Wang, G., Luo, P., Sharma, R.P., He, P., Li, M., Wang, M., Duan, G. (2020). Analysis of the spatial differences in canopy height models from UAV LiDAR and photogrammetry. Remote Sens. 12, 2884. https://doi.org/10.3390/RS12182884

Littell, R.C., Henry, P.R., Ammerman, C.B. (1998). Statistical analysis of repeated measures data using SAS procedures. J. Anim. Sci. 76, 1216–1231. https://doi.org/10.2527/1998.7641216x

Lombardi, E., Ferrio, J.P., Rodríguez-Robles, U., Resco de Dios, V., Voltas, J. (2021). Ground-Penetrating Radar as phenotyping tool for characterizing intraspecific variability in root traits of a widespread conifer. Plant Soil. https://doi.org/10.1007/s11104-021-05135-0

Lombardi, E., Shestakova, T.A., Santini, F., Resco de Dios, V., Voltas, J. (2022). Harnessing Tree-Ring Phenotypes to Disentangle Gene by Environment Interactions and Their Climate Dependencies in a Circum-Mediterranean Pine. Ann. Bot. 2, 1–15. https://doi.org/10.1093/aob/mcac092

Luo, L., Zhai, Q., Su, Y., Ma, Q., Kelly, M., Guo, Q. (2018). Simple method for direct crown base height estimation of individual conifer trees using airborne LiDAR data. Opt. Express. 26, A562-A578. https://doi.org/10.1364/oe.26.00a562

Mardia K.V. (1970). Measures of multivariate skewness and kurtosis with applications. in *Biometrika*; Publisher: Oxford University Press. 57, 519–530.

McGaughey, R.J. (2015). FUSION/LDV: Software for LIDAR data analysis and visualization, Version 3.50; US Department of Agriculture, Forest Service, Pacific Northwest Research Station, University of Washington: Seattle, WA, USA.

Mielcarek, M., Kamińska, A., Stereńczak, K. (2020). Digital Aerial Photogrammetry (DAP) and Airborne Laser Scanning (ALS) as Sources of Information about Tree Height: Comparisons of the Accuracy of Remote Sensing Methods for Tree Height Estimation. Remote Sens. 12, 1808. https://doi.org/10.3390/rs12111808

Moe, K.T., Owari, T., Furuya, N., Hiroshima, T., Morimoto, J. (2020). Application of Uav photogrammetry with Lidar data to facilitate the estimation of tree locations and Dbh values for high-value timber species in Northern Japanese mixed-wood forests. Remote Sens. 12, 1–19. https://doi.org/10.3390/rs12172865

Navarro-Cerrillo, R.M., Sánchez-Salguero, R., Manzanedo, R.D., Camarero, J.J., Fernández-Cancio, Á. (2014). Site and age condition the growth responses to climate and drought of relict *Pinus nigra* Subsp. *salzmannii* populations in southern Spain. Tree-Ring Res. 70, 145–155. https://doi.org/10.3959/1536-1098-70.2.145

Ne'eman, G., Goubitz, S., Nathan, R. (2004). Reproductive Traits of *Pinus halepensis* in the Light of Fire - A Critical Review. Plant Ecol. 171, 69–79. https://doi.org/10.1023/B:VEGE.0000029380.04821.99

Neuville, R., Bates, J.S., Jonard, F. (2021). Estimating forest structure from UAV-Mounted LiDAR point cloud using machine learning. Remote Sens. 13, 1–19, https://doi.org/doi:10.3390/rs13030352

Ordóñez, J.L., Retana, J., Espelta, J.M. (2005). Effects of tree size, crown damage, and tree location on post-fire survival and cone production of *Pinus nigra* trees. For. Ecol. Manage. 206, 109–117, https://doi.org/10.1016/j.foreco.2004.10.067

Patsiou, T.S., Shestakova, T.A., Klein, T., di Matteo, G., Sbay, H., Chambel, M.R., Zas, R., Voltas, J. (2020). Intraspecific responses to climate reveal nonintuitive warming impacts on a widespread thermophilic conifer. New Phytol. 228, 525-540. https://doi.org/10.1111/nph.16656

Plowright, A., Plowright, M.A. (2018). R Package 'ForestTools.' CRAN. Available online: https://github.com/andrew-plowright/ForestTools.

Poorter, L., Lianes, E., Moreno-de las Heras, M., Zavala, M.A. (2012). Architecture of Iberian canopy tree species in relation to wood density, shade tolerance and climate. Plant Ecol. 213, 707–722. https://doi.org/10.1007/s11258-012-0032-6

Popescu, S.C., and Wynne, R.H. (2004). Seeing the Trees in the Forest: Using Lidar and Multispectral Data Fusion with Local Filtering and Variable Window Size for Estimating Tree Height. Photogramm. Eng. Remote Sens. 70, 589–604. https://doi.org/10.14358/PERS.70.5.589

Ramírez-Valiente, J. A., del Santos del Blanco, L., Alía, R., Robledo-Arnuncio, J.J., Climent, J. (2022). Adaptation of Mediterranean forest species to climate: lessons from common garden experiments. J. Ecol. 110, 1022–1042. https://doi.org/10.1111/1365-2745.13730

Reutebuch, S.E, Mc Gaughey, R.J., Andersen, H.E. (2005). Accuracy of an IFSAR-Derived digital terrain model under a conifer forest canopy. Can. J. Remote Sens. 31, 283–288. https://doi.org/10.5589/m05-016

Resco de Dios, V., Arteaga, C., Hedo, J., Gil-Pelegrín, E., Voltas, J. (2018). A Trade-off between Embolism Resistance and Bark Thickness in Conifers: Are Drought and Fire Adaptations Antagonistic? Plant Ecol. Divers. 11, 253–258. https://doi.org/10.1080/17550874.2018.1504238

Ruiz-Peinado, R., Rio, M., Montero, G. (2011). New models for estimating the carbon sink capacity of Spanish softwood species. For. Syst. 20, 176–188. https://doi.org/10.5424/fs/2011201-11643

Santini, F., Kefauver, S.C., Resco de Dios, V., Araus, J.L., Voltas, J. (2019a). Using Unmanned Aerial Vehicle-Based Multispectral, RGB and thermal imagery for phenotyping of forest genetic trials: a case study in *Pinus halepensis*. Ann. Appl. Biol. 174, 262–276. https://doi.org/10.1111/aab.12484

Santini, F., Serrano, L., Kefauver, S.C., Abdullah-Al, M., Aguilera, M., Sin, E., Voltas, J. (2019). Morpho-Physiological Variability of *Pinus Nigra* Populations Reveals Climate-Driven Local Adaptation but Weak Water Use Differentiation. Environ. Exp. Bot. 166, 103828. https://doi.org/10.1016/j.envexpbot.2019.103828

Solvin, T.M., Puliti, S., Steffenrem, A. (2020). Use of UAV Photogrammetric data in forest genetic trials: measuring tree height, growth, and phenology in Norway spruce (*Picea Abies L.* Karst.). Scand. J. For. Res. 35, 322–333. https://doi.org/10.1080/02827581.2020.1806350

Stevens, J.T., Kling, M.M., Schwilk, D.W., Varner, J.M., Kane, J.M. (2020). Biogeography of Fire Regimes in Western U.S. Conifer Forests: A Trait-Based Approach. Glob. Ecol. Biogeogr. 29, 944–955. https://doi.org/10.1111/geb.13079

Tapias, R., Climent, J., Pardos, J.A., Gil, L. (2004). Life histories of Mediterranean pines. Plant Ecol. 171, 53–68. https://doi.org/10.1023/B:VEGE.0000029383.72609.f0

Topacoglu, O. (2013). Genetic Diversity among Populations in Black Pine (*Pinus Nigra Arnold*. Subsp. *Pallasiana* (Lamb.) Holmboe) Seed Stands in Turkey. Bulg. J. Agric. Sci. 19, 1459–1464.

Vauhkonen, J., Ene, L., Gupta, S., et al. (2012). Comparative testing of single-tree detection algorithms under different types of forest. Forestry. 85, 27–40. https://doi.org/10.1093/forestry/cpr051

Varelides, C., Brofas, G., Varelides, Y. (2001). Provenance variation in *Pinus nigra* at three sites in Northern Greece. Ann. For. Sci. 58, 893-900. https://doi.org/10.1051/forest:2001103

Vennetier, M., Ripert, C., Rathgeber, C. (2018). Autecology and growth of Aleppo pine (*Pinus halepensis Mill*.): a comprehensive study in France. For. Ecol. Manage. 413, 32–47. https://doi.org/10.1016/j.foreco.2018.01.028.

Voltas, J., Lucabaugh, D., Chambel, M.R., Ferrio, J.P. (2015). Intraspecific Variation in the Use of Water Sources by the Circum-Mediterranean Conifer *Pinus halepensis*. New Phytol. 208, 1031–1041. https://doi.org/10.1111/nph.13569

Voltas, J., Shestakova, T.A., Patsiou, T., di Matteo, G., Klein, T. (2018). Ecotypic variation and stability in growth performance of the thermophilic conifer *Pinus halepensis* across the Mediterranean basin. For. Ecol. Manage. 424, 205–215. https://doi.org/10.1016/j.foreco.2018.04.058

Yan, Z., Liu, R., Cheng, L., Zhou, X., Ruan, X., Xiao, Y. (2019). A Concave hull methodology for calculating the crown volume of individual trees based on vehicle-borne LiDAR data. Remote Sens. 11, 623. https://doi.org/10.3390/rs11060623

Chapter 3 – Tables and Figures

Table 1. Description of *in situ*, LiDAR- and RGB-derived phenotypic traits with their function or formula. The traits were obtained for two pine species evaluated in two provenance trials. The first trial was located in Valdeolmos (Madrid province, Spain) and consisted of 56 populations of *Pinus halepensis*. The second trial was located in Valsaín (Segovia province, Spain) and was composed by 18 populations of *Pinus nigra*.

Trait abbreviation	Trait description	Function/Formula	Valsaín	Valdeolmos	*in situ*	LiDAR-derived	RGB-derived
Traits related to main trunk							
h	Total tree height calculated from canopy height model	*Zonal statistic*, QGIS environment	X	X	X	X	X
half h	Half of the total tree height		X	X		X	
dbh	Estimated diameter at breast height	Multilinear model (for UAV-derived *dbh*) for black pine [65] and Aleppo pine [66]	X	X	X	X	X
Traits related to tree biomass							
Ws	Stem biomass	Allometric equation [67]	X	X	X	X	X
Wb2-7	Medium branches biomass	Allometric equation [67]	X	X	X	X	X
Wb2+n	Thin branches + needles biomass	Allometric equation [67]	X	X	X	X	X
Wr	Root biomass	Allometric equation [67]	X	X	X	X	X
Traits related to crown architecture							
CBH	Height of first living branch	Cubic smooth spline followed by calculation of first and second derivative	X			X	
CL	Total crown length	Total tree height minus *CBH*	X				
CL Skew	Crown height skewness	*skewness* function, R environment	X				
h Skew	Total height skewness	*skewness* function, R environment	X	X		X	
CV_{CL}	Coefficient of variation of crown length point dispersion around the mean	Standard deviation *CL* divided by mean *CL*	X	X		X	
QCD	Crown height quartile coefficient of dispersion	Q1 - Q3 / Q1 + Q3	X	X		X	
CA	Crown area calculated from the canopy height model	*Area* function, QGIS	X	X		X	X
h:CA	Ratio between crown height and crown area		X	X		X	X
WCS	Widest crown section	CHM derived tiles with the biggest area				X	
HWCS	Height of widest crown section		X	X		X	
h:HWCS	Total tree height to height of widest crown section ratio		X	X		X	
half h:HWCS	Half tree height to height of widest crown section ratio					X	
RI	Crown height rumple index	*rumple_index* function, R environment	X	X		X	

Traits related to crown volume					
Q99p	99th percentile of crown's points calculated from the point cloud		X	X	X
Q75p	75th percentile of crown's points calculated from the point cloud		X	X	X
Q50p	50th percentile of crown's points calculated from the point cloud		X	X	X
Q99d	99th percentile of crown's points density calculated from the point cloud		X	X	X
Q75d	75th percentile of crown's points density calculated from the point cloud		X	X	X
Q50d	50th percentile of crown's points density calculated from the point cloud		X	X	X
$Cvol_{025}$	Crown's volume using an alpha value of 0.25 calculated from the point cloud	*alpha shape* function, R environment	X	X	X
$CH{:}Cvol_{025}$	Ratio between crown height and crown volume		X	X	X
$3D_{025}{:}2D$	Ratio between $Cvol_{025}$ to crown area		X	X	X

Table 2. Mixed-effects model analysis of variance for *in situ*, LiDAR and RGB-derived phenotypic traits of 18 populations (Pop) of black pine grouped into five subspecies (Subs) grown in a common garden. Only traits with significant population effects are shown in the table.

			in situ		**LiDAR-derived traits**		**RGB-derived traits**	
Traits	Effect	Num *df*	*F* Value	*P* > *F*	*F* Value	*P* > *F*	*F* Value	*P* > *F*
Traits related to main trunk								
h	Subs	4	8.28	**<0.0001**	8.15	**<0.0001**	7.13	**<0.0001**
	Subs(Pop)	16	1.70	0.0537	1.57	0.0828	1.70	0.0534
half h	Subs	4	/	/	4.16	**0.0032**	/	/
	Subs(Pop)	16	/	/	2.37	**0.0037**	/	/
dbh	Subs	4	6.19	**<0.0001**	4.52	**0.0017**	4.48	**0.0018**
	Subs(Pop)	16	1.49	0.1103	1.21	0.2642	1.31	0.1942
Traits related to tree biomass								
Ws	Subs	4	6.30	**<0.0001**	5.55	**0.0003**	4.96	**0.0008**
	Subs(Pop)	16	1.53	0.0969	1.33	0.1854	1.42	0.1377
Wb2-7	Subs	4	6.16	**0.0001**	4.49	0.0018	4.21	**0.0028**
	Subs(Pop)	16	1.48	**0.0117**	1.18	0.2897	1.27	0.2213
Wb2+n	Subs	4	6.16	**0.0001**	4.49	**0.0018**	4.21	**0.0028**
	Subs(Pop)	16	1.48	0.1159	1.18	0.2897	1.27	0.2213
Wr	Subs	4	6.05	**0.0002**	4.44	**0.0020**	4.07	**0.0035**
	Subs(Pop)	16	1.45	0.1270	1.	0.3018	1.25	0.2339
Traits related to crown architecture								
CA	Subs	4	/	/	2.70	**0.0328**	2.74	**0.0309**
	Subs(Pop)	16	/	/	0.89	0.5767	0.99	0.4757
h:CA	Subs	4	/	/	2.84	**0.0265**	3.20	**0.0151**
	Subs(Pop)	16	/	/	1.14	0.3281	1.45	0.1253
CL	Subs	4	/	/	9.70	**<0.0001**	/	/
	Subs(Pop)	16	/	/	1.49	0.1120	/	/
WCS	Subs	4	/	/	2.94	**0.0226**	/	/
	Subs(Pop)	16	/	/	0.85	0.6219	/	/
HWCS	Subs	4	/	/	2.51	**0.0447**	/	/
	Subs(Pop)	16	/	/	2.30	**0.0049**	/	/
h:HWCS	Subs	4	/	/	2.19	0.0730	/	/
	Subs(Pop)	16	/	/	0.82	0.6563	/	/
half h:HWCS	Subs	4	/	/	2.53	**0.0433**	/	/
	Subs(Pop)	16	/	/	1.21	0.2694	/	/
h Skew	Subs	4	/	/	5.73	**0.0003**	/	/
	Subs(Pop)	16	/	/	1.89	**0.0257**	/	/
CL Skew	Subs	4	/	/	2.66	**0.0349**	/	/
	Subs(Pop)	16	/	/	1.74	**0.0457**	/	/
QCD	Subs	4	/	/	5.79	**0.0002**	/	/
	Subs(Pop)	16	/	/	1.20	0.2787	/	/
RI	Subs	4	/	/	14.88	**<0.0001**	/	/
	Subs(Pop)	16	/	/	1.29	0.2118	/	/
Traits related to crown volume								
Q99p	Subs	4	/	/	3.83	**0.0055**	/	/
	Subs(Pop)	16	/	/	1.21	0.2670	/	/
Q99d	Subs	4	/	/	2.86	**0.0257**	/	/
	Subs(Pop)	16	/	/	2.61	**0.0013**	/	/
Q75d	Subs	4	/	/	2.92	**0.0234**	/	/
	Subs(Pop)	16	/	/	2.58	**0.0015**	/	/
Q50d	Subs	4	/	/	2.92	**0.0234**	/	/

	Subs(Pop)	16	/	/	2.52	**0.0019**	/	/
CV_{CL}	Subs	4	/	/	8.88	**<0.0001**	/	/
	Subs(Pop)	16	/	/	1.18	0.2926	/	/
$Cvol_{025}$	Subs	4	/	/	4.98	**0.0009**	/	/
	Subs(Pop)	16	/	/	0.96	0.4994	/	/
$H{:}Cvol_{025}$	Subs	4	/	/	2.88	**0.0250**	/	/
	Subs(Pop)	16	/	/	1.11	0.3556	/	/
$3D_{025}{:}2D$	Subs	4	/	/	7.82	**<0.0001**	/	/
	Subs(Pop)	16	/	/	0.95	0.5152	/	/

Table 3. Stepwise discriminant analysis of *in situ*, LiDAR- and RGB-derived traits of 17 populations of black pine grouped into four subspecies and of 52 populations of Aleppo pine grouped into five ecotypes grown in common gardens in Spain. The only black pine population from subspecies *pallasiana* and four Aleppo pine populations from uncertain geographic origin have not been included in the analysis. Partial R^2, significance level and average squared canonical correlation values are shown for traits entering in the model ($P < 0.15$).

Pinus nigra						*Pinus halepensis*					
in situ traits						*in situ* traits					
Step	**Variable**	**Partial R2**	**F-value**	***P* > F**	**Average Squared Canonical Correlation**	**Step**	**Variable**	**Partial R2**	**F-value**	***P* > F**	**Average Squared Canonical Correlation**
1	*dbh*	0.73	11.46	0.001	0.24	1	*Wb2-7*	0.31	5.20	0.002	0.08
2	*h*	0.85	22.26	<0.001	0.51						
3	*Ws*	0.56	4.64	0.025	0.68						
UAV-LiDAR derived traits						UAV-LiDAR derived traits					
1	CV_{CL}	0.87	28.83	<0.001	0.29	1	*Q75d*	0.29	4.76	0.003	0.07
2	$Cvol_{025}$	0.77	13.27	<0.001	0.54	2	CV_{CL}	0.31	5.24	0.002	0.15
3	*h*	0.70	8.61	0.003	0.60						
UAV-RGB derived traits						UAV-RGB derived traits					
1	*h*	0.71	10.54	0.001	0.24	1	*Wb2-7*	0.22	3.29	0.019	0.06
2	*h:CA*	0.69	8.89	0.002	0.46	2	*dbh*	0.14	1.91	0.126	0.09
						3	*h*	0.19	2.54	0.053	0.13

Table 4. Mixed-effects model analysis of variance for *in situ*, LiDAR and RGB-derived phenotypic traits of 52 populations (Pop) of Aleppo pine grouped into five ecotypes grown in a common garden. Only traits with significant population effects are shown in the table.

			in situ		**LiDAR-derived traits**		**RGB-derived traits**	
Trait	**Effect**	**Num *df***	***F* Value**	***P* > *F***	***F* Value**	***P* > *F***	***F* Value**	***P* > *F***
Traits related to main trunk								
h	Ecotype	4	2.96	**0.0196**	4.22	**0.0023**	5.54	**0.0002**
	Pop(Ecotype)	47	2.41	**<0.0001**	2.71	**<0.0001**	2.65	**<0.0001**
half h	Ecotype	4	/	/	4.22	**0.0023**	/	/
	Pop(Ecotype)	47	/	/	2.71	**<0.0001**	/	/
dbh	Ecotype	4	6.28	**<0.0001**	2.79	**0.0261**	2.49	**0.0426**
	Pop(Ecotype)	47	1.54	**0.0152**	1.81	**0.0012**	1.60	**0.0088**
Traits related to tree biomass								
Ws	Ecotype	4	8.52	**<0.0001**	5.09	**0.0005**	5.11	**0.0005**
	Pop(Ecotype)	47	1.46	**0.0285**	1.87	**0.0007**	1.73	**0.0026**
Wb2-7	Ecotype	4	8.76	**<0.0001**	5.32	**0.0003**	4.93	**0.0007**
	Pop(Ecotype)	47	1.38	0.0539	1.67	**0.0048**	1.68	**0.0045**
Wb2+n	Ecotype	4	8.52	**<0.0001**	5.06	**0.0005**	5.06	**0.0005**
	Pop(Ecotype)	47	1.44	**0.0334**	1.79	**0.0015**	1.69	**0.0038**
Wr	Ecotype	4	8.10	**<0.0001**	3.72	**0.0055**	3.00	**0.0182**
	Pop(Ecotype)	47	1.44	**0.0334**	1.75	**0.0021**	1.47	**0.0265**
Traits related to crown architecture								
HWC	Ecotype	4	/	/	3.68	**0.0058**	/	/
	Pop(Ecotype)	47	/	/	1.85	**0.0009**	/	/
h Skew	Ecotype	4	/	/	1.98	0.0967	/	/
	Pop(Ecotype)	47	/	/	1.59	**0.0101**	/	/
CV_{CL}	Ecotype	4	/	/	4.30	**0.0020**	/	/
	Pop(Ecotype)	47	/	/	1.27	0.1126	/	/
QCD	Ecotype	4	/	/	1.81	0.1251	/	/
	Pop(Ecotype)	47	/	/	1.50	**0.0206**	/	/
Traits related to crown volume								
Q99d	Ecotype	4	/	/	7.38	**<0.0001**	/	/
	Pop(Ecotype)	47	/	/	1.33	0.0762	/	/
Q75d	Ecotype	4	/	/	7.27	**<0.0001**	/	/
	Pop(Ecotype)	47	/	/	1.33	0.0757	/	/
Q50d	Ecotype	4	/	/	5.54	**0.0002**	/	/
	Pop(Ecotype)	47	/	/	1.31	0.0903	/	/
3D025:2D	Ecotype	4	/	/	1.92	0.1068	/	/
	Pop(Ecotype)	47	/	/	2.35	**<0.0001**	/	/

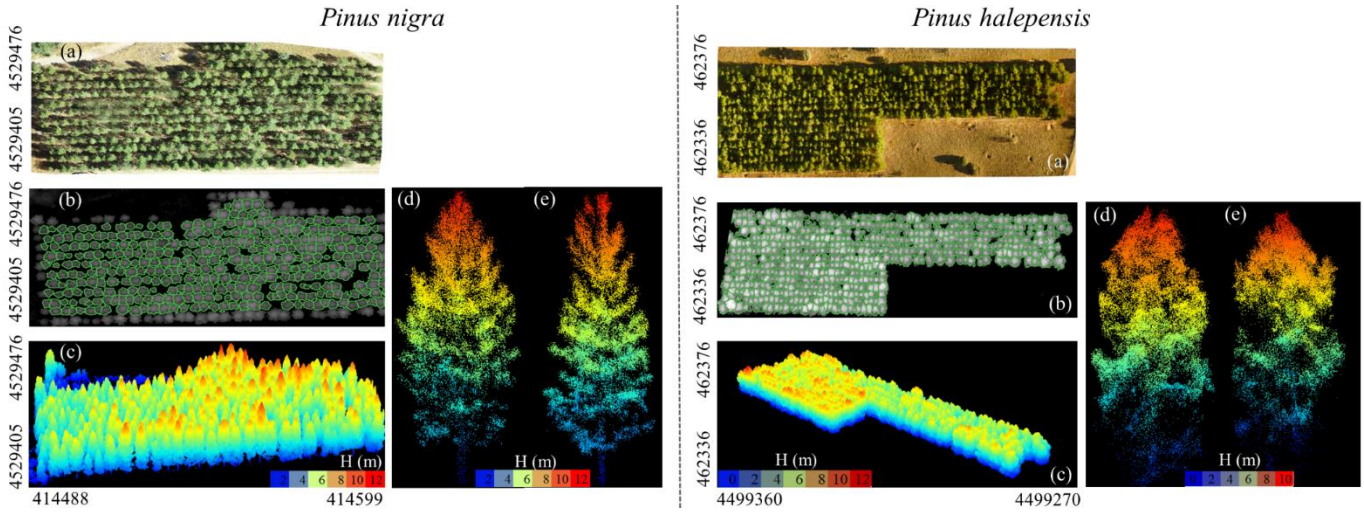

Fig. 1. Aerial RGB images and derived information of the two common gardens analysed in this study (**a**): *Pinus nigra* (left panels) and *Pinus halepensis* (right panels). Example of crown segmentation from the canopy height model of *P. nigra* and *P. halepensis* (**b**). Example of a normalized LiDAR point cloud of *P. nigra* and *P. halepensis* (**c**). Example of extracted tree individual point clouds for *P. nigra* subspecies *nigra* and *laricio* (**d-e**), and for Aleppo pine ecotype DHT (**d**) and DSC (**e**).

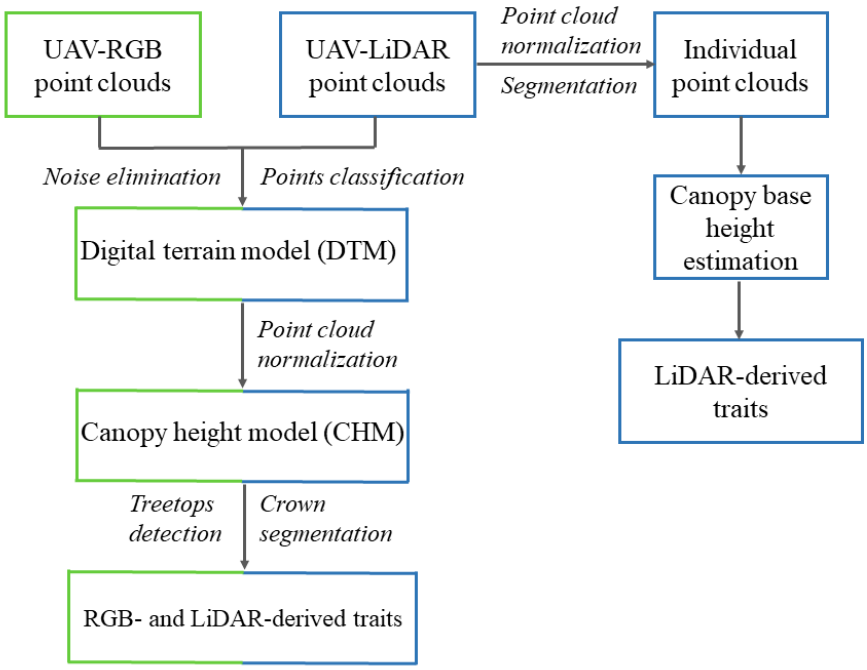

Fig. 2. Workflow of RGB and LiDAR point cloud processing. Green lines refer to the RGB-derived point cloud process and blue lines illustrate the LiDAR-derived point cloud process. The LiDAR-derived traits described in the right part of the workflow are those obtained from the segmentation applied directly to the LiDAR-derived point cloud.

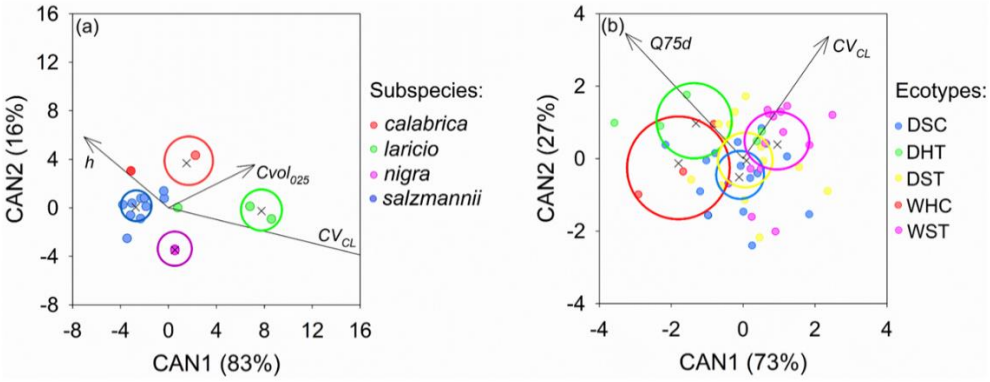

Fig. 3. Discriminant analysis plots showing the centroid (black crosses) and their 95% confidence ellipses of the first two canonical variables (CAN1 and CAN2) for four subspecies of *P. nigra* (a) and five ecotypes of *P. halepensis* (b) and their explanatory variables using LiDAR-derived traits. $Cvol_{025}$ = Crown volume calculate with alpha equal to 0.25; *h* = Total tree height; CV_{CL} = Coefficient of variation of crown length point dispersion; *Q75d* = 75th percentile of crown's point density calculated from the point cloud.

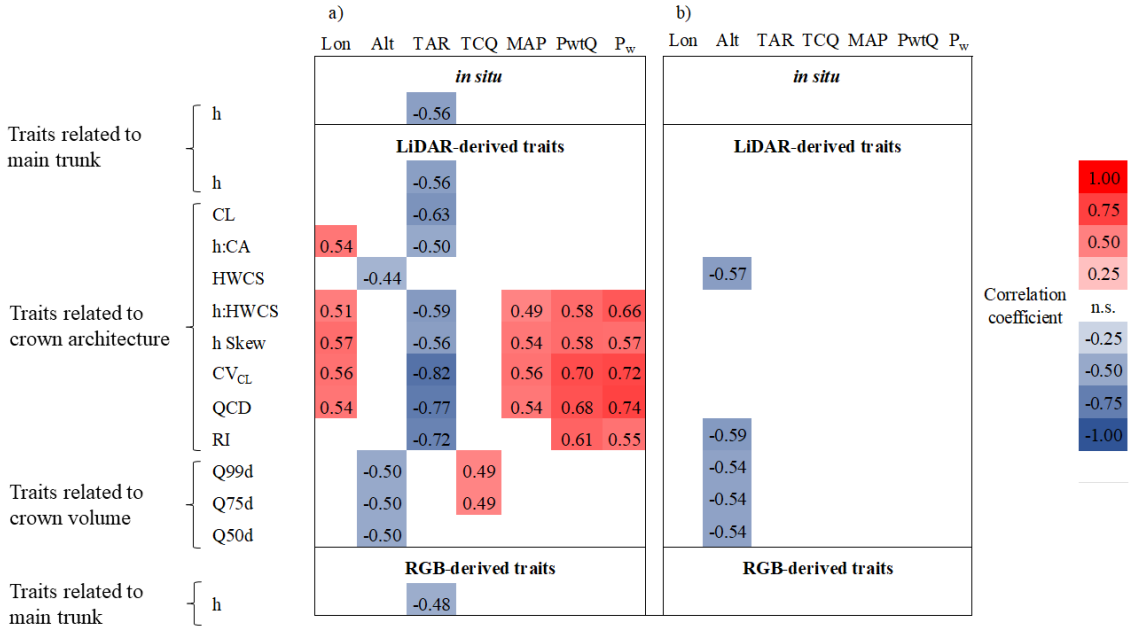

Fig. 4. Simple correlation (a) and partial correlation coefficients (b) between population means of *in situ*, RGB- or LiDAR-derived traits and climate factors at populations' origin for 16 populations of *Pinus nigra* tested in a common garden located in Valsaín (Spain). Only significant correlations ($P < 0.05$) with their respective correlation coefficients are shown.

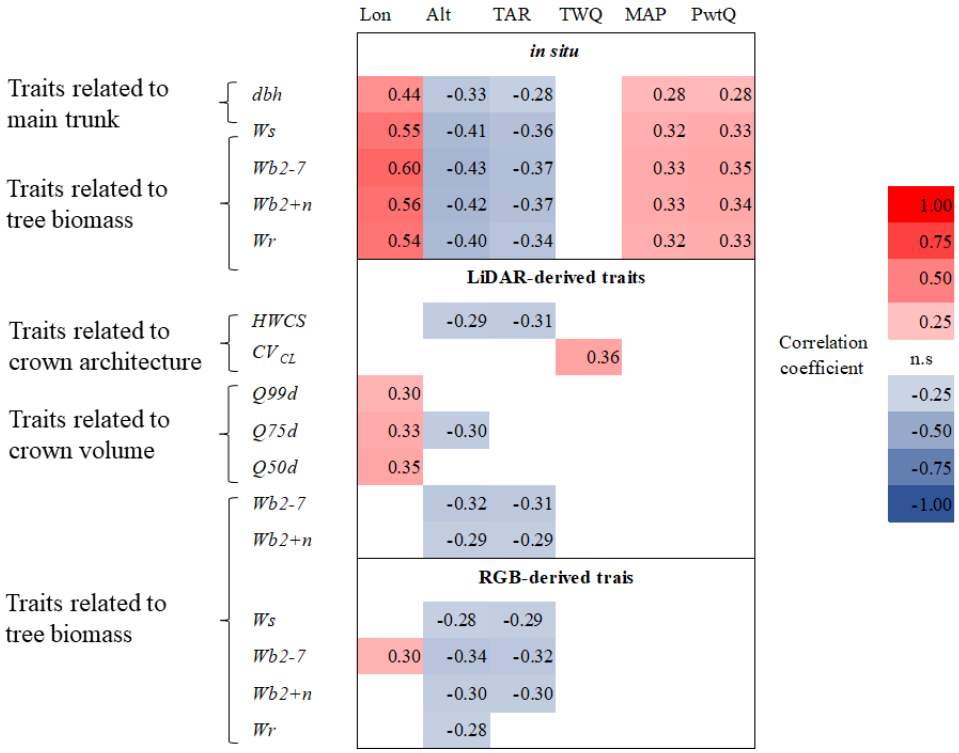

Fig. 5. Simple correlation coefficients between population means of *in situ*, RGB- or LiDAR-derived traits and climate factors at populations' origin for 48 populations of Aleppo pine tested in a common garden located in Valdeolmos (Spain). Only significant correlations ($P < 0.05$) with their respective correlation coefficients are shown.

Chapter 3 – Supplementary material

Table S1. Name, code, subspecies, geographic origin and environmental conditions of 18 populations of European black pine (*Pinus nigra*) grown in a common garden experiment located in Valsaín (Spain).

Population	Code	Subspecies	Country	Latitude	Longitude	Altitude (m, a.s.l)	MAT (°C)	TAR (°C)	TWQ (°C)	TCQ (°C)	MAP (mm)	PwtQ (mm)	PdrQ (mm)	P_w (mm)	P_s (mm)	PsP (%)
Ena	1	*salzmannii*	Spain	42° 31' 15" N	0° 45' 15" E	920	11.6	26.7	19.4	4.9	700	211	126	188	126	18
Solsonés	3	*salzmannii*	Spain	42° 02' 33" N	1° 31' 37" E	645	11.2	26.8	19.0	4.4	765	241	132	132	206	27
Cuenca	71	*salzmannii*	Spain	39° 59' 59" N	2° 03' 13" E	994	12.1	31.9	21.0	4.5	506	159	72.	143	79	16
Los Palancares	72	*salzmannii*	Spain	40° 01' 34" N	1° 58' 34" W	1221	10.7	31.6	19.7	3.3	545	172	80	148	89	16
Los Cadorzos	73	*salzmannii*	Spain	39° 50' 29" N	2° 00' 31" W	766	11.7	31.8	20.7	4.2	499	160	72	137	79	16
Paterna del Madera	81	*salzmannii*	Spain	37° 54' 60" N	2° 54' 25" W	1389	11.4	32.4	20.9	3.5	522	186	41	177	46	9
Navahondona	82	*salzmannii*	Spain	38° 34' 42" N	2° 19' 05" W	1125	11.9	33.9	21.7	3.8	475	161	48	145	54	11
Cazorla-Alcaraz	83	*salzmannii*	Spain	38° 13' 60" N	2° 37' 60" W	1329	11.0	33.2	20.7	3.0	530	181	46	170	53	10
Huéscar	84	*salzmannii*	Spain	37° 56' 55" N	2° 34' 48" W	1795	9.0	34.0	19.0	0.9	662	226	58	217	65	10
Gagniéres	150	*salzmannii*	France	44° 06' 60" N	4° 17' 00" E	277	12.9	26.8	21.0	5.7	826	285	137	206	137	17
Grancia	201	*calabrica*	Italy	39° 24' 59" N	16° 35' 09" E	1496	8.6	21.4	16.2	1.8	843	332	84	300	84	10
Macchia della tavola	202	*calabrica*	Italy	39° 22' 20" N	16° 35' 18" E	1544	7.6	21.6	15.3	0.8	831	323	86	292	86	10
Noceta	302	*laricio*	France (Corsica)	42° 09' 60" N	9° 11' 00" E	684	12.4	21.7	19.6	6.0	772	299	72	248	104	13
Sorba	303	*laricio*	France (Corsica)	42° 07' 60" N	9° 12' 00" E	1032	11.5	21.0	18.7	5.2	818	313	76	266	106	13
Ghisoni	304	*laricio*	France (Corsica)	42° 04' 60" N	9° 12' 00" E	699	12.4	21.3	19.6	6.1	747	290	68	241	99	13
Parabluerbeg	402	*nigra*	Austria	/	/	/	/	/	/	/	/	/	/	/	/	/
Milea	405	*nigra*	Greece	39° 45' 55" N	21° 11' 41" E	1111	9.4	27.1	17.7	1.6	879	315	114	278	114	13
Villetta Barrea	407	*nigra*	Italy	41° 46' 60" N	13° 46' 03" E	1360	8.0	24.2	16.2	0.7	787	254	166	175	166	21

MAT = Mean annual temperature; TAR = Annual range temperature; TWQ = Temperature of the warmest quarter; TCQ = Temperature of the coldest quarter; MAP Mean annual precipitation; PwtQ = Precipitation of the wettest quarter; PdrQ = Precipitation of the driest quarter; P_w = Winter precipitation; P_s = Summer precipitation; PsP = Summer to annual precipitation ratio.

Table S2. Name, code, ecotype, geographic origin, and environmental conditions of 56 populations of Aleppo pine (*Pinus halepensis*) grown in a common garden experiment located in Valdeolmos (Spain).

Population	Code	Ecotype	Country	Latitude	Longitude	Altitude (m, a.s.l)	MAT (°C)	TAR (°C)	TWQ (°C)	TCQ (°C)	MAP (mm)	PwtQ (mm)	PdrQ (mm)	P_w (mm)	P_s (mm)	PsP (%)
Cabanelles	11	WHC	Spain	42°15' N	2° 47' E	250	13.7	25.3	21.0	7.4	684	218	135	154	155	23
Tivissa	21	WST	Spain	42°20' N	0° 50' E	417	14.1	26.9	21.8	7.2	601	209	80	142	108	18
Sant Salvador Guardiola	31	WHC	Spain	41°40' N	1° 45' E	378	13.7	26.1	21.3	6.8	623	199	118	118	154	25
Zuera	61	WST	Spain	41°55' N	0° 55' E	582	13.1	28.5	21.4	5.7	441	146	87	98	95	22
Valdeconcha	82	DSC	Spain	40°27' N	2° 52' W	873	12.8	31.2	21.8	5.2	449	157	53	131	54	12
Alcantud	83	DSC	Spain	40°34' N	2° 18' W	683	13.6	32.7	22.7	5.8	422	164	45	125	45	11
Colmenar de Oreja	84	DSC	Spain	40°05' N	3° 20' W	1155	11.4	30.6	20.3	4.0	545	180	70	163	75	14
Cirat	91	DSC	Spain	40°03' N	0° 28' W	606	13.5	28.1	21.2	6.8	407	127	72	82	84	21
Tuéjar	92	DSC	Spain	39°49' N	1° 09' W	713	13.4	29.6	21.6	6.3	369	121	63	71	81	22
Enguidanos	93	DSC	Spain	39°38' N	1° 39' W	1009	12.1	31.9	21.2	4.5	443	148	76	103	82	19
Tibi	101	DSC	Spain	38°31' N	0° 39' W	976	12.4	32.3	21.5	4.7	420	138	61	95	61	15
Altura	102	DSC	Spain	39°47' N	0° 37' W	604	14.0	29.1	21.9	7.1	405	128	73	81	81	20
Villa de Ves	103	DSC	Spain	39°11' N	1° 15' W	817	13.1	31.5	22.1	5.4	394	133	69	83	70	18
Jarafuel	104	DSC	Spain	39°10' N	1° 01' W	564	14.4	30.0	22.9	7.0	376	120	60	80	60	16
Bicorp	105	DSC	Spain	39°06' N	0° 51' W	652	13.7	29.5	22.0	6.5	382	124	64	80	64	17
Commercial Seed	109		Spain	/	/											
Benicàssim	111	WST	Spain	40°05' N	0° 01' E	361	15.1	26.2	22.5	8.8	469	165	76	109	103	22
Gilet	112	DST	Spain	39°40' N	0° 21' W	734	14.0	33.0	23.5	6.0	422	154	46	130	47	11
Villajoyosa	131	DST	Spain	38°30' N	0° 18' W	50	17.6	26.1	24.5	11.5	308	124	31	72	50	16
Ricote	141	DST	Spain	38°09' N	1° 26' W	882	13.8	31.9	22.8	6.2	388	124	47	100	48	12

Monovar	142	DST	Spain	38°23' N	0° 57' W	778	13.9	31.9	22.7	6.2	385	125	52	89	52	14
Monovar II	143	DST	Spain	38°24' N	0° 55' W	493	15.2	30.0	23.5	7.9	350	117	43	79	50	14
Paterna	144	DSC	Spain	38°38' N	2° 17' W	1001	12.5	34.2	22.3	4.4	450	154	45	138	51	11
Abarán	145	DST	Spain	38°17' N	1° 16' W	702	14.4	30.8	23.0	6.9	362	115	46	89	46	13
Quéntar	151	DST	Spain	37°14' N	3° 25' W	1116	13.3	34.2	22.5	5.6	490	185	34	176	35	7
Benamaurel	152	DSC	Spain	37°42' N	2° 44' W	894	14.1	34.4	23.6	6.1	405	147	31	138	33	8
Vélez Blanco	153	DST	Spain	37°47' N	2° 01' W	875	13.6	32.7	22.7	5.9	381	130	37	117	38	10
Santiago de la Espada	154	DSC	Spain	38°14' N	2° 28' W	839	13.5	33.4	23.0	5.4	411	146	36	131	40	10
Lorca	156	DSC	Spain	37°52' N	1° 32' W	694	14.7	31.9	23.4	7.2	357	122	35	105	35	10
Alhama de Murcia	157	DSC	Spain	37°45' N	3° 01' W	831	13.6	30.9	22.3	6.1	382	125	40	105	40	10
Quesada	158	DSC	Spain	37°45' N	1° 57' W	653	15.0	32.0	23.9	7.4	381	142	29	131	30	8
Lentergi	171	DST	Spain	36°49' N	3° 41' W	364	16.9	26.6	24.1	10.7	436	187	20	173	23	5
Carratraca	172	DST	Spain	36°51' N	4° 50' W	501	15.7	26.4	23.0	9.5	651	308	20	286	26	4
Frigiliana	173	DST	Spain	36°49' N	3° 55' E	596	16.0	27.4	23.4	9.7	479	202	22	192	25	5
Palma de Mallorca	182	WST	Spain	39°09' N	2° 56' E	761	13.9	33.2	23.2	5.8	447	160	48	138	51	11
Santanyí	183	WST	Spain	39°17' N	3° 03' E	643	14.9	34.4	24.5	6.5	401	148	37	133	41	10
Alcudia	184	WST	Spain	39°52' N	03° 10' E	752	14.0	33.4	23.5	5.9	432	158	47	134	49	11
Calvia	185	WST	Spain	39°33' N	03° 08' E	668	14.7	33.9	24.3	6.4	404	147	41	130	44	11
Mercadal	186	WST	Spain	39°58' N	4° 10' E	532	15.3	32.0	24.4	7.4	352	119	43	100	50	14
Atàlix	187	WST	Spain	39°55' N	4° 03' E	555	15.5	31.8	24.8	7.6	368	123	44	103	50	14
Cala d'Hort	191	WST	Spain	38°53' N	1° 15' E	784	13.6	33.5	22.9	5.7	390	130	62	84	63	16
Ses Salines	192	DST	Spain	38°50' N	1° 24' E	907	13.0	33.8	22.4	5.0	409	139	64	88	66	16
Ses Salandres	193	DST	Spain	39°03' N	1° 20' E	1052	11.9	33.0	21.3	3.9	437	150	70	94	76	17
Valbuena de Duero	201		Spain	/	/											

Vega de Valdetronco	202		Spain	/	/										
Villavieja Tordesillas	203		Spain	/	/										
Istaia-eyboia	211	DHT	Greece	38°44' N	23°31'E	70	16.4	24.9	24.7	8.8	501	209	35	112	68	14
Amfilohia (likely seed orchard)	212	DHT	Greece	38°53' N	21°18'E	529	14.0	28.1	22.2	6.4	863	364	65	144	69	8
Tatoi-attica	213	DHT	Greece	38°27' N	23°28'E	252	15.3	27.9	23.9	7.6	532	226	36	134	66	12
Kassandra	214	DHT	Greece	40°05' N	23°54'E	347	14.2	25.4	23.0	6.1	507	187	65	205	35	7
Gemenos	221	WHC	France	43°25' N	5°40'E	392	13.3	25.8	20.9	6.6	708	243	93	197	93	13
Litorale Tarantino	231	WST	Italy	40°37' N	17°07'E	205	14.8	25.8	22.9	7.7	589	213	78	187	78	13
Gargano Monte Pucci	232	WST	Italy	41°54' N	15°57'E	457	15.2	22.6	21.8	8.6	204	68	36	48	36	18
Gargano Marzini	233	WST	Italy	41°33' N	15°51'E	0	16.2	26.7	24.4	9.0	443	146	76	117	76	17
Thala	241	DST	Tunisia	35°34' N	8°39'E	949	15.4	30.8	24.7	7.3	423	131	60	122	60	14
Tabarka	242	DHT	Tunisia	36°30' N	9°04'E	266	17.6	30.2	26.2	10.0	539	222	37	222	37	7

MAT = Mean annual temperature; TAR = Annual range temperature; TWQ = Temperature of the warmest quarter; TCQ = Temperature of the coldest quarter; MAP Meanannual precipitation; PwtQ = Precipitation of the wettest quarter; PdrQ = Precipitation of the driest quarter; P_w = Winter precipitation; P_s = Summer precipitation; PsP = Summer to annual precipitation ratio.

Table S3. Treetops accuracy detection of the local maxima algorithm applied to LiDAR and RGB canopy height models. Recall (R), precision (P) and F-score (F) are shown.

Species	LiDAR						RGB					
	Correctly detected treetops (TP)	Falsely detected treetops (FP)	Non-detected treetops (FN)	R	P	F	Correctly detected treetops (TP)	Falsely detected treetops (FP)	Non-detected treetops (FN)	R	P	F
P. nigra	317	3	28	0.919	0.991	0.953	314	6	31	0.910	0.981	0.944
P. halepensis	540	18	43	0.926	0.968	0.947	518	38	65	0.889	0.932	0.910

Table S4. Validation of *h* and *dbh* derived from LiDAR and RGB canopy height models against *h* and *dbh* measured *in situ*. Root mean square error (RMSE) and mean absolute error (MAE) are shown.

		P. nigra		*P. halepensis*	
	Traits	RMSE	MAE	RMSE	MAE
LiDAR-derived	*h*	0.36	0.24	0.43	0.31
	dbh	1.61	1.25	1.67	1.26
RGB-derived	*h*	0.40	0.29	0.45	0.34
	dbh	1.74	1.37	1.76	1.26

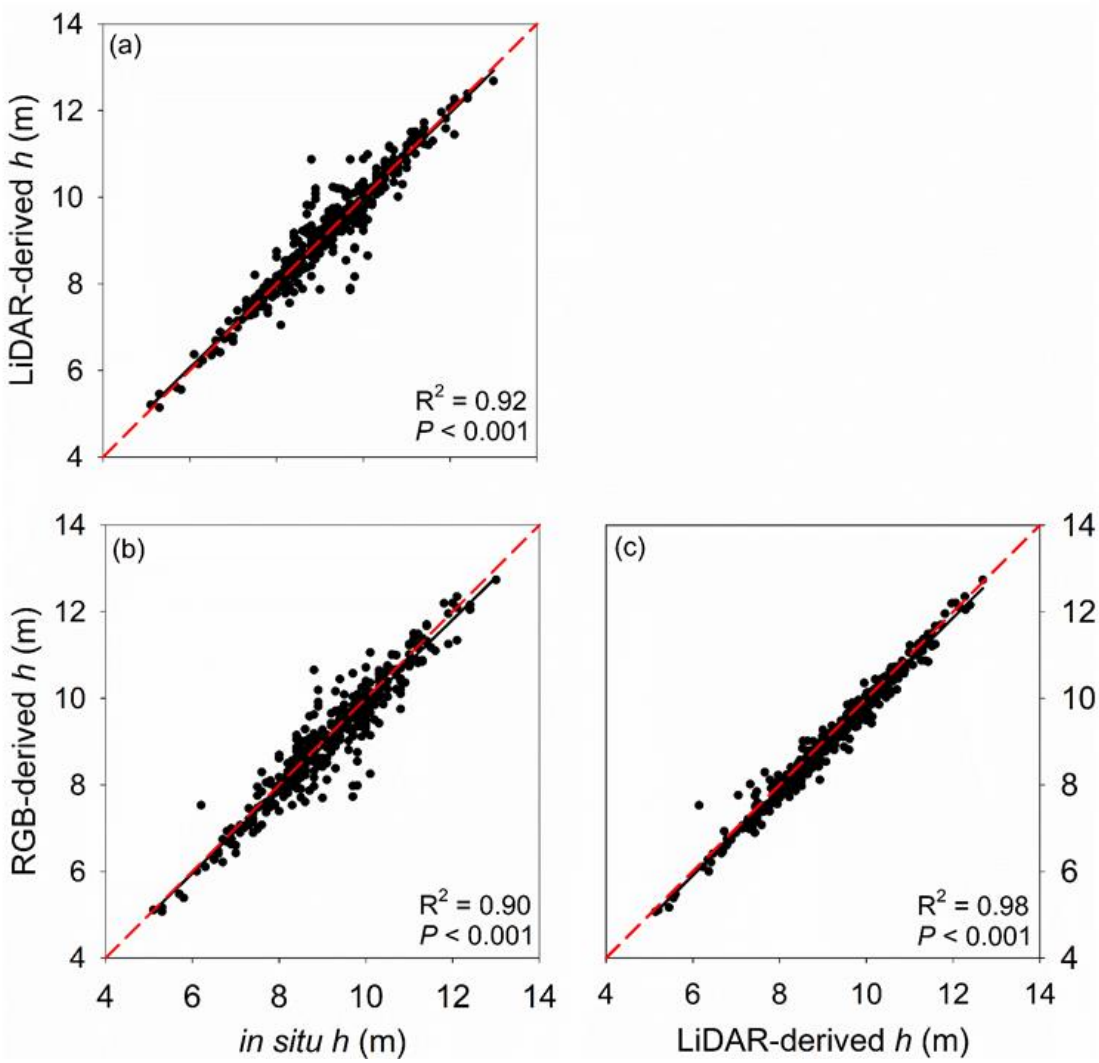

Fig. S1. Linear regressions between *in situ*-measured *h* and LiDAR- or RGB-derived *h* (a, b, respectively), and between LiDAR-derived *h* and RGB-derived *h* (c) for 345 black pine trees grown in a common garden located in Valsaín (Spain). R- squared and *P* values are shown.

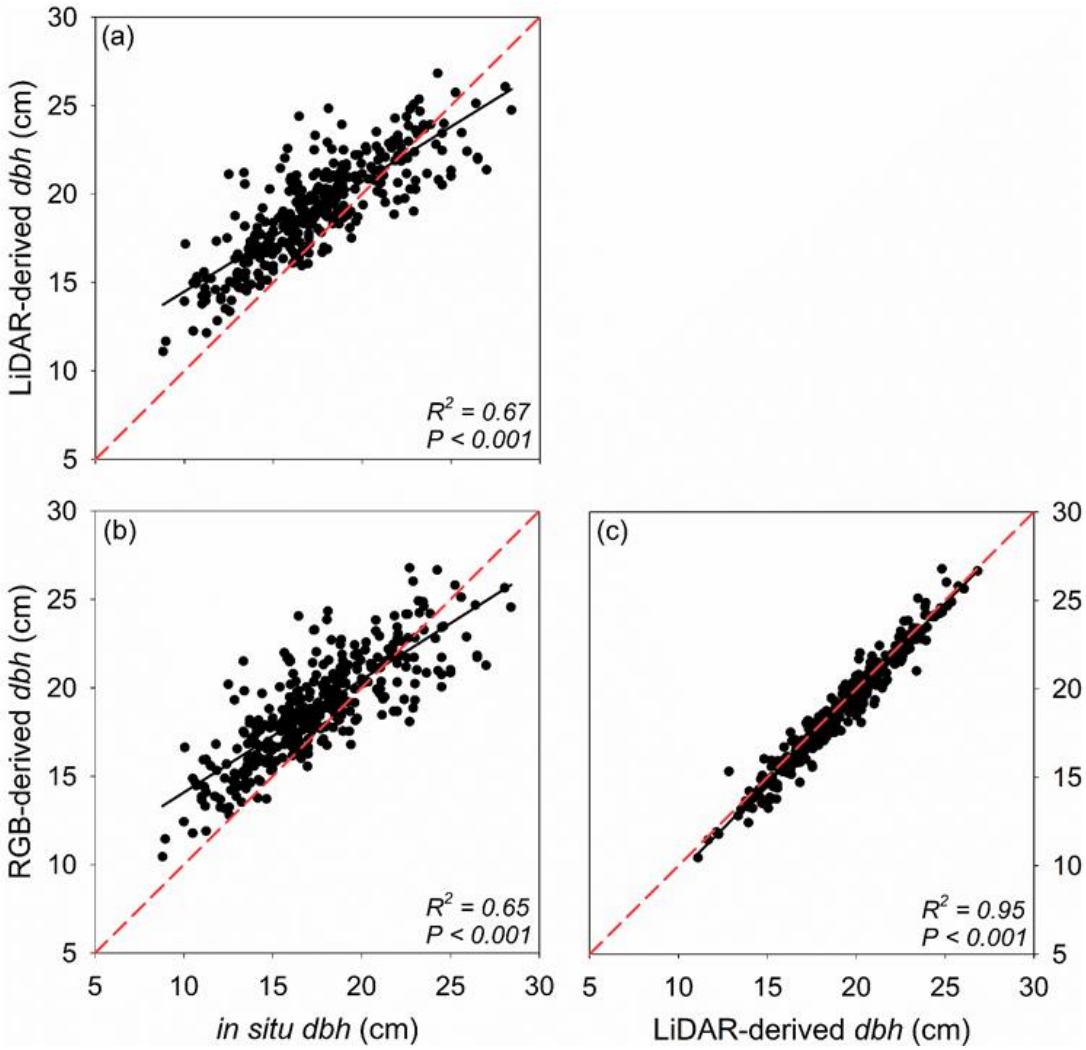

Fig. S2. Linear regressions between *in situ* measured *dbh* and LiDAR- or RGB-derived *dbh* estimation (a, b, respectively), and between LiDAR-derived *dbh* and RGB-derived *dbh* (c) for 345 black pine trees grown in a common garden located in Valsaín (Spain). R-squared and *P* values are shown.

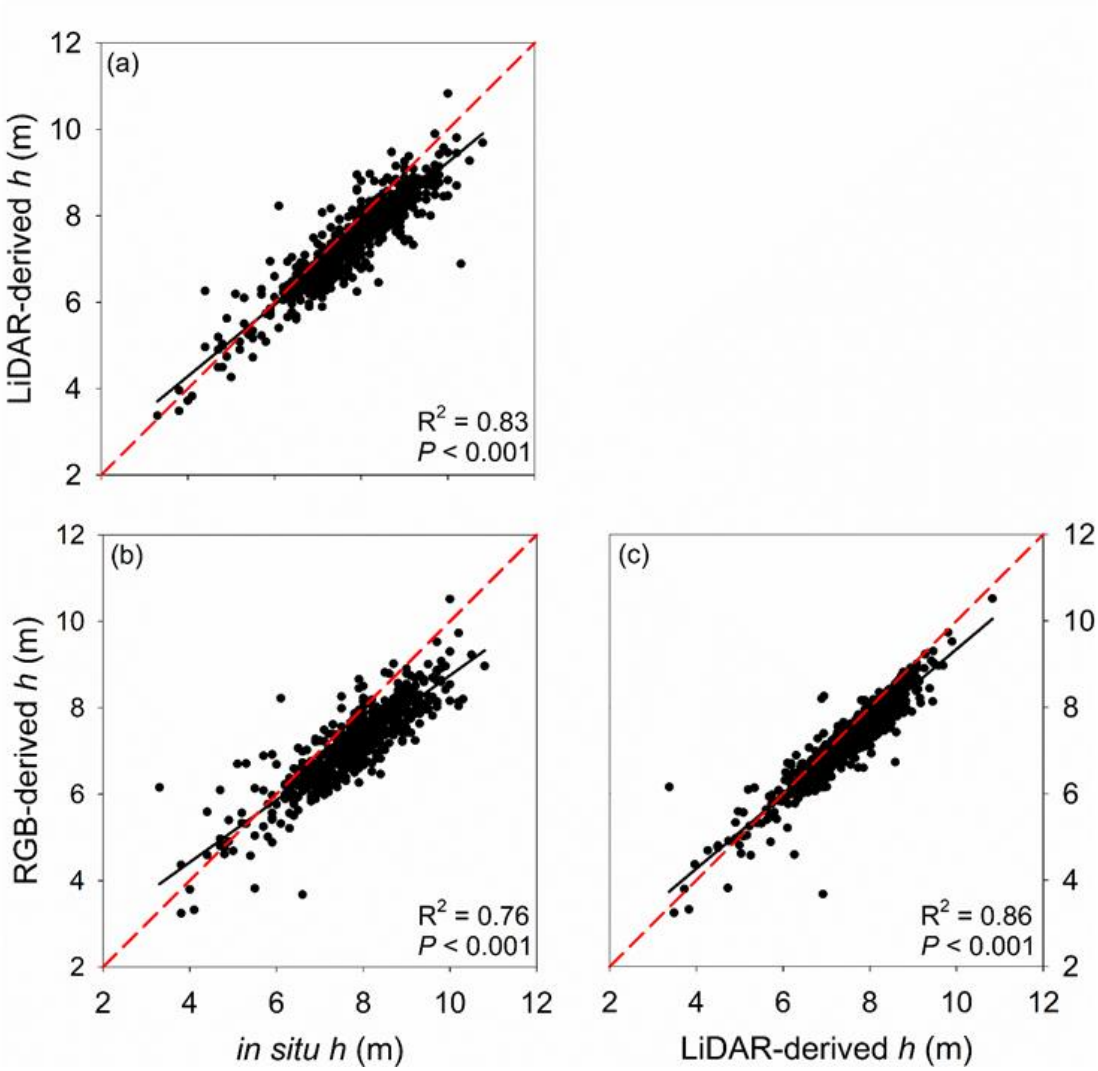

Fig. S3. Linear regression between *in situ* measured *h* and LiDAR- or RGB-derived *h* (a, b, respectively), and between LiDAR-derived *h* and RGB-derived *h* (c) for 583 Aleppo pine trees grown in a common garden located in Valdeolmos (Spain). R-squared and *P* values are shown.

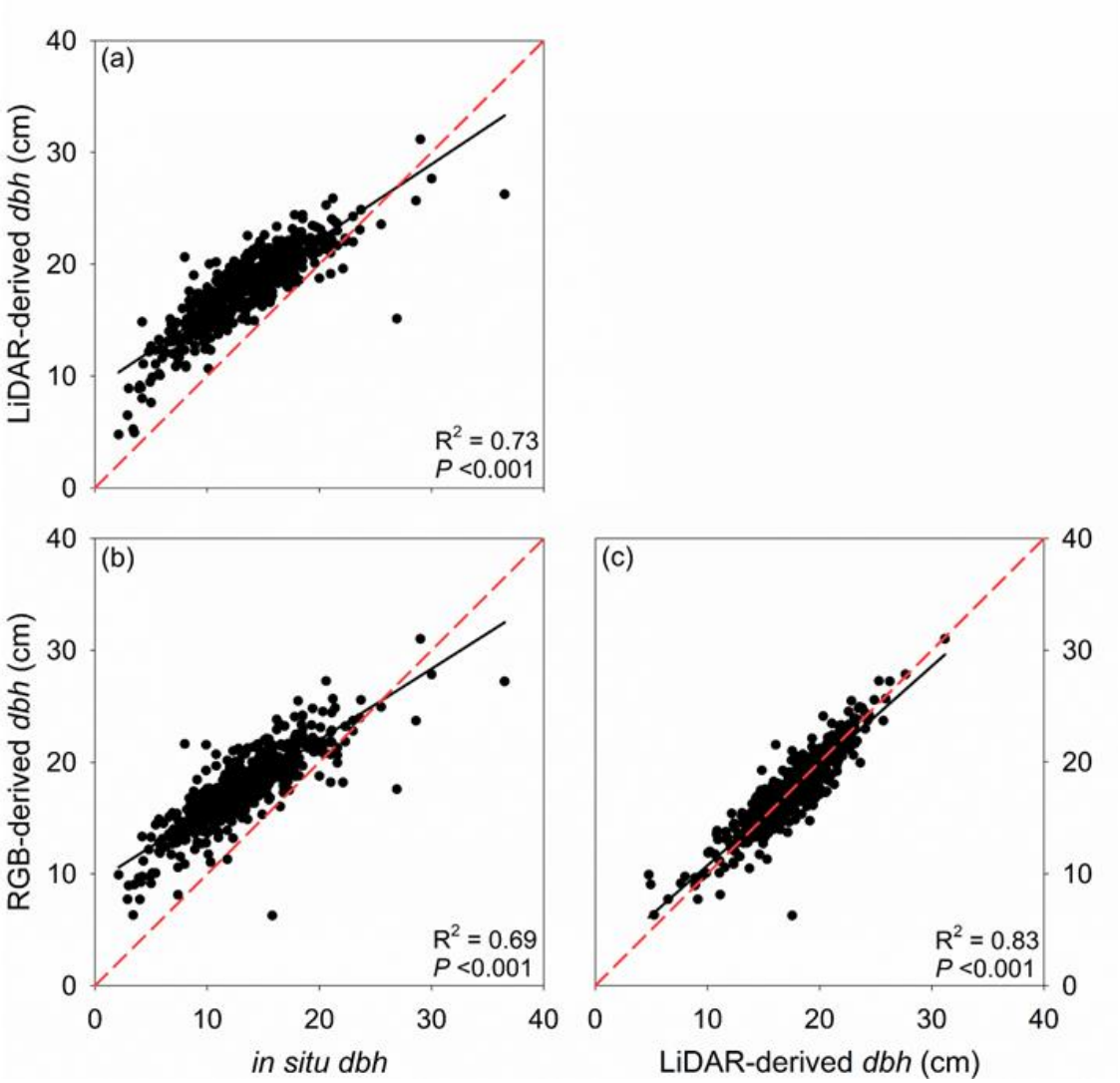

Fig. S4. Linear regressions between *in situ* measured *dbh* and LiDAR- or RGB-derived *dbh* estimation (a, b, respectively), and between LiDAR-derived *dbh* and RGB-derived *dbh* (c) for 583 Aleppo pine trees grown in a common garden located in Valdeolmos (Spain). R-squared and *P* values are shown.

Chapter 4

Remotely sensed and ground measurements reveal intraspecific differences in early season needle unfolding and senescence but lack of variability in litter flammability of *Pinus halepensis*

Erica Lombardi[1,2,*], Shawn Carlisle Kefauver[1,3], Luis Serrano[2], Ester Sin[2], Paula Piñas-Bonilla[4], Beatriz Pérez[4] , Belén Luna[4], Gonzalo Zavala[4], Víctor Resco de Dios[1,2], Jordi Voltas[1,2]

[1]Joint Research Unit CTFC – AGROTECNIO – CERCA, Av. Alcalde Rovira Roure 191, Lleida 25198, Spain

[2]Departament of Agricultural and Forest Sciences and Engineering, Av. Alcalde Rovira Roure 191, Lleida 25198, Spain

[3]Integrative Crop Ecophysiology Group, Plant Physiology Section, Faculty of Biology, University of Barcelona, Av. Diagonal 643, 08028 Barcelona, Spain

[4]Department of Environmental Sciences, University of Castilla-La Mancha, Av. Carlos III, 45071 Toledo, Spain

Abstract

Pinus halepensis Mill. is a conifer typical of Mediterranean pinewoods adapted to drought and fire. Although the timing of seasonal events in *P. halepensis* is strongly associated with these stressors and other environmental factors, needle phenology and litter flammability are insufficiently characterized at the intraspecific level. These traits can be informative of the existence of locally adapted populations across the species' distribution range, and remote sensing approaches are promising tools to infer phenological changes in forest trees. In this study, we investigated intraspecific differentiation of P. halepensis related to needle phenology at the onset of the fire season (May-June) through vegetation indexes (VIs) obtained from unmanned aerial vehicles. We collected aerial images using multispectral and RGB sensors for 56 adult populations of P. halepensis categorized into five ecotypes growing in two common gardens located in Spain under contrasting conditions (dry-continental *versus* wet-coastal). In the dry trial, we additionally monitored the temporal variation of RGB-derived indexes using two flights spaced over a one-month period. We also performed four consecutive ground measurements of needle pigments and fuel moisture content and obtained litter flammability traits for a subset of populations. Most *in situ* measurements and flammability traits did not show population differentiation. Regarding RGB-derived VIs, we did not detect obvious temporal patterns which differed among populations. However, we observed greener canopies in June than in May, which are indicative of the pace of current-year needle development. We also deduced an earlier phenology (i.e., earlier current-year needle unfolding) in the dry-continental trial. Ecotypic differentiation was found for some vegetation indexes related to needle unfolding (i.e., *TCARI/OSAVI*) and old needle senescence (i.e., *PRSI*). These differences were generally consistent across trials and time, and fundamentally indicated that sub-humid ecotypes typical of the eastern Mediterranean showed earlier needle unfolding and old needle senescence than semiarid ecotypes thriving in western continental Mediterranean areas. The intraspecific divergence observed in early season phenology is potentially related to the existence of contrasting life-history strategies present at the intraspecific level for the species. In particular, some semi-arid ecotypes, which are known to optimize the trade-off between carbon gain and water loss, exhibited an early old needle senescence (high likelihood of crown fire development) coupled with a late needle unfolding (conservative water use). These results indicate a possible trade-off between drought and fire resistance for the species, which suggest the importance of considering the intraspecific characteristics of Aleppo pine in forest management actions.

Keywords: Aleppo pine; vegetation indexes; intraspecific variability; litter flammability; needle phenology; remote sensing

Introduction

Pinus halepensis Mill. (Aleppo pine) is one of the most widespread conifer species in the Mediterranean basin (Picornell-Gelabert et al. 2021; Mauri et al. 2016). It presents high economic and ecological values (Chambel et al. 2013) and, as such, it is widely used in reforestation programs of Mediterranean ecosystems (Taïbi et al. 2014). The species is resistant to drought and prevails in fire-prone habitats due to its adaptive strategies to cope with fire, including serotiny, poor apical dominance and profuse branching (Pausas, 2015). Owing to its high intraspecific variability and plasticity, *P. halepensis* inhabits very contrasting ecological niches (Voltas et al. 2018). This differentiation among populations has been widely studied for many functional traits related to roots (Lombardi et al. 2021), crown structure (Lombardi et al. 2022), water use patterns (Voltas et al. 2015) and phenology (Klein et al. 2013), and also for remotely sensed vegetation indexes related to photosynthetic pigments, leaf area and water content (Santini et al. 2019b). On the contrary, knowledge on genetic variation in needle phenology is scarce in Aleppo pine (Santini et al. 2019b), and also on differentiation of flammability-related traits like litter flammability, which are widely studied at the interspecific level (Varner et al. 2022) but poorly investigated at the intraspecific level (Bastien & Ganteaume, 2020).

Understanding variation in the response of trees to disturbances has been a long-term goal of plant ecology (Grime, 1977). Some studies postulate that there is a fundamental trade-off between adaptations to drought and fire in pines (Karavani et al. 2018). It has been hypothesized that intraspecific variation in traits enhancing survival under drought occurs at the expense of increasing fire danger and, vice versa, that traits enhancing survival under fire may decrease performance under drought. A typical response from *P. halepensis* at the beginning of the fire season is to induce senescence in older leaves, which diminishes transpiration area and, consequently, water demand, but at the expense of increasing crown flammability. And concomitantly, *P. pinaster* individuals with thicker barks, which may survive under surface fires, show reduced tolerance to embolism (Resco de Dios et al. 2018). However, most evidence for this trade-off is anecdotal and lacking rigorous testing.

Phenology is a key driver of plant carbon and water cycles, and it can be described as the timing of reproduction and of other events related to e.g., growth or senescence of individuals (Ciocîrlan et al. 2022; Berra et al. 2019). The phenology of conifers comprises three main phases (bud dormancy, bud flush and needle senescence). Needle phenology in particular can be divided into needle unfolding, maturation, and

senescence and fall (Kumar et al. 2019), and it involves changes in photosynthetic pigments and nutrient pools dynamics (Fréchette et al. 2020; Springer et al. 2017). Needle phenology is strongly correlated with environmental condistions, especially temperature and water availability (Peaucelle et al. 2019). It can can influence fire behaviour by affecting live vegetation moisture, fuel vegetation structure or litter composition, for instance (Loudermilk et al. 2022; Silvério et al. 2015), and vice versa, fire can shape the composition and dynamics of forest ecosystems and thus affect tree phenology (e.g., timing of dormancy, growth and reproduction) (Miller et al. 2019; Risberg & Granström, 2009). Although field observations provide precise and important information on phenology, they are time-consuming and labour-intensive (Ciocîrlan et al. 2022). Lately, remote sensing is being used to effectively monitor tree phenology (Motohka et al. 2010), since images derived from satellites and especially from unmanned aerial vehicles (UAVs) can provide information at different spatiotemporal scales with high resolution (Wong et al. 2020; Berra et al. 2019). In particular, multispectral and RGB (Red, Green and Blue) sensors mounted on UAVs detect light reflectance variation, thereby providing reliable phenological data at the individual level (Kleinsmann et al. 2023; Santini et al. 2019b).

A vegetation index (VI) is a simple mathematical calculation that integrates two or more wavelengths of spectral reflectance image data (spectral bands or images) for the assessment (estimation or enhanced visualization) of surface biophysical properties (Huete, 2012). To date, hundreds of VIs have been evaluated from both visible and non-visible (including near infrared, short-wave infrared and even thermal infrared) wavelengths. VIs can provide information about chemical and pigment leaf composition, water content, leaf area, canopy cover and canopy health, for instance (Ciocîrlan et al. 2022; Santini et al. 2019b; Xue & Su 2017; Stimson et al. 2005). VIs have been used in field crops (Starý et al. 2020; Gracia-Romero et al. 2018) and, also, in forestry to estimate canopy properties at the landscape levels (Wong et al. 2019; Klosterman et al. 2018). Currently, many VIs are used to infer plant phenology, both multispectral-derived VIs (especially those using the reflectance in the near-infrared region) and also RGB-derived indexes. Tree level, RGB-derived indexes can be considered an affordable alternative to multispectral records if adquired through UAVs (Starý et al. 2020; Gracia-Romero et al. 2018; Kefauver et al. 2015). However, applications of VIs to assess crown properties and tree phenology at the intraspecific level is still scarce, especially for evergreen conifers (Ciocîrlan et al. 2022; Wong et al. 2022; Santini et al. 2019b).

In this study, we used VIs obtained from UAVs along withvegetation samples collected *in situ* to identify intraspecific differences in needle phenology of P. *halepensis*. We were especially interested in characterizing needle unfolding and old needle senescence at the onset of the wildfire season in the western Mediterranean (end of spring). Needle lifespan in *P. halepensis* is approximately three years, and three-years-old needles usually become dry and senesce towards the second half of June. Moreover, we evaluated intraspecific variation of litter flammability and flammability traits, such as live fuel moisture content (*FMC*). We used two common garden experiments characterised by a dry and continental climate (Zuera, northeastern Spain), and a coastal, sub-humid Mediterranean climate (Altura, eastern Spain). By using range-wide populations, we sought to describe intraspecific genetic variation in needle phenology related to photosynthetic pigments at the onset of the fire season (May-June), which can be potentially informative of differential plasticity and adaptation to varying conditions across the Mediterranean basin.

We expected an earlier phenology in the inland site (Zuera), as a consequence of drier conditions for the species related to higher temperatures and less available water, as previously described for needle unfolding (Camarero et al. 2022). We hypothesized that differences among populations for both *in situ* traits and RGB and multispectral indexes reflected different phenological responses (i.e., needle unfolding or old needle senescence) during late spring. In this regard, we also expected to detect intraspecific differences for flammability traits potentially related to contrasting evolutionary histories and adaptive intraspecific differentiation to fire-prone habitats. Specifically, we presumed that populations and ecotypes experiencing less water availability at their origin could show less *FMC,*, earlier old needle senescence and delayed needle unfolding as a result of a more conservative water-use strategy.. Because of their higher tolerance to drought, these populations may have less survival changes under surface and crown fires due to trade-offs among plant functional traits (i.e., enhanced flammability) (Karavani et al. 2018; Resco de Dios et al. 2018).

Material and Methods

Study sites

The study was performed in two provenance trials located in Zuera (Zaragoza province, Spain; 41°52′24″N, 00°38′57″W, 425 m a.s.l.) and Altura (Castellón province, Spain; 39°49′29″N, 00°34′22″W, 640 m a.s.l.) (Fig. 1). Zuera and Altura hold 721 (80% survival) and 807 (90% survival) adult trees respectively. These trees are

assigned to 56 populations of *P. halepensis* originating from mainland Spain, Balearic Islands, France, Greece, Italy and Tunisia (Table S1). The seeds were collected in 1995 from 20 to 30 adult individuals per population, spaced at least 100 m apart, and were sown in a forest nursery in Spain using standard container practices (Landis, 1990) the following year. In 1997, 896 one-year old seedlings (16 seedlings per population) were transplanted at both study sites. The experimental design was a Latinised row-column with four replicated blocks (John & Williams, 1998). This design efficiently controls intra-site variability, as systematic changes in both column and row directions can be incorporated into a linear mixed-effects model.

We used all trees available in both trials for obtaining UAV-based data, while a subset of trees from Zuera (a total of 36 individuals belonging to six populations) was used for ground truthing. This subset contained populations from the Iberian Peninsula, Balearic Islands, Tunisia and Greece, which are representative of most of the current distribution range of the species. Aleppo pine populations were further grouped into five climate-based ecotypes as proposed by Patsiou et al. (2020): dry-summer/semiarid/temperate (DST), dry-summer/semiarid/cold (DSC), dry-summer/sub-humid/temperate (DHT), wet-summer/semiarid/temperate (WST), and wet-summer/sub-humid/cool (WHC). This division stemmed from a hierarchical cluster analysis based on climatic information of populations for the purpose of delineating broad intraspecific patterns of growth performance under different climate change scenarios (Patsiou et al. 2020).

Plant material and climate data

We collected needles of six populations (#11, 142, 152, 182, 214 and 242; Table S1) during four sampling campaigns in 2021 (May 14th and 28th, June 11th and July 2nd). Needles were collected from healthy mid-canopy branches of six trees per population following the column direction of the trial. These branches were accessible with a telescopic lopper, while the sparse foliage of Aleppo pine made possible that full sunlight reached most of its crown. Two to five branchlets were sampled per tree (Minocha et al. 2009). Aleppo pine generally starts to develop new needles in spring, and these needles can be retained in the tree for three years before senescing (Balaguer-Romano et al. 2020; Girard et al. 2011). The sampled needles corresponded to the previous year (1-yr old) or older cohorts (≥2-yr old) (current year needles were just emerging and not clearly visible in the two earlier sampling campaigns). Needle tissue was used to quantify chlorophyll content (*Chl*), particularly chlorophyll *a* (Chl_a), chlorophyll *b* (Chl_b) and total chlorophyll (Chl_{a+b}), total carotenoid content (*Car*) and live

fuel moisture content (*FMC*). We collected additional needles during the last sampling campaign to infer specific leaf area (*SLA*) and stomatal conductance (g_{sw}).

The needles used to determine *Chl* and *Car* were immediately frozen in the field and stored in a dark place. *Chl* and *Car* were measured following the protocol by Minocha et al. (2009). We chopped 15 mg of unfrozen samples into 1.5 ml of 95% ethanol and afterwards they were stored in a water bath at 65 ºC for 16 hours. Once the samples were removed from the water bath, they were left few minutes at room temperature to equilibrate, and then vortexed for 1 min at low speed. Finally, the samples were centrifuged for 5 min at 13,500 g. We then recorded the absorbance at 649 nm, 664 nm and 470 nm using a UV spectrophotometer (UV-1600 PC, VWR International, Belgium). Chl_a, Chl_b, Chl_{a+b} and *Car* were estimated using the following equations:

$$Chl_a = (13.36 \times A664) - (5.19 \times A649) \quad (1)$$

$$Chl_b = (27.43 \times A649) - (8.12 \times A664) \quad (2)$$

$$Chl_{a+b} = Chl_a + Chl_b \quad (3)$$

$$Car = (1000 \times A470 - 2.13 \times Chl_a - 97.46 \times Chl_b) / 209 \quad (4)$$

The needle samples used to estimate *FMC* were stored in metallic tins sealed with parafilm. Once in the laboratory we weighted the fresh weight of samples, which were then oven-dried at 105 ºC during 48 h (Matthews, 2010). Afterwards the samples were weighted again, and the *FMC* was calculated as follows:

$$FMC = \frac{FW - DW}{DW} \times 100 \quad (5)$$

where *FW* represents the fresh weight and *DW* is the dry weight.

Leaf area (*LA*) was estimated using a scanner Area Meter (AM100, ADC, UK) using ten needles per population. After that, the samples were oven-dried at 105 ºC during 48 h (Matthews, 2010) to obtain leaf dry weight (*DW*), and *SLA* was calculated as:

$$SLA = \frac{LA}{DW} \quad (6)$$

Stomatal conductance was measured in the field using a LI-600 porometer (LI-COR Biosciences, Lincoln, NE, USA). We placed the needles in a plane across the leaf chamber aperture and we cover the side in contact with the atmosphere to avoid air leakage and ensure a stable reading for every measurement. We made three measurements per tree and their average was used for statistical analysis.

For each population, climate data at origin was obtained from the WorldClim database (Fick, 2017) at 1 km^2 spatial resolution. We used the total of 19 bioclimatic variables available in the database.

UAV-based flights and images processing

For the Zuera trial, RGB images were acquired through a UAV Mavic 2 Pro (DJI, China) equipped with an RGB camera of 20 MP, while multispectral images were acquired through a UAV Oktokopter 6S12 XL (Mikrokopter, Germany) equipped with a micro-MCA 11+ILS (Incident Light Sensor for dedicated band-wise spectral calibration) multispectral camera (Tetracam Inc., Chatsworth, CA, USA). The multispectral camera had 11 bands (the specific wavelengths captured by the sensor are described in Table S2). Two consecutive flights, each performed with UAV Mavic and UAV Oktokopter, were done at around midday on May 14th and on June 11th (2021) at an altitude of 57 m. A total of 385 images were obtained with the RGB camera, while 105 images were acquired with the micro-MCA camera. A field spectrometer ASD FieldSpec Pro FR^{TM} (USA) was used to measure, *a posteriori*, the absolute reflectance of the multi-colour landing panels in otimal light conditions and, hence, to provide a secondary empirical calibration to the micro-MCA data. Measurements made with the field spectrometer were employed to improve the instantaneous spectral calibration of the micro-MCA camera as flying conditions were sub-optimal, with some light cirrus clouds and moderate to heavy winds.

For the Altura trial, RGB and multispectral images were acquired on May 25th (2017) through the same Oktokopter 6S12 UAV by Mikrokopter described above. A Lumix GX7 RGB camera (Panasonic, Japan) with a 20 mm focal length and 16 MP resolution was used for the acquisition of RGB images, while a micro-MCA 12+ILS multispectral camera with 10 bands (Tetracam Inc., Chatsworth, CA, USA) and 15.6-megapixel resolution (1.3 MP for each of the 12 sensors) was employed to capture multispectral images (the wavelength capture by each sensor is described in Table S3).

The ILS processing to reflectance included in the Tetracam PixelWrench software includes all calibration steps to at-sensor reflectance, including parallax adjustments, DN and Dark Current.

Imagery processing

The Agisoft Metashape Professional software (Agisoft LLC, St. Petersburg, Russia, version 1.6.3.10732) was employed to align the multispectral or RGB images and produce dense points clouds and orthomosaic images and spectral calibration was done using ENVI 5.6.3 (USA). Unfortunately, we could not use the multispectral data retrieved in Zuera on May 14th due to technical reasons regarding the spectral calibration.

We used the open-source software LAStools (version 201003) (Isenburg 2017) and US Forest Service FUSION/LDV (version 4.21) (McGaughey, 2015) to eliminate noisy points, classify the valid points and normalize the RGB point clouds (through *lasnoise*, *lasclassify lasheight* functions in LAStools), and to obtain a digital terrain model (DTM) and a canopy height model (CHM) (through *GridSurfaceCreate* and *CanopyModel* functions in FUSION/LDV) (Lombardi et al. 2022). After that, we applied the *vwf* function (Popescu & Wynne, 2004) implemented in the ForestTools R package (version 4.1.2) (Plowright, 2018) to identify individual treetops. After visual inspection and manual correction of trees marked by the algorithm, we run the *mcws* function (Meyer & Beucher, 1990) of ForestTools to segment tree crowns, which were again visually inspected and manually corrected in QGIS (version 3.26.3). Afterwards, total tree height and crown area were estimated at the tree level. We did not validate tree height and crown area with ground-truth data; however, a validation procedure previously carried out in a twin common garden experiment to Zuera and Altura was highly satisfactory (R^2 of 0.8 and RMSE of 0.45 m) (Lombardi et al. 2022).

Multispectral and RGB vegetation indexes (VIs)

Vegetation indexes (VIs; Table 1) were calculated in QGIS through the raster calculator option for both the RGB and multispectral orthomosaics. Every index was calculated at the tree level (a workflow of the process is summarized in Fig. 2) using the zonal statistics function of QGIS. To this end, we used the average pixel value of each crown. We calculated four RGB-derived VIs: green percentage index (*G%*), green-red vegetation index (*GRVI**), green leaf index (*GLI*), and triangular green index (*TGI*). We also obtained six multispectral-derived VIs: normalized difference vegetation index (*NDVI*), plant senescence reflectance index (*PSRI*), green ratio vegetation index (*GRVI*), enhanced vegetation index (*EVI*), transformed chlorophyll absorption reflectance index (*TCARI*), and optimized soil adjusted vegetation index (*OSAVI*). We also calculated the ratio between the last two indexes (*TCARI/OSAVI*). Two additional multispectral VIs were also calculated in Zuera: chlorophyll/carotenoid index (*CCI*) and photochemical reflectance index (*PRI*), as micro-MCA sensors

partially changed between trial flights to improve the acquisition of vegetation information.

The two common gardens evaluated are free from understory. Thus, the reflected signal was unlikely affected by different backgrounds through time and among trial locations. A brief description of the VIs used in this study is as follows. *G%* is one of the mostly used RGB VI to track plant phenology (Larrinaga et al. 2019; Alberton et al. 2014; Sonnentag et al. 2012). It quantifies vegetation greenness through changes in leaf color (Alberton et al. 2014; Thapa et al. 2021). *GRVI** is sensitive to green color (Tucker, 1979) and it is also associated with leaf color changes (Motohka et al. 2010). It has been used in previous studies to monitor phenological changes (Anderson et al. 2016; Motohka et al. 2010). *GLI* is obtained using all three bands of the RGB camera (Louhaichi et al. 2001) and is sensitive to leaf chlorophyll content (Bulut, 2023). *TGI* is mostly associated with nitrogen and chlorophyll content (Hunt et al. 2011), and it has been used to detect changes in plant phenology (Starý et al. 2020, Hunt et al. 2012). *NDVI* is a commonly used VI calculated from the red and the near-infrared wavebands (Rouse et al. 1974) that has been used in many studies as a proxy for plant productivity and phenology (Wong et al. 2020; Santini et al. 2019b; Anderson et al. 2016). *PSRI* is also associated with photosynthetic pigments (Merzlyak et al. 1999) and has been used to monitor changes during leaf senescence (Li et al. 2022; Olmo et al. 2021). *GRVI* is sensitive to photosynthetic rates and can be used to estimate changes in leaf pigments (Sripada et al. 2006). *EVI* is considered an improved *NDVI* (Huete et al. 2002) that is less affected by atmospheric conditions and soil background. *TCARI* indicates leaf chlorophyll absorption (Haboudane et al. 2002) and it is often used in conjunction with *OSAVI* (Rondeaux et al. 1996) as a proxy for leaf area index (LAI) that minimizes soil background. Thus, *TCARI/OSAVI* can estimate leaf chlorophyll content independently of leaf area (Zarco-Tejada et al. 2004). *CCI* (Gamon et el. 2016) and *PRI* (Gamon et al. 1997) are sensitive to carotenoid and chlorophyll pigments, particularly to the ratio *Car* to *Chl*. These two indexes are associated to photosynthetic activity and can be considered proxies for photosynthetic phenology (Wong et al. 2020; Fréchette et al. 2016). Both are particularly suitable to monitor the phenology of photosynthesis in evergreen conifers (Wong et al. 2020; Springer et al. 2017).

To overcome noise caused by soil pixels contained into previously segmented single crowns, RGB and multispectral images were filtered as follows. For RGB images, negative values of *GRVI** were considered as soil pixels, since *GRVI** is also used to estimate biomass and green vegetation, with *GRVI** = 0 used as threshold (Chen et al. 2019; Motohka et al. 2010). For multispectral images, *NDVI* values were used by

choosing a pixel threshold of 0.5, since *NDVI* values close to 0 represent barren rocks and soil whereas values above 0.5 indicate healthy vegetation (Sharma et al. 2022; Santini et al. 2019b).

Flammability experiment

Needle litter was collected in July 2022 in Zuera (about 100 g per sample) from ten populations and three blocks (two populations per ecotype, as follows: #11, 31, 142, 143, 152, 154, 182, 186, 214 and 242; Table S1). Only needle litter fallen between the two central trees of each experimental unit was collected to minimize contamination from adjacent units. Needle length was measured at the nearest millimeter using the open software ImageJ (version 1.52a) (Schneider et al. 2012). In order to equilibrate needle temperature and humidity we weighted 75 g per sample, which was later put in an oven at 30 ºC for five days. Samples were removed from the oven one by one just before the experiment started in order to keep needle in equilibrium moisture content. As final checking, samples were re-weighed following the period in the oven. Their weight varied between 72 and 73 g, and their humidity (combustible humidity) ranged from 4.4% to 7.6%.

For the flammability experiment we followed established protocols (Varner et al. 2015, Fonda et al. 2001). The weighed needle samples were spread across a 20 × 20 cm grid with ethanol-soaked cotton strings placed on one side of the grid. Fuel bed depth was measured to the nearest mm in three different locations of each fuel bed. Fuel bed depth varied between 2.5 and 5 cm among samples. Two thermocouples were placed on top of each fuel bed approximately at 2 cm from each side, which recorded temperature every second, from which we calculated the mean peak heat (ºC). Right after the cotton was ignited the fuel burnt immediately, and we calculated (1) the time elapsed until the flame arrived to the opposed side of the grid (diffusion flame time), (2) the time elapsed until the flame extinguished (flame time), and (3) the time elapsed until the last ember extinguished and the smoke stopped (smoldering combustion time). The maximum height reached by the flame (flame height) was visually estimated to the nearest cm by an observer using a ruler mounted behind the fire chamber. A camera model Nikon d5300 (Nikon Corp., Japan) was mounted on a tripod to record the entire experiment and double check the estimation of the maximum flame height and the remaining parameters if needed. The amount of fuel combusted was calculated as the proportion of the initial litter mass to the remaining mass, while the mean rate weight loss was estimated by dividing the lost weight by smoldering combustion time (Fonda et al. 2001). An example of the experimental protocol can be visualized in a video

(available at https://www.kapwing.com/w/faCxHvtC86)

Statistical analyses

Population differentiation was first tested for each phenotypic trait measured *in situ*, independently for each of three field campaigns, through analysis of variance (ANOVA), with populations and replicates as fixed terms. One field campaign (June 11th) could not be analyzed independently due to large gaps in the dataset as a result of heavy rain preventing a complete collection of samples. Traits that had been continuously measured in at least two field work campaigns were then subjected to linear mixed-effects models with a repeated time structure that included all four field-work campaigns in order to estimate the temporal effect and its variability among populations, taking also into account needle age as main factor in the models.

For RGB- and multispectral-derived VIs, ANOVAs were run independently for each trial site (Zuera or Altura) to check for genetic variability among populations. In the case of Zuera, we used either (i) data acquired during the June flight, when both types of VIs (RGB and multispectral) were available, or (ii) RGB-derived data taken across flights, which were subjected to linear mixed-effects models with a repeated time structure for time-series analysis. In the latter case, this allowed to estimate temporal changes in VIs and its differential plasticity among populations. In all cases, the population effect was partitioned into an ecotype effect plus a population-nested-to-ecotype residual to evaluate the presence of a broad ecotypic structure in the dataset. Least significant difference tests (LSD) were used to statistically compare ecotype means.

Populations' means of VIs exhibiting significant population effects were correlated to climate at the origin of populations. Pearson's correlations were also performed between photsynthetic pigments (Chl_a, Chl_b, $Chl_{a/b}$, Chl_{a+b}, *Car* or Car/Chl_{a+b}) and RGB- or multispectral-derived VIs acquired in Zuera.

Regarding the flammability experiment, we divided the traits under evaluation into two groups: those associated with fuel characteristics (needle length, combustible humidity, and Fuel bed depth), or *fuel-related* traits, and those associated with flammability characteristics (diffusion flame time , flame time , smoldering combustion time, flame height, fuel combusted and mean peak heat), or *flammability-related* traits. Population differentiation was tested considering *fuel* and *flammability* traits as multidimensional traits through multivariate analysis of variance (MANOVA), and also considering each trait independently through ANOVA, with room temperature and relative humidity used as covariates in the analysis. Statistical analyses were

performed using SAS/STAT (Littell et al. 1998).

Results

Intraspecific variability of needle traits

For traits measured *in situ* only fuel moisture content (*FMC*) of one-year-old needles showed a significant population effect, with populations from the northern Iberian Peninsula and the eastern Mediterranean basin having higher *FMC* in July than continental and southern Iberian Peninsula populations in July 2nd. The remaining traits did not show significant variability among the subset of populations evaluated in the sampling campaigns (Table S4).

The mixed models with repeated time structure indicated that all traits varied across sampling dates. However, only *Car* and *FMC* showed significant (p <0.05) and marginally significant (p <0.10) population differentiation, respectively (Table 2). Needle age was significant only for *FMC*, while Chl_a and Chl_{a+b} were significant and marginally significant, respectively, for the interaction between needle age and sampling date (Table 2).

Relationships between VIs and in situ traits

Chl_a was negatively and significantly related to *G%* and *TGI*, and marginally related to *GLI* (Fig. 3). These associations seem counterintuitive, but they can be attributed to the fact that we did not measure *Chl* in current year needles because they were not fully developed at the time of sampling. *Car* showed marginally significant negative associations with *G%*, *GLI*, *NDVI* and *CCI*, and Car/Chl_{a+b} was also negatively related to *CCI*, and also marginally related to *NDVI* and *GRVI* (Fig. 3). These findings simply suggest that trees having more carotenoid in needle cohorts of 1-year-old and over had in turn more proportion of senescent needles.

Differences in growth and vegetation indexes between trials, populations and ecotypes

Populations exhibited significant differences for total height at both sites, while no differences were found among populations at both sites for crown area (Table S5). Total height showed a clear ecotypic pattern in Altura, but not in Zuera. In both cases, the population-nested-to-ecotype term was significant (Table S5). All RGBderived VIs (*G%*, *GLI*, *GRVI** and *TGI*) differed significantly among populations in Altura. In turn

all VIs exhibited significant ecotypic differences, and also differences among populations nested to ecotypes (Table 3). In Zuera, on the other hand, only TGI showed a marginally significant population differentiation in Zuera for the June flight (Table 3). Marginally significant ecotypic differences were found for *TGI* and *GLI* for the June flight (Table 3), and only for *GRVI** across flights (Table 4). Although significant time effects were found for *G%* and *GLI*, none of them showed significant interactions between populations (or ecotypes) and time (Table 4).

For multispectral-dervied VIs, population differentiation was detected in the case of *NDVI* and *PSRI* in Altura (Table 3). Also, *NDVI*, *PSRI* and *TCARI/OSAVI* showed ecotypic differences, and there were also population differences within ecotypes in the case of *NDVI* and *PSRI* (Table 3). In Zuera, *EVI*, *TCARI* and *TCARI/OSAVI* disclosed significance population differentiation (Table 3; Table S6). The ecotype term was significant for *NDVI*, *EVI*, *TCARI/OSAVI* (Table 3) and *TCARI* and *OSAVI* (Table S6). A schematic representation of the trials along with an example of spatial variation of VIs (for the case of *NDVI*) are provided in supplementary material (Fig. S1, S2). Results regarding vegetation indexes that provided somewhat redundant information (i.e., *TCARI* or *OSAVI*) or did not display population or ecotypic differentiation are also shown in supplementary material (Table S6).

Relationships between VIs and climate at the origin of populations

In Altura, all RGB-derived VIs of populations (and also *NDVI*) increased eastward along the Mediterranean basin (i.e., positive relationship between longitude and VIs), while *PSRI* increased westward (i.e., negative relationship between longitude and *PSRI*) (Fig. 4). This suggested that populations from the eastern Mediterranean had an earlier phenology (i.e., having earlier needle unfolding or old neelde senescence, or both) than their western counterparts. Moreover, *PSRI* was negatively related to mean annual temperature and showed a positive association with latitude and temperature annual range (Fig. 4). Mean diurnal range and isothermality exhibited negative relationships with *NDVI* (Fig. 4). In addition, all RGB-derived VIs showed negative correlations with isothermality (Fig. 4), suggesting that populations exposed to high temperature evenness over the year at origin were phenologically less advanced when grown under mesic climatic conditions (Altura). Climate variables related to precipitation did not show significant relationships with VIs (Fig. 4). In Zuera, on the other hand, a significant eastward gradient was found for *TCARI/OSAVI* and

(marginally significant) for *GLI* and *TCARI* (Fig. 4).

Lack of intraspecific variability in flammability traits

Our results did not show any differentiation among populations or ecotypes for the suite of traits obtained in the flammability experiment, neither when analyzed together for fuel or flammability traits through MANOVA (Table S7), nor independently through ANOVA (Table S8).

Discussion

Aleppo pine is a dominant species in fire-prone habitats of the Mediterranean basin adapted to crown fires. However, intraspecific differences in fire-related traits are still poorly studied (Martín-Sanz et al. 2019), especially those related to early season needle unfolding and old needles senescence (Karavani et al. 2018). The latter leads to about one-third of the canopy (that is, all 3 years-old leaves) being dry just before the peak fire season. This increases the probability of crown fire in Aleppo pine at the onset of the fire season (Balaguer-Romano et al. 2020). Needle phenology (e.g., needle unfolding and senescence) may differ among Aleppo pine populations as a result of different adaptive strategies related to water use (Voltas et al. 2015), growth (Lombardi et al. 2022; Patsiou et al. 2020), or fire (Karavani et al. 2018). Needle senescence affecting the old leaves cohort can be triggered by climate factors, especially drought and nutrient availability, and also by specific growth events as a result of remobilization of nutrients from old to young leaves (Peaucelle et al. 2019; Munné-Bosch & Alegre, 2004).

Here, we applied UAV-derived VIs and *in situ* measurements to assess intraspecific variation in the timing of needle unfolding and senescence of Aleppo pine at the onset of the fire season in a range-wide common garden experiment. This assessment was supplemented by an analysis of plastic spatial responses for the same traits by combining results from the Zuera common garden (typical of dry continental conditions) with those of a second, contrasting common garden (representative of a coastal Mediterranean climate).

Needle traits measured in situ and their relationships with vegetation indexes (VIs)

Most *in situ* measuraments related to pigments content as well as the suite of traits related to the litter flammability experiment showed inconclusive patterns regarding intraspecific differentiation. As an exception,

population differentiation in early season live fuel moisture content suggests adaptive divergence potentially associated to fire responses. Additionally, the variability in carotenoids content among populations could be related to their different phenological stage or, alternatively, to its photo-protection role under the dry, continental conditions of the trial since our results did not show a clear temporal trend for this pigment indicative of phenological changes. However, these results should be re-examined by securing a larger set of representative populations than the exploratory subset used in this study. With regard the counterintuitive relationships between needle pigments and RGB-derived VIs, these could have been influenced by the different mixing of needles of different ages among populations (Kuusk et al. 2018). Current-year needles were emerging at the time of the first sampling, and they were not collected for pigments determination, in contrast, the RGB sensor registered reflectance of all needle cohorts. Generally, current-year needles have greater reflections, especially in the green wavelength, as previously reported for other conifers. Therefore, reflectance is likely to decrease with needle age (Hejtmánek et al. 2022; Lhotákova et al. 2021). On the other hand, the relationships between some multispectral indexes (*CCI* and *NDVI*) and the ratio of carotenoids to total chlorophyll content were is in line with previous studies conducted in other pine species at their adult (Fréchette et al. 2020, Wong et al, 2019) or seedling stage (D'Odorico et al. 2020). This result points to the existence of population differentiation in pigment contents, especially carotenoids, during the early growing season (Fréchette et al. 2020). It may be related to different intraspecific responses to the onset of summer drought that lead to pre-programmed cell death of old needles or cause changes in photosynthetic phenology, or both (Wong et al. 2020; Peaucelle et al. 2019).

Do vegetation indexes differ among trials, populations and ecotypes?

Based on the limited time series of VIs available in the continental trial (Zuera), we did not observe any obvious temporal pattern which may have differed among populations. However, the ecotypic means of VIs plotted independently for each flight time (May and June), reveal that canopies were in general greener in June, which we interpret as related to the pace of current-year needle development (Fig. 5). On the other hand, we observed higher values of RGB-derived VIs (Fig. 6) and also of NDVI-based VIs (*NDVI*, *EVI*, *TCARI* and *TCARI/OSAVI*) and, *PSRI* (Fig. 7) in continental trial (Zuera) than in the coastal trial (Altura). This observation is probably indicating anearlier phenology of trees (i.e., earlier current-year needle unfolding), potentially

coupled with an earlier old needle senescence in (high *PSRI*), in the continental trial during late spring-early summer. In both trials, the observed population and ecotypic differentiation for many VIs (i.e., *GLI*, *NDVI*, *TCARI/OSAVI*) suggest variable early season needle phenology related to needle unfolding at the intraspecific level, although with conserved patterns (i.e., similar population plasticity) across sites.

As aforementioned, ecotypes diverged in VIs in a rather consistent manner across trials and suggested that DHT and WST have opposing early season phenology (i.e., timing of needle unfolding and old needle senescence) (Fig. 7). Since variation in needle pigments and water content can be interpreted as differences in the timing of needle unfolding among populations (Wong & Gamon, 2015), our results indicate that DHT (an ecotype originating from sub-hunid climates) had the earliest phenology (i.e., the earliest needle unfolding), among all ecotypes. This result is in concordance with previous studies pointing to important functional differences among Aleppo pine populations in the same Altura trial (Voltas et al. 2015; Santini et al. 2019a; Lombardi et al. 2021). These studies revealed that drought-sensitive eastern Mediterranean populations (i.e., DHT ecotype) invest comparatively more in aerial growth than in other functional traits such as storage (Santini et al. 2019a), reproduction (Climent et al. 2008) or roots (Lombardi et al. 2021) compared to drought-tolerant western Mediterranean populations (i.e., DSC or DST ecotypes). In turn, they have higher photosynthetic capacity coupled with higher summer transpiration than its western counterparts (Santini et al. 2019b). The early needle unfolding of DHT may partly be related to both its high growth plasticity (Lombardi et al. 2022; Patsiou et al. 2020) and its ability to grow well under different climates (Patsiou et al. 2020).

While DHT and WST showed the most contrasting differences for all VIs, ecotypes DST and DSC performed generally closer to WST, and ecotype WHC closer to DHT (Figs. 6 and 7). This observation that DHT, showed an earlier phenology compared with semi-arid ecotypes probably indicates the existence of adaptive responses linked to a more conservative strategy of populations from drought-prone environments (e.g., higher water-use efficiency, higher root investment), as previously reported for the species (Voltas et al. 2015).

In addition, our findings disclosed ecotypic differentiation in old needle senescence not previously reported for this species, although such differences were clearest in the coastal trial. While WST showed delayed senescence (i.e., high *PSRI*), other semi-arid ecotypes (DSC, DST) showed an opposite pattern (Fig. 7). his observation may effectively indicate changes in early season needle phenology of ecotypes, in particular WST (with a delayed phenology and, thus, later needle development and old needle senescence) and DHT

(with an earlier phenology and, thus, earlier needle unfolding and old needle senescence). It may also reflect adaptive differentiation to fire-prone habitats and a trade-off between fire- and drought-related traits, since old needle senescence may be triggered under drought conditions but together it can favor crown fires. This could be the case of ecotypes DST and DSC, which showed late needle unfolding but early old needle senescence (i.e., high *PSRI*), the latter probably triggered by the beginning of the summer drought period (Grulke et al. 2020). The existence of such intraspecific differentiation may be related to the strategy adopted by different populations as driven by their local fire regime, in the same way as other fire-related traits like cone serotiny, which has been estimated to be modulated by fire and, indeed, increases its importance under stronger fire regimes (Romero et al. 2023). However, this conclusion should be taken with caution, and particularly so since our flammability analysis suggested lack of genetic differentiation in litter flammability traits.

The relationships found between height growth and VIs corroborate the findings above, in particular those involving needle development (i.e., earlier current-year needle unfolding related to enhanced growth). These relationships were partially described by Santini et al. (2019b) for Aleppo pine, particularly the association between aerial growth (volume over bark) and *NDVI*-related indexes, which is primarily linked to differences in total leaf area.

Finally, our results revealed few conclusive associations between climate factors at origin of populations and VIs. In the coastal trial, where climate is wetter, temperature-related factors at origin were the main drivers of population differentiation in VIs. Under these conditions, we could detect a clear longitudinal pattern that indicates earlier needle phenology for populations from the eastern Mediterranean basin compared with their western counterparts. On the other hand, we did not find a clear climatic pattern in the continental trial.

Methodological limitations

A main limitation of this study is the lack of a complete time series fully covering the onset of the growing season. Instead, we performed two flights spaced one month in late spring (May-June) in the same common garden experiment and, unfortunately, we could only use a single flight (June) for obtaining multispectral VIs due to technical reasons. A higher frequency of flights could definitely improve the characterization of phenological changes in the canopy and, eventually, unveil population or ecotypic differences which may have

gone unnoticed using a two-point series of records.

With regard ground truth measurements, we had availability of a larger time series covering one and a half month; however, we sampled a relatively small subset of populations because of personnel and technical constraints, a typical drawback that hampers conventional ecophysiological studies. As a consequence, the development of current-year needles was likely incompletely captured at the intraspecific level. The alternative target of sampling a larger subset of populations or, even, the entire trial could have increased the scope of inferences by disclosing additional patterns of intraspecific differentiation. A similar flaw applies to the litter flammability experiment.

On a separate issue, and regarding both ground measurements and UAV-derived data, the lack of a time series covering multiple years (instead of a single year) also prevented a more complete characterization of genetic patterns. Indeed, a multiyear time-series of records would be desirable to test for consistency of phenological variability across populations and ecotypes of the species. Finally, although previous studies carried out in the Altura trial have revealed important intraspecific differences in Aleppo pine, the joint characterization of functional traits characterizing drought responses across trials (in addition to needle phenology and senescence) would add relevant information about such differentiation and its plasticity, especially regarding the issue of a potential trade-off between fire resistance and drought tolerance.

Conclusions

This study showcases the existence of intraspecific variation in needle unfolding and old needle senescence of *P. halepensis*. In turn, this variability is informative of differential plasticity and local adaptation to contrasting conditions across the Mediterranean basin. We found that ecotypes DHT (exposed to dry summers, but with a sub-humid, temperate climate)) and WST (with wet summers, but with a semiarid, temperate climate) exhibited the most obvious differences in VIs. Also, ecotypes with semiarid climates shared, in general, similar similar traits to WST. These findings are likely a result of different life-history strategies and, eventually, trade-offs between fire- and drought-related traits, as exemplified by ecotypes DST and DSC, which seemingly exhibited an early old needle senescence coupled with late needle unfolding. On the other hand, the lack of population differentiation for flammability traits suggested similar adaptations to fire for *P. halepensis*. This study represents a first attempt to understand changes in early season needle unfolding and old needle

senescence using UAV-derived RGB and multispectral VIs in common garden experiments of adult individuals for a widespread conifer. Our result point to the importance of taking into account the intraspecific characteristics of this species in forest management actions. Particularly, populations (or ecotypes) with high growth potential show increased risk of crown flammability at the onset of the fire season in the Mediterranean basin.

Acknowledgments: We would like to thank Javier Madrigal (CIFOR-INIA), for his assistance regarding the flammability protocol and Maria Josep Pau for technical assistance.

Funding: This work was partly supported by the Spanish Government, grant numbers: RTI2018-094691-B-C31 and RTI2018-094691-B-C33 (MCIU/AEI/FEDER, EU), E. Lombardi was supported by a AGAUR FI-2022 pre-doctoral fellowship (with the support from the Secretariat for Universities and Research of the Ministry of Business and Knowledge of the Government of Catalonia and the European Social Found).

Data Availability Statement: The data supporting the results of this study will be made available at the CORA open repository (https://dataverse.csuc.cat/) upon acceptance of this article.

References

Alberton, B., Almeida, J., Helm, R., Torres, R. da S., Menzel, A., Morellato, L.P.C. **(**2014). Using phenological cameras to track the green up in a cerrado savanna and its on-the-ground validation. Ecol. Inform. 19, 62–70. https://doi.org/10.1016/j.ecoinf.2013.12.011

Anderson, H.B., Nilsen, L., Tømmervik, H., Karlsen, S.R., Nagai, S., Cooper, E.J. **(**2016). Using ordinary digital cameras in place of near-infrared sensors to derive vegetation indices for phenology studies of High Arctic vegetation. Remote Sens. 8, 847. https://doi.org/10.3390/rs8100847

Balaguer-Romano, R., Díaz-Sierra, R., Madrigal, J., Voltas, J., Resco de Dios, V. (2020). Needle senescence affects fire behavior in aleppo pine (*Pinus halepensis* mill.) stands: A simulation study. Forests 11, 1–14. https://doi.org/10.3390/f11101054

Bastien, R., Ganteaume, A. (2020). Correction to: Does recent fire activity impact fire-related traits of *Pinus halepensis* Mill. and *Pinus sylvestris* L. in the French Mediterranean area? Ann. For. Sci. 77, 1-19. https://doi.org/10.1007/s13595-020-01021-4

Berra, E.F., Gaulton, R., Barr, S. (2019). Assessing spring phenology of a temperate woodland: A multiscale comparison of ground, unmanned aerial vehicle and Landsat satellite observations. Remote Sens. Environ. 223, 229–242. https://doi.org/10.1016/j.rse.2019.01.010

Bulut, S. (2023). Machine learning prediction of above-ground biomass in pure Calabrian pine (*Pinus brutia* Ten.) stands of the Mediterranean region, Türkiye. Ecol. Inform. 74, 101951. https://doi.org/10.1016/j.ecoinf.2022.101951

Camarero, J.J., Campelo, F., Colangelo, M., Valeriano, C. (2022). Agricultural and Forest Meteorology Decoupled leaf-wood phenology in two pine species from contrasting climates: Longer growing seasons do

not mean more radial growth. Agr. For. Meteorol. 327, 109223. https://doi.org/10.1016/j.agrformet.2022.109223

Chambel, M.R., Climent, J., Pichot, C., Ducci, F. (2013). Mediterranean Pines (*Pinus halepensis* Mill. and *brutia* Ten.). In: Pâques, L. (eds) Forest Tree Breeding in Europe. Managing Forest Ecosystems, Publ. Springer, Dordrecht. 25, 229-265. https://doi.org/10.1007/978-94-007-6146-9_5

Chen, A., Orlov-Levin, V., Meron, M. (2019). Applying high-resolution visible-channel aerial imaging of crop canopy to precision irrigation management. Agricultural water management. Agric. Water Manag. 216, 196-205. https://doi.org/10.1016/j.agwat.2019.02.017

Ciocîrlan, C., Curtu, A.L., Radu, G.R. (2022). Predicting Leaf Phenology in Forest Tree Species Using UAVs and Satellite Images: A Case Study for European Beech (*Fagus sylvatica* L.). Remote Ens. 14, 6198. https://doi.org/10.3390/rs14246198

Climent, J., Prada, M.A., Calama, R., Chambel, M.R., De Ron, D.S., Alía, R. (2008). To grow or to seed: Ecotypic variation in reproductive allocation and cone production by young female Aleppo pine (*Pinus halepensis, Pinaceae*). Am. J. Bot. 95, 833–842. https://doi.org/10.3732/ajb.2007354

D'Odorico, P., Besik, A., Wong, C. Y., Isabel, N., Ensminger, I. (2020). High-throughput drone-based remote sensing reliably tracks phenology in thousands of conifer seedlings. New Phytol. 226, 1667-1681. https://doi.org/10.1111/nph.16488

Fady, B., Semerci, H., Vendramin, G.G. (2003). EUFORGEN Technical Guidelines for genetic conservation and use for Aleppo pine (*Pinus halepensis*) and Brutia pine (*Pinus brutia*). International Plant Genetic Resources Institute, Rome, Italy.

Fick, S.E. (2017). WorldClim 2: new 1-km spatial resolution climate surfaces for global land areas. Int. J. Climatol. 4315, 4302–4315. https://doi.org/10.1002/joc.5086

Fonda, R.W. (2001). Burning characteristics of needles from eight Pine species. For. Sci. 47, 390–396.

Fréchette, E., Chang, C.Y.Y., Ensminger, I. (2020). Variation in the phenology of photosynthesis among eastern white pine provenances in response to warming. Glob. Chang. Biol. 26, 5217–5234. https://doi.org/10.1111/gcb.15150

Fréchette, E., Chang, C.Y., Ensminger, I. (2016). Methods paper Photoperiod and temperature constraints on the relationship between the photochemical reflectance index and the light use efficiency of photosynthesis in *Pinus strobus*. Tree Physiol. 36, 311–324. https://doi.org/10.1093/treephys/tpv143

Gamon, J.A., Huemmrich, K.F., Wong, C.Y.S., Ensminger, I., Garrity, S., Hollinger, D.Y., Noormets, A., Peñuelask, J. (2016). A remotely sensed pigment index reveals photosynthetic phenology in evergreen conifers. Proc. Natl. Acad. Sci. U. S. A. 113, 13087–13092. https://doi.org/10.1073/pnas.1606162113

Gamon, J.A., Serrano, L., Surfus, J.S. (1997). The photochemical reflectance index: An optical indicator of photosynthetic radiation use efficiency across species, functional types, and nutrient levels. Oecologia 112, 492–501. https://doi.org/10.1007/s004420050337

Girard, F., Vennetier, M., Ouarmim, S., Caraglio, Y., Misson, L. (2011). Polycyclism, a fundamental tree growth process, decline with recent climate change: The example of *Pinus halepensis* Mill. in Mediterranean France. Trees - Struct. Funct. 25, 311–322. https://doi.org/10.1007/s00468-010-0507-9

Gracia-Romero, A., Vergara-Díaz, O., Thierfelder, C., Cairns, J.E., Kefauver, S.C., Araus, J.L. (2018). Phenotyping conservation agriculture management effects on ground and aerial remote sensing assessments of maize hybrids performance in Zimbabwe. Remote Sens. 10, 1–21. https://doi.org/10.3390/rs10020349

Grime, J.P. (1977). Evidence for the Existence of Three Primary Strategies in Plants and Its Relevance to Ecological and Evolutionary Theory. Am. Nat. 111, 1169–1194. https://doi.org/10.1086/283244

Grulke, N., Maxfield, J., Riggan, P., Schrader-Patton, C. (2020). Pre-emptive detection of mature pine drought stress using multispectral aerial imagery. Remote Sens. 12, 1–23. https://doi.org/10.3390/rs12142338

Haboudane, D., Miller, J.R., Tremblay, N., Zarco-tejada, P.J., Dextraze, L. (2002). Integrated narrow-band vegetation indices for prediction of crop chlorophyll content for application to precision agriculture. Remote Sens. Environ. 81, 416–426. https://doi.org/10.1016/S0034-4257(02)00018-4

Hejtmánek, J., Stejskal, J., Čepl, J., Lhotáková, Z., Korecký, J., Krejzková, A., Dvořák, J., Gezan, S.A. (2022). Revealing the Complex Relationship Among Hyperspectral Reflectance, Photosynthetic Pigments, and Growth in Norway Spruce Ecotypes. Front. Plant Sci. 13. https://doi.org/10.3389/fpls.2022.721064

Huete, A., Didan, K., Miura, T., Rodriguez, E.P., Gao, X., Ferreira, L.G. (2002). Overview of the radiometric and biophysical performance of the MODIS vegetation indices. Remote Sens. Environ. 83, 195–213. https://doi.org/10.1016/S0034-4257(02)00096-2

Huete, A. R. (2012). Vegetation indices, remote sensing and forest monitoring. Geography Compass 6(9), 513-532. https://doi.org/10.1111/j.1749-8198.2012.00507.x

Hunt, E.R., Daughtry, C.S.T., Eitel, J.U.H., Long, D.S. (2011). Remote sensing leaf chlorophyll content using a visible band index. Agron. J. 103, 1090–1099. https://doi.org/10.2134/agronj2010.0395

Hunt, E.R., Doraiswamy, P.C., McMurtrey, J.E., Daughtry, C.S.T., Perry, E.M., Akhmedov, B. (2012). A visible band index for remote sensing leaf chlorophyll content at the Canopy scale. Int. J. Appl. Earth Obs. Geoinf. 21, 103–112. https://doi.org/10.1016/j.jag.2012.07.020

John, J.A., Williams, E.R. (1998). t-Latinized Designs. Australian & New Zealand Journal of Statistics, 40, 111-118. https://doi.org/10.1111/1467-842X.00012

Karavani, A., Boer, M.M., Baudena, M., Colinas, C., Díaz-Sierra, R., Pemán, J., de Luis, M., Enríquez-de-Salamanca, A., Resco de Dios, V. (2018). Fire-induced deforestation in drought-prone Mediterranean forests: drivers and unknowns from leaves to communities. Ecol. Monogr. 88, 141–169. https://doi.org/10.1002/ecm.1285

Kefauver, S.C., El-haddad, G., Consultancy, S.S., Diaz, O.V., Araus, J.L. (2015). RGB picture vegetation indexes for High-Throughput Phenotyping Platforms RGB picture vegetation indexes for High-Throughput Phenotyping Platforms (HTPPs). *In Remote sensing for agriculture, ecosystems and hydrology XVII. SPIE conference*. https://doi.org/10.1117/12.2195235

Klein, T., Di Matteo, G., Rotenberg, E., Cohen, S., Yakir, D. (2013). Differential ecophysiological response of a major Mediterranean pine species across a climatic gradient. Tree Physiol. 33, 26–36. https://doi.org/10.1093/treephys/tps116

Kleinsmann, J., Verbesselt, J., & Kooistra, L. (2023). Monitoring Individual Tree Phenology in a Multi-Species Forest Using High Resolution UAV Images. Remote Sensing, 15, 3599.

Klosterman, S., Melaas, E., Wang, J., Martinez, A., Frederick, S., O'Keefe, J., Orwig, D.A., Wang, Z., Sun, Q., Schaaf, C., Friedl, M., Richardson, A.D. (2018). Fine-scale perspectives on landscape phenology from unmanned aerial vehicle (UAV) photography. Agric. For. Meteorol. 248, 397–407. https://doi.org/10.1016/j.agrformet.2017.10.015

Kumar, M., Kalra, N., Khaiter, P., Ravindranath, N.H., Singh, V., Singh, H., Sharma, S., Rahnamayan, S. (2019). PhenoPine: A simulation model to trace the phenological changes in *Pinus roxhburghii* in response to ambient temperature rise. Ecol. Modell. 404, 12–20. https://doi.org/10.1016/j.ecolmodel.2019.05.003

Kuusk, V., Niinemets, Ü., Valladares, F. (2018). Structural controls on photosynthetic capacity through juvenile-to-adult transition and needle ageing in Mediterranean pines. Funct. Ecol. 32, 1479–1491. https://doi.org/10.1111/1365-2435.13087

Larrinaga, A. R., Brotons, L. (2019). Greenness indices from a low-cost UAV imagery as tools for monitoring post-fire forest recovery. Drones, 3, 6.

Landis, T. (1990). Characteristics of Containers for Forest Nurseries Types of Containers Chemical Root Pruning Conclusions and Recommendations Literature Cited. North 1–39.

Lhotáková, Z., Kopačková-Strnadová, V., Oulehle, F., Homolová, L., Neuwirthová, E., Švik, M., Janoutová, R., Albrechtová, J. (2021). Foliage biophysical trait prediction from laboratory spectra in norway spruce is more affected by needle age than by site soil conditions. Remote Sens. 13, 1–24. https://doi.org/10.3390/rs13030391

Li, Xiangcai, Tian, J., Li, Xiaojuan, Wang, L., Gong, H., Shi, C., Nie, S., Zhu, L., Chen, B., Pan, Y., He, J., Ni, R., Diao, C. (2022). Developing a sub-meter phenological spectral feature for mapping poplars and willows in urban environment. ISPRS J. Photogramm. Remote Sens. 193, 77–89. https://doi.org/10.1016/j.isprsjprs.2022.09.002

Littell, R.C., Henry, P.R., Ammerman, C.B. (1998). Statistical Analysis of Repeated Measures Data Using SAS Procedures. J. Anim. Sci. 76, 1216–1231. https://doi.org/10.2527/1998.7641216x

Lombardi, E., Ferrio, J.P., Rodríguez-Robles, U., Resco de Dios, V., Voltas, J. (2021). Ground-Penetrating Radar as phenotyping tool for characterizing intraspecific variability in root traits of a widespread conifer. Plant Soil 468, 319–336. https://doi.org/10.1007/s11104-021-05135-0

Lombardi, E., Rodríguez-Puerta, F., Santini, F., Chambel, M.R., Climent, J., Resco de Dios, V., Voltas, J. (2022). UAV-LiDAR and RGB Imagery Reveal Large Intraspecific Variation in Tree-Level Morphometric Traits across Different Pine Species Evaluated in Common Gardens. Remote Sens. 14, 1–21. https://doi.org/10.3390/rs14225904

Loudermilk, E.L., O'Brien, J.J., Goodrick, S.L., Linn, R.R., Skowronski, N.S., Hiers, J.K. (2022). Vegetation's influence on fire behavior goes beyond just being fuel. Fire Ecol. 18, 1-10. https://doi.org/10.1186/s42408-022-00132-9

Louhaichi, M., Borman, M. M., Douglas, E. J. (2001). Spatially Located Platform and Aerial Photography for Documentation of Grazing Impacts on Wheat. Geocarto Int. 16, 65-70, https://doi.org/10.1080/10106040108542184

Martín-Sanz, R.C., San-Martín, R., Poorter, H., Vázquez, A., Climent, J. (2019). How does water availability affect the allocation to bark in a Mediterranean conifer? Front. Plant Sci. 10, 1–13. https://doi.org/10.3389/fpls.2019.00607

Matthews, S. (2010). Effect of drying temperature on fuel moisture content measurements. International Journal of Wildland Fire, 19, 800-802, https://doi.org/10.1071/WF08188

Mauri, A., Di Leo, M., Rigo, D., de Caudullo, G. (2016). *Pinus halepensis* and *Pinus brutia* in Europe: distribution, habitat, usage and threats. In: San-Miguel-Ayanz J, de Rigo D, Caudullo G, Houston Durrant T, Mauri A (Eds.) European Atlas of Forest Tree Species. Publ. Off. EU, Luxembourg, e0166b8

McGaughey, R.J. (2015). FUSION/LDV: Software for LIDAR data analysis and visualization, Version 3.50; US Department of Agriculture, Forest Service, Pacific Northwest Research Station, University of Washington: Seattle, WA, USA.

Merzlyak, M.N., Gitelson, A.A., Chivkunova, O.B., & Rakitin, V.Y. (1999). Non-destructive optical detection of pigment changes during leaf senescence and fruit ripening. Physiol. Plant. 106, 135-141. https://doi.org/10.1034/j.1399-3054.1999.106119.x

Meyer, F., & Beucher, S. (1990). Morphological segmentation. J. Vis. Comm. Image Represent. 1, 21-46. https://doi.org/10.1016/1047-3203(90)90014-M

Miller, R.G., Tangney, R., Enright, N.J., Fontaine, J.B., Merritt, D.J., Ooi, M.K.J., Ruthrof, K.X., Miller, B.P. (2019). Mechanisms of Fire Seasonality Effects on Plant Populations. Trends Ecol. Evol. 34, 1104–1117. https://doi.org/10.1016/j.tree.2019.07.009

Minocha, R., Martinez, G., Lyons, B., Long, S. (2009). Development of a standardized methodology for quantifying total chlorophyll and carotenoids from foliage of hardwood and conifer tree species. Can. J. For. Res. 39, 849–861. https://doi.org/10.1139/X09-015

Motohka, T., Nasahara, K.N., Oguma, H., Tsuchida, S. (2010). Applicability of Green-Red Vegetation Index for remote sensing of vegetation phenology. Remote Sens. 2, 2369–2387. https://doi.org/10.3390/rs2102369

Munné-Bosch, S., Alegre, L. (2004). Die and let live: Leaf senescence contributes to plant survival under drought stress. Funct. Plant Biol. 31, 203–216. https://doi.org/10.1071/FP03236

Olmo, V., Tordoni, E., Petruzzellis, F., Bacaro, G., Altobelli, A. (2021). Use of sentinel-2 satellite data for windthrows monitoring and delimiting: The case of "vaia" storm in friuli venezia Giulia region (north-eastern Italy). Remote Sens. 13, 1530. https://doi.org/10.3390/rs13081530

Pausas, J.G. (2015). Evolutionary fire ecology: Lessons learned from pines. Trends Plant Sci. 20, 318–324. https://doi.org/10.1016/j.tplants.2015.03.001

Patsiou, T.S., Shestakova, T.A., Klein, T., di Matteo, G., Sbay, H., Chambel, M.R., Zas, R., Voltas, J. (2020). Intraspecific responses to climate reveal nonintuitive warming impacts on a widespread thermophilic conifer. New Phytol. 228, 525-540. https://doi.org/10.1111/nph.16656

Peaucelle, M., Ciais, P., Maignan, F., Nicolas, M., Cecchini, S., Viovy, N. (2019). Representing explicit budburst and senescence processes for evergreen conifers in global models. Agric. For. Meteorol. 266–267, 97–108. https://doi.org/10.1016/j.agrformet.2018.12.008

Picornell-Gelabert, L., Servera-Vives, G., Carrión Marco, Y., Burjachs, F., Currás, A., Llergo, Y., Dufraisse, A., De Luís Arrillaga, M., Mus Amézquita, M. (2021). Late Holocene Aleppo pine (*Pinus halepensis* Miller) woodlands in Mallorca (Balearic Islands, Western Mediterranean): Investigation of their distribution and the role of human management based on anthracological, dendro-anthracological and archaeopalynological data. Quat. Int. 593–594, 346–363. https://doi.org/10.1016/j.quaint.2020.11.006

Plowright, M.A. (2018). R Package 'ForestTools.' CRAN. Available online: https://github.com/andrew-plowright/ForestTools.

Popescu, S. C., & Wynne, R. H. (2004). Seeing the trees in the forest: Using lidar and multispectral data fusion with local filtering and variable window size for estimating tree height. Photogramm. Eng. Remote Sens. 70, 589-604.

Resco de Dios, V., Arteaga, C., Hedo, J., Gil-Pelegrín, E., Voltas, J. (2018). A trade-off between embolism resistance and bark thickness in conifers: are drought and fire adaptations antagonistic? Plant Ecol. Divers. 11, 253–258. https://doi.org/10.1080/17550874.2018.1504238

Risberg, L., Granström, A. (2009). The effect of timing of forest fire on phenology and seed production in the fire-dependent herbs *Geranium bohemicum* and *G. lanuginosum* in Sweden. For. Ecol. Manage. 257, 1725–1731. https://doi.org/10.1016/j.foreco.2009.01.031

Romero, B., Scotti, I., Fady, B., Ganteaume, A. (2023). Fire frequency, as well as stress response and developmental gene control serotiny level variation in a widespread pioneer Mediterranean conifer, *Pinus halepensis.* Ecol. Evol. 13, e9919. https://doi.org/10.1002/ece3.9919

Rondeaux, G., Steven, M., Baret, F. (1996). Optimization of Soil-Adjusted Vegetation Indices. Remote Sens. Environ. 107, 95–107. https://doi.org/10.1016/0034-4257(95)00186-7

Rouse, J.W., Haas, R.H., Schell, J.A. and Deering, D.W. (1974). Monitoring vegetation systems in the Great Plains with ERTS. NASA Spec. Publ, 351, 309.

Santini, F., Climent, J.M., Voltas, J. (2019a). Phenotypic integration and life history strategies among populations of *Pinus halepensis*: an insight through structural equation modelling. Ann. Bot. 124, 1161–1171. https://doi.org/10.1093/aob/mcz088

Santini, F., Kefauver, S.C., Resco de Dios, V., Araus, J.L., Voltas, J. (2019b). Using unmanned aerial vehicle-based multispectral, RGB and thermal imagery for phenotyping of forest genetic trials: A case study in *Pinus halepensis*. Ann. Appl. Biol. 174, 262–276. https://doi.org/10.1111/aab.12484

Schneider, C., Rasband, W., Eliceiri, K. (2012). NIH Image to ImageJ: 25 years of image analysis. Nat Methods 9, 671–675. https://doi.org/10.1038/nmeth.2089

Sharma, Y., Ahmed, R., Sajjad, H. (2022). Assessing vegetation condition across topography in Nainital district, India using temperature vegetation dryness index model. Model. Earth Syst. Environ. 8, 2167–2181. https://doi.org/10.1007/s40808-021-01208-2

Silvério, D.V., Pereira, O.R., Mews, H.A., Maracahipes-Santos, L., Santos, J.O. dos, Lenza, E. (2015). Surface fire drives short-term changes in the vegetative phenology of woody species in a Brazilian savanna. Biota Neotrop. 15, e20140077. https://doi.org/10.1590/1676-0611-bn-2014-0077

Sonnentag, O., Hufkens, K., Teshera-Sterne, C., Young, A.M., Friedl, M., Braswell, B.H., Milliman, T., O'Keefe, J., Richardson, A.D. (2012). Digital repeat photography for phenological research in forest ecosystems. Agric. For. Meteorol. 152, 159–177. https://doi.org/10.1016/j.agrformet.2011.09.009

Springer, K.R., Wang, R., Gamon, J.A. (2017). Parallel seasonal patterns of photosynthesis, fluorescence, and reflectance indices in boreal trees. Remote Sens. 9, 1–18. https://doi.org/10.3390/rs9070691

Sripada, R.P., Heiniger, R.W., White, J.G., Meijer, A.D. (2006). Aerial color infrared photography for determining early in-season nitrogen requirements in corn. Agron J. 98, 968-977.

Starý, K., Jelínek, Z., Kumhálova, J., Chyba, J., Balážová, K. (2020). Comparing RGB-based vegetation indices from UAV imageries to estimate hops canopy area. Agron. Res. 18, 2592–2601. https://doi.org/10.15159/AR.20.169

Stimson, H.C., Breshears, D.D., Ustin, S.L., Kefauver, S.C. **(**2005). Spectral sensing of foliar water conditions in two co-occurring conifer species: *Pinus edulis* and *Juniperus monosperma*. Remote Sens. Environ. 96, 108–118. https://doi.org/10.1016/j.rse.2004.12.007

Taïbi, K., del Campo, A.D., Mulet, J.M., Flors, J., Aguado, A. (2014). Testing Aleppo pine seed sources response to climate change by using trial sites reflecting future conditions. New For. 45, 603–624. https://doi.org/10.1007/s11056-014-9423-y

Thapa, S., Garcia Millan, V.E., Eklundh, L. (2021). Assessing forest phenology: A multi-scale comparison of near-surface (UAV, spectral reflectance sensor, phenocam) and satellite (MODIS, sentinel-2) remote sensing. Remote Sens. 13, 1597. https://doi.org/10.3390/rs13081597

Tucker, C.J. (1979). Red and photographic infrared linear combinations for monitoring vegetation. Remote Sens. Environ. 8, 127–150. https://doi.org/10.1016/0034-4257(79)90013-0

Varner, J.M., Kane, J.M., Banwell, E.M., Kreye, J.K. (2015). Flammability of litter from southeastern trees: a preliminary assessment. In *Southern Silvicultural Research Conference*.

Varner, J.M., Shearman, T.M., Kane, J.M., Banwell, E.M., Jules, E.S., Stambaugh, M.C. (2022). Understanding flammability and bark thickness in the genus *Pinus* using a phylogenetic approach. Sci. Rep. 12, 1–10. https://doi.org/10.1038/s41598-022-11451-x

Voltas, J., Lucabaugh, D., Chambel, M.R., Ferrio, J.P. (2015). Intraspecific variation in the use of water sources by the circum-Mediterranean conifer *Pinus halepensis*. New Phytol. 208, 1031–1041. https://doi.org/10.1111/nph.13569

Voltas, J., Shestakova, T.A., Patsiou, T., di Matteo, G., Klein, T**.** (2018). Ecotypic variation and stability in growth performance of the thermophilic conifer *Pinus halepensis* across the Mediterranean basin. For. Ecol. Manage. 424, 205–215. https://doi.org/10.1016/j.foreco.2018.04.058

Woebbecke, D.M., Meyer, G.E., Von Bargen, K., Mortensen, D.A. (1995). Color indices for weed identification under various soil, residue, and lighting conditions. Trans. Am. Soc. Agric. Eng. 38, 259–269. https://doi.org/10.13031/2013.27838

Wong, C.Y.S., D'Odorico, P., Arain, M.A., Ensminger, I. (2020). Tracking the phenology of photosynthesis using carotenoid-sensitive and near-infrared reflectance vegetation indices in a temperate evergreen and mixed deciduous forest. New Phytol. 226, 1682–1695. https://doi.org/10.1111/nph.16479

Wong, C.Y.S., D'Odorico, P., Bhathena, Y., Arain, M.A., Ensminger, I. (2019). Carotenoid based vegetation indices for accurate monitoring of the phenology of photosynthesis at the leaf-scale in deciduous and evergreen trees. Remote Sens. Environ. 233, 111407. https://doi.org/10.1016/j.rse.2019.111407

Wong, C.Y.S., Gamon, J.A. (2015). Three causes of variation in the photochemical reflectance index (PRI) in evergreen conifers. New Phytol. 206, 187–195. https://doi.org/10.1111/nph.13159

Wong, C.Y.S., Mercado, L.M., Arain, M.A., Ensminger, I. (2022). Remotely sensed carotenoid dynamics improve modelling photosynthetic phenology in conifer and deciduous forests. Agric. For. Meteorol. 321, 108977. https://doi.org/10.1016/j.agrformet.2022.108977

Xue, J., Su, B. (2017). Significant remote sensing vegetation indices: A review of developments and applications. J. Sensors 2017. https://doi.org/10.1155/2017/1353691

Ye, J., Bao, W., Liao, C., Chen, D., Hu, H. (2023). Corn Phenology Detection Using the Derivative Dynamic Time Warping Method and Sentinel-2 Time Series. Remote Sens. 15. https://doi.org/10.3390/rs15143456

Zarco-Tejada, P.J., Miller, J.R., Morales, A., Berjón, A., & Agüera, J. (2004). Hyperspectral indices and model simulation for chlorophyll estimation in open-canopy tree crops. Remote sensing of environment, 90, 463-476. https://doi.org/10.1016/j.rse.2004.01.017

Chapter 4 – Tables and Figures

Table 1. RGB and multispectral-based vegetation indexes (VIs) used in this study. The calculation of VIs was based on reflectance (*R*) of particular wavelengths. The table shows the abbreviation of each index, the wavelengths involved, the formula applied and the appropriate reference. Where G = green colour channel (0-255); R = red colour channel (0-255); and B = blue colour channel (0-255). *G%* = green percentage index; *GRVI**= green-red vegetation index; *GLI* = green leaf index; *TGI* = triangular green index; *NDVI* = normalized difference vegetation index; *CCI* = chlorophyll/carotenoid index; *PRI* = photochemical reflectance index; *PSRI* = plant senescence reflectance index; *GRVI* = green ratio vegetation index; *EVI* = enhanced vegetation index; *TCARI* = transformed chlorophyll absorption reflectance index; *OSAVI* = optimized soil adjusted vegetation index.

	VI abbreviation	Formula	References
RGB VIs	G%	$G / (R + G + B)$	Woebbecke et al. 1995
	$GRVI_{RGB}$	$(G - R) / (G + R)$	Tucker et al. 1979
	GLI	$((G - R) + (G - B)) / 2G + R + B$	Louhaichi et al. 2001
	TGI	$-0.5 \times [190 \times (R - G) - 120 \times (R - B)]$	Hunt et al. 2011
Multispectral VIs	NDVI	$(R_{840} - R_{670}) / (R_{840} - R_{670})$	Rouse et al. 1973
	CCI	$(R_{532} - R_{670}) / (R_{532} + R_{670})$	Gamon et el. 2016
	PRI	$(R_{532} - R_{570}) / (R_{532} + R_{570})$	Gamon et al. 1992
	PSRI	$(R_{670} - R_{570}) / (R_{840})$	Merzlyak et al. 1999
	GRVI	R_{840} / R_{570}	Sripada et al. 2006
	EVI	$2.5 \times (R_{840} - R_{670}) / [(R_{840} + 6 \times R_{670} - 7.5 \times R_{450}) + 1]$	Huete et al. 2002
	TCARI	$3 \times (R_{700} - R_{670}) - 0.2 \times (R_{700} - R_{570}) \times (R_{700} / R_{670})$	Haboudane et al. 2002
	OSAVI	$(1 + 0.16) \times (R_{840} - R_{670}) / (R_{840} + R_{670} + 0.16)$	Rondeaux et al. 1996

Table 2. Mixed-effects model analysis of variance with repeated time structure for several needle pigments and fuel moisture content of a subset of six populations of Aleppo pine grown in a common garden in Zuera (Spain). Only fixed effects are reported. Chl_a = Chlorophyll a; Chl_b = Chlorophyll b; $Chl_{a/b}$ = ratio between chlorophyll a and b; Chl_{a+b} = total chlorophyll; *Car* = total carotenoids; Car/Chl_{a+b} = ratio between carotenoids and chlorophyll; *FMC* = fuel moisture content. $P < 0.05$ is indicated with bold characters.

			Chl_a		Chl_b		$Chl_{a/b}$		Chl_{a+b}		Car		Car/Chl		FMC		
Source of variation	Num df	Den df	F-value	$P > F$	F-value	$P > F$	F-value	$P > F$	F-value	$P > F$	F-value	$P > F$	F-value	$P > F$	Den df	F-value	$P > F$
Block	2.0	22.0	1.58	0.229	0.15	0.864	1.36	0.278	0.51	0.607	2.51	0.104	0.31	0.739	22.0	0.45	0.825
Population (Pop)	5.0	22.0	1.93	0.131	0.07	0.900	0.38	0.855	1.07	0.405	3.39	**0.020**	0.78	0.573	22.0	2.53	*0.059*
Needle age (NA)	1.0	22.0	0.01	0.909	0.62	0.439	0.08	0.780	0.16	0.693	2.47	0.131	1.56	0.225	22.0	288.17	**<0.001**
Pop × NA	5.0	22.0	0.74	0.620	0.86	0.520	1.21	0.338	0.25	0.937	1.68	0.271	0.48	0.784	22.0	0.87	0.518
Time (T)	3.0	51.0	53.87	**<0.001**	59.27	**<0.001**	6.31	**0.001**	85.96	**<0.001**	26.12	**<0.001**	22.98	**<0.001**	26.0	11.33	**<0.001**
Pop × T	15.0	51.0	1.31	0.230	0.89	0.575	1.19	0.308	0.94	0.528	1.47	0.154	0.66	0.814	26.0	1.93	*0.086*
NA × T	3.0	51.0	3.31	**0.027**	0.24	0.868	0.07	0.975	2.20	*0.099*	1.09	0.363	0.64	0.591	26.0	1.71	0.200
Pop × T × NA	15.0	51.0	1.27	0.258	0.86	0.608	1.26	0.261	0.82	0.654	1.19	0.310	0.5	0.931	26.0	1.69	0.138
Mean effect size (Population)			0.473 mg g^{-1}		0.068 mg g^{-1}		0.769 mg g^{-1}		0.595 mg g^{-1}		0.186 mg g^{-1}		0.024			1.9 %	

Table 3. Mixed-effects model analysis of variance for RGB and multispectral vegetation indexes of 56 populations of Aleppo pine categorized in five ecotypes and grown in two common gardens (Altura, eastern Spain; Zuera, northeastern Spain). Analysis of variance was fitted independently for each site. Only fixed effects are reported. *G%* = green percentage index; *GRVI** = green-red vegetation index; *GLI* = green leaf index; *TGI* = triangular green index; *NDVI* = normalized difference vegetation index; *PSRI* = plant senescence reflectance index; *EVI* = enhanced vegetation index; *TCARI/OSAVI* = ratio between the transformed chlorophyll absorption reflectance index and the optimized soil adjusted vegetation index. *P* < 0.05 is indicated with bold characters.

				G%		*GLI*		*GRVI**		*TGI*		*NDVI*		*PSRI*		*EVI*		*TCARI/OSAVI*	
Site	Source of variation	Num df	Den df	F-value	P > F	F-value	P > F	F-value	P > F	F-value	P > F	F-value	P > F	F-value	P > F	F-value	P > F	F-value	P > F
Altura	Column	6	18	23.31	**<0.001**	23.06	**<0.001**	9.96	**<0.001**	16.31	**<0.001**	4.20	**0.008**	2.85	**0.039**	14.81	**<0.001**	7.85	**<0.001**
	Block	3	18	4.65	**0.014**	4.47	**0.016**	3.25	**0.046**	2.11	0.134	2.15	0.13	6.25	**0.004**	0.97	0.428	2.22	0.121
	Population	55	112	1.91	**0.002**	1.90	**0.002**	1.93	**0.002**	2.01	**0.001**	1.64	**0.014**	1.92	**0.002**	1.00	0.486	1.28	0.138
	Ecotype	4	100	3.56	**0.009**	3.42	**0.012**	3.27	**0.014**	4.06	**0.004**	3.74	**0.007**	4.07	**0.004**	0.87	0.486	2.64	**0.038**
	Population [Ecotype]	47	100	1.72	**0.012**	1.72	**0.012**	1.79	**0.008**	1.81	**0.007**	1.49	**0.05**	1.80	**0.007**	1.12	0.310	1.33	0.120
	Mean effect size (Population)			0.004		0.008		0.002		0.675		0.014		0.005		0.024		0.015	
Zuera	Column	6	18	3.15	**0.027**	3.40	**0.02**	1.45	0.252	5.00	**0.004**	1.55	0.218	0.36	0.892	0.40	0.872	1.02	0.442
	Block	3	18	8.77	**0.001**	4.97	**0.011**	9.67	**0.001**	3.87	**0.027**	1.75	0.193	1.08	0.381	0.99	0.42	0.71	0.558
	Population	55	112	1.16	0.254	1.14	0.278	1.25	0.161	1.36	0.086	1.09	0.35	1.10	0.332	1.62	**0.017**	1.92	**0.002**
	Ecotype	4	100	1.81	0.132	2.36	0.058	1.80	0.135	2.97	**0.023**	2.59	**0.041**	1.05	0.386	3.73	**0.007**	6.13	**<0.001**
	Population [Ecotype]	47	100	1.16	0.266	1.08	0.363	1.28	0.154	1.29	0.148	0.92	0.624	0.98	0.525	1.58	**0.029**	1.74	**0.011**
	Mean effect size (Population)			0.003		0.006		0.003		0.543		0.011		0.005		0.050		0.014	

Table 4. Mixed-effects model analysis of variance for RGB and multispectral vegetation indexes of 56 populations of Aleppo pine categorized in five ecotypes and grown in a common garden located in Zuera (northeastern Spain). Analysis of variance was fitted for a time series comprising two consecutive UAV flights (May and June). Only fixed effects are reported. *G%* = green percentage index; *GRVI** = green-red vegetation index; *GLI* = green leaf index; *TGI* = triangular green index. $P < 0.05$ is indicated with bold characters.

			G%		*GLI*		*GRVI**		*TGI*	
Source of variation	Num df	Den df	F-value	P > F	F-value	P > F	F-value	P > F	F-value	P > F
Column	6	18	3.64	**0.015**	3.46	**0.019**	2.15	**0.097**	7.04	**0.001**
Block	3	18	1.49	0.250	0.68	0.573	2.12	0.133	1.33	0.295
Population (Pop)	55	112	1.44	0.055	1.26	0.153	1.02	0.455	1.44	0.054
Ecotype	4	100	1.78	0.140	1.61	0.178	3.05	**0.021**	1.59	0.182
Time	1	155	658.61	**<0.001**	571.21	**<0.001**	0.93	0.336	1.15	0.286
Ecotype × Time	4	155	0.34	0.847	0.60	0.666	0.83	0.506	0.47	0.757
Pop[Ecotype]	47	100	1.28	0.153	1.33	0.117	1.19	0.230	1.52	**0.041**
Time × Pop[Ecotype]	47	155	0.47	0.998	0.50	0.997	0.70	0.921	0.52	0.995
Mean effect size (Population)			0.003		0.005		0.094		0.524	

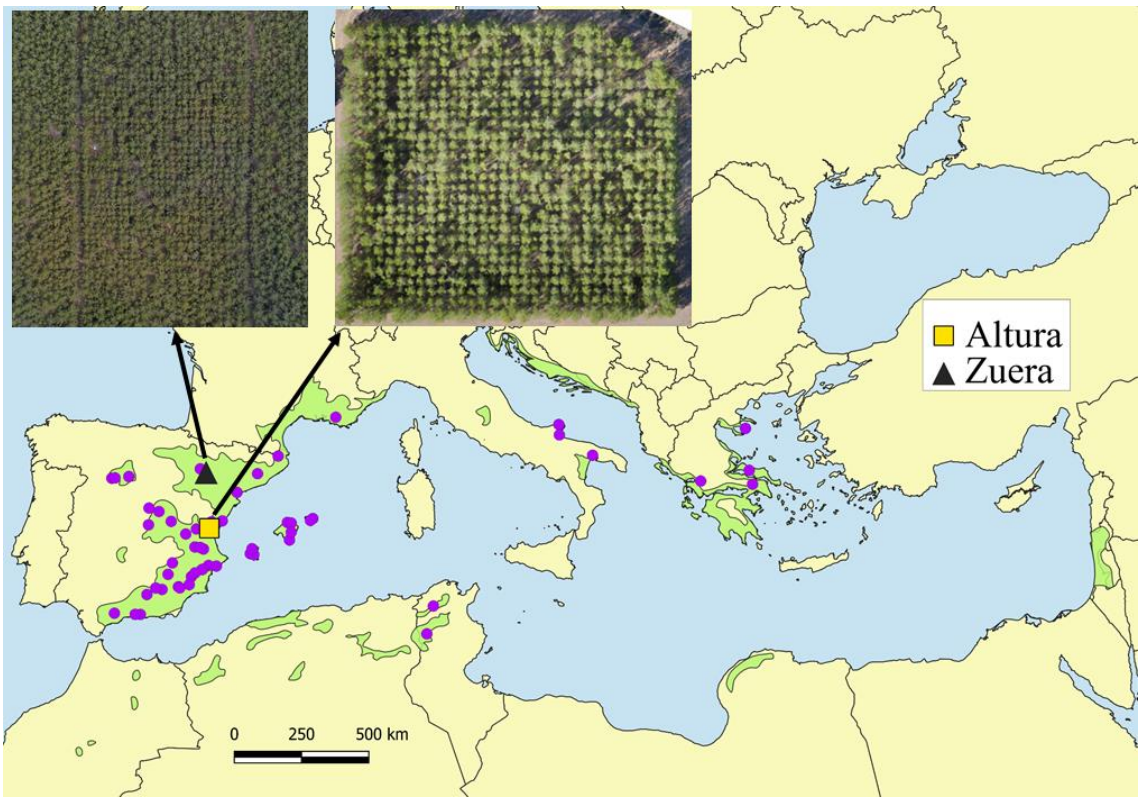

Fig. 1 Geographic origin of 56 *Pinus halepensis* populations (purple dots), evaluated in two common gardens experiments used in this study: Altura (Castellón province, Spain) and Zuera (Zaragoza province, Spain). The green area represents the natural distribution of *P. halepensis* according to EUFORGEN (http://www.euforgen.org/species).

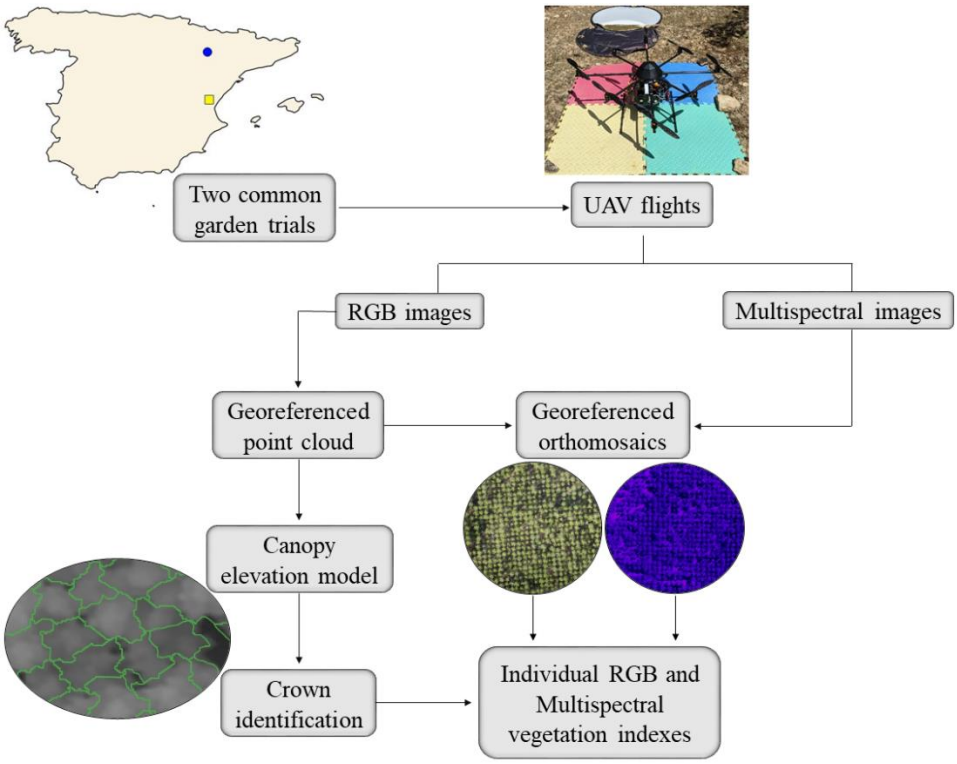

Fig 2. Flowchart summarizing the processing of RGB and multispectral images to obtain vegetation indexes at the tree level (i.e., phenotypic data).

	Chl_a	Chl_b	$Cha_{a/b}$	Chl_{a+b}	Car	Car/Chl_{a+b}	FMC
G%	**-0.54**	-0.09	0.09	-0.44	*-0.49*	-0.32	0.10
GLI	*-0.51*	-0.08	0.11	-0.41	*-0.46*	-0.29	0.06
GRVI*	-0.34	0.05	-0.17	-0.22	-0.26	-0.17	-0.35
TGI	**-0.54**	-0.13	0.32	-0.45	-0.38	-0.17	0.29
NDVI	-0.13	0.31	-0.32	0.06	*-0.51*	*-0.53*	0.02
CCI	-0.09	0.42	-0.30	0.16	*-0.57*	**-0.62**	0.25
PRI	0.22	-0.25	0.38	0.04	0.42	0.41	-0.47
PSRI	0.10	-0.16	0.22	-0.01	0.37	0.33	-0.32
GRVI	-0.15	0.24	-0.35	0.02	-0.45	*-0.46*	-0.19
EVI	-0.16	0.15	-0.23	-0.04	-0.30	-0.28	-0.07
TCARI	-0.23	0.07	-0.16	-0.14	-0.13	0.06	0.03
OSAVI	-0.16	-0.21	-0.27	-0.01	-0.40	-0.39	-0.03
TCARI/OSAVI	-0.17	-0.21	0.12	-0.24	0.36	0.46	0.10

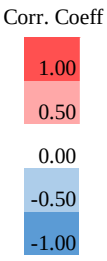

Fig. 3. Pearson correlation coefficients between population means of VIs and several needle pigments or fuel moisture content of a subset of six populations growing in a common garden located in Zuera, eastern Spain. *G%* = green percentage index; *GRVI** = green-red vegetation index; *GLI* = green leaf index; *TGI* = triangular green index; *NDVI* = normalized difference vegetation index; *CCI* = chlorophyll/carotenoid index; *PRI* = photochemical reflectance index; *PSRI* = plant senescence reflectance index; *GRVI* = green ratio vegetation index; *EVI* = enhanced vegetation index; *TCARI* = transformed chlorophyll absorption reflectance index; *OSAVI* = optimized soil adjusted vegetation index. Chl_a = Chlorophyll a; Chl_b = Chlorophyll b; $Chl_{a/b}$ = ratio between chlorophyll a and b; Chl_{a+b} = total chlorophyll; *Car* = total carotenoids; Car/Chl_{a+b} = ratio between carotenoids and chlorophyll; *FMC* = fuel moisture content. $P < 0.05$ is indicated with bold characters.

	G%		GLI		GRVI*		TGI		NDVI		PSRI		EVI		TCARI/OSAVI	
	(Altura)	(Zuera)	(Altura)	(Zuera)	(Altura)	(Zuera)	(Altura)	(Zuera)	(Altura)	(Zuera)	(Altura)	(Zuera)	(Altura)	(Zuera)	(Altura)	(Zuera)
Longitude	**0.52**	-	**0.50**	0.23	**0.44**	-	**0.47**	-	**0.60**	-	**-0.28**	-	-	0.17	0.04	**0.31**
Latitude	-0.14	-	-0.14	-0.26	-0.13	-	*-0.26*	-	0.03	-	**0.29**	-	-	-0.20	-0.21	-0.10
Altitude	-0.05	-	-0.05	-0.06	-0.04	-	-0.04	-	-0.25	-	0.24	-	-	0.03	-0.12	-0.16
MAT	0.04	-	0.04	0.23	0.01	-	0.09	-	0.08	-	**-0.30**	-	-	-0.05	0.20	0.13
MDR	-0.21	-	-0.21	-0.14	-0.21	-	-0.17	-	**-0.42**	-	0.20	-	-	0.00	0.11	-0.18
ISO	**-0.37**	-	**-0.36**	-0.13	**-0.33**	-	**-0.28**	-	**-0.48**	-	0.03	-	-	0.06	0.22	-0.18
TAR	-0.07	-	-0.07	-0.13	-0.09	-	-0.05	-	**-0.28**	-	**0.28**	-	-	-0.06	-0.01	-0.14
MAP	0.07	-	0.07	-0.13	0.06	-	0.06	-	0.18	-	-0.08	-	-	0.09	0.08	0.16

Coeff corr.
1.00
0.50
0.00
-0.50
-1.00

Fig. 4. Pearson correlation coefficients between population means of VIs and climate variables at origin of 56 populations growing in two common garden experiments located in Zuera (northeastern Spain) and Altura (eastern Spain). *GLI* = green leaf index; *TGI* = triangular green index; *PSRI* = plant senescence reflectance index; *EVI* = enhanced vegetation index; *TCARI/OSAVI* = ratio between the transformed chlorophyll absorption reflectance index and the optimized soil adjusted vegetation index. MAT = mean annual temperature; MDR = mean diurnal range; ISO = isothermality; TAR = temperature annual range; MAP = mean annual precipitation. Significant correlations are indicated in bold ($P < 0.05$).

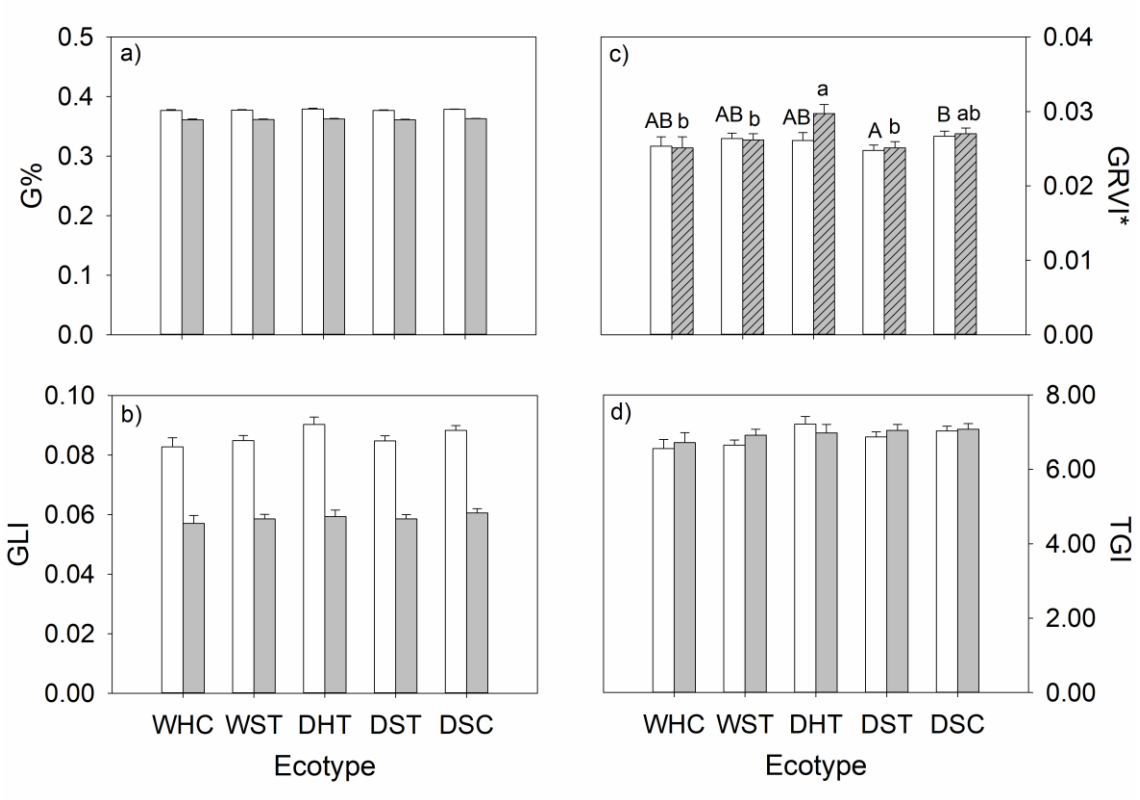

Fig. 5. Barplots summarizing ecotypic differences of RGB- derived vegetation indexes measured in Zuera (northeastern Spain) in two consecutive flights: May (grey bars), June (white bars). Hatched bars denote significant ecotypic differences within a flight and different letters indicate significantly different ecotypes (uppercase letters for June, lowercase letters for May) (LSD test, $P = 0.05$). *G%* = green percentage index; *GRVI** = green-red vegetation index; *GLI* = green leaf index; *TGI* = triangular green index.

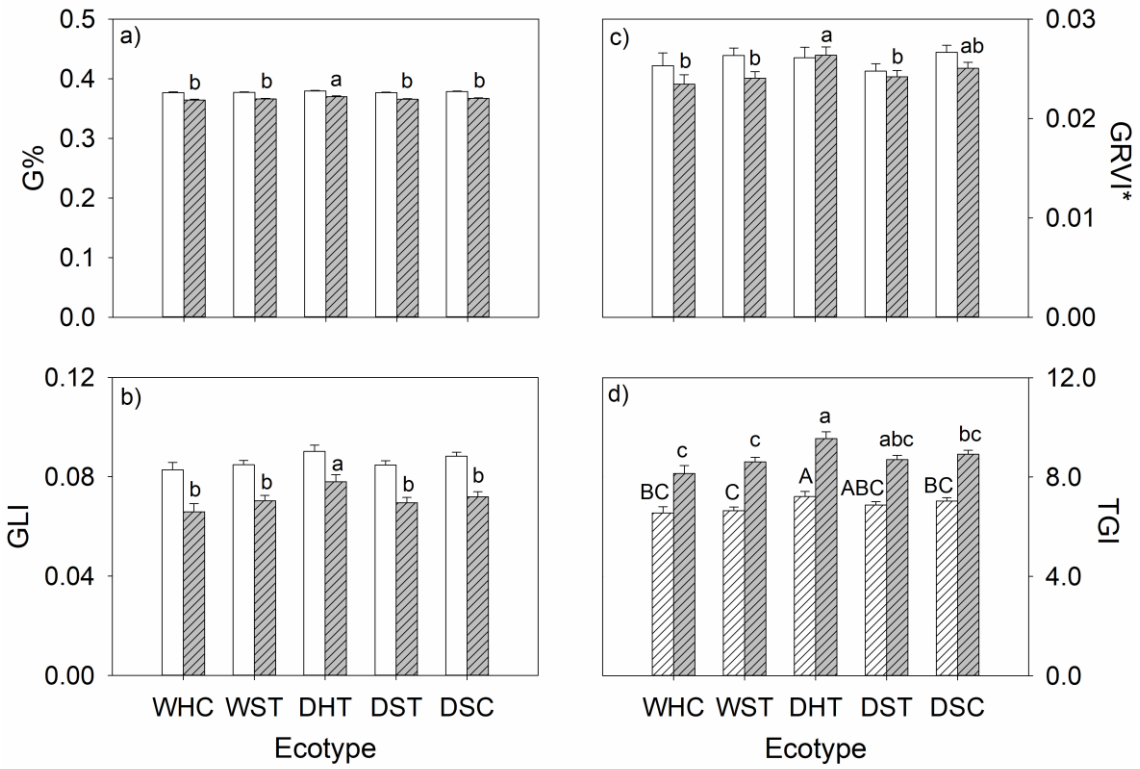

Fig. 6. Barplots summarizing ecotypic differences of RGB- derived vegetation indexes measured in two common garden trials: Altura, eastern Spain (grey bars), and Zuera, northeastern Spain (white bars). Hatched bars denote significant ecotypic differences within trial and different letters indicate significantly different ecotypes (uppercase letters for Zuera, lowercase letters for Altura) (LSD test, $P = 0.05$). *G%* = green percentage index; *GLI* = green leaf index; *GRVI** = green-red vegetation index; *GLI* = green leaf index; TGI = triangular green index.

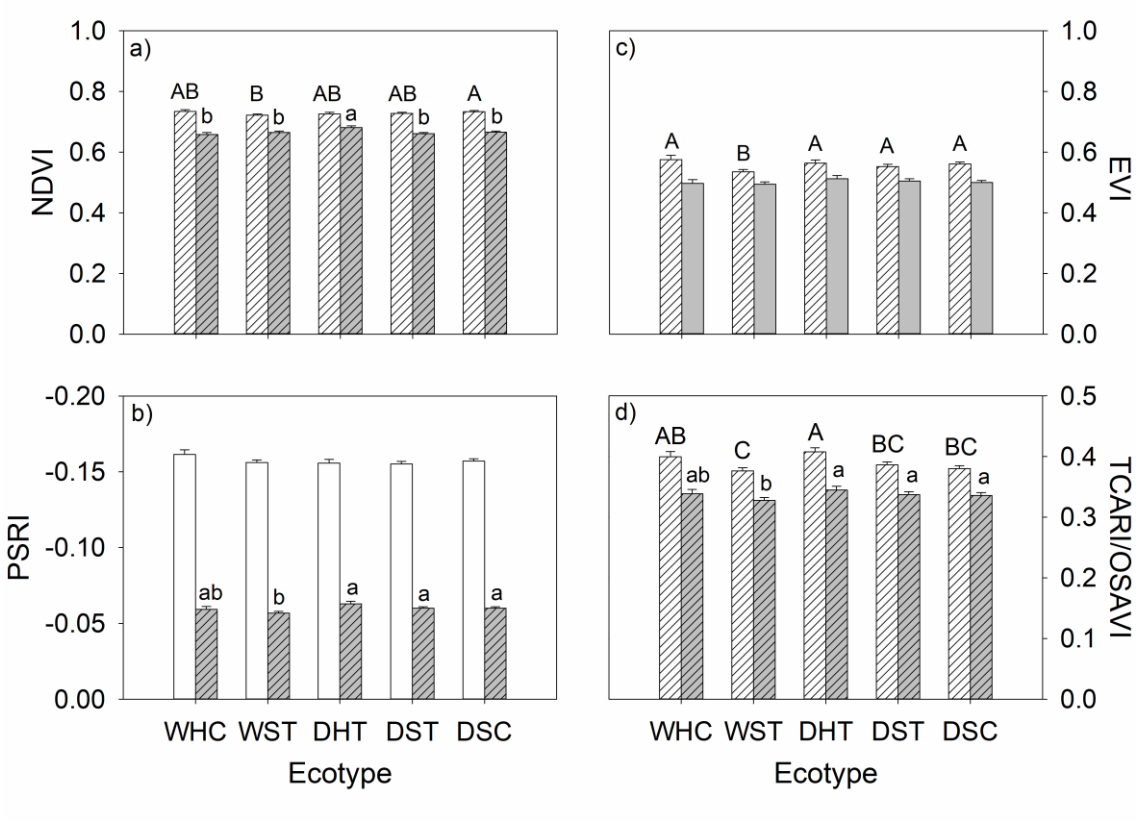

Fig. 7. Bar plots summarizing ecotypic differences of multispectral-derived vegetation indexes measured in two common garden trials: Altura, eastern Spain (grey bars), and Zuera, northeastern Spain (white bars). Hatched bars denote significant ecotypic differences within a trial and different letters indicate significantly different ecotypes (uppercase letters for Zuera, lowercase letters for Altura) (LSD test, P = 0.05). *NDVI* = normalized difference vegetation index; *PSRI* = plant senescence reflectance index; *EVI* = enhanced vegetation index; *TCARI/OSAVI* = ratio between the transformed chlorophyll absorption reflectance index and the optimized soil adjusted vegetation index.

Chapter 4 – Supplementary material

Table S1. Characteristics of the 56 populations of Aleppo pine used in this study and grouped into 5 ecotypes.

Name of provenances	Population code	Ecotype	Region	Longitutde	Latitude	Altitude	MAT (°C)	MAP (mm)
Cabanelles	11	WHC	Catalonia	2°47'E	42°15'	258	14.56	720.00
Tivissa	21	WST	Catalonia	0°50'E	42°20'	336	14.83	587.00
Sant Salvador Guardiola	31	WHC	Catalonia	1°45'E	41°40'	318	14.39	628.00
Zuera	61	WST	Ebro Depression	0°55'E	41°55'	576	11.95	474.00
Valdeconcha	82	DSC	Southern Plateau	2°52'W	40°27'	837	12.76	433.00
Alcantud	83	DSC	Southern Plateau	2°18'W	40°34'	1057	10.84	505.00
Colmenar de Oreja	84	DSC	Southern Plateau	3°20'W	40°05'	692	13.70	433.00
Cirat	91	DSCS	Iberian Range	0°28'W	40°03'	445	14.62	440.00
Tuéar	92	DSC	Iberian Range	1°09'W	39°49'	729	13.18	424.00
Enguidanos	93	DSC	Iberian Range	1°39'W	39°38'	990	11.87	485.00
Altura	102	DSC	Iberian Range	0°37'W	39°47'	662	13.07	546.00
Benicàssim	111	WST	Iberian Range	0°01'E	40°05'	468	13.80	472.00
Gilet	112	DST	Iberian Range	0°21'W	39°40'	152	13.11	462.00
Tibi	101	DSC	East Spain	0°39'W	38°31'	976	14.76	428.00
Villa de Ves	103	DSC	East Spain	1°15'W	39°11'	864	14.71	454.00
Jarafuel	104	DSC	East Spain	1°01'W	39°10'	563	15.17	386.00
Bicorp	105	DSC	East Spain	0°51'W	39°06'	587	14.65	523.00
Commercial Seed	109		East Spain	1°00'W	39°09'		16.57	451.00
Villajoyosa	131	DST	N. Betic Mts	0°18'W	38°30'	126	17.70	422.00
Ricote	141	DST	N. Betic Mts	1°26'W	38°09'	688	14.75	398.00
Monovar	142	DST	N. Betic Mts	0°57'W	38°23'	820	13.97	467.00
Monovar	143	DST	N. Betic Mts	0°55'W	38°24'	601	15.11	416.00
Paterna	144	DSC	N. Betic Mts	2°17'W	38°38'	1028	12.84	470.00
Abarán	145	DST	N. Betic Mts	1°16'W	38°17'	657	14.85	403.00
Quéntar	151	DST	S. Betic Mts	3°25'W	37°14'	1226	12.81	578.00
Benamaurel	152	DSC	S. Betic Mts	2°44'W	37°42'	908	14.15	452.00
Vélez Blanco	153	DST	S. Betic Mts	2°01W	37°47'	785	14.14	416.00
Santiago de la Espada	154	DSC	S. Betic Mts	2°28'W	38°14'	842	14.14	432.00
Lorca	156	DSC	S. Betic Mts	1°32'W	37°52'	831	14.13	427.00
Alhama de Murcia	157	DSC	S. Betic Mts	3°01'W	37°45'	765	15.05	449.00
Quesada	158	DSC	S. Betic Mts	1°57'W	37°45'	757	15.09	373.00

Lentergi	171	DST	South Spain	3°41'W	36°49'	363	16.73	378.00
Carratraca	172	DST	South Spain	4°50'W	36°51'	635	15.38	695.00
Frigiliana	173	DST	South Spain	3°55'E	36°49'	595	15.66	456.00
Palma de Mallorca	182	WST	Majorca	2°56'E	39°09'	32	16.68	563.00
Santanyí	183	WST	Majorca	3°03'E	39°17'	19	16.84	568.00
Alcudia	184	WST	Majorca	03°10'E	39°52'	185	15.74	704.00
Calvia	185	WST	Majorca	03°08'E	39°33'	243	15.75	526.00
Marcadal	186	WST	Menorca	4°10'E	39°58'	85	16.56	613.00
Atàlix	187	WST	Menorca	4°03'E	39°55'	67	16.93	608.00
Cala d'Hort	191	WST	Ibiza	1°15'E	38°53'	329	15.89	542.00
Ses Salines	192	DST	Ibiza	1°24'E	38°50'	10	17.50	443.00
Ses Salandres	193	DST	Ibiza	1°20'E	39°03'	65	17.10	467.00
Istaia-eyboia	211	DHT	Greece	23°31'E	38°44'	53	17.47	506.00
Amfilohia	212	DHT	Greece	21°18'E	38°53'	429	14.20	975.00
Tatoi-attica	213	DHT	Greece	23°28'E	38°27'	253	16.31	552.00
Kassandra	214	DHT	Greece	23°54'E	40°05'	402	14.37	510.00
Gemenos	221	WHC	France	5°40'E	43°25'	391	12.44	707.00
Litorale Tarantino	231	WST	Italy	17°07'E	40°37'	204	15.17	551.00
Gargano Monte Pucci	232	WST	Italy	15°57'E	41°54'	382	14.18	524.00
Gargano Marzini	233	-WST	Italy	15°51'E	41°330	0	16.11	472.00
Thala	241	DST	Tunisia	8°39'E	35°34'	948	14.89	467.00
Tabarka	242	DHT	Tunisia	9°04'E	36°30'	287	17.75	558.00
Valbuena de Duero	201		North Plateau (Reforestation)	04°16'W	41°39'	825		
Vega de Valdetronco	202		North Plateau (Reforestation)	05°04'W	43°35'	820		
Villavieja Tordesillas	203		North Plateau (Reforestation)	04°55'W	41°36'	820		

Table S2. Wavelength specification of the spectral bands of the sensor micro-MCA 11+ILS multispectral camera used in the Zuera trial (northeastern Spain). CW = central spectral band; FWHM = bandwidth.

Band number	CW (nm)	FWHM (nm)
1	450	40
2	490	10
3	532	3
4	570	10
5	670	10
6	700	10
7	740	10
8	780	10
9	840	10
10	860	10
11	950	40

Table S3. Wavelength specification of the spectral bands of the sensor micro-MCA 12+ILS multispectral camera used in the Altura trial (eastern Spain). CW = central spectral band; FWHM = bandwidth.

Band number	CW (nm)	FWHM (nm)
1	450	40
2	550	10
3	570	10
4	670	10
5	700	10
6	720	10
7	840	10
8	860	10
9	900	10
10	950	40

Table S4. Mixed-effects model analysis of variance for needle pigment content, fuel moisture content, stomatal conductance and specific leaf area of a subset of six populations of Aleppo pine grown in a common garden in Zuera (northeastern Spain). Analysis of variance was fitted independently for each field campaign and needle age class: (a) one-year-old needles, (b) ≥ two-year-old needles.

(a) one-year-old needles

				Chl$_a$		*Chl*$_b$		*Chl*$_{a/b}$		*Chl*$_{a+b}$		*Car*		*Car/Chl*$_{a+b}$		*FMC*		*GSW*		*SLA*	
Source of variation	Time	Num df	Den df	F-value	P > F	F-value	P > F	F-value	P > F	F-value	P > F	F-value	P > F	F-value	P > F	F-value	P > F	F-value	P > F	F-value	P > F
Block	May 14th	2	10.0	0.70	0.521	0.26	0.777	1.42	0.287	0.05	0.951	4.33	**0.044**	2.95	0.099	/	/	/	/	/	/
Population		5	10.0	1.30	0.337	0.64	0.672	1.01	0.460	0.21	0.949	2.62	*0.092*	1.03	0.449	/	/	/	/	/	/
Block	May 28th	2	10.0	0.15	0.862	0.25	0.783	0.90	0.438	0.21	0.817	0.54	0.599	0.32	0.734	0.78	0.486	/	/	/	/
Population		5	10.0	0.40	0.838	1.06	0.436	1.51	0.271	0.90	0.520	0.62	0.686	0.54	0.745	2.24	0.131	/	/	/	/
Block	Jul 02nd	2	10.0	0.55	0.594	0.32	0.732	1.67	0.237	0.58	0.578	0.99	0.404	0.24	0.793	0.65	0.541	/	/	/	/
Population		5	10.0	1.35	0.320	0.48	0.784	1.20	0.377	1.41	0.302	1.04	0.444	0.50	0.772	3.91	**0.032**	/	/	/	/

(b) ≥ two-year-old needles

				Chl$_a$		*Chl*$_b$		*Chl*$_{a/b}$		*Chl*$_{a+b}$		*Car*		*Car/Chl*$_{a+b}$		*FMC*		*GSW*		*SLA*	
Source of variation	Time	Num df	Den df	F-value	P > F	F-value	P > F	F-value	P > F	F-value	P > F	F-value	P > F	F-value	P > F	F-value	P > F	F-value	P > F	F-value	P > F
Block	May 14th	2	10.0	0.62	0.556	2.06	0.178	4.10	**0.050**	0.95	0.419	0.94	0.423	2.54	0.129	/	/	/	/	/	/
Population		5	10.0	1.61	0.245	1.36	0.317	1.65	0.233	1.52	0.269	0.70	0.635	0.76	0.596	/	/	/	/	/	/
Block	May 28th	2	10.0	0.70	0.517	0.28	0.762	1.53	0.262	0.54	0.569	0.02	0.982	0.87	0.447	0.09	0.912	15.46	**0.001**	/	/
Population		5	10.0	0.86	0.538	0.19	0.958	0.97	0.478	0.39	0.842	0.59	0.709	0.27	0.918	1.33	0.325	1.62	0.242	/	/
Block	Jul 02nd	2	10.0	1.01	0.367	0.17	0.843	0.99	0.406	0.26	0.778	3.26	0.081	0.04	0.959	1.46	0.278	0.01	0.985	2.89	0.102
Population		5	10.0	0.75	0.605	0.03	0.999	1.00	0.464	0.17	0.970	1.29	0.341	0.20	0.953	1.3	0.339	0.57	0.725	0.79	0.581

Table S5. Mixed-effects model analysis of variance for total height (*H*) and crown area (*CA*) of 56 populations of Aleppo pine categorized in five ecotypes and grown in two common gardens (Altura, eastern Spain; Zuera, northeastern Spain). Analysis of variance was fitted independently for each site. Only fixed effects are reported. $P < 0.05$ is indicated with bold characters.

				H		*CA*	
Site	Source of variation	Num df	Den df	F-value	P > F	F-value	P > F
Altura	Column	6	18.0	3.23	**0.025**	3.44	**0.019**
	Block	3	18.0	3.63	**0.033**	0.77	0.526
	Population (Pop)	55	111.0	2.27	**<0.001**	1.00	0.488
	Ecotype	4	100.0	4.23	**0.003**	0.69	0.602
	Pop [Ecotype]	47	100.0	2.19	**0.001**	1.11	0.332
Zuera	Column	6	18.0	1.49	0.238	1.92	0.132
	Block	3	18.0	2.46	*0.096*	1.38	0.281
	Population Pop	55	112.0	2.01	**0.001**	1.00	0.486
	Ecotype	4	100.0	1.70	0.155	0.23	0.920
	Pop [Ecotype]	47	100.0	2.08	**0.001**	1.12	0.314

Table S6. Mixed-effects model analysis of variance for multispectral vegetation indexes of 56 populations of Aleppo pine categorized in five ecotypes and grown in two common gardens (Altura, eastern Spain; Zuera, northeastern Spain). Analysis of variance was fitted independently for each site. Only fixed effects are reported. $P < 0.05$ is indicated with bold characters.

				CCI		*PRI*		*GRVI*		*TCARI*		*OSAVI*	
Site	Source of variation	Num df	Den df	F-value	*P* > F	F-value	*P* > F	F-value	*P* > F	F-value	*P* > F	F-value	*P* > F
Altura	Column	6	18	-	-	-	-	2.7	**0.047**	13.34	**<0.001**	9.45	**<0.001**
	Block	3	18	-	-	-	-	3.48	**0.038**	0.85	0.483	2.49	0.093
	Population (Pop)	55	112	-	-	-	-	1.15	0.265	1.11	0.315	0.8	0.819
	Ecotype	4	100	-	-	-	-	2.18	0.077	2.14	0.081	0.25	0.909
	Pop [Ecotype]	47	100	-	-	-	-	1.14	0.284	1.15	0.279	0.95	0.569
	Mean effect size (Population)							0.150		0.007		0.010	
Zuera	Column	6	18	1.98	0.123	0.39	0.875	1.47	0.242	0.47	0.825	0.74	0.626
	Block	3	18	2.83	0.068	4.12	**0.022**	1.11	0.37	1.08	0.384	1.19	0.34
	Population (Pop)	55	112	1.16	0.251	0.96	0.55	0.98	0.519	1.92	**0.002**	1.41	0.065
	Ecotype	4	100	1.64	0.169	0.87	0.484	1.4	0.241	5.14	**0.001**	3.4	**0.012**
	Pop [Ecotype]	47	100	0.99	0.503	0.95	0.564	0.79	0.812	1.83	**0.006**	1.28	0.151
	Mean effect size (Population)			0.014		0.013		0.150		0.011		0.018	

Table S7. Multivariate Analysis of Variance (MANOVA) of the following groups of variables: Fuel traits (needle length, combustible humidity and fuel bed depth) and Flammability traits (diffusion flame time, flame time, smoldering combustion time, flame height, fuel combusted and mean peak heat). The MANOVA table shows the fixed effects of population and block of ten populations of Aleppo pine grown in a common garden located in Zuera (northeastern Spain). $P < 0.05$ is indicated with bold characters.

		Fuel traits					Flammability traits				
Main effect	df	Wilks	Num df	Den df	F value	*P* > F	Wilks	Num df	Den df	*F* value	*P* > F
Block	2	0.572	6.0	26.0	1.34	0.254	0.266	12.0	16.0	1.15	0.332
Population	9	0.362	27.0	38.6	0.62	0.920	0.022	54.0	45.4	1.02	0.600

Table S8. Mixed-effects model analysis of variance for (a) fuel-related traits and (b) flammability-related traits of 56 populations of Aleppo pine categorized in five ecotypes and grown in a common gardens located in Zuera, northeastern Spain. (a) Combustible humidity (*CH*), fuel bed depth (*FBD*), needle length (*NL*); (b) Diffusion of flame time (*DFT*), flame time (*FL*), smoldering combustion time (*SCT*), maximum flame height (*FH*), fuel combusted (*FC*), mean rate of weight loss (*W*L), and mean peak temperature (*MH*). Analysis of variance was fitted independently for each site. Only fixed effects are reported. $P < 0.05$ is indicated with bold characters.

(a)				*CH*		*FBD*		*NL*	
Source of variation	Trait type	Num df	Den df	F value	P > F	F-value	P > F	F-value	P > F
Block	Fuel	2	15.0	1.66	0.223	0.24	0.793	0.96	0.404
Population (Pop)		9	15.0	0.63	0.759	0.28	0.971	0.46	0.878
Ecotype		4	15.0	0.31	0.866	0.29	0.880	0.13	0.970
Ecotype [Pop]		5	15.0	0.84	0.542	0.26	0.927	0.72	0.613

(b)				*DFT*		*FL*		*SCT*		*FL*		*FC*		*ML*		*MH*	
Source of variation	Trait type	Num df	Den df	F-value	P > F	F-value	P > F	F-value	P > F	F-value	P > F	F-value	P > F	F-value	P > F	F-value	P > F
Block	Flammability	2	13.0	2.12	0.160	1.03	0.383	0.52	0.608	0.88	0.438	0.23	0.799	0.10	0.903	0.66	0.536
Population (Pop)		9	13.0	0.75	0.661	0.69	0.706	1.25	0.345	0.66	0.730	0.83	0.601	2.07	0.113	0.26	0.973
Ecotype		4	13.0	0.60	0.671	0.29	0.882	1.22	0.350	0.85	0.516	1.12	0.391	2.18	0.129	0.28	0.887
Ecotype [Pop]		5	13.0	0.86	0.535	0.97	0.472	1.17	0.373	0.54	0.742	0.65	0.666	2.34	0.100	0.27	0.919

a)

b)

B IV								B III								B II								B I							
143	171	131	242	21	201	192	104	183	61	102	154	202	192	112	232	84	242	156	183	141	221	103	191	101	201	187	152	142	183	31	232
211	231	191	142	145	102	31	173	201	111	152	191	83	241	157	103	102	82	185	192	152	109	144	212	213	143	141	83	203	102	184	151
141	153	93	214	232	186	185	83	101	182	212	21	158	141	231	172	201	186	91	112	21	151	233	145	172	91	11	221	192	231	153	111
151	193	156	11	101	109	202	111	11	173	184	242	144	92	214	145	153	131	213	241	182	101	173	61	158	84	242	193	173	212	112	93
103	144	61	187	213	172	158	233	203	156	151	211	93	82	187	131	142	104	193	214	172	83	154	203	109	171	145	103	82	105	214	182
84	92	203	157	182	152	112	221	193	104	105	185	233	221	153	31	157	143	231	11	202	105	187	93	21	191	185	131	92	154	233	202
184	212	183	91	105	82	241	154	143	109	84	142	186	171	91	213	184	171	31	92	232	158	211	111	144	241	211	157	156	186	104	61

c)

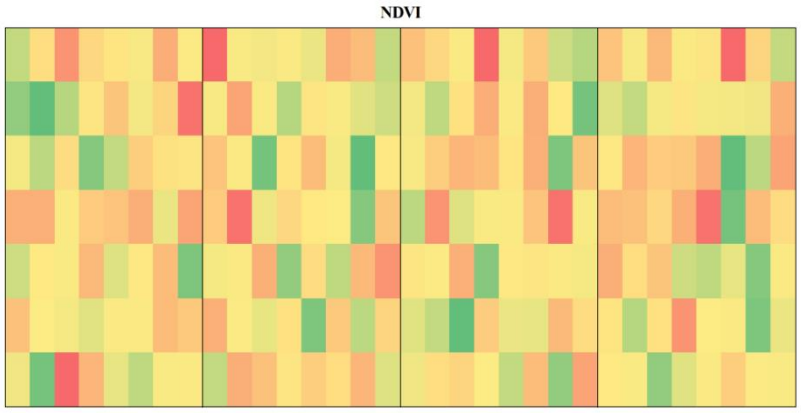

Fig. S1. Composite illustration showing (a) an aerial image of the Altura trial (eastern Spain), (b) a scheme of the experimental design (B I, II, III, IV refer to each of the four blocks of the experiment, and numbers represent the population codes with population codes available at Table S1), and (c) the spatial variation of NVDI (greener colours indicate higher NDVI values, redder colours indicate lower NDVI values).

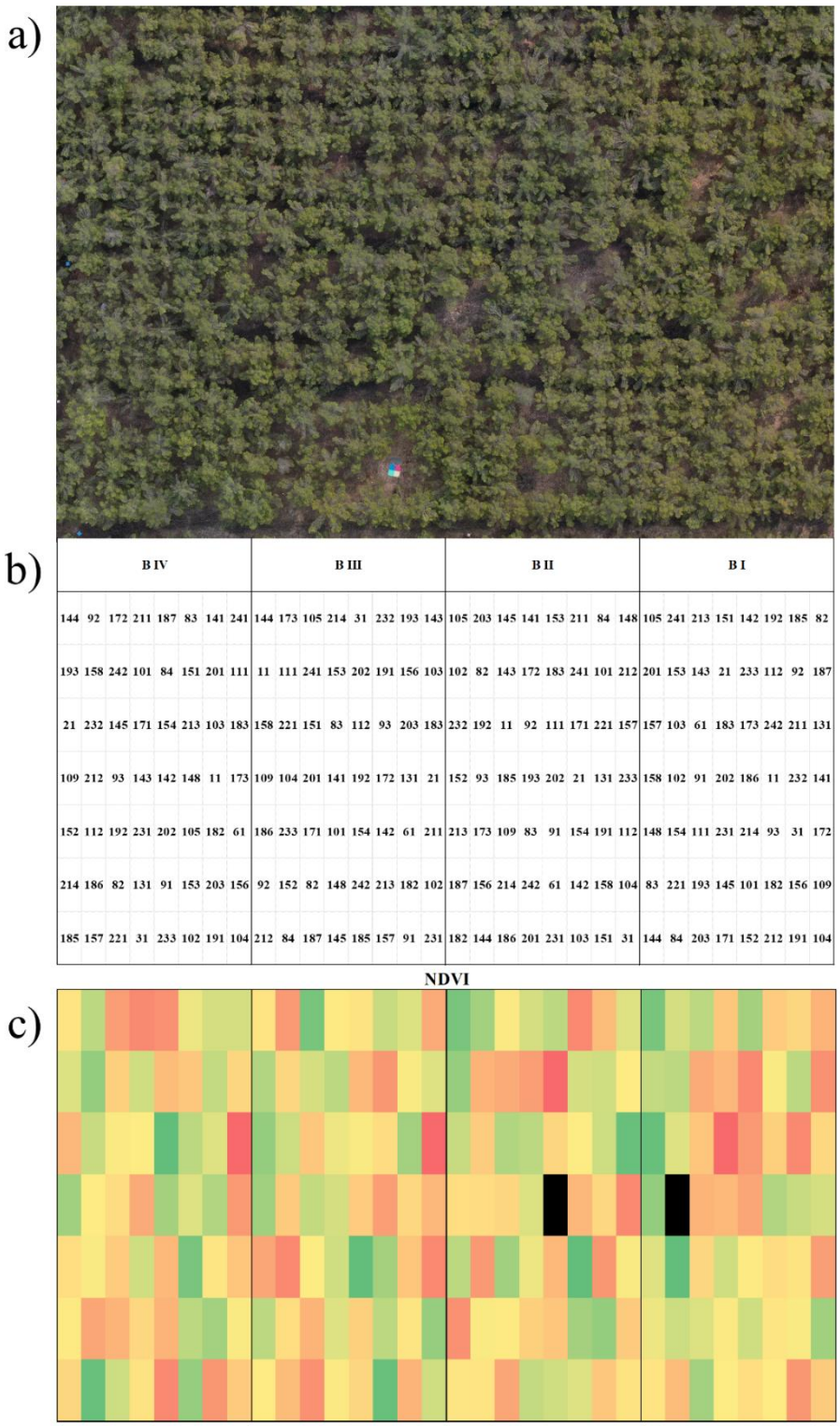

Fig. S2. Composite illustration showing (a) an aerial image of the Zuera trial (northeastern Spain), (b) a scheme of the experimental design (B I, II, III, IV refer to each of the four blocks of the experiment, and numbers represent the population codes with population codes available at Table S1), and (c) the spatial variation of NVDI (greener colours indicate higher NDVI values, redder colours indicate lower NDVI values, and black cells indicate missing observations).

General discussion

Phenotypic variation indicative of adaptive syndromes in Mediterranean pines

P. halepensis and *P. nigra* are two widely distributed pine species across the Mediterranean basin. Although these species can naturally co-occur in some environments, they present high interspecific differences for many adaptive traits that allow them to occupy contrasting ecological niches (Jevšenak and Saražin, 2023). *P. halepensis* is a thermophilic species well adapted to drought that dominate fire-prone habitats (Pasho et al. 2012; Pausas, 2015) while *P. nigra* is most commonly found in mountain areas, it is well adapted to cold, and it is a fire-tolerant species (Enescu et al. 2016; Kreyling et al. 2012). In addition to the high interspecific differences, both species present high intraspecific differentiation for functional traits potentially related to life-history strategies of their different populations. In spite of the importance that intraspecific variability plays in the determination of long-term adaptations of a species, it has not received the consideration it deserves for the purpose of revising silvicultural strategies and adaptive forest management for optimizing tree performance under global change. In this regard, this work provides new clues on phenotypic and genotypic intraspecific differentiation to assist unraveling local adaptation and phenotypic plasticity of two conifers with high ecological value in Mediterranean forests. In particular, the traits analyzed in this thesis for these two pine species are summarized in Table 1.

Table 1. Summary of functional traits analyzed at the intraspecific level in this thesis using four common garden experiments.

Traits	*P. halepensis*	*P. nigra*
Root morphology	✓	
Total height	✓	✓
DBH	✓	✓
Tree-ring width	✓	
Tree biomass	✓	✓
Crown architecture	✓	✓
Crown volume	✓	✓
Needle phenology	✓	
Litter flammability	✓	

Intraspecific differentiation in Pinus halepensis

P. halepensis was evaluated in all four chapters of this thesis, thereby providing an overview of the existing intraspecific variability of many plant compartments, from roots (Chapter 1) to canopy (Chapters 3 and 4) through secondary growth (Chapter 2). It is known that water availability, temperature and fire are the main environmental drivers that shape the distribution and genetic differentiation of the species across its distribution range. Populations coming from xeric environments, which are grouped in several semi-arid ecotypes (Patsiou et al. 2020), adopt generally a more conservative resource-use strategy than mesic populations. They present a high water-use efficiency (Voltas et al. 2015), and they invest more in early reproduction (Climent et al. 2008), in defense (Santos-del-Blanco et al. 2013) and in reserves (Santini et al. 2019a) at the expenses of growth. This differential adaptive strategy of inhibited or enhanced tree growth was clearly noticeable in all the chapters (chapters 1 to 4).

The general pattern described for the genus *Pinus* is that species originating from harsher conditions allocate more in root growth than species inhabiting mesic areas (Andivia et al. 2019). This pattern was not straightforward at the intraspecific level (Chapter 1), highlighting the complex adaptive syndromes of the species, and suggesting possible trade-offs between plant compartments. Thus, populations (or ecotypes) coming from xeric conditions do invest less resources in growth in general, both below- and aboveground growth (Chapter 1 and 3) in order to allocate more resources to other functions. In fact, when combining below- and aboveground growth (i.e. the ratio between root diameter or depth and total tree height), I could notice that even if populations belonging to semi-arid ecotypes do not always exhibit larger allocation to roots compared to populations from sub-humid ecotypes, they do invest comparatively more in roots than in total tree height (Lombardi et al. 2022) (Fig. 1).

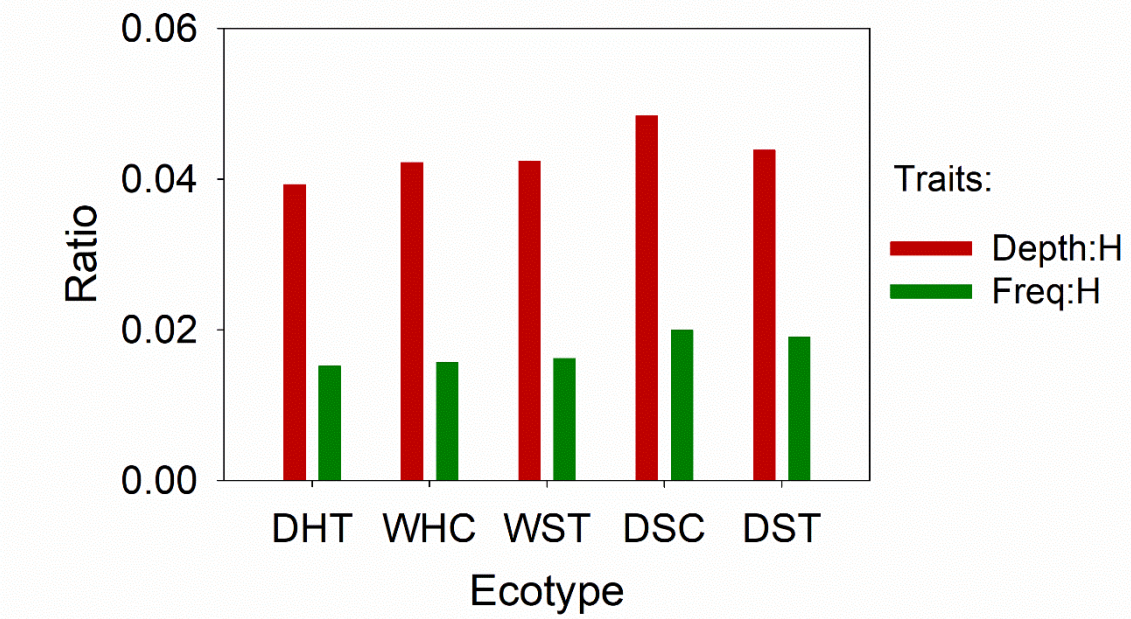

Fig. 1. Barplot showing mean ecotypic values for the ratio between root depth (cm) or frequency and total tree height (cm) (Depth:H, Freq:H, respectively) inferred in an adult *P. halepensis* experiment garden located in Altura, Castellón province (Spain). DHT = dry-summer/sub-humid/temperate; WHC = wet-summer/sub-humid/cool (WHC); WST = wet-summer/semiarid/temperate; DSC = dry-summer/semiarid/cold; DST = dry-summer/semiarid/temperate.

The enhancing aerial growth pattern of populations belonging to sub-humid ecotypes was described with more details in chapters 3 and 4. In addition to total tree height, those populations exhibited larger crown density and crown volume, and also advanced current-year needle sprouting (Fig. 2).

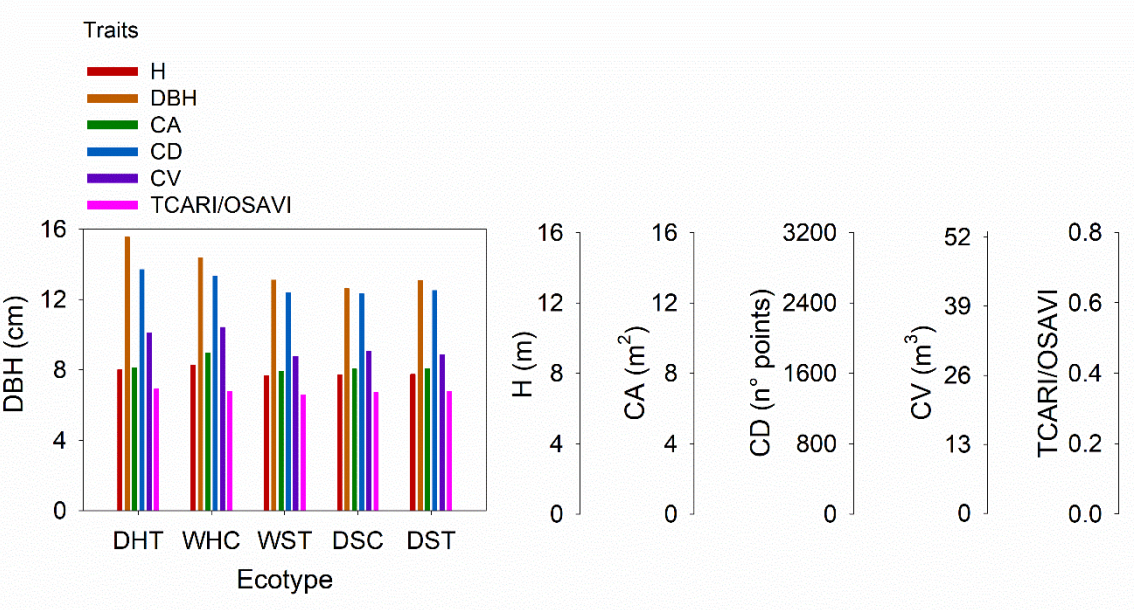

Fig 2. Barplot showing ecotypic values for total tree height (H), diameter at breast height (DBH), crown area (CA), crown density (CD), crown volume (CV) and the vegetation index TCARI/OSAVI measured in an adult *P. halepensis* common garden located in Altura, Castellón province (Spain). Units are indicated for each trait separately. DHT = dry-summer/sub-humid/temperate; WHC = wet-summer/sub-humid/cool (WHC); WST = wet-summer/semiarid/temperate; DSC = dry-summer/semiarid/cold; DST = dry-summer/semiarid/temperate.

Altogether, these results disclosed a clearly larger investment in aerial growth of populations belonging to sub-humid ecotypes, suggesting a potentially genetically based shade-avoidance strategy adopted by ecotypes from more favorable environments to outcompete their neighbors. In favorable environments the productivity is generally higher (Vennetier et al. 2018) and, therefore, subjected to higher intra- and interspecific competition, and a more expanded crown enhances light capture and carbon gain (Duursma et al. 2007). Also, these populations are characterized by a higher growth plasticity and, hence, they usually grow well under different climates (Patsiou et al. 2020) because they can adjust the timing of earlywood formation in relation to climate, especially spring and early summer temperature (chapter 2). Alternatively, populations (and ecotypes) from semi-arid environments could assign more resources to the production of serotine cones as a post-fire regeneration strategy at the expense of primary growth.

This points to possible trade-offs between drought- and fire-related traits (Karavani et al. 2018). Indeed, limited tree height and enhanced needle senescence may promote tree flammability, favoring surface fire to become crown fire. On the other hand, results of this thesis indicated lack of intraspecific differentiation in other flammability traits, such as litter flammability, among Aleppo pine populations.

Intraspecific genetic differentiation in Pinus nigra

P. nigra was analysed in one chapter (chapter 3). Previous studies have documented intraspecific variation in miscellaneous traits such as radial growth (Fkiri et al. 2018), wood structure (Esteban et al. 2012), total height and tree survival (Varelides et al. 2001), and vegetation indices and reserves (Santini et al. 2019b). The high genetic divergence among populations of this species have traditionally led to its taxonomic division into a number of subspecies with contrasting morphophysiological characteristics. The results of this thesis indicated that the high differentiation among populations and subspecies for traits related to crown architecture and crown structure is potentially related to the different degree of cold hardiness characteristics within the species (Fig. 3).

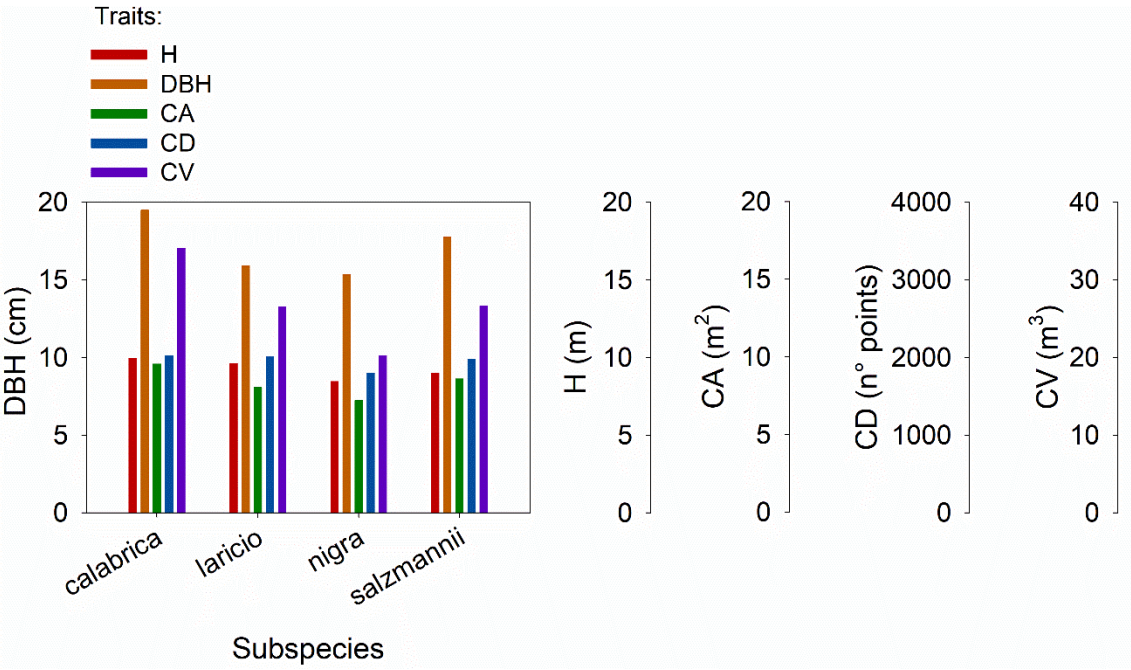

Fig. 3. Barplot showing ecotypic values for the total tree height (H), diameter at breast height (DBH), crown

area (CA), crown density (CD) and crown volume (CV) measured in an adult *P. nigra* common garden located in Valsaín, Segovia province (Spain). Units are indicated for each trait separately.

In this regard, precipitation, intra-annual temperature fluctuations and altitude were found to be the principal external drivers of these intraspecific differentiations. Subspecies with higher cold hardiness experienced a slower growth, along with a slender and shorter canopy that may protect the tree from snow canopy damage. This finding is in agreement with previous studies that highlighted intraspecific variation in winter cold resistance among *P. nigra* populations (Santini et al. 2019b; Kreyling et al. 2012), with *calabrica* the most freeze-sensitive subspecies, generally from mesic environments, exhibiting fast growing characteristics. In the other extreme of its ecological niche, the *salzmannii* and *nigra* subspecies occupies areas, where drought and snowfall are the main limiting factors for growth. In addition, fire regime can also play an important role for this fire-tolerant species (Resco de Dios et al. 2018) and, in this regard, subspecies from xeric environments showed characteristics potentially associated to prioritize storage (i.e., reserve accumulation) at the expenses of aboveground growth.

High-throughput phenotyping methods in common garden experiments

A central and important part of this thesis was the assessment of different high-throughput phenotypic techniques to retrieve information about phenotypic variability in common garden experiments of adult pines (chapter 1, 3 and 4). The complexity and time-consuming nature of field-based measurements are the two major limitations when phenotyping forest trees, especially in their adult stage. In this regard, an array of high-throughput phenotyping tools (HTPTs) have been developed in the last decade (Camarretta et al. 2020; Ganz et. al. 2019; Guo et al. 2013). The most common HTPTs utilized in forest phenotyping are remote sensing tools obtained from e.g. satellites, unmanned aerial vehicles (UVAs), or aerial and terrestrial LiDAR. In this thesis I provided valuable information about the potentiality of HTPTs to derive phenotypic traits at the individual or plot level in adult forest pines growing in common garden experiments. Different approaches have been used along the thesis (Table 2). UAV-records used in chapter 3 and 4

delivered accurate data (at the individual level) useful to characterize phenotypic variability in two forest species (*P. halepensis* and *P. nigra*) growing in three genetic trials. These results indicate that UAVs equipped with RGB and multispectral cameras coupled with widely used (and mostly free) software are cost-effective tools suitable to infer a wide array of phenotypic traits informative of morphology, phenology and physiology in adult forest trees with enough accuracy.

Table 2. Summary of high throughput phenotyping techniques (HTPTs) used in the different chapters of this thesis for two conifer species (*P. halepensis* and *P. nigra*) at different levels: plot (PL) and individual level (IL).

HTPTs	Chapter	*P. halepensis*	*P. nigra*
Ground penetrating radar	1	✓ (PL)	
UAVs with RGB camera	3, 4	✓ (IL)	✓ (IL)
UAVs with multispectral camera	4	✓ (IL)	
UAVs with LiDAR sensor	3	✓ (IL)	✓ (IL)

Limitations of HTPTs

Even though this thesis demonstrates and corroborates the high competence of HTPTs for tree phenotyping, they are not devoid of technical issues. On one hand, GPR detection capacity is seriously impaired in both nearly saturated (Hirano et al. 2009; Rodríguez-Robles et al 2017) and very dry soils (Hirano et al. 2009). In this regard I suggest to carry out these measurements in periods of full vegetative activity of trees, when roots would be active, but at the same time avoiding extremes in soil water status as a result of abundant precipitation or a prolonged drought. Moreover, root orientation can influence the detection of coarse roots, since overlapping roots and roots underneath the tree trunk are underestimated by the GPR device (Butnor et al. 2016). Also, soil type can influence root detection, and for this reason it is necessary to know about soil site characteristics and which antenna's frequency perform better under those conditions before collecting the data (Rodríguez-Robles et al. 2017). Lastly, I suggest collecting the data by making concentric circles around the main trunk of each tree, when the experiment design allows that, in order to minimize underestimating root detection due to roots' position and orientation (Butnor et al. 2016). On the other hand, UAV-derived records, especially RGB and multispectral images, are

influenced by environmental conditions, even if to a lesser extent than satellites. Wind can affect the performance of small UAVs (Wang et al. 2019), and clouds can influence vegetation reflectance values, thereby affecting vegetation indices as well as shadowing other objects or neighbor trees (Yamazaki et al. 2009). In this way, it is recommended to make flights under optimal atmospheric conditions, and around noon (preferably from late spring till early autumn). Moreover, RGB and multispectral sensors capture images from the top of the canopy, and despite it is possible to reconstruct a 3D point clouds, the information at different crown levels are not recorded. For this reason, the use of LiDAR is particularly meaningful to retrieve detailed within-crown information; however, this tool is significantly more expensive than a RGB camera. Finally, when UAV-derived phenotypic tools are applied at the individual tree level, it is necessary a previous knowledge of the trial even if tree segmentation can be done with a semi-automatic process in order to identify the individual of interest, otherwise difficult in homogeneous stands.

References

Andivia, E., Zuccarini, P., Grau, B., de Herralde, F., Villar-Salvador, P., Savé, R. (2019). Rooting big and deep rapidly: the ecological roots of pine species distribution in southern Europe. Trees - Struct. Funct. 33, 293-303. https://doi.org/10.1007/s00468-018-1777-x

Butnor, J. R., Samuelson, L. J., Stokes, T. A., Johnsen, K. H., Anderson, P. H., González-Benecke, C. A. (2016). Surface-based GPR underestimates below-stump root biomass. Plant Soil 402, 47-62. https://doi.org/10.1007/s11104-015-2768-y

Camarretta, N., Harrison, P.A., Lucieer, A., Potts, B.M., Davidson, N., Hunt, M. (2020). From drones to phenotype: Using UAV-LiDAR to detect species and provenance variation in tree productivity and structure. Remote Sens. 12, 1-16. https://doi.org/10.3390/rs12193184

Climent, J., Prada, M.A., Calama, R., Chambel, M.R., De Ron, D.S., Alía, R. (2008). To grow or to seed: Ecotypic variation in reproductive allocation and cone production by young female Aleppo pine (*Pinus halepensis*, Pinaceae). Am. J. Bot. 95, 833-842. https://doi.org/10.3732/ajb.2007354

Duursma, R.A., Mäkelä, A. (2007). Summary models for light interception and light-use efficiency of non-homogeneous canopies. Tree Physiol. 27, 859-870. https://doi.org/10.1093/treephys/27.6.859

Enescu, C. M., de Rigo, D., Caudullo, G., Mauri, A., Houston Durrant, T. (2016). *Pinus nigra* in Europe: distribution, habitat, usage and threats. In: San-Miguel-Ayanz J, de Rigo D, Caudullo G, Houston Durrant T, Mauri A (Eds.), European Atlas of Forest Tree Species. Publ. Off. EU, Luxembourg.

Esteban, L.G., Martín, J.A., de Palacios, P., Fernández, F.G. (2012). Influence of region of provenance and climate factors on wood anatomical traits of *Pinus nigra* Arn. subsp. *salzmannii*. Eur. J. For. Res. 131, 633-645. https://doi.org/10.1007/s10342-011-0537-x

Fkiri, S., Guibal, F., Fady, B., Khorchani, A. El, Khaldi, A., Khouja, M.L., Nasr, Z. (2018). Tree-rings to climate relationships in nineteen provenances of four black pines sub-species (*Pinus nigra* Arn.) growing in a common garden from Northwest Tunisia. Dendrochronologia. 50, 44-51. https://doi.org/10.1016/j.dendro.2018.05.001

Ganz, S., Käber, Y., Adler, P. (2019). Measuring tree height with remote sensing-a comparison of photogrammetric and LiDAR data with different field measurements. Forests. 10, 694. https://doi.org/10.3390/f10080694

Guo, L., Chen, J., Cui, X., Fan, B., Lin, H. (2013). Application of ground penetrating radar for coarse root detection and quantification: A review. Plant Soil. 362, 1-23. https://doi.org/10.1007/s11104-012-1455-5

Hirano, Y., Dannoura, M., Aono, K., Igarashi, T., Ishii, M., Yamase, K., Makita, N., Kanazawa, Y., 2009. Limiting factors in the detection of tree roots using ground-penetrating radar. Plant Soil 319, 15-24. https://doi.org/10.1007/s11104-008-9845-4

Jevšenak, J., Saražin, J. (2023). *Pinus halepensis* is more drought tolerant and more resistant to extreme events than *Pinus nigra* at a sub - Mediterranean flysch site. Trees. 3-8. https://doi.org/10.1007/s00468-023-02413-5

Karavani, A., Boer M. M., Baudena, M., Colinas, C. Díaz-Sierra, R., Pemán J., de Luis M., Enríquez-de-Salamanca A., Resco de Dios V. (2018). Fire-induced deforestation in drought-prone Mediterranean forests: drivers and unknowns from leaves to communities. Ecolo. Monogr. 88, 141-169. https://doi.org/10.1002/ecm.1285

Kreyling, J., Wiesenberg, G.L.B., Thiel, D., Wohlfart, C., Huber, G., Walter, J., Jentsch, A., Konnert, M., Beierkuhnlein, C. (2012). Cold hardiness of *Pinus nigra* Arnold as influenced by geographic origin, warming, and extreme summer drought. Environ. Exp. Bot. 78, 99-108. https://doi.org/10.1016/j.envexpbot.2011.12.026

Lombardi, E., Ferrio, J. P., Rodíguez-Robles, U., Resco de Dios, V., Voltas, J. (2022). Uso del Georradar como herramienta de fenotipado del sistema radical de especies forestales. Actas 8º Congreso Forestal Español (CFE). Lleida, Spain, 27 June-1 July.

Pasho, E., Camarero, J.J., Vicente-Serrano, S.M. (2012). Climatic impacts and drought control of radial growth and seasonal wood formation in *Pinus halepensis*. Trees - Struct. Funct. 26, 1875-1886. https://doi.org/10.1007/s00468-012-0756-x

Patsiou, T.S., Shestakova, T.A., Klein, T., di Matteo, G., Sbay, H., Chambel, M.R., Zas, R., Voltas, J. (2020). Intraspecific responses to climate reveal nonintuitive warming impacts on a widespread thermophilic conifer. New Phytol. https://doi.org/10.1111/nph.16656

Pausas, J.G. (2015). Evolutionary fire ecology: Lessons learned from pines. Trends Plant Sci. 20, 318-324. https://doi.org/10.1016/j.tplants.2015.03.001

Resco de Dios, V., Arteaga, C., Hedo, J., Gil-Pelegrín, E., Voltas, J. (2018). A trade-off between embolism resistance and bark thickness in conifers: are drought and fire adaptations antagonistic? Plant Ecol. Divers. 11, 253-258. https://doi.org/10.1080/17550874.2018.1504238

Rodríguez-Robles, U., Arredondo, T., Huber-Sannwald, E., Ramos-Leal, J. A., Yépez E. A. (2017). Technical note: Application of geophysical tools for tree root studies in forest ecosystems in complex soils. Biogeosciences 14, 5343-5357. https://doi.org/10.5194/bg-14-5343-2017

Santini, F., Climent, J.M., Voltas, J. (2019a). Phenotypic integration and life history strategies among populations of *Pinus halepensis*: an insight through structural equation modelling. Ann. Bot. 124, 1161-1171. https://doi.org/10.1093/aob/mcz088

Santini, F., Serrano, L., Kefauver, S.C., Abdullah-Al, M., Aguilera, M., Sin, E., Voltas, J. (2019b). Morpho-physiological variability of *Pinus nigra* populations reveals climate-driven local adaptation but weak water use differentiation. Environ. Exp. Bot. 166, 103828. https://doi.org/10.1016/j.envexpbot.2019.103828

Santos-del-Blanco, L., Bonser, S.P., Valladares, F., Chambel, M.R., Climent, J. (2013). Plasticity in reproduction and growth among 52 range-wide populations of a Mediterranean conifer: Adaptive responses to environmental stress. J. Evol. Biol. 26, 1912-1924. https://doi.org/10.1111/jeb.12187

Varelides, C., Brofas, G., Varelides, Y. (2011). Provenance variation in *Pinus nigra* at three sites in Northern Greece. Ann. For. Sci. 58, 893-900. https://doi.org/10.1051/FOREST:20011003

Vennetier, M., Ripert, C., Rathgeber, C. (2018). Autecology and growth of Aleppo pine (Mill.): A comprehensive study in France. For. Ecol. Manage. 413, 32-47. https://doi.org/10.1016/j.foreco.2018.01.028

Voltas, J., Lucabaugh, D., Chambel, M.R., Ferrio, J.P. (2015). Intraspecific variation in the use of water sources by the circum-Mediterranean conifer *Pinus halepensis*. New Phytol. 208, 1031-1041. https://doi.org/10.1111/nph.13569

Wang, B.H., Wang, D.B., Ali, Z.A., Ting Ting, B., Wang, H. (2019). An overview of various kinds of wind effects on unmanned aerial vehicle. Meas. Control (United Kingdom) 52, 731-739. https://doi.org/10.1177/0020294019847688

Yamazaki, F., Liu, W., and Takasaki, M. (2009). Characteristics of shadow and removal of its effects for remote sensing imagery‖, In: Proc. International Geoscience and Remote Sensing Symposium, IGARSS, Cape Town, South, Africa, 12-17 July. 4, 426-429.

Final Conclusions

Intraspecific genetic differentiation and its environmental drivers in P. halepensis and P. nigra

1. Both species exhibited large intraspecific differentiation among populations and ecotypes (or subspecies) in morphological (*P. halepensis*, *P. nigra*), phenological and physiological traits (*P. halepensis*) (all Chapters).
2. *P. halepensis* populations were characterized by differences in below- and aboveground growth, in the last case involving traits related to both primary and secondary growth (chapters 1, 2, 4).
3. Intraspecific variability of phenotypic traits among *P. halepensis* populations indicated contrasting adaptive syndromes: populations originating from semi-arid environments showed lower growth than their mesic counterparts, particularly: less allocation to roots, lower tree height and DBH, lower crown volume and density, lower ring-width, and delayed current-year needle development (all Chapters).
4. Intraspecific differentiation of secondary growth among *P. halepensis* populations was under genetic control, with variation in SNPs associated to metabolism and responses to environmental signals influencing ring-width and early- to latewood ratio. Water availability and temperature at origin during spring were the main climate factors that affected secondary growth of *P. halepensis* populations (Chapter 2).
5. The complex evolutionary differentiation of *P. nigra* was earmarked by its high intraspecific variability of phenotypic traits related to main trunk, crown architecture and crown density. Phenotypic variation in *P. nigra* was modulated by water availability at origin of populations, but mostly by continentality, with subspecies more adapted to low temperatures showing less aerial growth and a simpler and sparser crown (Chapter 3).
6. Phenotypic differentiation among *P. halepensis* populations exhibited a geographical pattern that followed an east-west cline. Water availability at origin of populations was the main driver modulating intraspecific differences in this species (Chapters 1, 3 & 4).

HTPTs and traditional in situ methods

7. The GPR device is a high-throughput non-destructive method capable of detecting and phenotyping the architecture of coarse roots in pine species (Chapter 1).
8. Dendrochronological analysis can be successfully combined with candidate-gene approaches to assess growth responses and their genetic control at the intra-annual level in pine species, particularly with the purpose of assessing the effects of SNP-based allelic substitutions in relation to the influence of climate variables (Chapter 2).
9. UAV-imagery and LiDAR are effective tools for the assessment of phenotypic differentiation of morphological traits at the individual level in forest genetic trials (Chapter 3).
10. RGB and multispectral records are meaningful to characterize intraspecific differences in needle phenology especially related to senescence in an evergreen, fire-embracer conifer such as *Pinus halepensis* (Chapter 4).

This thesis has been carried out at the Laboratory of Silviculture, Deparment of Agricultural and Forestry Science and Engineering, University of Lleida. Erica Lombardi was supported by AGAUR FI pre-doctoral fellowship (with the support from the Secretariat for Universities and Research of the Ministry of Business and Knowledge of the Government of Catalonia and the European Social Found). The research was supported by the Spanish Government, grant numbers: AGL2015-68274-C3-3-R (MINECO/FEDER); RTI2018-094691-B-C31 and RTI2018-094691-B-C33 (MCIU/AEI/FEDER, EU).

Acknowledgments

It is time to thank the people who contributed to the realization of this thesis.

First of all, I would like to thank my supervisors. Jordi, thanks for your constant support, for your suggestions and for your guidance, always gave with patience. You are an amazing person and supervisor, always ready to help, your passion and your knowledge have inspired me during these years. Thanks to encourage me and for helping me to fulfil my PhD step by step. Victor, thank you for believing in me since the beginning, unfortunately we did not have the opportunity to see each other that much, but I always knew that you were there for everything I needed. Many thanks to both of you for giving me this great opportunity to come to Lleida and to complete my PhD.

I also would like to thank Filippo, who shared with me a lot of knowledge (and data), your help has been fundamental for the realization of this thesis, I truly appreciate all the time that you have spent for me. I am also grateful to Tatiana, who shared with me her knowledge about dendrochronology giving me a great help for the realization of Chapter 2. Thanks to Sveta for the company and for the shared lunches and to Maria Josep for the talks during tea time and for the help with my lab work. I would like to extent the acknowledgment to Luis and Tatiana, to stop by the lab for a chat and for the nice field trip to Rome.

Thanks to Paco Rodríguez, who hosted me in Soria for two weeks, your knowledge and your hints have been fundamental for the development of Chapter 3 and 4.

I am also really grateful to Beatriz Pérez, María Belén Luna, Gonzalo Zavala and Paula Piñas for hosting me one week in your lab in Toledo, I really enjoyed my short stay and without your support the flammability experiment in Chapter 4 would not have been possible.

Thanks to Andrea Hevia and Raul Sanchez to start a beautiful collaboration between their lab DendrOlavide and the Laboratory of Silvicolture of the University of Lleida.

I would like to acknowledge Shwan Kefauver, who provide the drone, flew it and pre-process the images that I have been used in Chapter 4, thanks for your work and your patience.

I am grateful to all the co-authors of my papers, their effort and their contribution for the success of this thesis has been huge.

Acknowledgments

I would like to thank all the people that I met during this years, everyone has contributed in a certain way to make this PhD an unforgettable life experience. In particular, I would like to thank Irene, Albert and Breno, to be there always, especially during the “not so easy” Covid time, thanks to be my “burbuja” during that period. I will always remember all the laugh and the good moments that we have spent together. Also a special thanks to Filippo, Alicia and Priya to welcome me in the best way and to make me feel at home as only you can do.

A huge thanks to my family, for being always present and ready to help. I doubt I would be at this point of my life without you.

And of course, thanks to Matteo for everything and especially for always supporting my decisions, no matter what.